A PARAMETRIC STUDY OF FORMATION FLIGHT OF A WING BASED ON PRANDTL'S BELL-SHAPED LIFT DISTRIBUTION

A Thesis

presented to

the Faculty of California Polytechnic State University,

San Luis Obispo

In Partial Fulfillment

of the Requirements for the Degree

Master of Science in Aerospace Engineering

By

Kyle Sean Lukacovic

June 2020

COMMITTEE MEMBERSHIP

TITLE:	A Parametric Study of Formation Flight of a Wing Based on Prandtl's Bell-Shaped Lift Distribution
AUTHOR:	Kyle Sean Lukacovic
DATE SUBMITTED:	June 2020
COMMITTEE CHAIR:	Aaron Drake, Ph.D. Professor of Aerospace Engineering
COMMITTEE MEMBER:	Paulo Iscold, Ph.D. Associate Professor of Aerospace Engineering
COMMITTEE MEMBER:	David Marshall, Ph.D. Professor of Aerospace Engineering, Department Chair
COMMITTEE MEMBER:	Russell Westphal, Ph.D. Professor of Mechanical Engineering

ABSTRACT

A Parametric Study of Formation Flight of a Wing Based
on Prandtl's Bell-Shaped Lift Distribution

Kyle Sean Lukacovic

The bell-shaped lift distribution (BSLD) wing design methodology advanced by Ludwig Prandtl in 1932 was proposed as providing the minimum induced drag. This study used this method as the basis to analyze its characteristics in two wing formation flight. Of specific interest are the potential efficiency savings and the optimal positioning for formation flight. Additional comparison is made between BSLD wings and bird flight in formation.

This study utilized Computational Flow Dynamics (CFD) simulations on a geometric modeling of a BSLD wing, the Prandtl-D glider. The results were validated by modified equations published by Prandtl, by CFD modeling published by others, and by Trefftz plane analysis. For verification, the results were compared to formation flight research literature on aircraft and birds, as well as published research on non-formation BSLD flight.

The significance of this research is two part. One is that the BSLD method has the potential for significant efficiency in formation flight. The optimal position for a trailing wing was determined to be partially overlapping the leading wing vortex core. For a BSLD wing these vortices are located inboard from the wingtips resulting in wingtip overlap and have a wider impact downstream than the elliptical lift distribution (ELD) wingtip vortices. A second aspect is that avian research has traditionally been studied assuming the ELD model for bird flight, whereas this study proposes that bird flight would be better informed using the BSLD.

Keywords: [Bell Shaped Lift Distribution, BSLD, Formation Flight, Computational Fluid Dynamics, CFD, Prandtl, Prandtl-D, Avian Flight, Birds, Vortex, Optimization, Induced Drag, Efficiency]

ACKNOWLEDGMENTS

First and foremost, I would like to thank my Dad, John Lukacovic. A father's love is the compass by which his children learn to navigate, to sail, and to reach their dreams. I would not be here without you. From the bottom of my heart I send my appreciation for all that you do.

I would like to thank Dr. Graham Doig for giving me the opportunity to pursue graduate education at Cal Poly. Without this opportunity and his guidance, I would not be at NASA Ames working as a wind tunnel test director. It is a step or two up from the lab in Building 41 but in the grand scheme of things it operates the same.

I would also like to thank my advisor Dr. Aaron Drake for his patience and time. Their expertise and professionalism in the field of aerospace engineering and knowledge of aerodynamics has propelled my drive to shoot for excellence. His acceptance of the advisor position at an advanced stage in the project reflects his dedication to his students.

I send my deepest gratitude to my distinguished committee members. The feedback I received from Dr. Paulo Iscold, Dr. David Marshall, and Dr. Russell Westphal helped push my thesis. I especially appreciate their willingness to step in and help with my extended thesis process.

I thank Albion Bowers and Oscar Murillo for the experience of a lifetime out in the Mojave Desert where I learned of a little thing called the Bell-Shaped Lift Distribution. My internship sending the Prandtl-D wing soaring into the sky led me to the hypotheses I present herein for the wing in formation flight. This research would not have been published to the world without turning me into a believer of the impossible.

I would also like to acknowledge my science and math teachers at Sehome High School; Ms. Hankinson, Mr. Toney, Mr. Swets, and Mr. Criez. From the catalytic chemistry, basswood bridge building, composite canoe manufacturing, and robotic design, their enthusiasm had my young mind always striving for more to soak up. They inspired me to pursue a degree in engineering.

A big shout out also goes Dr. Nancy Squires at Oregon State University. Her classes in aerospace engineering and many long office hour talks persuaded me to reach towards the stars and fly towards a masters in aeronautics.

I also send thanks to two of my best friends and roommates from my time at Cal Poly, Sabir Utamsing and Matt Nguyen. From the countless hours of watching movies with popcorn, to the uncountable hours sitting in the lab trying to determine how to get the schlieren to work, my fondest memories will always be the experiences I shared with them. I can't wait to see what they do in the future.

To the rest of my family, friends, coworkers, and everyone else who has touched me throughout this journey we call life, I thank you. A whole book can be written for how they have shaped me into the person I am today.

Lastly, I want to send love to my Mom for all the support you have given me from day one. This thesis is dedicated to you.

TABLE OF CONTENTS

LIST OF TABLES

LIST OF FIGURES

NOMENCLATURE

VARIABLES

γ	Vortex sheet strength
Γ	Circulation
Γ_0	Circulation at the wing center, y = 0
Γ	Circulation
δ	Boundary layer thickness
ϵ	Dissipation rate
ϵ	GCI solution comparison
ζ	Non-dimentional distance along the chord
μ	Ratio of circulation
μ	Dynamic viscosity
ν	Kinematic viscosity
ξ	Semispan location
π	Pi
ρ	Density
τ_{wall}	Wall Shear Stress
φ_x	X direction velocity perturbation
φ_y	Y direction velocity perturbation
φ_z	Z direction velocity perturbation
b	Span of a bell-shaped wing
b_e	Span of an elliptical wing
c	Chord length
c_l	Local lift coefficient
c_p	Local coefficient of pressure
C_D	Drag coefficient
$C_{D,i}$	Induced drag coefficient
C_f	Friction coefficient
C_L	Lift coefficient
D	Drag
D_f	Skin friction drag
D_i	Induced drag

D_p	Pressure drag
E	Error
f	Numerical solution obtained with grid spacing h
F_s	Factor of safety
h	Characteristic mesh length
I	Moment of inertia
k	Kinetic energy
l	Local lift force
L	Defined length
L	Lift of a bell-shaped wing
L_0	Lift at center of a bell-shaped wing
M	Bending moment
p	Pressure
q	Dynamic pressure
r	Radius of gyration of an elliptical wing
r	Refinement factor
Re	Reynolds number
s	Semispan of a bell-shaped wing
s_e	Semispan of an elliptical wing
S	Wing area
S_T	Trefftz plane area
u	x velocity component
V	Flow velocity
V_∞	Freestream velocity
V_*	Friction velocity
w	Downwash
w_0	Downwash at the wing center
$\hat{x}$	Cartesian x unit vector
y	Nondimensional spanwise location, 0 = wing center
y	Distance away from wing surface
Y	Dimensional spanwise location, 0 = wing center
Y	Wingtip spacing (WTS)
y^+	Wall y+

ABBREVIATIONS

AFRC	Armstrong Flight Research Center
AoA	Angle of Attack
AR	Aspect Ratio
BSLD	Bell-Shaped Lift Distribution
CAD	Computer Aided Design
CFD	Computational Fluid Dynamics
ELD	Elliptical Lift Distribution
GCI	Grid Convergence Index
L/D	Lift-to-drag ratio
MAC	Mean Aerodynamic Chord
NASA	National Aeronautical and Space Administration
RANS	Reynolds-Averaged Navier-Stokes
S.D.	Standard Deviation
WTS	Wingtip Spacing

Chapter 1

INTRODUCTION

In the last century the aviation industry has been using the elliptical lift distribution (ELD) published by Ludwig Prandtl in 1922. But there is another spanload proposed by Prandtl in 1932 that has received little attention [1]: this spanload is known as the bell-shaped lift distribution (BSLD). To achieve the BSLD a wing design can incorporate twist to result in less lift at the wingtips. One of the key characteristics of the BSLD is that downwash gradually transitions to upwash at 70.4 percent of the semispan, producing a weak vortex roll-up inboard of the wingtips.

For most of the last century, little experimental testing of the BSLD had been performed. In recent years former Chief Scientist Albion Bowers and Oscar Murillo at the National Aeronautical and Space Administration (NASA) Armstrong Flight Research Center delved deeper into the application and conducted flight research on a flying wing glider using the BSLD model, called the Prandtl-D [2]. Their collected data and published work demonstrated the high efficiency of the design, as well as a potential new control scheme called proverse yaw. This means that the BSLD wing can fly with no vertical tail control which is needed to counter the adverse yaw of ELD wing designs. They also theorized that bird flight is better described by the BSLD methodology. The Prandtl-D glider is a prime candidate for further study of the BSLD because the geometry of the wing is published by NASA [2].

Research and observation by avian scholars show that birds in formation flight fly with their wingtips significantly overlapped but make the assumption that bird flight can be modeled with the ELD loading (Section 2.4). Since the ELD results in wingtip vortices, this assumption fails to identify why birds in formation flight overlap their wings. Modeling bird flight using the BSLD, which has a vortex core inboard of the wingtip, would better explain why birds flying in formation benefit with their wings overlapped.

1.1. Hypotheses

The purpose of this thesis is to determine the aerodynamic characteristics, efficiencies, and the optimal position for a BSLD wing in formation flight. Several hypotheses were made going into the study. The first is that formation flight for the BSLD is highly beneficial. The second hypothesis is that the trailing BSLD wing would benefit most when its tip is aligned with the leading wing vortex. This was suggested by Bowers and Murillo in their report [2]. This is similar to the configuration identified as being optimal for an ELD wing where the trailing wing's tip is closer in-line with the leading wing's vortex (Section 2.5), except the BSLD vortex is inboard of the tip which results in wingtip overlap. Further discussions on this subject are presented in Sections 5.4 and 6.2. The third, as mentioned above, is that bird formation flight is best modeled using BSLD rather than ELD. This was proposed in the Prandtl-D report [2] and observational avian research data implies it (Section 2.4). These hypotheses will be confirmed and/or modified within this report.

1.2. Methodology

The approach to a study of formation flight can go four routes: either analytically using CFD simulations or equation-based methods, or experimentally via tests in a wind tunnel or research flights. These four methods (equations, CFD, wind tunnel test, research flights) were all used in the selected literature review (Section 2.5) for the determination of the optimal position for drag reduction of the ELD wing in formation flight. For this study the author chose to perform a parametric study of a BSLD wing using Computational Fluid Dynamics (CFD) on the Prandtl-D in formation flight to determine the optimal lateral position of the trailing wing. This was determined to be more cost effective than building multiple research vehicles or designing and manufacturing wind tunnel models with instrumentation to capture the experimental data.

The parametric study was broken up into three phases. The first step was to create the CAD model of a BSLD wing. As mentioned in Section 2.3, the Prandtl-D glider wing designed by Bowers accurately displayed the characteristics of the BSLD as determined by Prandtl. Because

the wing's geometry is published it becomes the primary candidate for a study of formation flight of a BSLD wing. It is also beneficial that previous studies have been done on this same wing and published results can be used as additional validation. Chapter 3 takes the geometry of the Prandtl-D P3-C wing and creates a three-dimensional CAD model to be used in the simulation. Providing a detailed overlook on how the model was produced is important so that others can recreate the study. The chapter also highlights any differences between the published geometry and that of the studied model.

The second step was to set up the CFD simulation and to verify a baseline configuration (Chapter 4). The simulation setup is comprised of determining the flow physics continua, setting a fluid domain, and establishing an adequate mesh. As it is important to make sure the right data is being produced and everything is up to the right standards, a baseline configuration was run. Validation of this study was performed by comparing the output to the previous studies on the Prandtl-D glider.

The third phase was to run a determined test matrix and to analyze the results (Chapter 5). The test matrix selected consists of 23 configurations where the trailing wing is moved laterally behind the leading wing. An analysis of the lift and drag characteristics of both the individual trailing wing and the two wings as a combined system will help identify the best position for flight. A Trefftz plane analysis was performed to determine the reduction of induced drag for the two-wing system (Section 5.3). An additive section is also included showing how the lift distribution changed for the trailing wing at the various positions (Section 5.5). The conclusion (Chapter 6) provides a summation of the study results found, as well as comparisons between the results and the previous bird and ELD research.

Validating this work presents some challenge as no other known lab or field observations have been performed on wings with the BSLD in formation flight. As such a review of previous formation flight research as seen by both aircraft with the ELD and by birds will better inform the results of this study.

Chapter 2

PREVIOUS WORK

This chapter details previous work done on bell-shaped lift distributions and on formation flight. First, an introduction to the equations behind the BSLD will be presented followed by how it is implemented in the NASA Armstrong Flight Research Center's aircraft. This chapter will conclude with a literature review of formation flight of birds as well as of aircraft with elliptically loaded wings.

2.1. The Bell-Shaped Lift Distribution

In this section the underlying equations for the bell-shaped lift distribution are introduced. First, a solution is presented of Prandtl's proposed method showing a reduction in induced drag of 11% for the BSLD. Next, simplified equations from Prandtl's study for the lift and downwash distribution as derived by Bowers and Murillo are given. Finally, a look into additional studies of the minimum induced drag is presented as insight into other approaches to the derivation of BSLD solutions.

2.1.1. Discovering the Minimum Induced Drag Solution

In the 1920s Ludwig Prandtl demonstrated that, assuming a wing with a given lift and a specified wingspan, one can obtain the minimum induced drag using an ELD. Later in 1932 Prandtl published a paper with the translated titled "On Wings with the Least Induced Drag" [1] in the German Society for Aeronautics and Astronautics early journal the "Journal of Aviation Engineering and Motorized-Airship Aeronautics." In this paper he asked a very fundamental question: "Is there another spanload with the same lift and the same structure that has less drag?" To this Prandtl was able to find a solution to minimizing induced drag (Equation 2.1) by specifying both the total lift (Equation 2.2) and the moment of inertia of the lift distribution (Equation 2.3).

$$D_i = \rho \int_{-s}^{s} \Gamma w dy \tag{2.1}$$

$$L = \rho V \int_{-s}^{s} \Gamma dy \tag{2.2}$$

$$I = Lr^2 = \rho V \int_{-s}^{s} \Gamma y^2 dy \tag{2.3}$$

In these equations ρ is density, V_∞ is freestream velocity, Γ is circulation, w is downwash, y is the nondimensional spanwise location with 0 being the center of the wing, s is the semispan of the new spanloaded wing, and r is the radius of gyration for an ELD wing. Solving a variational problem, Prandtl was able to transform Equation 2.2 and Equation 2.3 into Equation 2.4 and Equation 2.5, respectively. Here, there are a few additional variables where b is the span of the new spanloaded wing, Γ_0 is the circulation at the center of the wing, L is lift, and μ is a ratio of circulations across the span (Equation 2.6). This ratio is used to define the spanload distribution with μ=0 being for the ELD. μ is derived out of Equation 2.7 which is the equation for the circulation distribution across a finite wing [3]. Note Equation 2.7 uses the variable ξ, an abbreviation for the semispan location (Equation 2.8)

$$L = \frac{\pi}{4} \rho b V_\infty \Gamma_0 \left(1 - \frac{\mu}{4}\right) \tag{2.4}$$

$$Lr^2 = \frac{\pi}{64} \rho b^3 V_\infty \Gamma_0 \left(1 - \frac{\mu}{2}\right) \tag{2.5}$$

$$\mu = -\frac{\Gamma_2}{\Gamma_0} \tag{2.6}$$

$$\Gamma = (\Gamma_0 - \Gamma_2 \xi^2)\sqrt{1 - \xi^2} \tag{2.7}$$

$$\xi = \frac{y}{s} \tag{2.8}$$

Through division it is directly revealed that:

$$r^2 = \frac{1}{16} b^2 \frac{1 - \frac{\mu}{2}}{1 - \frac{\mu}{4}} \tag{2.9}$$

Or:

$$b = 4r\sqrt{\frac{1-\frac{\mu}{4}}{1-\frac{\mu}{2}}} \tag{2.10}$$

These are relationships between the radius of gyration for an elliptical wing and the span of the new wing with a modified spanload. Reinserting Equation 2.10 back into Equation 2.4 results in Equation 2.11, the circulation at the center of the wing with a new spanload.

$$\Gamma_0 = \frac{L}{\pi\rho V_\infty r}\sqrt{\frac{1-\frac{\mu}{2}}{\left(1-\frac{\mu}{4}\right)^3}} \tag{2.11}$$

From Prandtl's analysis substituting Equation 2.11 into the induced drag Equation 2.12 gives the final equation for the induced drag of a modified spanload, Equation 2.13. Induced drag in these equations is represented by the variable D_i. This equation is important to the study as it shows that changing the circulation ratio also changes the induced drag.

$$D_i = \frac{\pi\rho{\Gamma_0}^2}{8}\cdot\left(1-\frac{\mu}{2}+\frac{\mu^2}{4}\right) \tag{2.12}$$

$$D_i = \frac{L^2}{8\pi\rho{V_\infty}^2 r^2}\cdot\frac{\left(1-\frac{\mu}{2}\right)\left(1-\frac{\mu}{2}+\frac{\mu^2}{4}\right)}{\left(1-\frac{\mu}{4}\right)^3} \tag{2.13}$$

One can tabulate the variation of the circulation ratio, μ, compared to the progression of the functions of μ within equations Equation 2.10, Equation 2.11, and Equation 2.13 as seen in Table 2.1. These functions will be denoted as $f(\mu)_b$, $f(\mu)_{\Gamma_0}$, as $f(\mu)_{D_i}$ for the respective ratios of span, the circulation at the center of the wing, and induced drag at different spanload distributions.

Table 2.1: μ Variation in Relation to Aerodynamic Characteristics Ratios

	$f(\mu)_b$	$f(\mu)_{\Gamma_0}$	$f(\mu)_{D_i}$
μ	$\sqrt{\frac{1-\frac{\mu}{4}}{1-\frac{\mu}{2}}}$	$\sqrt{\frac{1-\frac{\mu}{2}}{\left(1-\frac{\mu}{4}\right)^3}}$	$\frac{\left(1-\frac{\mu}{2}\right)\left(1-\frac{\mu}{2}+\frac{\mu^2}{4}\right)}{\left(1-\frac{\mu}{4}\right)^3}$
0.00	1.000000	1.000000	1.000000
0.25	1.035098	1.030498	0.945778
0.50	1.080123	1.058080	0.909621
0.75	1.140175	1.079456	0.892126
1.00	1.224745	1.088662	0.888889

One recognizes easily that the minimum of $f(\mu)_{D_i}$ occurs when μ=1, which can also be demonstrated by analyzing the differential of $f(\mu)_{D_i}$ which disappears at exactly μ=1. The function does not have a usual minimum here but rather an inflection point (see Figure 2.1), where the function lowers even further for values of μ>1. However, past this inflection point our task loses its rational meaning because negative lift will occur at the wingtip and consequently also negative bending moments (*M*), and of course the negative bending moments do not correspond with negative spar weight. Thus, in the case of the bending moment changing sign, one does not have to take the integral over *M* but instead the integral over the absolute value of *M*, and thus the basis for the whole calculation falls away and the solution becomes invalid. It therefore follows that the largest reasonable value of μ is 1, which at the same time is also the optimal value to achieve the lowest induced drag.

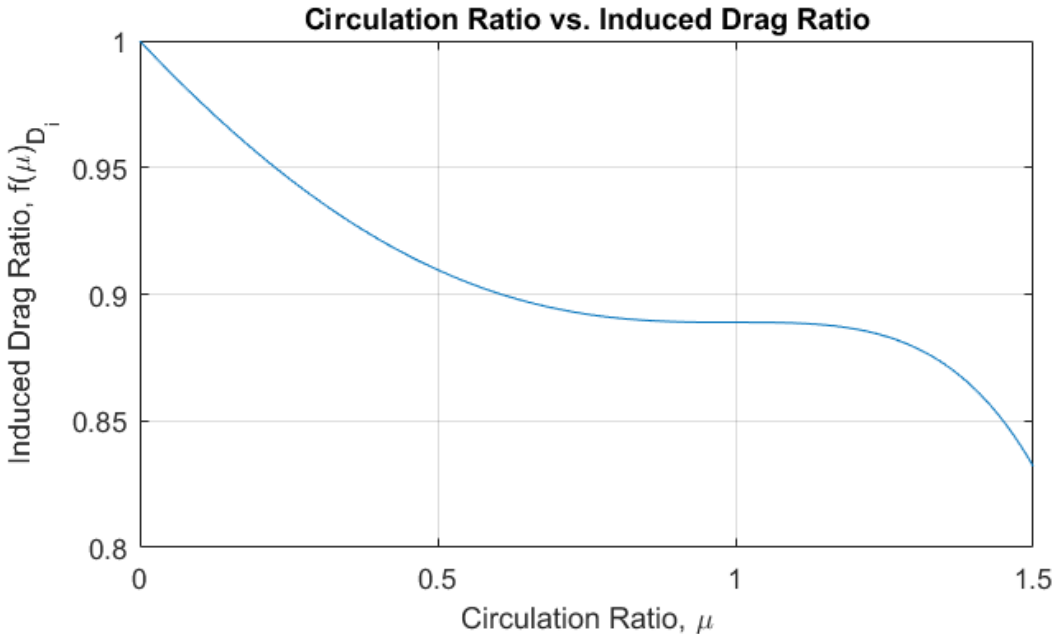

Figure 2.1: Induced drag ratio compared to the circulation ratio

$$\Gamma = \Gamma_0(1 - \mu\xi^2)\sqrt{1 - \xi^2} \tag{2.14}$$

$$w = -\frac{\Gamma_0}{2b_e}\left(1 + \frac{\mu}{2} - 3\mu\xi^2\right) \tag{2.15}$$

Figure 2.2 and Figure 2.3 plot the circulation distributions (Equation 2.14) and downwash velocity (Equation 2.15) respectively in association to μ of 0, 0.25, 0.5, 0.75, and 1. Note in Equations 2.14 and 2.15 the variable ξ from Equation 2.8 for the semispan location is used. Also recognize Equation 2.14 for the circulation distribution is Equation 2.7 when μ is substituted in. One also can produce the nondimensional curves in Figure 2.2 as a relationship with lift on the y axis as lift and circulation are correlated by a constant. As seen in Figure 2.2, the curve for μ=0 represents the standard ELD while the curve for μ=1 represents what we now call the bell-shaped lift distribution (BSLD), the optimal lift distribution for minimum drag based on the assumptions. This is where Ludwig Prandtl's 1932 analysis ended, as he did not continue to look at the optimization of his derived solution in this paper.

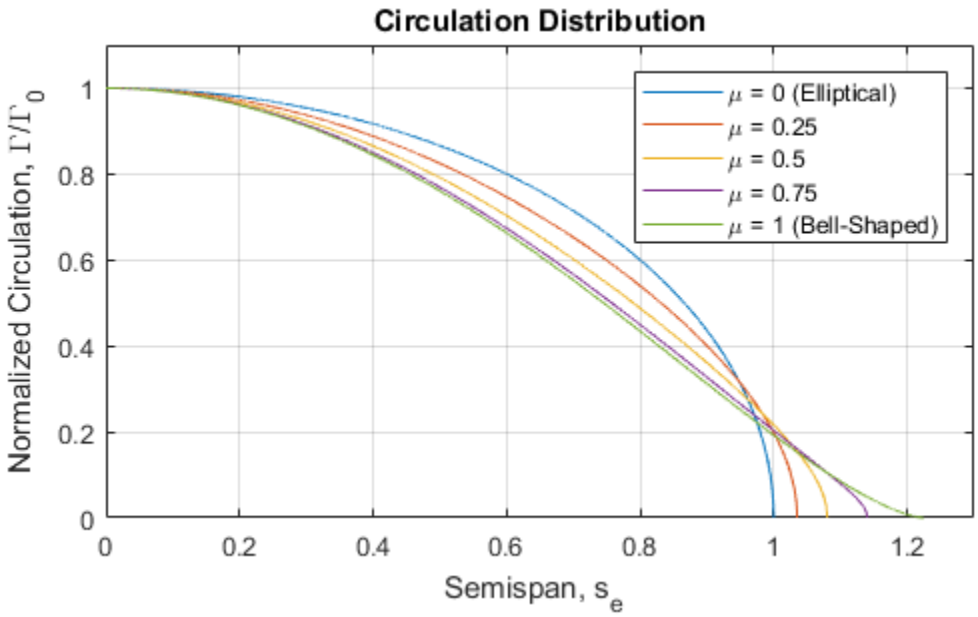

Figure 2.2: Circulation distribution of various spanloads

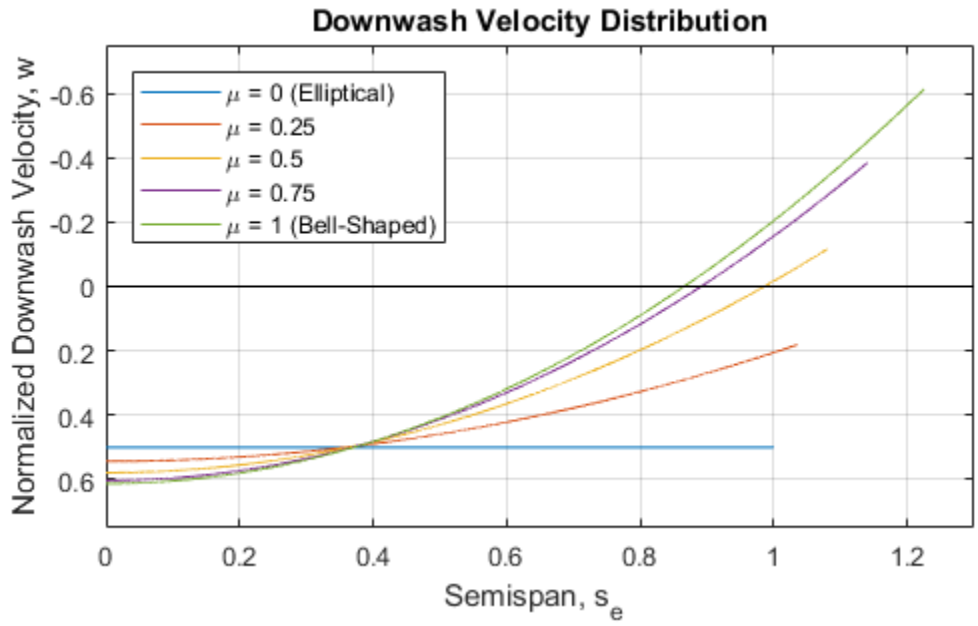

Figure 2.3: Downwash velocity distribution of various spanloads

In Figure 2.3 the downwash distribution for the ELD wing is constant along the entire span of the wing. In contrast it is shown for the BSLD wing the downwash crosses the zero line and becomes upwash near the wingtip. This transition occurs at 0.8622 of the 1.2247 semispan on the graph, or 70.4 percent of the semispan of the BSLD wing. This phenomenon creates induced thrust

towards the wingtips, which is negative induced drag. It should still be noted that the total sum of the induced thrust and induced drag still creates a net drag on the wing.

A comparison of the flow fields resulting from the elliptical and bell-shaped spanloads is shown in Figure 2.4. For the ELD wing there is a sharp discontinuous slope at the wingtip. Where the constant downwash becomes a sudden upwash is where a strong vortex is created located at the wingtip. As for the BSLD wing, there is a smooth transition between the downwash and upwash with no discontinuity (also seen in Figure 2.3) in which a weaker vortex forms at the 0.704 location on the semispan. This is an important difference between the two lift distributions. The gradual downwash-upwash transition of the BSLD means a less intense velocity shear, resulting in a weaker vortex. However, the upwash continues from this inboard vortex core all the way out to the wingtip, resulting in a wide vortex of almost 30% of the span. This provides a potentially wider range of beneficial positioning for a trailing wing versus the ELD which has a smaller range imposed by the stronger and more compact wingtip vortex. This characteristic is seen in the wide range of positioning selected by birds (Subsection 2.4.4) and in the tight range of benefit for aircraft (Subsection 2.5.3). The conclusion in Sections 6.2 and 6.4 discusses the difference more.

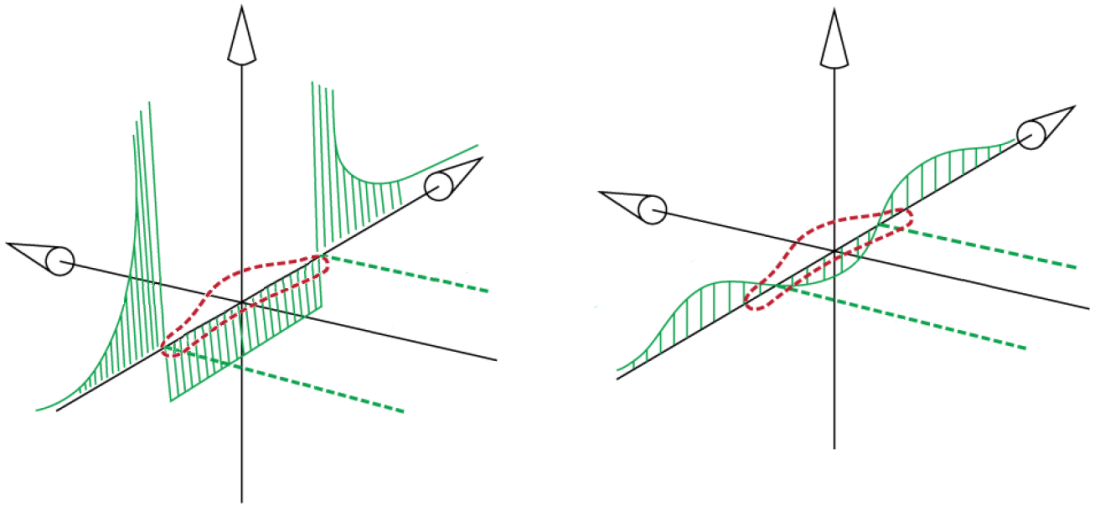

Figure 2.4: Flow fields resulting from the elliptical (a. Left) and bell-shaped (b. Right) spanloads

To continue with the derivation of the BSLD equations, μ=1 can now be plugged back into the previously discussed equations for simplification. Progressing off Prandtl's work, the author found that the equation for lift now becomes Equation 2.16 where the area under the lift distribution curve is no longer $\pi/4$ but $3\pi/16$. The moment of inertia Equation 2.5 can also be simplified to Equation 2.17.

$$L = \frac{\pi}{4}\rho b V_\infty \Gamma_0 \cdot \left(\frac{3}{4}\right) = \frac{3\pi}{16}\rho b V_\infty \Gamma_0 \tag{2.16}$$

$$I = Lr^2 = \frac{\pi}{64}\rho b^3 V_\infty \Gamma_0 \cdot \left(\frac{1}{2}\right) = \frac{\pi}{128}\rho b^3 V_\infty \Gamma_0 \tag{2.17}$$

A few more of Prandtl's equations can be simplified down. Equation 2.9, the relationship between the radius of gyration of the elliptical wing to the span of the bell-shaped wing becomes Equation 2.18. This can also be displayed as Equation 2.19 when Equation 2.10 is reduced with μ=1.

$$r^2 = \frac{1}{16}b^2 \cdot \left(\frac{2}{3}\right) = \frac{2}{48}b^2 \tag{2.18}$$

$$b = 4r\sqrt{\frac{3}{2}} \approx 4r \cdot (1.22) \tag{2.19}$$

For a standard ELD wing with a given span (b_e), the radius of gyration (r) is equal to a quarter of the span (Equation 2.20) acting at half the semispan (s_e). Therefore, the relationship between the span of the ELD wing (b_e) to the span of the BSLD wing (b) as well as the relationship between the semispan of the ELD wing (s_e) to the semispan of the BSLD wing (s) can be displayed as Equation 2.21 and Equation 2.22 respectively.

$$r = \frac{b_e}{4} = \frac{s_e}{2} \tag{2.20}$$

$$b = 1.22 \cdot b_e \tag{2.21}$$

$$s = 1.22 \cdot s_e \tag{2.22}$$

A couple more simplifications can be made when substituting μ=1 into Ludwig Prandtl's equations. Equation 2.11 for circulation at the center of the wing now becomes Equation 2.23. Most importantly though for our analysis is the simplification of Equation 2.13 for induced drag. The 0.89 factor in Equation 2.24 shows that there is a total reduction of 11% in induced drag with a wing that has 22% greater span than an elliptically loaded wing with the same total lift, while using the same exact amount of structure (approximated by the moment of inertia of the lift distribution). This factor of 8/9 is the underlying conclusion of Prandtl's 1932 study for the minimum induced drag of the BSLD.

$$\Gamma_0 = \frac{L}{\pi\rho V_\infty r}\sqrt{\frac{32}{27}} \approx \frac{L}{\pi\rho V_\infty r}\cdot(1.09) \tag{2.23}$$

$$D_i = \frac{L^2}{8\pi\rho {V_\infty}^2 r^2}\cdot\left(\frac{8}{9}\right) \approx \frac{L^2}{8\pi\rho {V_\infty}^2 r^2}\cdot(0.89) \tag{2.24}$$

2.1.2. A Simplification of Prandtl's Equations

Albion H. Bowers and Oscar J. Murillo took Prandtl's work one step further in their paper "On Wings of the Minimum Induced Drag: Spanload Implications for Aircraft and Birds" [2]. Therein they simplified Prandtl's equation for the circulation distributions (Equation 2.14) to the nondimensional local load Equation 2.25. As the lift distribution follows the same distribution as circulation, Equation 2.26 can also be composed. In these cases, y is the span location between -1 and 1 (wingtip to wingtip). As shown in Figure 2.5, a plot of the simplified equation is similar to that of the BSLD in Figure 2.2 for μ=1 (scaled for the x-axis). In Section 4.5, the lift distribution of the Prandtl-D aircraft as determined by the CFD data will be overlaid on this plot (Figure 4.6) for verification to make sure the analysis within this report represents Prandtl's optimal lift distribution.

$$\Gamma = (1-y^2)^{3/2} \tag{2.25}$$

$$L = (1-y^2)^{3/2} \tag{2.26}$$

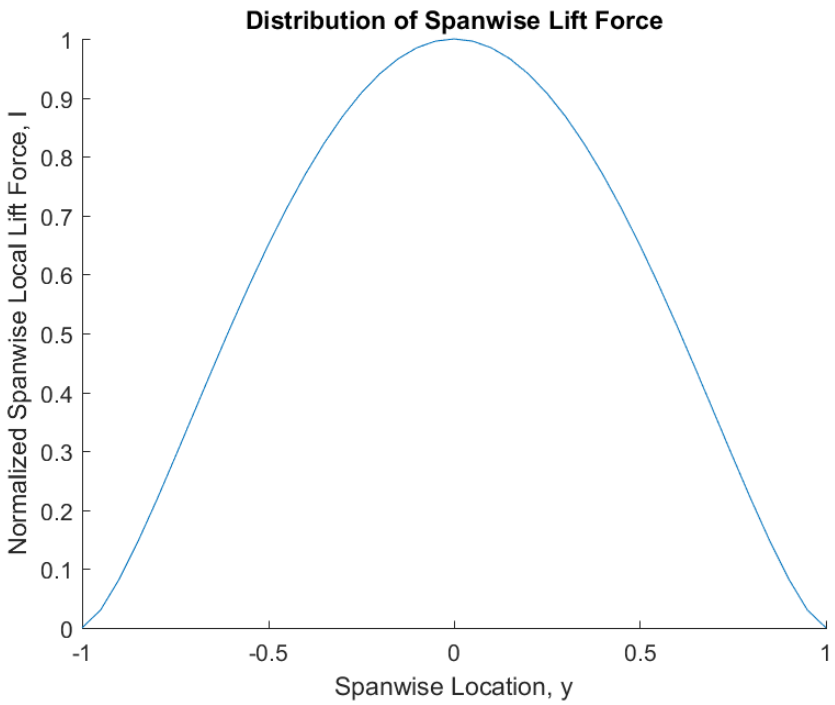

Figure 2.5: Distribution of spanwise local lift

Going a step further than Bowers and Murillo [2], these nondimensional equations can be scaled to the dimensional space in equations Equation 2.27 and 2.28 when *Y* is the dimensional spanwise location on the BSLD wing and the wing center is Y = 0.

$$\Gamma(Y) = \Gamma_0(1 - \left(\frac{2Y}{b}\right)^2)^{3/2} \tag{2.27}$$

$$\mathrm{L(Y)} = \mathrm{L_0}(1 - \left(\frac{2\mathrm{Y}}{\mathrm{b}}\right)^2)^{3/2} \tag{2.28}$$

Bowers and Murillo [2] also simplified Equation 2.15 for the nondimensional downwash velocity as seen in Equation 2.29. Taking this one step further than their published work, the equation can be scaled dimensionally with Equation 2.30.

$$\mathrm{w} = \frac{3}{2}(\mathrm{y}^2 - 1/2) \tag{2.29}$$

$$\mathrm{w(Y)} = \mathrm{w_0}\frac{3}{2}\left(\left(\frac{2\mathrm{Y}}{\mathrm{b}}\right)^2 - 1/2\right) \tag{2.30}$$

2.1.3. Additional Minimum Induced Drag Studies

After Ludwig Prandtl, a few other studies were performed on the new lift distribution. Though these are not as vital for the current study that is based on Prandtl's work, it is important to be aware of these reports for future studies. In 1950 Robert T. Jones published his paper "The spanwise distribution of lift for minimum induced drag of wings having a given lift and a given bending moment" [4]. In his final equation (Equation 2.31) Jones solved for the induced drag of a BSLD that corresponds to the elliptically loaded equivalent wing using the ratio of their spans as seen in the brackets. The difference between Prandtl's conclusion and Jones's was their initial assumptions, where Prandtl used a given moment of inertia and Jones used a given root bending moment.

$$D_i = \frac{L^2}{\pi \frac{\rho}{2} {V_\infty}^2 (2s_e)^2} \cdot \left[8 \left(\frac{s_e}{s} \right)^4 - 16 \left(\frac{s_e}{s} \right)^3 + 9 \left(\frac{s_e}{s} \right)^2 \right] \tag{2.31}$$

In 1973, Armin Klein and S. P. Viswanathan arrived at the same conclusion as Jones without knowledge of the 1950's report [5]. Their equations for induced drag differ only as the span ratio is inversed (Equation 2.31 vs. Equation 2.32). This function has its minimum induced drag ratio when $s/s_e = 4/3$, equivalent to 1.333. This in result gives an induced drag ratio of 27/32 or 0.844 as noted in Equation 2.33. Consequently, this gives the optimum loading Equation 2.34.

$$D_i = \frac{L^2}{\pi \frac{\rho}{2} {V_\infty}^2 (2s_e)^2} \cdot \frac{\left(\frac{s}{s_e} \right)^2 + 8(1 - \frac{s}{s_e})^2}{\left(\frac{s}{s_e} \right)^4} \tag{2.32}$$

$$D_i \approx \frac{L^2}{\pi \frac{\rho}{2} {V_\infty}^2 (2s_e)^2} \cdot \frac{27}{32} \tag{2.33}$$

$$\Gamma = \sqrt{1 - y^2} + \frac{y^2}{2} \log \frac{1 - \sqrt{1 - y^2}}{1 + \sqrt{1 - y^2}} \tag{2.34}$$

Progressing further, Klein and Viswanathan published in the Journal of Aircraft an additional study [6] in 1975 where they also included the spanwise shear-force into their analysis. Solving for the induced drag, they found Equation 2.35 where the optimal s/s_e was found to be 1.160 with a

minimum induced drag ratio of 0.929 (Equation 2.36). As a result, the optimal spanload is given in Equation 2.37.

$$D_i = \frac{L^2}{\pi \frac{\rho}{2} {V_\infty}^2 (2s_e)^2} \cdot \frac{4}{\left(\frac{s}{s_e}\right)^6}\left(9\left(\frac{s}{s_e}\right)^4 - 40\left(\frac{s}{s_e}\right)^3 + \frac{145}{2}\left(\frac{s}{s_e}\right)^2 - 60\left(\frac{s}{s_e}\right) + \frac{75}{4}\right) \tag{2.35}$$

$$D_i \approx \frac{L^2}{\pi \frac{\rho}{2} {V_\infty}^2 (2s_e)^2} \cdot 0.929 \tag{2.36}$$

$$\Gamma = 3.3008((1-y^2)^3)^{1/2} - 2.3008 \times (1-y^2)^{\frac{1}{2}} - 1.1075 y^2 \log_e \frac{1-(1-y^2)^{1/2}}{1+(1-y^2)^{1/2}} \tag{2.37}$$

For the purpose of this study, as the Prandtl-D wing that will be analyzed was based on Prandtl's 1932 solution (see Section 2.3), Equations 2.31 through 2.37 are not used to evaluate the performance.

2.2. Far-Field Induced Drag

The analysis on induced drag in the previous section were using the near-field assessment of forces on the body. Another method to analyze drag is to use an idealized far-field approach. This is done by identifying the forces of the wake trailing the lifting body, relating the perturbation velocities to the aerodynamic parameters on a downstream Trefftz plane. It is also noted that the velocity perturbations far behind an aircraft are less than those directly behind the aircraft, thus this method does not fully capture the total induced drag but is relatively close. Mark Drela in "Flight Vehicle Aerodynamics" [7] identifies the total drag force on the plane with the following in Equation 2.38. In this idealization the vortex sheet thickness is assumed to be small with a net strength γ in the x-direction. This sheet generates crossflow perturbation velocity $\nabla\varphi$ which defines induced drag. This can be visualized in Figure 2.6.

$$D = \iint_{TP} [p_\infty - p - \rho u(u - V_\infty)]\, dy\, dz \tag{2.38}$$

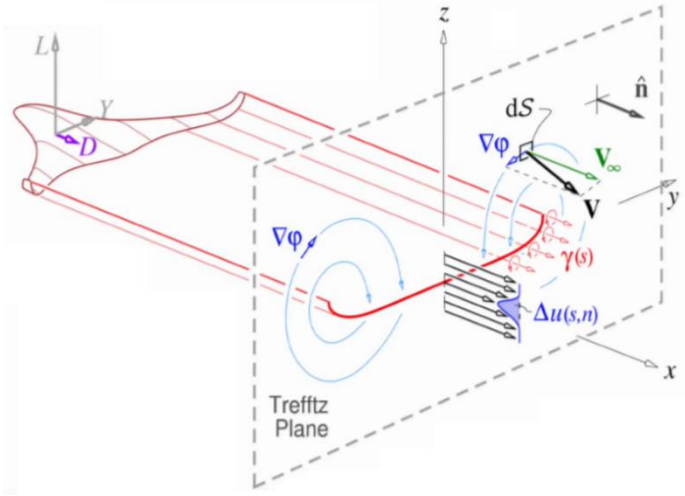

Figure 2.6: Flow on the Trefftz plane behind a lifting body [7]

By substituting the velocity and pressure, as defined by Equation 2.39 and Equation 2.40 respectively, into Equation 2.38 the induced drag and profile drag can be determined. The induced drag on the Trefftz plane can now be defined as Equation 2.41.

$$V = (V_\infty + \Delta u)\hat{x} + \nabla\varphi \tag{2.39}$$

$$p = p_\infty - p_\infty V_\infty \varphi_x - \frac{1}{2} p_\infty \left(\varphi_x{}^2 + \varphi_y{}^2 + \varphi_z{}^2\right) \tag{2.40}$$

$$D_i = \frac{1}{2}\rho \iint_{S_{TP}} \left(\varphi_y{}^2 + \varphi_z{}^2 - \varphi_x{}^2\right) dS \tag{2.41}$$

The final step is to note that the far downstream $x-$ velocity perturbation (φ_x) must die out as the trailing vortices cannot induce an $x-$ component of velocity far downstream. This in result simplifies the solution to Equation 2.42 which concludes that the induced drag is the crossflow kinetic energy (per unit distance) transferred by the lifting body. Using this approach, a Trefftz plane can be positioned behind two wings in formation flight to calculate the overall system induced drag.

$$D_i = \frac{1}{2}\rho \iint_{S_T} \left(\varphi_y{}^2 + \varphi_z{}^2\right) dS \tag{2.42}$$

2.3. Prandtl-D Research

Figure 2.7: NASA Armstrong's Prandtl-D P2 in an early flight in 2015 [8]

In 2016 Albion Bowers and Oscar Murillo published the paper "On Wings of the Minimum Induced Drag: Spanload Implications for Aircraft and Birds" detailing the work they had been conducting for more than a decade [2]. To validate Prandtl's theory the research team conducted an experiment using flying wings that incorporate twist to achieve the bell-shaped spanload defined in Equation 2.26. This research performed at NASA Armstrong Flight Research Center (AFRC) was designated as the PRANDTL-D program, which is an acronym for Preliminary Research Aerodynamic Design To Lower Drag. The first two aircraft studied had a span of 3.749 m (12.3 ft) which are considered to be 25 percent subscale models as a correlation to a full scale Horten H Xc aircraft. These first flying wings were identified as P1 and P2 (Figure 2.7) and have a design lift coefficient of 0.6. A third aircraft, designated as P3-C, was also developed and flown. As the geometry for the Prandtl-D wing is published (see Section 3.1), it becomes the primary candidate for an investigation into formation flight of a BSLD wing. This unmanned glider, which is the basis of the CFD study in this report, is a 50 percent scale with a wingspan of 7.50 m (24.6 ft). The

overall objective of the Prandtl-D experiments was to demonstrate that a wing with the bell-shaped spanload and no vertical surfaces flies with proverse yaw. The results of the flight research were successful in exhibiting proverse yaw and a sample output from a flight is shown in Figure 2.8.

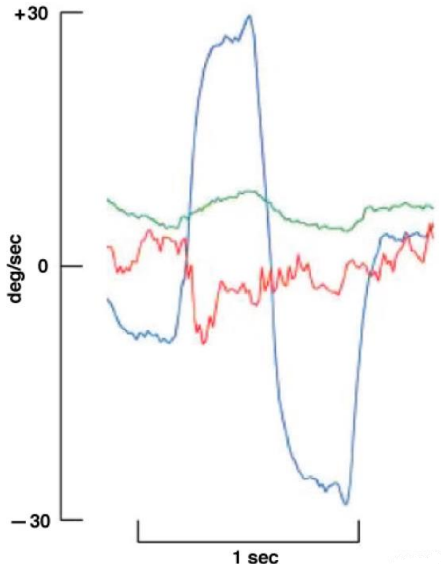

Figure 2.8: Angular momentum data from an onboard Inertial Measurement Unit on the Prandtl-D wing. The red is pitch rate, blue is roll rate, and green is yaw rate. [2]

For a wing with an elliptical spanload, as the lift increases near one wingtip so does induced drag. Thus, when an aircraft deflects the control surfaces to create more lift near a wingtip to bank, more drag is created on the wing which causes the aircraft to yaw in the opposite direction of roll and requires a vertical stabilizer to correct the aircraft desired flight path. As seen in the figure above, this is not the case for an aircraft with a bell-shape spanload. When the aircraft rolls by use of elevons, which have an equal and opposite throw on port and starboard, the aircraft increases lift near one wingtip resulting in an increase of induced thrust at the raised wing which causes yaw in the direction of the roll. Note, there is still induced thrust at both wingtips, but the side of the wing that now sees an increase in lift will have an induced thrust that has more strength than the other side, resulting in the controlled yaw. This can be seen in the positive angle for roll and yaw of the aircraft in Figure 2.8. This is proverse yaw, which could allow an aircraft to achieve coordinated flight without the need of a vertical tail or rudder.

As discussed briefly in 2.1.1, an important characteristic of the BSLD wing is that the trailing vortex is wider and considerably less intense than that of an elliptical lift distribution wing because the shear velocities of the adjacent downwash and upwash are much less pronounced (see Figure 2.4). Instead of two adjacent streams heading in opposite directions (upwash vs, downwash) causing a tight shear at the tip per the ELD, the BSLD wing has a gradual and continuous transition from downwash to upwash which results in a less intense and wider vortex core. The importance of this wider vortex is that there is a wider lateral range of vortex upwash providing benefits to a trailing wing. See Conclusion, Section 6.2 for more discussion.

The location of this vortex-creating shear is also at a different point along the wing than the current standard. The elliptical design has a vortex initiated at the wingtip, whereas the bell-shape design is inboard, at s = 0.704 for the wing as described by Prandtl. Experimental flight performed at NASA AFRC was able to confirm the vortex core locations inboard of the wingtips of the Prandtl-D P2. Figure 2.9, presented by Bowers and Murillo [2], shows the downwash field and the vortex roll-up behind the Prandtl-D wing found analytically. Their analysis confirmed the location of the vortex cores for the glider at 70.4% of the semispan. Orange dots have been added to identify these spanwise locations. Also pictured is an experiment conducted where VHS tape was strung behind the wing positioned at the theoretical vortex cores as well as a two more about a foot outward towards the wingtip. As seen (and more visibly evident on the left side of the wing) the streamers attached at 70.4% of the semispan are curling up identifying the vortices while those outward towards the wingtips stay relatively straight with the streamwise flow.

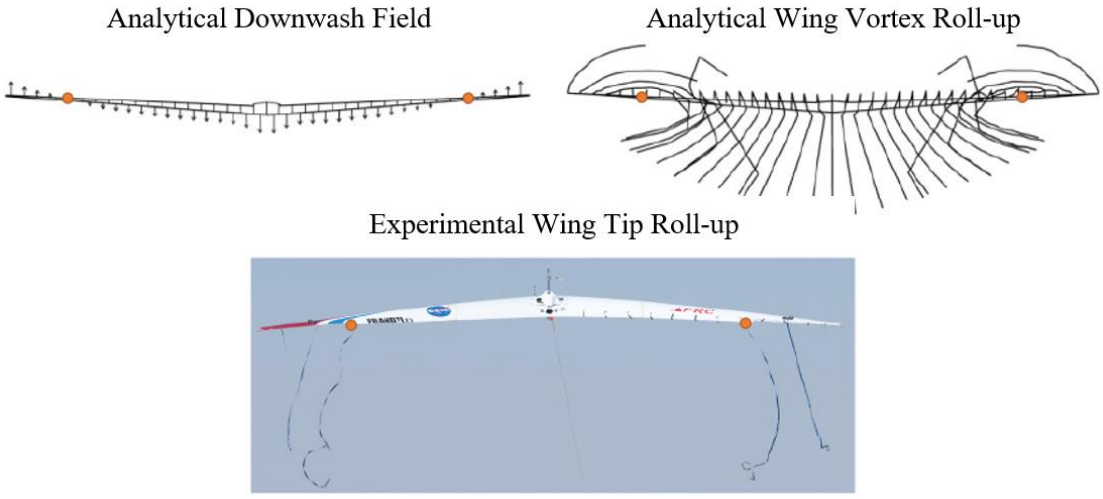

Figure 2.9: Analytical and experimental downwash and vortex roll-up on the P2 [2]

2.4. Birds and Avian Formation Flight

When analyzing a wing with a bell-shaped lift distribution, why consider birds in flight? In their paper, Bowers and Murillo report that there is an important implication of their study: the flight of birds is better explained by the BSLD model as opposed to the ELD model. Several points help explain this conclusion. First is that birds have no vertical tails, whereas wings following the ELD model require the horizontal control provided by a vertical control surface to counteract the inherent adverse yaw. As discussed earlier, demonstrating the proverse yaw of the BSLD wing is a specific part of their study. A second characteristic is apparent when looking at the wings of birds that fly in formation. Also note that their wings tend to taper to a sharp point at the wingtip (refer to the albatross in Figure 2.10 for example). This sharp wingtip is rarely seen on aircraft wings. The reason for this difference is a result of the higher load carried nearly to the wingtip of an elliptically loaded aircraft wing versus the tapering load of a bell-shaped spanload (see Figure 2.2). Again, consider the wing of a bird, the structure of the wingtip feathers would not be able to carry the load if the wing followed the ELD design. The load capacity of the primary feathers at the wingtip of a bird is small, but so is the effective surface area.

This report takes this hypothesis that bird flight is better described by the BSLD method and looks to existing research papers for confirmation. One aspect of bird flight that is pertinent to this paper is when birds fly in formation. For decades, avian researchers have studied the wake of birds in flight and have gathered data to confirm that birds benefit by flying in formation. Formation flight allows trailing birds to capture upwash in the air from the wing vortex roll-up of leading birds. There is no dispute that birds maximize the lift from the vortex upwash. What is disputed is where along the wing that vortex occurs, and what is the most beneficial position for a trailing bird.

When viewing birds in formation flight, it is readily noted that they fly with their wings significantly overlapped (see Figure 2.11). The hypothesis that bird wings follow the BSLD model would explain why this overlap is optimal. Since the vortex roll up on the leading bird is not close to the wingtip (as per the elliptical model) but closer to the inboard vortex position of the BSLD model (at 0.704), the following bird needs to adjust inward and overlap wings with the leading bird to better benefit from the vortex upwash. Another visual is provided in Figure 2.12 which shows a formation of brown pelicans flying with wingtips considerably overlapped, which is an optimal arrangement with the bell-shaped load (but suboptimal for the elliptical load) because in this model the vortex roll-up is not at the wingtip but well inboard of the wingtip.

Figure 2.10: A laysan albatross (phoebastria immutabilis) flying at Kaena Point, O'ahu, Hawaii [9]

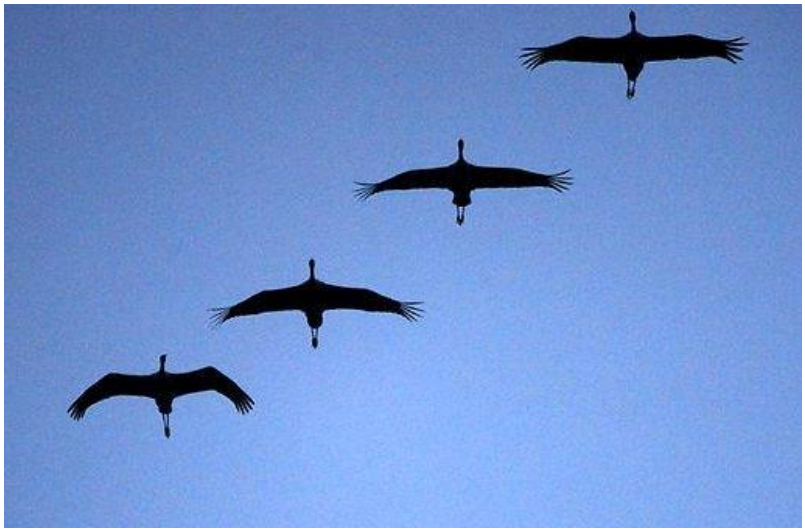

Figure 2.11: Common cranes (grus grus) flying in formation over lake Fehér near Sándorfalva, Hungary [10]

Birds position themselves in overlapped formation flight based on the location of the actual vortex roll-up, and the bell-shaped spanload generates a vortex roll-up in that location. Observational data of birds in formation flight confirms this. As exhibited in the selected references below, for over 50 years researchers have assumed the ELD model for bird wings. However, they

have all had to explain the differences between their observational data and their expected findings by adjusting and conforming their findings to fit the standard elliptical model of rigid aircraft wings.

Figure 2.12: Formation flight of brown pelicans (pelecanus occidentalis) photographed by Michael Cox [2]

Lissaman and Schollenberger [11] (revised 1970) performed bird formation flight analyses based on generic ELD aircraft airfoils. They stated that "analyzing the bird as a fixed-wing aircraft gives a good estimate of its cruise power requirements. So, we considered a fixed-wing vehicle of the same geometry as the bird." Their understanding was that "classical aerodynamics states that, for a single monoplane, minimum induced power occurs when the wing generates a uniform downwash behind it", therefore they "considered only elliptically loaded fixed-wing monoplanes, for which the mathematics are quite simple."

This analysis, based on elliptically loaded monoplane wings and in gliding posture (external propulsion rather than flapping) may have some application to aircraft formation flight, but shows no stated connection to bird formation. However, an unintended consequence that resulted is that this early study from 50 years ago is the most cited article in the bird formation literature and has influenced the assumptions and conclusions of the majority of academic studies since it was published.

To better understand the research that has been conducted, five papers have been selected that seem unique in the history of bird formation flight research or that show considerable effort in data

collection and quantification. In 1986 Spedding [12] conducted novel studies with a trained kestrel, taking visual data to analyze the vortices created by its gliding flight. This report required an adjustment to explain the location of the trailing vortex. In a 1987 paper, Hainsworth [13] filmed and analyzed Canada geese in formation. He developed useful data showing a wide range of positions but based his quantitative analysis on the models of Lissaman and Schollenberger [11], which impaired his conclusions. In another 1987 paper, Hainsworth [14] filmed brown pelicans in formation flight and analyzed the frames. He also analyzed data on white pelicans that had been reported by others. Yet he could not explain why his data shows a wide variation in formation location of trailing pelicans. Speakman with Banks [15] in 1998 published an article detailing the spacing of greylag geese in formation, with considerable data collected by taking and analyzing photographs. Although their assumptions of vortices based on elliptical loading made many of their results inconclusive, the spacing data presented in the study strongly validates a BSLD wing. In 2014 Portugal [16] reported on a wonderfully crafted study on the formation flight of northern bald ibises. He collected a great amount of data and analyzed it, trying quite unconvincingly to fit the results into a conclusion matching the ELD model. The observational data collected and reported on in these five papers required considerable analysis by the study teams. The following subsections summarize the findings and conclusions of these research reports and highlight those parameters which are pertinent to the current study.

2.4.1. Beneficial Positioning vs Position Frequency

In general, the authors started with the expectation that birds are adept at positioning themselves where they can maximize the benefits of vortex upwash. The accepted general aerodynamic theory of elliptical loaded wings (ELD) predicts a tight range of strong vortex upwash that would be greatly beneficial, and so they predicted that birds would frequent this tight range. What they found, however, was that the birds occupied a significantly wide range of wingtip spacing (WTS) positioning. The observational data collected by the various studies include position

frequency data. Assuming that the authors were right in thinking that birds will find beneficial positions, then it would follow that a graph of frequency vs WTS may reflect the level and range of benefits. Correlations to the position frequencies used in this report assumes this connection between frequency and benefits in the analyses that follow. Note that in these discussions, the symbol Y is used for the lateral wingtip spacing (WTS) of the trailing wing relative to the leading wing. Values for Y/b assume 0.0 at wingtip alignment, with -1.00 being centerline alignment, and >0.0 being lateral space between the wingtips. Y is considered a negative value when there is wing overlap.

2.4.2. Induced Drag Reduction

Some of the papers calculated induced drag. Most of these were based solely on elliptical loaded wings and so the results are of no practical use in this report. The paper by Spedding, however, did include a Trefftz Plane analysis of the wake of a single kestrel hawk and found it correlates to the energy expenditure predicted. The margin of error in the data/prediction, though, would include both ELD and BSLD models and so is inconclusive for our purposes.

2.4.3. Optimal Bird Position

The observational data is used to determine an optimal position for the birds. This is taken as the modal point of the frequency chart. That is the point that is frequented more often than any other point. The authors used mean and median points in their analyses, which have some validity but are also skewed by the outliers (data points that don't fit the "curve") and are also thrown off by a naturally skewed graph that falls off at Y/b = -1.00. The papers reported the following data. Hainsworth's report on Canada geese [13] had a wingspan b = 150 cm, and a median WTS of -28.2 cm (eliminating outlying data for distant trailing birds more than 500 cm behind). This provided an optimal median position of Y/b = -0.188. Hainsworth's report of the brown and white pelicans [14] was inconclusive because there was a scattered range of positioning with no clustering at a particular location. Speakman and Banks [15] (greylag geese) reported b =143.9 cm and median

WTS = -17.5 cm on a skewed frequency distribution. This corresponds to a median at Y/b = -0.122. Portugal [16], recording northern bald ibises in formation, had a wide scattering of position data. He reported the highest frequency (modal) region was noted at a centerline separation of 0.904m, which is Y/b = -0.246. The variation between all the results (see Table 2.3) from these studies could be due to a combination of median vs modal, skewed graphs, and different bird species physiology. Either way, they show a significant wingtip overlap selected by the trailing birds with the optimal position at an average at Y/b = -0.185.

2.4.4. Beneficial Range

A more revealing outcome of the observational data is the wide range of positions that the birds found to be beneficial. Hainsworth (Canada geese) [13] had 451 measurements for 55 birds in 8 separate formations. There is a wide variation, skewed (Figure 2.13) towards a negative WTS, however with a significant number with positive spacings. The median of all the data was -20 cm., but the median for each formation varied from -44 cm to +12 cm (Table 2.2). One way of determining beneficial range is to consider the modal as the optimal and determining the range as being where 50% of the maximum is achieved. This is the data from -70 cm to +20 cm (the center three bars in Figure 2.13) where the number in the bar is above 53.5. For a wingspan b = 150 cm, this correspond to a Y/b range of -0.47 to +0.13, or 0.60b (a width of 60% of the wingspan).

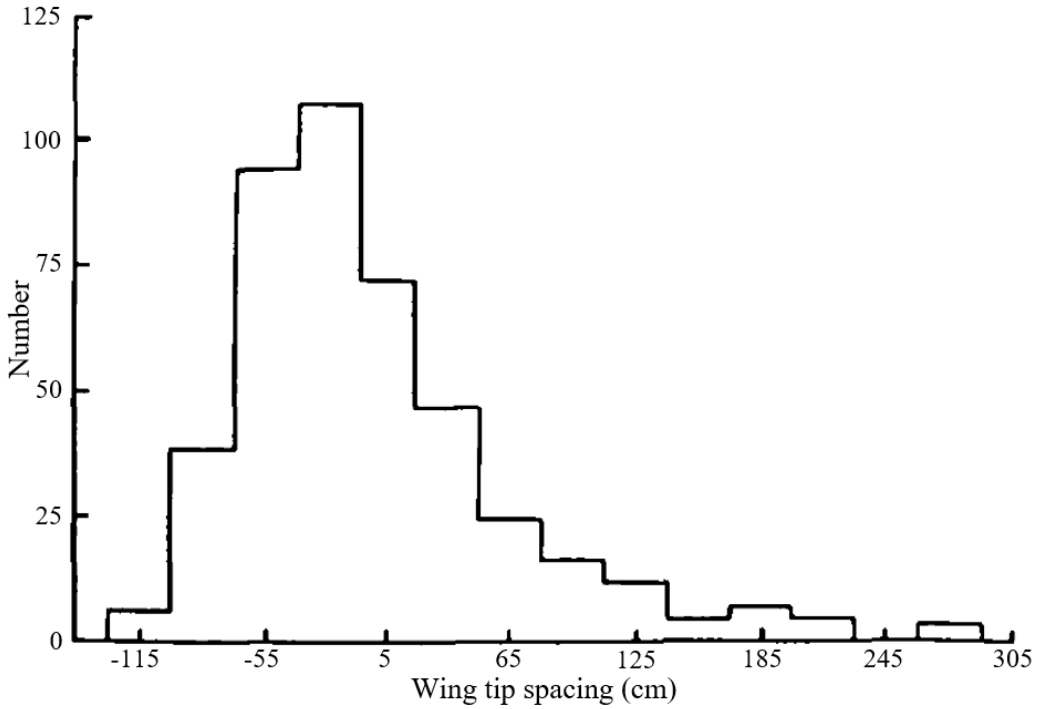

Figure 2.13: Frequency distribution of wingtip spacing for Canada geese (branta canadensis) [13]

The data this value is taken from is a composite of widely varying formation positions. This is seen both in the differences between the eight formations he filmed (Table 2.2), and in the number of birds that lagged considerably behind and wide from their leading bird.

Table 2.2: Median and Range for Wingtip Spacing (WTS, in cm) for Canada Geese in Eight Formations

Formation	N	Range	Median
1	81	-100 to 289	-18.9
2	109	-91 to 129	-16.6
3	30	-73 to 134	-0.5
4	36	-84 to 54	-37.5
5	60	-128 to 194	-44.4
6	62	-105 to 189	12.0
7	30	-106 to 84	-35.5
8	43	-98 to 109	-24.4
Total	451	-128 to 289	-19.8

Hainsworth also reported on brown and white pelicans [14]. For these he found a variation of points that did not allow him to conscientiously determine a mathematical conclusion concerning

WTS. He states that “The pelicans differed in their formation flight positioning. There was little to suggest that they were sensitive to the location of a particular position yielding high savings”. Considering the modal 50% approach, the beneficial range of 2m is found to be between -2.5m and -0.5m, where Y/b = -0.92 and -0.18. From this a range of 0.73b is calculated. Note that this is an imperfect value with an admittedly large margin of error due to the fact that each bar on the histogram represents 1m.

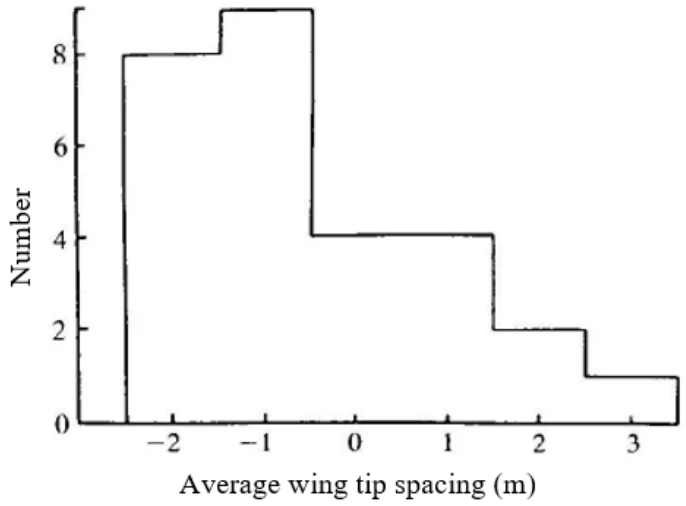

Figure 2.14: Frequency distribution of average wingtip spacing of white pelicans (pelecanus erythrorhynchos) in formation flight [14]

Speakman and Banks (greylag geese) [15] also provided a skewed frequency distribution (Figure 2.15), but he was able to calculate a mean WTS of -8.3 cm (est. S.D. 30cm) and median WTS of -17.5 cm (on a skewed distribution) with a 143.9 cm wingspan. If 50% of maximum benefit (modal frequency) is taken to be 32.5, then the range of 60 cm is determined (-40 cm to +20 cm). Therefore, from Y/b =-0.28 to Y/b = 0.14 with a range of 0.42b.

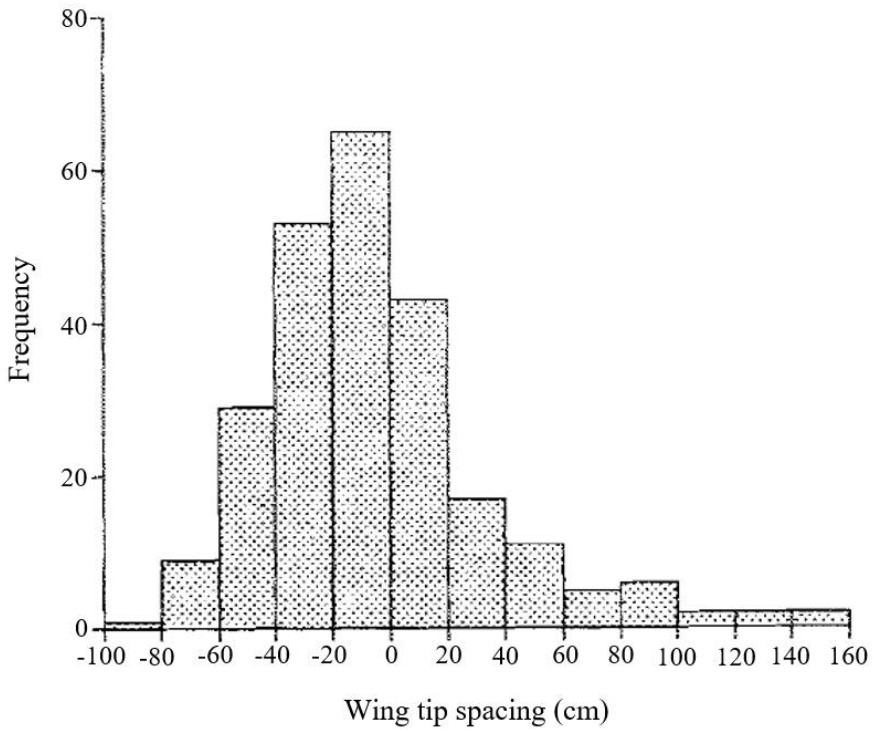

Figure 2.15: Frequency distribution of wingtip spacing for Greylag geese (anser anser) [15]

Portugal [16] studied northern bald ibis with a wingspan b = 1.2 m. An important aspect is that the position data falls within a very wide range of significant readings. The histogram provided (Figure 2.16) plots the centerline separation between the leading and trailing bird pairs vs the number of flaps the trailing bird takes at that position. The more flaps in a region indicates that the bird stayed in that position longer. Portugal shaded gray (in Figure 2.16) the optimal relative positioning which is based on fixed-wing aerodynamics using the $\pi/4$ contraction assumption. It was expected that the birds would not find themselves flying outside this range, which differs from the plotted data. This plot helps to identify a modal point centered around 0.904 m between bird centerlines, but it does not give a clear indication of an effective range of positioning. If the 50% of benefit (frequency) is determined, the highest position is at 22,000 flaps and 50% would be 11,000 flaps. However, the entire graph is above 11,000 flaps, which could be interpreted as beneficial all across. Instead, one can consider 50% of the data being above 18,000 flaps (halfway

between 14,000 and 22,000). With this the modal beneficial range is determined to be between Y/b = -0.66 to 0.53 for a 1.19b.

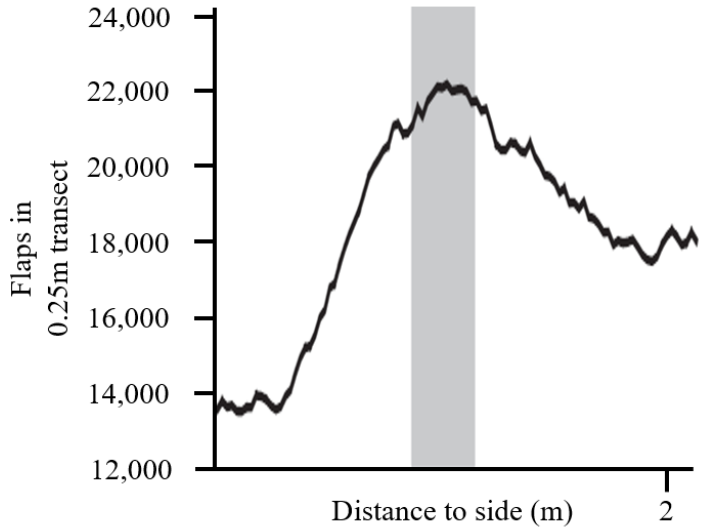

Figure 2.16: Histogram detailing the total number of flaps recorded between each bird–bird pair, with respect to position of the following bird [16]

Together, the data from these papers present a great variation in results of beneficial positioning (see Table 2.3 for tabulation). The important aspect of this, however, is that the birds were able to find beneficial upwash over a wide (rather than narrow) range of positions. Analyses performed for wings with an ELD (see Section 2.5) indicates that the beneficial range is relatively small, whereas the wider bird position range is consistent with the wider beneficial range provided by a BSLD wing (Section 5.4).

2.4.5. Vortices

The primary vortex position study in these papers was by Spedding (kestrel hawk) [12]. He flew a trained hawk over a stream of hydrogen bubbles and photographed the turbulence of the bubbles in the wake. The two-dimensional motion (direction and velocity) of these were determined and plotted for use in a Trefftz Plane analysis. It showed the centerline of the two wing vortices as being 0.513m apart. With a wingspan b = 0.676 m, the vortex position is at 0.76 of the semispan. The author had seven readings of vortex centers and they appeared to be well in line (Figure 2.17),

but he preferred to illustrate it as a wingtip vortex that immediately contracted inboard. To explain the discrepancy of having inboard vortices, the author claimed that wingtip vortices contract by a factor of π/4 (0.79). This vortex contraction, or "horseshoe vortex" is described in traditional textbooks (such as Milne-Thompson [17], Subsection 2.5.4). In fact, all five papers assumed ELD wingtip vortices with an immediate vortex contraction and used it to explain why their observations show significant inboard WTS positioning.

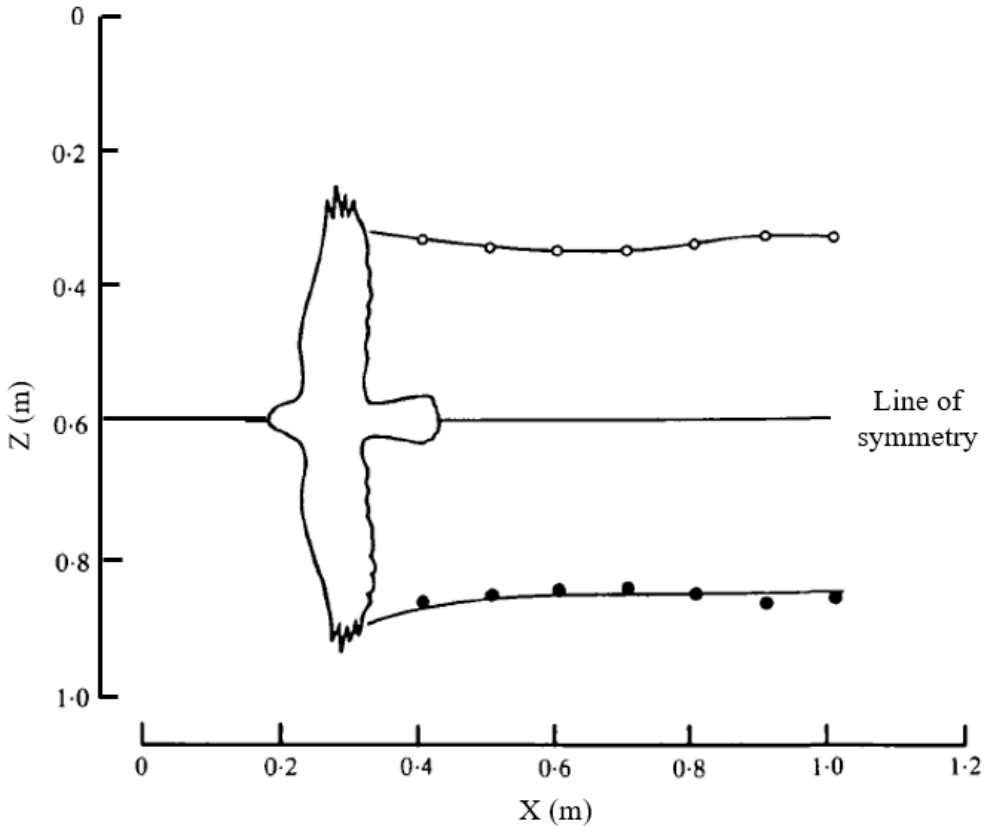

Figure 2.17: Spedding's kestrel (falco tinnunculus) trailing vortex location data [12]

In 1966 professor L.M. Milne-Thompson published his "Theoretical Aerodynamics" textbook [17]. It quickly became an academic standard. Several articles and papers, including the ones cited above, utilized calculation methods from his book. They also used his discussion of vortex contraction to explain why birds flying in formation tend to position themselves with well overlapped wings. However, this instable tendency of the vortex in the far field has been incorrectly

applied to the near field. The discrepancy can be seen in the title of the book section: “11.7 The Wake Far Down Wind.” Milne-Thompson notes that this contraction takes time and that “at a sufficient distance behind the aerofoil a section of the wake…would show two cylindrical vortices whose distance is less than the span.” The point is that the claims by the various authors that they can explain the discrepancy of their trailing bird position by using vortex contraction described by Milne-Thompson is misapplied and simply incorrect. As this contraction takes time, it is impossible for a bird one to two spans behind the leading bird to see this change.

2.4.6. Reported Findings

The papers each included several findings, depending on their emphasis. Those pertinent to this study are mentioned here. These address the discrepancies between expected and observed positioning of the birds in formation. In general, the authors assumed that birds are adept at finding beneficial upwash from the leading birds and expected a tight grouping of data around the vortex with little variation since the ELD model predicts a sharp drop in benefit if the bird strays a small distance laterally. However, what they found was that they centered well inboard away from the wingtip, and that their positioning was wide ranging rather than tightly grouped. These findings needed explanation.

Hainsworth [13] claimed (1) that the abilities of the geese were imperfect, (2) that “it is clear that other constraints influence performance so only some individuals behave 'optimally' and only some of the time”, and (3) that “local differences in turbulence may have contributed to variation between formations”. In his second paper [14] Hainsworth claimed that (1) imprecision in WTS may be due to …difficulty in maintaining position under windy conditions”, and (2) “there was little to suggest that they were sensitive to the location of a particular position yielding high savings”.

Speakman and Banks [15] speculated “First, the model was derived for fixed wings and did not account for flapping. Second, the vortex locations were predicted for still air and did not account

for wind strength and direction. Alternatively, the birds may have been attempting to track the trailing vortices to save energy but were imperfect at doing so".

Portugal [16] admitted that "the precise aerodynamic interactions that birds use to exploit upwash capture have not been identified". He felt "that flock structure is highly dynamic" and that this indicates remarkable awareness of, and ability to respond to, the wing path—and thereby the spatial wake structure—of nearby flock-mates". He also noted that trailing "birds may be able to benefit from 'drafting' while, to a certain extent, avoiding an increased cost of weight support by evading localized regions of downwash". In other words, although the birds are very adept at beneficial positioning, the dynamics of the flock present a higher priority.

2.4.7. Summary – Bird Formation Flight

Despite the ELD-based predictions made by the authors of bird formation literature, the observational data they provided show consistent discrepancies. As tabulated in Table 2.3, the optimal bird positioning is well inboard from the wingtip, at an average Y/b = -0.185. Also noted in the table is that the range of beneficial positioning is wide (and not consistent) with an average modal of 0.735b. Hainsworth [13][14] and Speakman & Banks [15] said the birds were insensitive and imperfect at positioning, whereas Portugal [16] said they were adept. Most claimed turbulence as a primary factor. All incorrectly claimed vortex contraction to explain the optimal position. However, these data discrepancies could be explained by assuming the BSLD methodology when analyzing bird flight. The CFD simulation results presented in Chapter 5 describe an inboard vortex with weaker, but wider vortices that act on a larger area of the wing and allow beneficial flight over a much wider range of positions.

An elaborate physical study would need to be conducted to confirm these characteristics on an individual bird wing. The physiology of a bird's ability to change the shape of a wing in flight would be difficult to model, as well as the dynamics of flapping. Add to this the vast differences of wing dimensions and proportions between species. To conduct such a study in an academically

definitive manner may be far beyond the capacity of any paper. However, for the purpose of this study, the intent is primarily to demonstrate that the characteristics of bird wings and bird flight are better described by the BSLD model, and that numerous past studies have been performed that have observational data that validates this premise.

Table 2.3: Optimal Position and Beneficial Range from Avian Observation

	Optimal Position, Y/b	Beneficial Range (Modal 50%)	
		Y/b	b
Canadian Geese - Hainsworth [13]	-0.188	-0.47 to +0.13	0.60
White Pelican - Hainsworth [14]	NA	-0.91 to -0.18	0.73
Greylag Geese - Speakman & Banks [15]	-0.122	-0.28 to 0.14	0.42
Ibises – Portugal [16]	-0.246	-0.66 to 0.53	1.19
Average	-0.185	NA	0.735

2.5. Formation Flight of Aircraft

There have been numerous published studies of the drag reduction benefit of aircraft flying in formation. A review of published articles pertaining to formation flight and vortex production was conducted to gain knowledge about specific aerodynamic conditions of rigid elliptically loaded wings that would be relevant to this study. These center around formation efficiency, the range of the beneficial flight positioning, and fixed wing vortex properties.

The seven studies selected cover a wide range of data collection methods, ranging from theoretical calculations using traditional formulas, to CFD modeling, to wind tunnel testing, and aircraft flights. They were chosen for their pertinent data and results. Andrew Ning at Stanford [18] (2011) performed formulaic simulations comparing several vortex propagation and decay methods. His analysis was on the benefits of extended flight formations of 10-40 wingspans. H.S. Shin at Cranfield University in the UK [19] (2018) ran CFD simulations on multiple unmanned aerial vehicles (UAV) in various formations (echelon, v-type, and diamond) with 2 to 10 aircraft. The two UAV echelon case is reported below. William Blake in the Air Force Research Lab [20] (2001)

conducted wind tunnel tests on 1/13 scale model delta wing models. He used strain gauge balances to collect data and varied the x, y, and z coordinates. M. Jake Vachon and Jennifer Hansen at NASA [21] [22] (2002) summarized the results of NASA tests on two fully-instrumented F/A-18 aircraft. They utilized autonomous formation flight (AFF) autopilot to maintain selected positions to determine the beneficial position for the trailing wing. James Frazier from North Carolina State University [23] (2003) studied multiple wings in formation using Trefftz plane analysis and a formulaic (calculus-of-variations) simulation approach. J.E. Kless from NASA [24] (2013) performed CFD modeling with an added vortex propagation package (Betz method) to consider extended flight formation (30 wingspans). He analyzed NACA 0012 wings at subsonic and transonic speeds. Rather than submit a summary review of each of these articles, the pertinent results are taken and compared below. Note that not every paper presented results for all of these parameters.

2.5.1. Induced Drag Reduction

The efficiency of formation was usually presented as the reduction of the induced drag for the system (both leading and trailing wing) in an echelon formation. Some provided lift or energy savings to indicate efficiencies, but four provided values for D_i of the system. The reported values varied yet were rather close together with Ning at 30% [18] for extended formation vortex calculations, Shin at 26% [19] for CFD modeling, Blake at 25% [20] for wind tunnel tests, and Vachon at 20% [21] for the transonic F/A-18 aircraft. As a result, from these studies one can consider the system induced drag reduction of on average 25% for a two aircraft formation. This is important to take note of while analyzing the reduction of the system induced drag for the current analysis, so as to find a comparison between the two lift distributions.

2.5.2. Optimal Wing Position

These induced drag reductions maximized around a tight position when considering lateral wingtip spacing (WTS), Y. Although different streamwise (x coordinate) distances were assumed

for the wings, the optimal tip to tip spacing was closer. Values for Y/b_e given assume 0.0 being wingtip alignment, -1.00 being centerline alignment, and >0.0 being lateral space between wingtips. The optimal Y/b_e for Ning is -0.15 [18] for extended formation vortex calculations, Blake is -0.15 [20] for wind tunnel tests, Vachon and Hansen is -0.13 [21][22] for transonic F/A-18 aircraft, Frazier is -0.11 [23] for formulaic calculations, and Kless is -0.10 [24] for extended formation CFD modeling. Note the tight grouping even though different methods were used to determine them. Summarized, this results in an optimal positioning of Y/b_e = -0.10 to -0.15 with an average at -0.13. This additional 13% overlap for the optimal total drag reduction of the trailing wing is noteworthy because it is inboard from the generation point of the vortex core of the leading wing. It is close to that of the position concluded from the bird studies at 16% overlap and the results of this study will better inform the reasoning behind this.

2.5.3. Beneficial Range

Because elliptical loaded fixed wings produce strong wingtip vortices, then the trailing wing needs to contact primarily the upwash of a vortex to gain higher efficiency benefits. This specific positioning means that the range of lateral spacing is fairly tight. Hansen [22] said that incremental forces are very sensitive to position, and Kless [24] noted that 90% of energy benefits can be lost with a 10% variation in spanwise position. Even Hainsworth [13] who reported on bird formation but used elliptical lift distribution calculations said that a "slight variation in WTS in either direction drastically lowers benefits". The authors providing a Y/b_e range for maximum benefits were Frazier with -0.10 to +0.05 [23] for formulaic calculations, Ning with -0.25 to 0.00 [18] for extended formation vortex calculations, Blake with -0.30 to 0.00 [20] for wind tunnel tests, and Vachon with -0.25 to -0.05 [21] for transonic F/A-18 aircraft. This can be summarized as a beneficial range of Y/b_e = -0.25 to 0.00 range at $0.25b_e$. Note that this is one-third the range found in the bird studies where an average range of 0.735b was found. This suggests that birds tend to shift more, which as mentioned before is a direct correlation to the strength of the vortex of a BSLD wing.

2.5.4. Vortices

The vortex properties were also reported by several authors. The question of vortex contraction is one of interest, since contraction would affect the lateral position that is most beneficial for energy reduction. Historically, there is a "horseshoe vortex" theory that says the wingtip vortices tend to eventually move inward towards each other (contract) to $\pi/4$ of the span apart, a vortex core separation of $0.79b_e$. This was best presented in a textbook by Milne-Thompson in 1966 [17] (see the previous discussion on this topic in Section 2.4). One author, Hansen [22], studying F/A-18 aircraft in formation, does not note any contraction. Kless [24] and Ning [18], both conducting vortex-specific modeling, say there is no vortex contraction. And Frazier [23] said his vortex was at 0.78. However, he assumed an immediate onset of the horseshoe vortex as a basis of his calculation method, so his conclusion was directly dependent on his assumptions. Overall, there is no observed or modeled data in these reports showing a vortex contraction. This should be taken as a direct contradiction to the avian studies' assumption that vortex contraction is the explanation for the observed bird wing overlap.

2.5.5. Summary – Aircraft Formation Flight

The conclusion of the review of literature on the formation flight of aircraft is (1) that the beneficial lateral position (WTS) range for trailing aircraft is much tighter than that reported for birds (about $0.25b_e$ for aircraft vs. 0.74b for birds), (2) that the optimal wingtip position for drag reduction on an aircraft is close to, yet inboard of, the wingtip ($Y/b_e = -0.128$), (3) that for the optimal position there is a an average system induced drag reduction of 25%, and (4) that credit for a vortex contraction should not be applied for near-field formation flying as it is not bourne out by observation or by up-to-date vortex modeling. Table 2.4 summarizes the results from the previous subsections.

Table 2.4: Optimal Wing Position, Beneficial Range, and Induced Drag from Aircraft Research

Report Author	Optimal Position, Y/b_e	Beneficial Range		System induced drag reduction, %
		Y/b_e	b_e	
Ning [18]	-0.15	-0.25 to 0.00	0.25	-30.0
Shin [19]	Not listed	Not listed	Not listed	-26.0
Blake [20]	-0.15	-0.30 to 0.00	0.30	-25.0
Vachon [21]	-0.13	-0.25 to -0.05	0.30	-20.0
Frazier [23]	-0.11	-0.10 to +0.05	0.15	Not listed
Kless [24]	-0.10	Not Listed	Not Listed	Not listed
Average	-0.128	-0.25 to 0.00	0.25	-25.25

Chapter 3

THREE-DIMENSIONAL MODELING

This chapter describes the creation of the wing's CAD model, which consisted of two steps. The first was the manipulation of points using MATLAB to generate an array of points outlining the wing in three-dimensional space. The second step implemented the use of the CAD software SolidWorks to import the array of points to create 3D model surfaces. These surfaces were then divided to make mesh management more variable in areas of interest, particularly where the vortex core is shed. This chapter begins with an introduction of the Prandtl-D wing geometry and concludes with a correlation between the final geometry of the CAD model and the actual glider (as published).

The intention of including this description in the report is to allow any future duplication of the research for whatever reason, whether it is for validation of other CFD models on the Prandtl-D wing, or for progressing this research, or just for providing an approach to CFD modeling.

3.1. Prandtl-D Geometry

The geometry of the Prandtl-D aircraft is provided in Bowers' and Murillo's publication [2]. The aircraft's airfoils transition linearly from the centerline to the wingtip. Figure 3.1 plots the two airfoil profiles against one another from the non-dimensional coordinate points provided in the NASA report, which are tabulated in Appendix A for reference. These profiles are before any twist or chord scaling are applied.

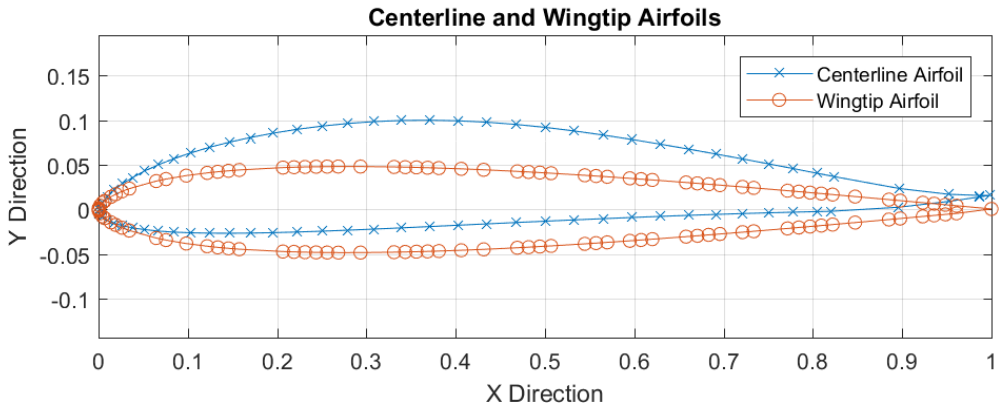

Figure 3.1: Plot of the nondimensional centerline and wingtip airfoil profiles

The Prandtl-D P2 has a centerline chord length of 0.400 m (15.75 in) and a wingtip chord length of 0.100 m (3.94 in). As mentioned in Section 2.3, for the purpose of this study an analysis was done of the P3-C aircraft, which is twice the size of P2. Therefore, a centerline chord of 0.800 m (31.5 in) and wingtip chord of 0.200 m (7.88 in) were specified. The wing also has a nonlinear twist that is specified at 20 intervals between the centerline and the wingtip. The twist distribution along the semispan is plotted in degrees in Figure 3.2 and tabulated in Appendix A. As the aircraft was designed with control surfaces in the trailing 25 percent of the chord, the axis the twist has been applied to is at the three-quarter chord point of each airfoil section. Lastly, there is a leading edge sweep of 24 degrees, as well as a dihedral of 2.5 degrees enacted along the 75 percent chord axis (the axis of twist). Unlike the Prandtl-D wing, the one modeled in this study does not include the rounded wingtip to reduce mesh inconsistencies that arose in preliminary CFD studies. This does not change the results in the study. The wingspan of the P2 aircraft was 3.75 m (12.3 ft). As the wing studied is twice in size following suit with P-3C, a wingspan of 7.50 m (24.6 ft) is used.

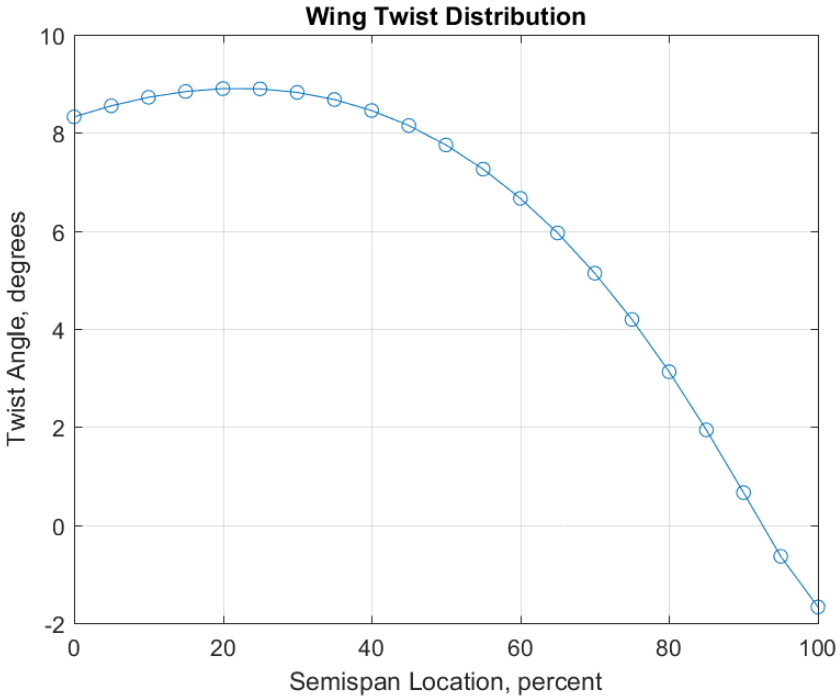

Figure 3.2: Wing twist angle as a function of the semispan

3.2. Three-Dimensional Point Manipulation

The software MATLAB R2017a was used to manipulate the data provided in the section above to create an array of points to import into CAD. There were three main steps to creating the airfoil points, namely interpolation between the centerline and wingtip, applying twist, and applying translations that included sweep and dihedral.

Before these steps were performed it was found that the data presented by Bowers and Murillo [2], Appendix A, introduced a complication as the centerline airfoil consists of 79 points while the wingtip is comprised of 119 points. Due to the limitations of the software, which uses matrix multiplication, it is difficult to manipulate two arrays of different sizes. Thus, 40 points in the wingtip were chosen to be removed for interpolation. A plot of the removed and retained points as well as a table of the final wingtip coordinates can be found in Appendix A.

The MATLAB code to fill out the wing point coordinates can be found in Appendix B. While initially the points were created for the right side of the wing they were then mirrored about the x-

z plane to create the left side of the wing. Each airfoil section was then split into a top and bottom to create two surfaces for the practicality of a CFD pressure analysis (Sections 4.5 and 5.5). Matrices were also made for the leading edge, trailing edge, and 75 percent chord axis. Each set of points was then tabulated as .txt files to be uploaded for CAD. The airfoil section point coordinates that were outputted from MATLAB are presented in Appendix C.

3.3. CAD Creation

The next step after all the airfoils sections points were found was to create the CAD model using SolidWorks. First, the points for the top and bottom surfaces as well as the leading and trailing edge were imported into CAD and the curves produced are showed in Figure 3.3.

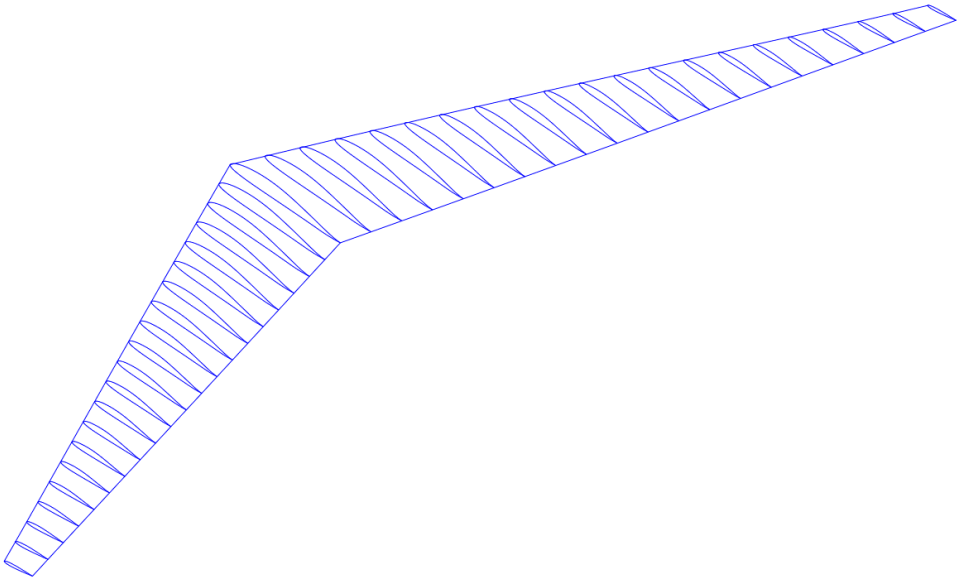

Figure 3.3: Imported curves consisting of airfoil profiles, leading edge, and trailing edge

With the wing outlined, curved surfaces were then extrapolated. A total of six surfaces were formed; a top and a bottom surface of the left half of the wing, a top and bottom surface of the right half of the wing, and a left and right wingtip cap. The surfaces were then combined, merging the entities to make a solid. The result is shown in Figure 3.4.

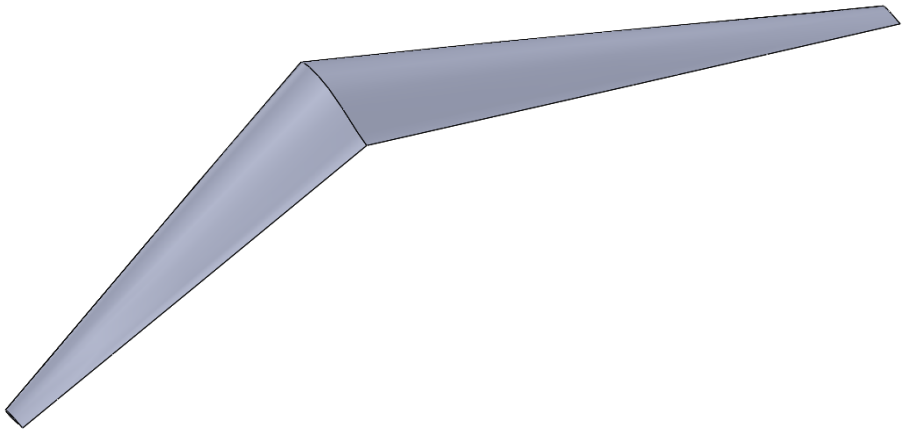

Figure 3.4: Knitted wing surfaces

The final step in creating the CAD model was to prepare the surfaces for CFD mesh allocation. From preliminary studies it was determined that more mesh was desirable in the wake around the vortex core at the 70.4% semispan points. As a result, three regions were created for a fine, medium, and course wake refinement seen in Figure 3.5 as red, orange, and yellow respectively.

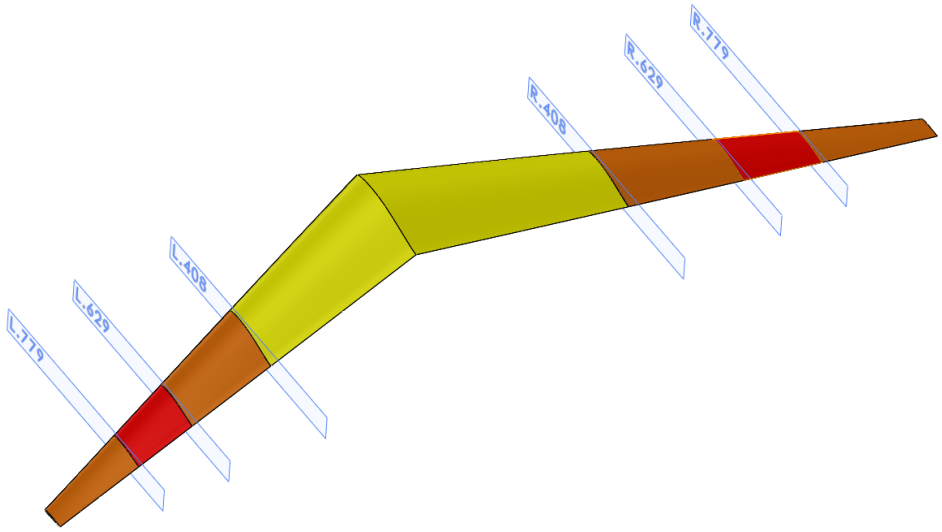

Figure 3.5: Divided surfaces and section planes

The first two planes are ±7.5% from the theoretical vortex core location, thus positioned at 62.9% and 77.9% of the semispan. The next plane was placed the same distance away from the vortex as the wingtip, therefore positioned at 40.8% of the semispan. This was done on both the

left and right side of the wing. These split line locations that divided the wing surfaces are tabulated in Table 3.1.

Table 3.1: Surface Split Line Locations from Centerline

Meters	Percent
-2.921	-77.9
-2.358	-62.9
-1.530	-40.8
1.530	40.8
2.358	62.9
2.920	77.9

3.4. Final Geometry

In this section additional dimensions of the finalized geometry of the wing are presented. Figure 3.6 shows the dimensioned final CAD model used for the report.

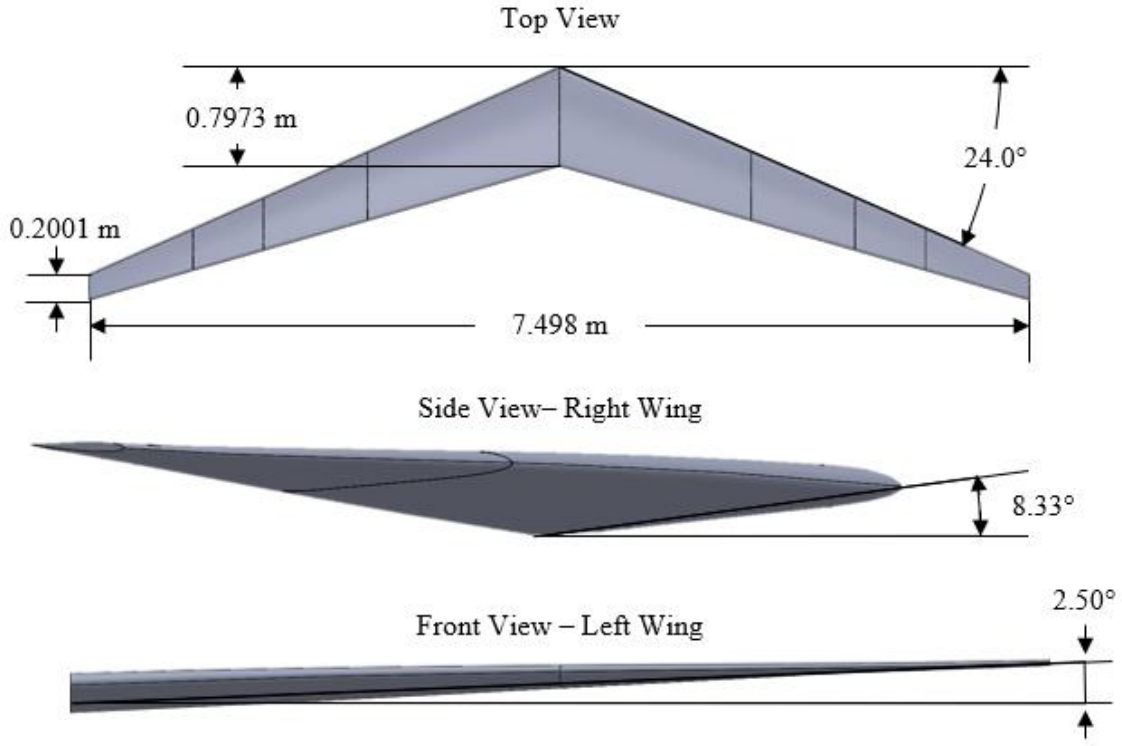

Figure 3.6: Final CAD Model

The wing of the model had a centerline chord length of 0.7973 m while the wingtip has a chord length of 0.2001 m after MATLAB manipulation. As mentioned in Section 2.2, a centerline chord

of .8001 m and wingtip chord of .2002 m were desired. The variance in the goal and final chord lengths is due to two reasons. The first is due to inherent rounding errors when rotating and translating the matrix of points. The second, is due to the nondimensional centerline chord matrix (Appendix A) as provided in the Prandtl-D report which presents a chord length of 0.998 instead of 1. The final chord lengths of all 21 sections are tabulated in Table 3.2.

Table 3.2: Section Chord Lengths

Span Location (%)	Span Location (m)	Chord Length (m)
0	0.000	0.797
5	0.187	0.767
10	0.375	0.737
15	0.562	0.708
20	0.750	0.678
25	0.937	0.648
30	1.125	0.618
35	1.312	0.588
40	1.500	0.558
45	1.687	0.529
50	1.875	0.499
55	2.062	0.469
60	2.249	0.439
65	2.437	0.409
70	2.624	0.380
75	2.812	0.350
80	2.999	0.320
85	3.187	0.290
90	3.374	0.260
95	3.562	0.230
100	3.749	0.200

A simple linear regression was performed on the chord lengths to insure a linear translation between the centerline and wingtip chord lengths. Using MATLAB's regression function, Equation 3.1 was determined for the relationship between the chord length (c) and a given span location (y) in meters. The function also gives the correlation coefficient (r) of -0.999 resulting in a r^2 coefficient of determination of 0.999. These values were deemed acceptable to proceed. Equation 3.2 calculates the chord length at various span locations based on the data provided in the NASA report and shows the small discrepancy between the wing geometry used in this analysis.

$$c(y) = -0.1592 \times y + 0.7971 \quad (3.1)$$

$$c(y) = -0.1600 \times y + 0.8001 \quad (3.2)$$

Using the linear regression equation (3.1) a couple more chord lengths of interest were calculated. These are the geometrical Mean Aerodynamic Chord (MAC) and the chord length at the vortex core location. The MAC can be calculated for the tapered wing using Equation 3.3 by substituting in Equation 3.1. With a semispan of 3.749 m, the MAC exists at 1.478 m with a chord length of 0.562 m. The vortex core is located at 70.4% of the semispan, or 2.639 m along the semispan. Using Equation 3.1, the chord length at the vortex core is 0.377 m. These additional chord lengths are tabulated in Table 3.3. The chord length at the vortex chord was chosen for the Reynolds number calculation in the following section.

$$MAC = \frac{2}{S}\int_0^{b/2} c(y)^2 dy \quad (3.3)$$

Table 3.3: Additional Section Chord Lengths

Chord	Span Location (%)	Span Location (m)	Chord Length (m)
MAC	39.42	1.159	0.562
Vortex Chord	70.40	2.639	0.377

The planform area (S) of the wing was calculated using two methods. The wing area is the projected area of the planform which is bounded by the leading and trailing edge. Using MATLAB, the X and Y coordinates of the leading and trailing edge (Appendix D) was uploaded and the planform area was calculated to be 3.713 m^2. The wing area was also calculated later using STAR-CCM+ by calculating the area normal to the z direction. This was determined by the software to be 3.715 m^2. Between the two areas, there is a 0.07 percent difference. As there was not much variance between the two calculated values it was deemed that the area calculated by STAR-CCM+ would be used as all other data produced for this report came from the software. As reference, in the report "Computational Fluid Dynamics Analysis of the Stall Characteristics of a Wing Designed Based on Prandtl's Minimum Induced Drag." by Seung Yoo in 2018 [25], which will be discussed further

in Section 4.5, it was determined that reference area for the Prandtl-D P3C wing was 3.763 m^2 (40.5 ft^2). This is 1.27 percent larger than what was determined for the model analyzed in this report and is because rounded wingtip extensions were included in Yoo's analysis.

Using a wing area of 3.715 m^2 and a span of 7.498 m, the aspect ratio using Equation 3.4 was calculated to be 15.1. Wings with higher aspect ratios will have less induced drag than wings with lower aspect ratios of the same area. As induced drag is more significant at low airspeeds it makes sense that gliders like Prandtl-D or birds like the albatross have longer slender wings. The important reference quantities are presented in Table 3.4.

$$AR = \frac{b^2}{S} \tag{3.4}$$

Table 3.4: Model Reference Dimensions

Variable	Value	Unit
Planform Area, S_{ref}	3.715	m^2
Mean Aerodynamic Chord, C_{MAC}	0.562	m
Chord at Vortex Core, C_V (C_{ref})	0.377	m
Span, b_{ref}	7.498	m
Aspect Ratio, AR	15.1	NA

Chapter 4

SIMULATION SETUP

This chapter reviews the set up of the CFD simulation. Like a calculator, the software only gives the answer in response to the user inputs, thus making sure the simulation is set up correctly is important to justify the results. A simulation requires three primary inputs: the fluid characteristics, the domain in which the fluid is bounded, and the allocation of mesh in the domain that the software uses to calculate how the fluid flows. A baseline configuration was used to set up these parameters after which a validation of the simulation was made proving that the CFD model was established properly.

4.1. CFD Software and Resources

The CFD simulations were all meshed, solved, and post processed in STAR-CCM+ version 12.06.011. As mentioned above, the CAD was generated in Solidworks and then exported as a Parasolid file type (.x_b) into STAR-CCM+. The data outputted from STAR-CCM+ was exported and then manipulated in MATLAB.

The domain sizing, grid independence, and final geometry simulations were all run on California Polytechnic State University's Bishop High Performance Computer Cluster (Bishop Cluster). The Bishop Cluster is a high-performance computer that features four nodes with 240 processing cores and 1.1 terabytes of RAM. Post processing was done on a campus lab computer that had 64.0 gigabytes of RAM.

4.2. Physics Continua

The physics continua define the three-dimensional flow field environment of the CFD simulation using the fluid properties of air. At 25 °C, the air was modeled as incompressible with a constant density of $\rho = 1.184\ kg\ m^{-3}$ and a dynamic viscosity of $\mu = 1.855\ \times 10^{-5} Pa\ s$. The freestream velocity (V) was determined to be 30 ft/s, or 9.144 m/s, from correspondence with Al

Bowers. The pressure was set at $101.325 \times 10^3 Pa$. Using the vortex core chord length (L) of 0.377 m, the Reynolds number of the aircraft was determined to be $Re = 2.195 \times 10^5$ by means of Equation 4.1.

$$\mathrm{Re} = \frac{\rho \mathrm{V} \mathrm{L}}{\mu} \tag{4.1}$$

The steady Reynolds-Averaged Navier-Stokes (RANS) equations with segregated flow were used for the solver. In actuality the flow over the wing would be unsteady but capturing this would have required significantly more computational time with no appreciable differences in results and was therefore deemed unnecessary.

STAR-CCM+ offers both coupled and segregated flow solvers to solve the conservation equations of mass and momentum. The segregated flow solver resolves these equations sequentially for pressure and velocity while the coupled flow model solves the mass, moment, and energy simultaneously. The coupled flow solver also requires more time to converge and can help with convergence for compressible flow, which was not necessary for this simplified study. As a result, the segregated flow model was chosen.

The realizable k-epsilon ($k - \epsilon$) model was used for the turbulence model with a two-layer all wall y+ treatment. The $k - \epsilon$ turbulence model is composed of two equations, one solving for the turbulent kinetic energy (k) while the other solves for the dissipation rate (ϵ). This turbulence model uses a version of the transport equations and more accurately predicts boundary layers, separation, and round jets. This makes the model ideal for capturing vortex formation off the trailing edge of the Prandtl-D wing. The two-layer approach allows the model to be applied in the mesh close to the wall, in the viscous-affected layer, and is accurate for low Reynolds number. This model works best with a wall y+ value of 1, see Subsection 4.4.1 for more detail.

The Reynolds number of 2.195 x 10^5 may be low for the fully turbulent approximation. Yet, as is also noted by Yoo [25], “although the Reynolds number is low, turbulent flow would exist in the pressure recovery of the airfoil. As such, it [is] not anticipated that laminar separation would be an

issue and turbulent separation [is] anticipated" as the Angle of Attack (AoA) approaches stall for the Prandtl-D wing. This separation can be seen in the pressure coefficient contours and surface streamlines of the upper surface of the P-3C (Figure 4.1) [25]. The wings in this report are at 8.33 degrees AoA (Subsection 4.3.1) while this scalar has the wing at 8 degrees AoA. Note that a portion of the upper surface is turbulent, and flow over the wing is transitional, rather than fully laminar. Therefore, it was assumed that the use of a turbulence model was acceptable for this study.

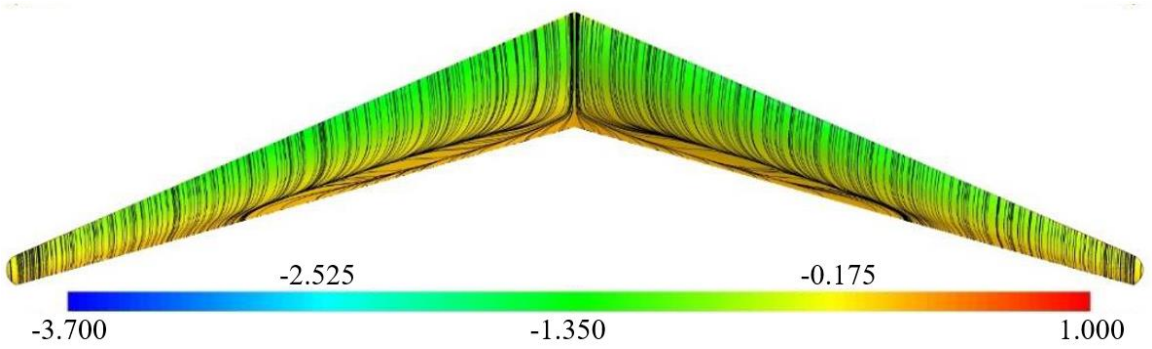

Figure 4.1: Pressure coefficient contours and surface streamlines on the upper surface of the P-3C at 8° AoA [25].

4.3. Fluid Domain

The fluid domain is the confined volume defined by boundaries that limit the flow field for CFD simulations. The domain also limits the area that is to be volumetrically meshed. For this analysis the fluid domain was defined as a rectangular prism where the flow enters from a velocity inlet and the flow exits a pressure outlet. There are four surrounding walls, each set to be a slip wall with no boundary layer growth. Two staggered wings in an echelon formation were placed within the domain for the study, shown in Figure 4.2.

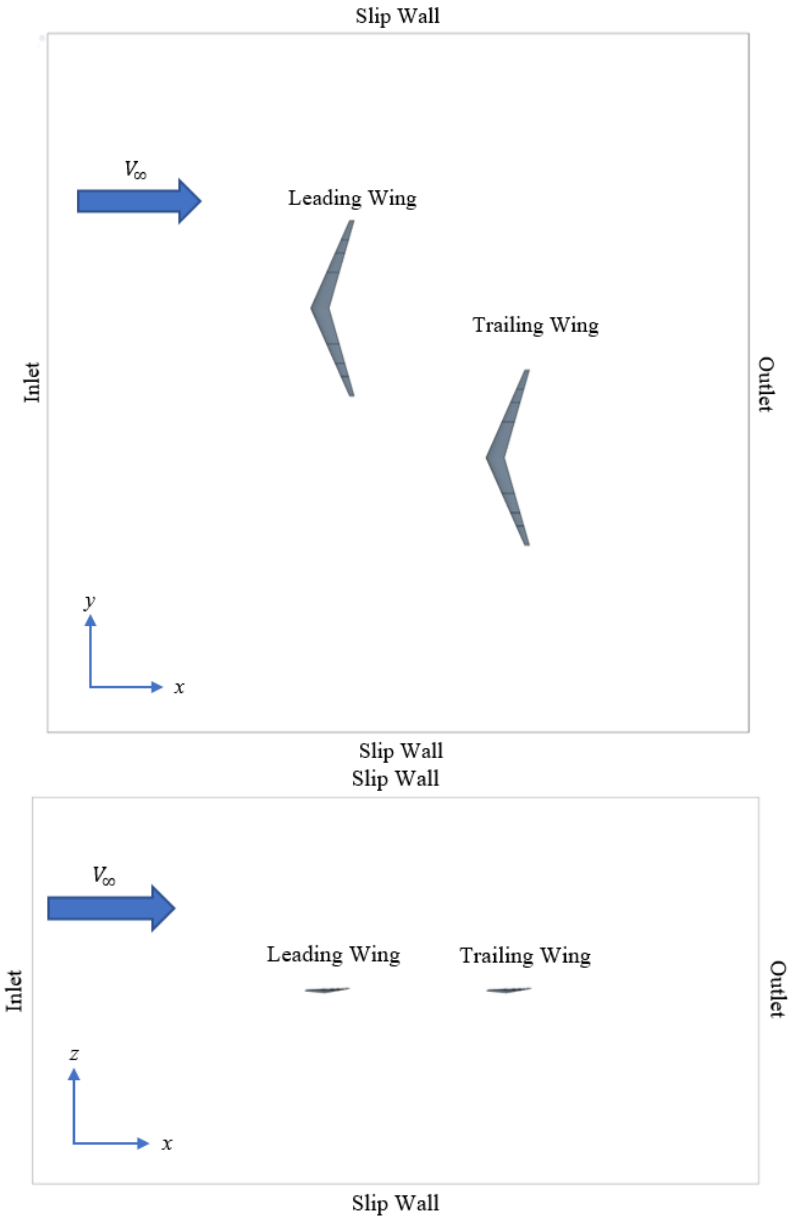

Figure 4.2: Domain boundary settings. (a) Top view and (b) Side view

4.3.1. Trailing Wing Placement

The placement of the trailing wing is key because where it is positioned determines how the downstream wake of the leading wing affects it. For this study, the key parameter of interest was the lateral position in the y direction. Section 5.1 defines how wing overlap changes for the test matrix. The nose of the leading wing was defined as the origin of the model (0 m, 0 m, 0 m) with positive x pointing downstream along the flow, positive y pointed towards the wings starboard, and

positive z pointing up. To start off, the baseline model had the trailing wing's right wingtip positioned at the location of the leading wing's left wing vortex, which was determined to be .704 of the semispan or located at -2.639 m from the origin in the y direction. This results in the baseline case having a Y/b of -0.148. and was based on the hypothesis going into the analysis. For placement, review of bird formation literature was informative. There is no discernable displacement between the birds in the vertical direction, so the trailing wing was set at z = 0.000. For depth in the X-axis, the literature varied. Hainsworth [13] reports on Canada geese with a wingspan of 150 cm and trailing at a median 305 cm. Speakman and Banks [15] studied Greylag geese with a wingspan of 144 cm and trailing at a median of 123 cm. Portugal [16] noted ibises with a wingspan of 120 cm and trailing at a median of 100+ cm. The analysis by Spedding [12] on a kestrel with a 68 cm wingspan measured vortex roll-up at about 60 cm. These x/b ratios (span to the distance) between birds of 2.0, 0.8, 0.8, and 0.9 are dependent on the species, but are likely synchronized with the roll-up of the vortices. In Portugal's report, ibises were studied flying in formation flight. In that study, there was an x/b ratio of 1. With the variation in depth from these five reports averaging a little over one span, the trailing wing in this report was positioned one span length aft of the leading. This allowed for a developed vortex and still a close formation where the weaker vortex of a BSLD wing has not broken up and so greater benefits are more likely. This positioned the nose of the trailing wing at (7.498 m, -6.388 m, 0 m). Both wings were left at 8.33 degrees AoA for this analysis, which is the centerline airfoil twist angle.

4.3.2. Domain Sizing

With the wings positioned the next step is to size the domain. This was done by generating an unstructured mesh and changing boundary distances away from the wings. The mesh settings, tabulated in Table 4.1, were not the final ones used, as those were determined afterwards in the mesh generation phase. For each domain size both lift and total drag were reported. When there was no sizeable difference in the forces between two domain sizes it indicated that the boundaries

were no longer influencing the results. For this analysis, a change of less than 2% was deemed acceptable, in which case the smaller of the two domains was chosen. Each simulation was run to 2,500 iterations at which point the residuals of the software were lower than 1.0×10^{-3}. The definitions of each of the settings in Table 4.1 are explained further in Section 4.4.

Table 4.1: Domain Sizing Mesh Settings

Domain Size	**Wing Surface Size**	**Wake Size**	**Growth Rate**
1.00 m	0.02 m	0.05 m	1.2
Prism Layer Total Thickness		**Number of Prism Layers**	
.02 m		5	

Table 4.2 summarizes the three domain sizes studied. To visualize these settings Figure 4.3 was drawn with key dimensions labeled, which are recorded in Table 4.3.

Table 4.2: Summary of Three Domain Sizes

Domain Size	**Inlet** Leading Wing Nose	**Outlet** Trailing Wing Nose	**Top & Bottom** Origin	**Sides** Outer Wingtips
Small	- *b*	*b*	+/- 6	+/- 6
Medium	-1.5 *b*	1.5 *b*	+/- 8	+/- 8
Large	-2 *b*	2 *b*	+/- 12	+/- 12

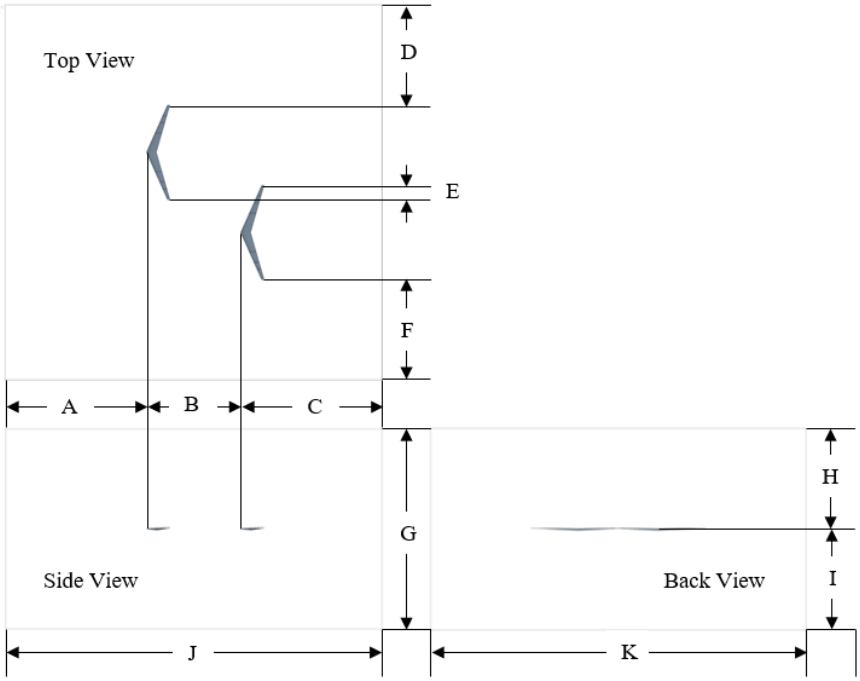

Figure 4.3: Three view drawing of the fluid domain sizing parameters

Table 4.3: Fluid Domain Sizing Parameters

Domain Size Parameter	Small	Medium	Large
A	7.498	11.247	14.996
B	7.498	7.498	7.498
C	7.498	11.247	14.996
D	6.000	8.000	12.000
E	1.110	1.110	1.110
F	6.000	8.000	12.000
G	12.000	16.000	24.000
H	6.000	8.000	12.000
I	6.000	8.000	12.000
J	22.494	29.992	37.490
K	25.886	29.886	37.886

The results of the study are documented in Table 4.4. There was very little change in both lift and total drag when increasing the domain size. As the cut off for an acceptable difference in force was set to be 2.00% the small domain was not able to be chosen over the large because the total drag was a difference of 2.05%. The difference in the forces between the small and medium domains would be acceptable with this 2.00% cutoff but the difference between the medium and large domains were more reasonable. Lift only had a decrease in 0.15% while total drag saw a decrease of 0.37%. With this recognition the medium sized domain was chosen for the continuation of the analysis. It was also an acceptable choice because a majority of the mesh cells in the study were identified to be those in the wake of the aircraft, and an increase in the domain size would greatly increase the number of cells, the size of the simulation file, and the time to run the simulation.

Table 4.4: Change in Forces between Domain Sizes

Domain Size Change	Lift % Diff.	Total Drag % Diff.
Small to Medium	0.53%	1.67%
Medium to Large	0.15%	0.37%
Small to Large	0.68%	2.05%

4.4. Mesh Generation

With the domain sized the next step was to generate a mesh for the geometry. The mesh for the study was unstructured and trimmed with the settings in Table 4.1 used as the baseline mesh that was iterated for the desired settings. First, the boundary layer to be captured by prism layers was found using the determined Wall-Y+ value. Then a two stem grid convergence study was preformed, first looking at the cells around the leading wing to view their influence on the lift and drag, followed by an analysis on the wake of the leading wing's effect on the trailing wing's aerodynamic forces.

4.4.1. Prism Layers

One of the key aspects in obtaining accurate drag and lift forces from CFD is capturing the boundary layer properly. This can be identified using the wall y^+, which is a non-dimensional distance that correlates the distance y to the wall with the friction velocity V_* and the kinematic viscosity ν. This correlation is noted in Equation 4.2.

$$y^+ = \frac{yV_*}{\nu} \tag{4.2}$$

As mentioned in Section 4.2, for the realizable $k-\epsilon$ two-layer turbulence model, at low Reynolds numbers the y^+value should be on average 1 for the model. Prism layers are orthogonal prismatic cells that reside close to wall boundaries or surfaces and are used to capture the large flow field gradient within the inner layer of the boundary layer. The prism layers were sized to capture the boundary layer thickness as well as to size the first prism layer to achieve the recommended wall y^+ value. To solve for the boundary layer thickness, Equation 4.3 was used as an approximation of laminar flow over a flat plate [26]. The distance x (length of chord) and Reynolds number Re where chosen at the 70.4% semispan location. These values were 0.377 m and 2.195 x 10^5 respectively. This resulted in a total boundary layer thickness of 1.189 mm.

$$\delta = \frac{0.37x}{Re_x^{1/5}} \tag{4.3}$$

The following step was to determine the height of the first prism cell layer. First the coefficient of friction, C_f, was calculated in Equation 4.4. This was followed by using Equation 4.5 to find the wall shear stress, τ_{wall}, and then Equation 4.6 to determine friction velocity, V_*. The final step was to solve for the first layer prism height, Δy, using Equation 4.7, which was found to be 35.6 μm.

$$C_f = \frac{0.026}{Re^{1/7}} \tag{4.4}$$

$$\tau_{wall} = \frac{C_f \rho V_\infty^2}{2} \tag{4.5}$$

$$V_* = \sqrt{\frac{\tau_{wall}}{\rho}} \tag{4.6}$$

$$\Delta y = \frac{V_* y^+}{u_* \rho} \tag{4.7}$$

By setting the first prism layer and total prism layer thicknesses, and after the following grid convergence studies, the following scalar in Figure 4.4 was produced for the leading wing. On average the wall y^+ was around 1 for the overall aircraft, and the settings were deemed acceptable.

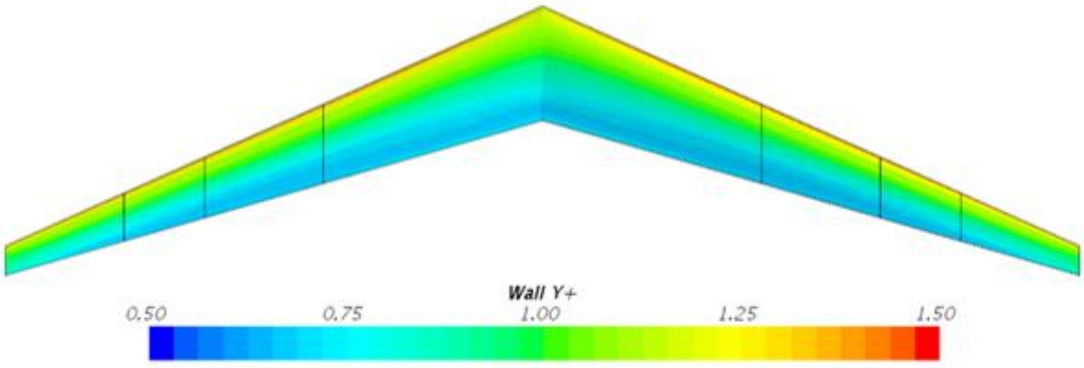

Figure 4.4: Wall y^+ scalar scene of the leading wing

4.4.2. Grid Convergence Studies

After setting the mesh near the wings, the next step was to determine the settings of the mesh in the surrounding volume of the domain. This was done in two phases; first the mesh around the wings was resolved, secondly the mesh refinement in the wake was set. In each case three meshes of coarse, medium, and fine qualities were considered. In the study determining cell size around the wing's surfaces, the lift and drag were reported from the leading wing as there is no affect from the following wing. In the analysis for determining the wake cell sizes, the lift and drag of the following wing were reported due to the refinement of the wake influence by the leading wing. In reporting the lift and drag values, tabulated in Tables 4.5 and 4.6, grid convergences for the best settings were found.

Table 4.5: Lift and Drag Values with Increased Mesh Density Close to the Wing

Mesh Size	Leading Wing Lift (N)	Leading Wing Total Drag (N)	Number of Cells
Coarse	126.88	5.59	1.83E+07
Medium	129.32	5.69	2.19E+07
Fine	132.08	5.80	3.27E+07

Table 4.6: Lift and Drag Values with Increased Wake Mesh Density

Mesh Size	Trailing Wing Lift (N)	Trailing Wing Total Drag (N)	Number of Cells
Coarse	133.61	4.58	3.99E+07
Medium	136.47	4.68	4.77E+07
Fine	138.73	4.75	6.49E+07

The grid convergence index (GCI) method as detailed in "Quantification of Uncertainty in Computational Fluid Dynamic" by Roache was used in narrowing down which mesh settings to use [27]. In both cases, mesh around the wing and mesh in the wake, the fine mesh had less than a 4 percent difference in the lift and drag values between the coarse and fine mesh. As a result, the finest mesh was ruled out and the GCI was calculated for the medium and coarse meshes using Equation 4.8. F_s is the factor of safety and is dependent on the number of mesh intervals to be considered, which Roache recommends setting to 3 for the sake of uniform reporting and adequate

conservatism. Equation 4.9 calculates the error (E) in the corresponding grid by comparing the solution to that of the other grid, either medium to coarse or coarse to medium. The characteristic mesh length (h) in the case of the mesh close to the wing was $h_{coarse} = 1.25$ mm and $h_{med} = 0.5$ mm. For the study on the mesh in the wake the mesh lengths were $h_{coarse} = 1.5$ cm and $h_{med} = 1$ cm.

$$\mathrm{GCI}^{\mathrm{med}} = \mathrm{F_s}\left|\mathrm{E}^{\mathrm{med}}\right| \tag{4.8a}$$

$$\mathrm{GCI}^{\mathrm{coarse}} = \mathrm{F_s}\left|\mathrm{E}^{\mathrm{coarse}}\right| \tag{4.8b}$$

$$\mathrm{E}^{\mathrm{med}} = \frac{\epsilon}{(\mathrm{r}^{\mathrm{p}} - 1)} \tag{4.9a}$$

$$\mathrm{E}^{\mathrm{coarse}} = \frac{\mathrm{r}^{\mathrm{p}}\epsilon}{(\mathrm{r}^{\mathrm{p}} - 1)} \tag{4.9b}$$

$$\epsilon = \frac{\mathrm{f_{coarse}} - \mathrm{f_{med}}}{\mathrm{f_{coarse}}} \tag{4.10}$$

$$\mathrm{r} = \frac{\mathrm{h_{coarse}}}{\mathrm{h_{med}}} \tag{4.11}$$

The results from the two grid convergence studies are shown in Table 4.7 and 4.8. In both cases there is little change between the GCI of the coarse mesh and the medium mesh settings, and as a result the medium mesh settings were chosen. For clarification, after the medium mesh settings were chosen for around the wing these settings were carried over into the wake study where three mesh cases were devised. There was no wake refinement in the initial wing surface mesh analysis.

Table 4.7: CGI and Error Values with Increased Mesh Density Close to the Wing

	Coarse		Medium	
	E	CGI	E	CGI
Lift	-0.023	0.069	-0.004	0.011
Drag	-0.022	0.065	-0.003	0.010

Table 4.8: CGI and Error Values with Increased Wake Mesh Density

	Coarse		Medium	
	E	CGI	E	CGI
Lift	-0.039	0.116	-0.017	0.051
Drag	-0.040	0.121	-0.018	0.054

The final settings were those of the medium mesh found in the wake grid convergence study. The initial settings determined from the grid convergence study on the wing surface are listed in Table 4.9. The base size was equivalent to the chord length at the vortex core location, set at 0.38 m. Both the target surface size and minimum surface size were set to 100% of the base size to allow manipulation in the surface controls. The prism layer settings were set to those determined in Subsection 4.4.1 with the prism layers disabled on the outer slip walls to reduce redundant meshing. For the wings surfaces themselves, surface and line controls were applied. The target surface size of the wing was 1 cm with 5 mm set close to the trailing edge. Over the whole wing the allowable minimum surface size was set to 0.5 mm allowing for a finer mesh around the leading edge.

Table 4.9: Mesh Settings Determined from Wing Surface Mesh Convergence Study

Default Controls	
Base Size	0.38 m
Target Surface Size – Relative to Base	100
Minimum Surface Size – Relative to Base	100
Maximum Cell Size – Relative to base	100
Surface Curvature – Pts/circle	36
Surface Growth Rate	1.1
Number of Prism Layers	10
Prism Layer Near Wall Thickness	3.56E-05 m
Prism Layer Total Thickness – Absolute size	3.98E-04 m
Volume Growth – Default Growth Rate	Very Slow
Volume Growth – Surface Growth Rate	Disable
Surrounding Walls – Surface Control	
Prism Layers	Disable
Wing Surface – Surface Control	
Target Surface Size – Absolute	0.01 m
Minimum Surface Size – Absolute	5.00E-04 m
Trailing Edge – Line Control	
Target Surface Size – Absolute size	0.005 m
Minimum Surface Size – Absolute size	5.00E-04 m

The additional settings added after the addition of wake refinement from the second grid convergence study are listed in Table 4.10. As displayed in Figure 3.5, the wings were divided into three regions: fine refinement at the vortex (red), medium refinement near the vortex cores (orange), and coarse refinement in the center of the wing (yellow). The wake refinement behind each wing extended all the way back to the pressure outlet, 18.7452 m behind the leading wings

nose. One reason the fine wake refinement settings were not applied across the whole wing was because including finer mesh significantly increased the size of the file and the time required to mesh, run, and post process. In the vortex the wake refinement was set to 1 cm with volume growth rate set to a slow transition, meaning as the cell size transition between a cell in the wake with a size of 1 cm to the base cell size of 38 cm away from the wake was gradual and not abrupt. Near the vortex, the wake refinement was set to 2 cm with a medium volumetric growth rate. The final wake refinement set was for the center of the wing, which was set to 4 cm with a fast transition to the surrounding mesh. These determined mesh settings, with those listed in Table 4.9, were used for the remainder of the report.

Table 4.10: Additional Mesh Settings Determined from Wake Mesh Convergence Study

Wake Center – Surface Control	
Wake Refinement – Absolute size	0.04 m
Wake Refinement – Volume Growth Rate	Fast
Wake Near Vortex – Surface Control	
Wake Refinement – Absolute size	0.02 m
Wake Refinement – Volume Growth Rate	Medium
Wake Vortex – Surface Control	
Wake Refinement – Absolute size	0.01 m
Wake Refinement – Volume Growth Rate	Slow

4.5. Baseline Validation

Once the mesh was finalized a validation simulation of the baseline case was run. For justification of the CFD, a comparison was made to the study by Seung Y. Yoo [25]. He analyzed the stall characteristics of the Prandtl-D P3-C aircraft using CFD. Yoo used the RANS solver OVERFLOW with a fully turbulent flow approximation. Unlike this report where the $k-\epsilon$ turbulence model was applied Yoo used the Spalart-Allmaras turbulence model with rotational and curvature correction. Yoo also performed a grid convergence study but didn't focus on wake refinement as there was no object behind the wing that was being evaluated. There are a few differences between flow characteristics in this report and his which are listed in Table 4.11. In

general, the flow was run at a different altitude and freestream velocity. One other note is that while the analysis in this report removed the rounded wingtips, Yoo kept them in the glider's geometry.

Table 4.11: Differences to Yoo's Physics Set Up

Characteristic	Yoo	Lukacovic
Velocity	8.775 m/s	9.144 m/s
Density	$1.145\ kg\ m^{-3}$	$1.184\ kg\ m^{-3}$
Pressure	$93.182\ \times 10^{3} Pa$	$101.325\ \times 10^{3} Pa$
Temperature	10.443 °C	25 °C
Dynamic Viscosity	$3.5281\ \times 10^{-6} Pa\ s$	$1.855\ \times 10^{-5} Pa\ s$
Mach Number	0.026	0.027

For grid convergence Yoo studied four different grid resolutions varying parameters such as the surface spacing, y+ value, stretching ratios, and near field grids. To evaluate success, the coefficient of lift (C_{L_stall}) at the stall AoA was used, which was determined for the aircraft to be around $17.25° \pm .25°$. The coefficient of drag and lift at the various angles of attack analyzed and four grid resolutions are plotted below in Figure 4.5.

Overlaid on top of Yoo's plots indicated by orange and yellow stars are the leading wing's C_L and C_D values respectively as determined from the finalized baseline mesh settings in this study. These values were found to be 0.702794 and 0.030969 when calculated using Equations 4.12 and 4.13 respectively. The lift (L) and drag (D) were outputs from STAR-CCM+ and calculated to be 129.237 N and 5.695 N. When comparing the results visually from the baseline to Yoo's the C_L and C_D line up exactly. From this it was determined that the mesh settings used in this report achieved a level suitable for this study and the findings here and forthcoming are considered accurately justified.

$$C_L = \frac{L}{\frac{1}{2}\rho S V_\infty{}^2} \tag{4.12}$$

$$C_D = \frac{D}{\frac{1}{2}\rho S V_\infty{}^2} \tag{4.13}$$

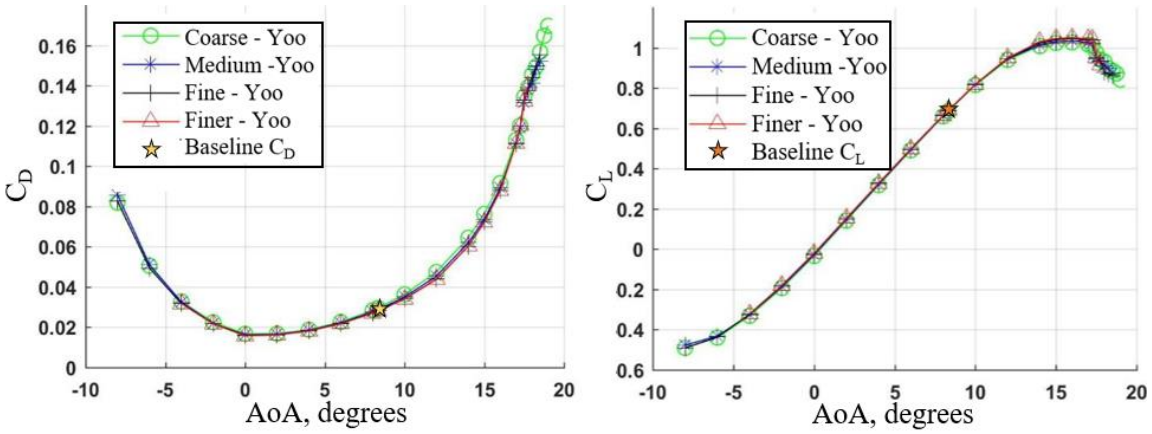

Figure 4.5: C_L and C_D comparison between current baseline and Yoo's analysis

Another means of verification was to identify how closely the model conforms to the BSLD (Figure 2.5). For this some additional setup was required within STAR-CCM+ to get pressure profiles. A macro was built to distribute 41 planes spanwise across the leading wing at equal intervals, lining up with the section profiles used to create the wing in CAD. Line probes were applied at the intersection of each plane and the top and bottom wing surfaces, resulting in 82 probes. Data points along these lines containing the x location within the simulation as well as the coefficient of pressure were exported as .csv files. In MATLAB the x location was converted into the non-dimensional distance along the chord length, $\zeta = x/c$ ranging from 0 to 1. The next step is to convert the coefficient of pressure distributions to the local lift coefficient (c_l). This was done using Equation 4.14 where $c_{p,l}$ and $c_{p,u}$ are upper and lower coefficients of pressure. Knowing the local lift coefficient, the lift force per unit span of the wing (l) was calculated using Equation 4.15 where q is the dynamic pressure and c is the chord length. Finally, these values were converted to the non-dimensional range of 0 to 1 by dividing the values by the maximum local lift force and the span location was changed to the non-dimensional spanwise location of 2y/b. Figure 4.6 plots the spanwise local lift from the CFD results against Prandtl's BSLD (Equation 2.26).

$$c_l = \int_0^1 \left(c_{p,l} - c_{p,y}\right) d\zeta \tag{4.14}$$

$$c_l = \frac{l}{qc} \tag{4.15}$$

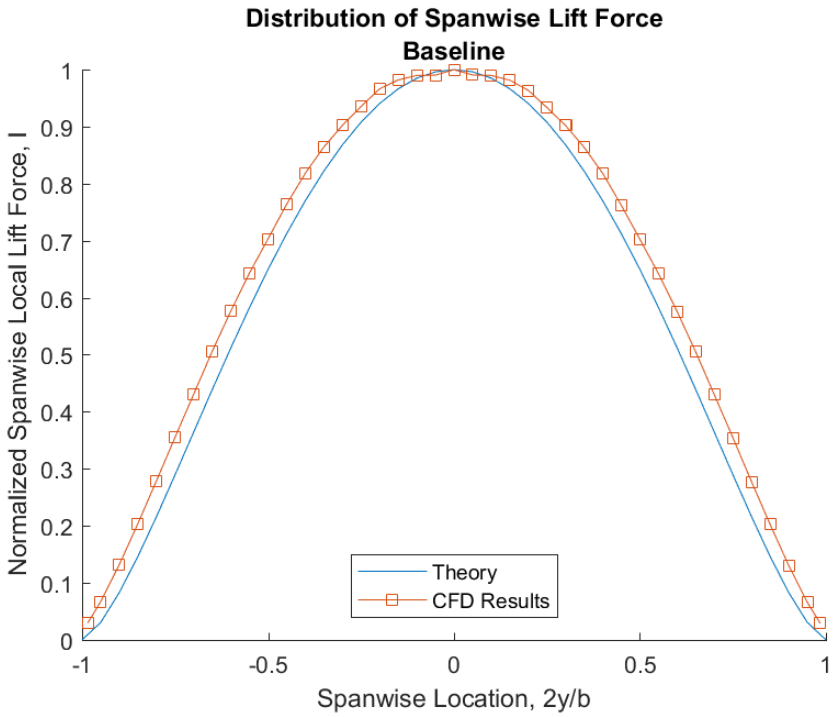

Figure 4.6: Verification of the spanwise local lift distribution

From viewing this graph there is some discrepancy yet overall, the curve of the CFD results follows the same trend as the theory. Note also that the coefficients of pressure were not able to be gathered directly at the wingtip, and the furthest points outward were taken at 0.98 of the semispan. Therefore, the wingtip does not display zero lift, though it is still assumed. From this comparison it was determined to be an acceptable representation of the lift distribution to continue to study as there was only a maximum of 5% difference along the wing.

Chapter 5

RESULTS AND ANALYSIS

This chapter presents the simulation parameters, the results, and the analysis. In Section 5.1 there is a presentation of the lateral positions selected for testing and the standards set to ensure a good convergence for all of the simulations. In Section 5.2, the simulation output is processed to provide the results for the parameters selected. The formulas used for calculating these results are given. Then the numerous parameters and simulation results are combined and presented in graphs and tables. Section 5.3 discusses a Trefftz Plane analysis that was conducted to find the induced drag of the wings in formation flight. In Section 5.4 there is a more detailed discussion of the study findings specifically concerning optimal trailing wing positioning that is most beneficial with regards to lift, drag, and other parameters. A comparison to the bird formation research data analyzed in Section 2.4 is also presented. Section 5.5 presents a study of the changes to the lift distributions along the entire wingspan, comparing results at each wing position.

5.1. Test Matrix and Convergence

To conduct the simulations of positions in the Y coordinate, a finite number of points need to be selected. Instead of selecting evenly spaced points, it was more pertinent to select more points close to the expected parameter maximums around the BSLD vortex and fewer points further away. This section discusses the selection of those points, as well as the configuration of the test domain, the size of the cells, and the convergence criteria.

With the baseline configuration for the study complete and validated the next step is to shift the following wing laterally in the Y-direction to identify the optimal position for both the trailing wing and for the two wings as system. For this a test matrix was developed with the primary focus around the baseline location, which hypothetically should result in the best placement for the trailing wing's benefit.

For this study values for Y/b are used to identify the various configurations, assuming 0.0 being wingtip alignment, -1.00 being centerline alignment (100% overlap), and >0.0 being lateral outboard space between wingtips. Y in this case is the WTS and b is the span. Figure 5.1 provides a visualization of this parameter in a few configurations. The lateral location ranged from Y/b = -1 (which has a WTS of -7.498 m) to Y/b = 2 (a WTS of two spans, 14.996 m). For example, the baseline configuration ran in the previous chapter is denoted at Y/b = -.148 for having 14.8% of the trailing wing overlapping the leading wing. To investigate more detail around this hypothetical optimal position for the BSLD, it was decided to have five evenly spaced points from the wingtip to the vortex (at 0.000, -0.037, -0.074, -0.111, and -0.148). Two more points at the same spacing were selected outside the wings (at =0.037 and =0.074). Six points were similarly spaced inboard (from -0.148 to -0.370) to mirror the six outboard points just noted. This gave a full coverage of points from tip-to-tip (0.00) and vortex-to-vortex (-0.296), and then some. Then selections were made to cover the rest of the three wingspan field. Inboard a double step was taken to -0.444, then a quadruple step to -0.592, then the end at -1.000. Outboard matched this pattern with double to +0.148, then quadruple spacing to +0.296, +0.444, and +0.592 then a six space step to +0.814, ending with points at +1.000 and +2.000. With 23 points covering the full field and detailed around the more critical vortex position, it seemed a good selection for the purposes of this study. The finalized test matrix configurations can be seen in the first column of Table 5.1.

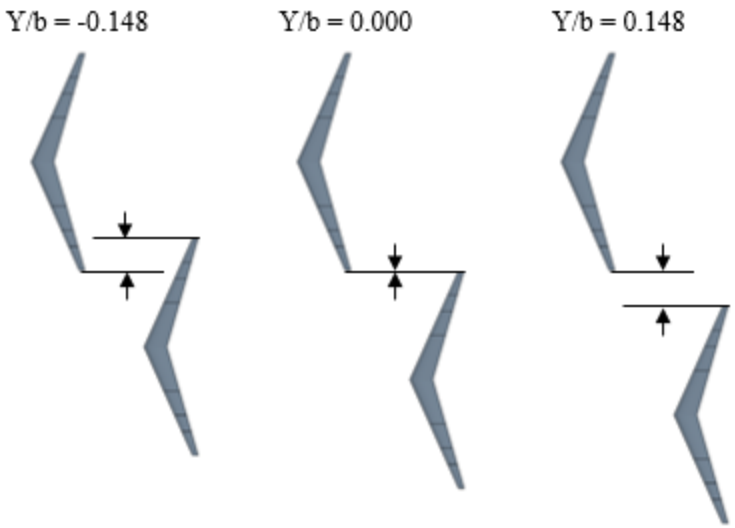

Figure 5.1: Visualization of Y/b in three configurations (-0.148, 0.000, and 0.148)

A macro written in java script was used to transition the trailing wing from the baseline model to the additional 22 configurations. The macro not only repositioned the trailing wing but was used to set up the new boundary locations within the domain, mesh the geometry, create monitors and reports (Section 5.2), add Trefftz planes (Section 5.3), and add pressure planes (Section 5.4).

The domain size changed from configuration to configuration but the overall spacing from the wing models to the boundaries stayed the same, as defined by the medium domain size in Table 4.3. As a result, the only wall location that moved was the left wall leaving a spacing of 8m from the left wingtip of the traversed trailing wing. See Table 5.1 for the configuration domain sizes.

Table 5.1: Configuration Domain Sizes

Wing Spacing, Y/b	Inlet (m)	Outlet (m)	Left Wall (m)	Right Wall (m)	Top (m)	Bottom (m)	Volume (m^3)
-1.000	-11.247	18.745	-11.749	11.749	8.000	-8.000	11276
-0.592	-11.247	18.745	-14.808	11.749	8.000	-8.000	12744
-0.444	-11.247	18.745	-15.918	11.749	8.000	-8.000	13277
-0.370	-11.247	18.745	-16.473	11.749	8.000	-8.000	13543
-0.333	-11.247	18.745	-16.750	11.749	8.000	-8.000	13676
-0.296	-11.247	18.745	-17.028	11.749	8.000	-8.000	13809
-0.259	-11.247	18.745	-17.305	11.749	8.000	-8.000	13942
-0.222	-11.247	18.745	-17.583	11.749	8.000	-8.000	14076
-0.185	-11.247	18.745	-17.860	11.749	8.000	-8.000	14209
-0.148	-11.247	18.745	-18.137	11.749	8.000	-8.000	14342
-0.111	-11.247	18.745	-18.415	11.749	8.000	-8.000	14475
-0.074	-11.247	18.745	-18.692	11.749	8.000	-8.000	14608
-0.037	-11.247	18.745	-18.970	11.749	8.000	-8.000	14741
0.000	-11.247	18.745	-19.247	11.749	8.000	-8.000	14874
0.037	-11.247	18.745	-19.525	11.749	8.000	-8.000	15007
0.074	-11.247	18.745	-19.802	11.749	8.000	-8.000	15141
0.148	-11.247	18.745	-20.357	11.749	8.000	-8.000	15407
0.296	-11.247	18.745	-21.467	11.749	8.000	-8.000	15939
0.444	-11.247	18.745	-22.576	11.749	8.000	-8.000	16472
0.592	-11.247	18.745	-23.686	11.749	8.000	-8.000	17004
0.814	-11.247	18.745	-25.351	11.749	8.000	-8.000	17803
1.000	-11.247	18.745	-26.745	11.749	8.000	-8.000	18473
2.000	-11.247	18.745	-34.243	11.749	8.000	-8.000	22071

After the geometry of each configuration was set the simulations were meshed. The number of vortices, faces, and cells are plotted in Figure 5.2. The total cells in the simulations ranged from 120 to 160 million cells while the number of vortices and faces ranged from 40 to 58 million. This variation is due to the change in wake refinement as the trailing wing position is changed. Overall, as there is no overlap in the Y/b > 0.0 cases thus the total number of cells stayed relatively the same. As the trailing wing slowly moves laterally to the where the two wings have their high density meshed vortices lined up (Y/b = -0.296) the configurations reaches a lower cell count. Moving the trailing wing further right behind the leading wing increases the number of cells as the vortices are

no longer in line. Then at the Y/b = -1 case there are about 14% fewer cells than the Y/b =1 case, since the wake refinement mesh behind the wing is not duplicated.

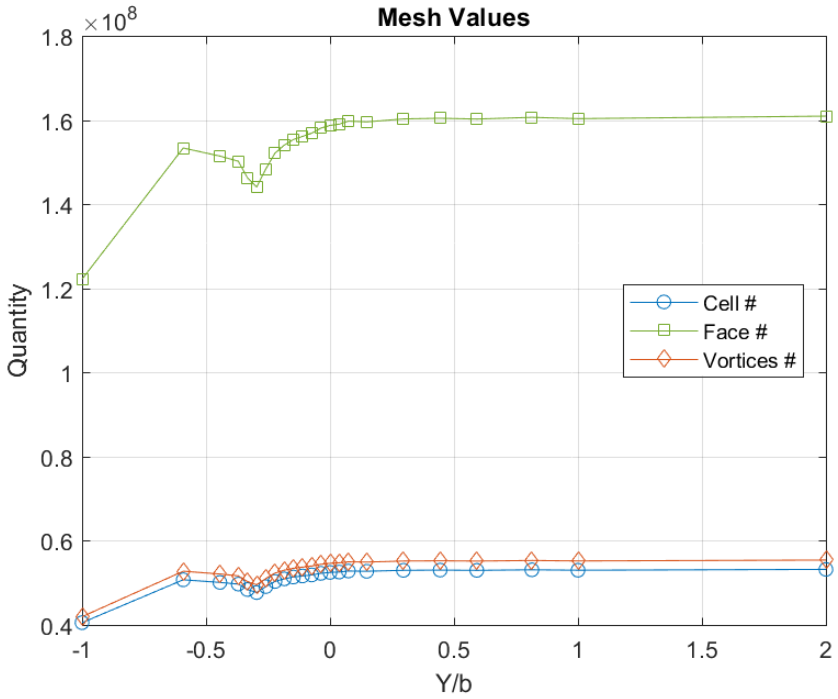

Figure 5.2: Number of cells, faces, and vortices once meshed

One of the key attributes to any CFD simulation are the residuals, which are one way to identify when a simulation has converged to a solution. While the primary source to identify convergence for this study was when the values of lift and drag did not fluctuate within +/- 0.05% after 2500 iterations, the residuals were also monitored as they directly quantify the error in the solution of the system equations. Residual levels of 1E-04 are considered to be loosely converged, levels of 1E-05 are considered to be well converged, and levels of 1E-06 are considered to be tightly converged. For complex solutions it may not always be possible to achieve residuals this low. The average value, max value, and minimum value for each residual across all 23 cases are tabulated in Table 5.2 below along with the standard deviation of the sample (S.D.). Apart from two outliers in the Tdr residual, the results were deemed acceptable for the resolution and complexity of this study. The value of each residual for all 23 configurations and their S.D. are tabulated in Appendix E with some additional plots. Of all the configurations the Y/b = 2 case had the worst residuals.

Table 5.2: Residual Values

Residual Parameter	Mean Value	Max Value	Min Value	S.D.
Continuity	2.28E-04	2.81E-04	2.02E-04	1.61E-05
Tdr	1.24E-02	2.51E-01	4.36E-06	5.48E-02
Tke	6.86E-05	8.52E-04	2.30E-05	1.68E-04
X Momentum	2.20E-04	2.27E-03	1.13E-04	4.38E-04
Y Momentum	2.87E-04	3.52E-03	1.17E-04	6.88E-04
Z Momentum	4.66E-05	7.92E-04	1.15E-05	1.59E-04

The conclusion of Section 5.1 is that a successful effort was made to select monitoring points surrounding the areas of interest (the leading wing vortex position) and other points further far afield. Also, proper domain and cell configurations were set to ensure adequate to good convergence. The output from these converged simulations were processed and discussed in the following Section 5.2.

5.2. Data Processing and Results

This section presents the analysis and results of the data provided by the simulations. It shows the formulas used in the analyses and displays the results in tabular and graphical formats. Four parameters were monitored for each of the two wings: lift (L), total drag (D), pressure drag (D_P), and skin friction drag (D_f). The variables below are denoted with a subscript "l" for the leading wing and a subscript "t" for the trailing wing. Using these outputs, the following parameters were calculated: coefficient of lift, coefficient of drag, and the lift-to-drag ratio. For each of these calculated aerodynamic parameters, as well as the four output from STAR-CCM+, a percent change between the leading and trailing wing was computed. The equations below (5.1-5.13) were used to calculate these parameters. Using MATLAB, the last 200 iterations for each configuration were analyzed resulting in a mean value and a standard deviation for each parameter. Note that the S.D. of all these parameters for the 23 cases were between 1E-04 to 1E-07, except for the lift and pressure drag of the Y/b = 2 case which seemed to have the largest S.D, resulting in the variables

derived at that position having larger S.D. as well. The results are plotted below in the following subsections and tabulated in Appendix F. Additional conclusions are made in Section 5.4.

$$\text{Lift \% Change} = \frac{L_t - L_l}{L_l} * 100 \tag{5.1}$$

$$C_{L,l} = \frac{L_l}{\frac{1}{2}\rho S V_\infty{}^2} \tag{5.2}$$

$$C_{L,t} = \frac{L_t}{\frac{1}{2}\rho S V_\infty{}^2} \tag{5.3}$$

$$\text{Lift Coefficient \% Change} = \frac{C_{L,t} - C_{L,l}}{C_{L,l}} * 100 \tag{5.4}$$

$$\text{Total Drag \% Change} = \frac{D_t - D_l}{D_l} * 100 \tag{5.5}$$

$$C_{D,l} = \frac{D_l}{\frac{1}{2}\rho S V_\infty{}^2} \tag{5.6}$$

$$C_{D,t} = \frac{D_t}{\frac{1}{2}\rho S V_\infty{}^2} \tag{5.7}$$

$$\text{Total Drag Coefficient \% Change} = \frac{C_{D,t} - C_{D,l}}{C_{D,l}} * 100 \tag{5.8}$$

$$\frac{L}{D}\text{Ratio, l} = \frac{L_l}{D_l} \tag{5.9}$$

$$\frac{L}{D}\text{Ratio, t} = \frac{L_t}{D_t} \tag{5.10}$$

$$\text{Lift to Drag Ratio \% Change} = \frac{\frac{L}{D_t} - \frac{L}{D_l}}{\frac{L}{D_l}} * 100 \tag{5.11}$$

$$\text{Pressure Drag \% Change} = \frac{D_{p,t} - D_{p,l}}{D_{p,l}} * 100 \tag{5.12}$$

$$\text{Skin Friction Drag \% Change} = \frac{D_{f,t} - D_{f,l}}{D_{f,l}} * 100 \tag{5.13}$$

5.2.1. Lift

The following plots in Figures 5.3 to 5.15 were created in MATLAB using the calculated results of the equations above. In Figures 5.3 and 5.4, lift (a direct output of STAR-CCM+) and the lift coefficient are plotted for both the leading and trailing wings. Figure 5.5 shows the percent change in the lift (and equivalently the lift coefficient as it is scaled) for the trailing wing as compared to the leading wing. The first thing to note is the difference in the resulting lift for the leading wing. There is a 0.62% increase in lift for the leading wing at Y/b = -1 compared to the Y/b = 2 position, with an average lift coefficient of 0.702 from all configurations. This small, yet evident, increase in lift for the leading wing is caused by some upstream influences of the trailing wing when there is overlap. Another note to make is that when the wings are at two wingspans apart there is still some influence in lift on the trailing wing, an increase of 0.05%. This indicates that the analysis of a couple additional cases of increased separation could have been conducted until there was a zero percent difference, but for the purpose of this report the author deemed this unnecessary. As the wingtip spacing decreases the lift increases gradually and then, once overlap occurs, lift spikes up topping out at Y/b = -0.185. At this point there is an increase in lift of 5.89% for the following wing compared to the leading wing. After this peak as the wing overlap increases the lift for the trailing wing decreases slowly and then drastically to the point where, when there is complete overlap, there is a 19.61% reduction of lift due to the wake induced by the leading wing. The hypothesis going into this study was that the best position for a wing with the BSLD would be the wingtip to vortex configuration at Y/b = -0.148, but when it comes to lift the results conclude that with an increased overlap of 3.7% is marginally better (at Y/b = -0.185).

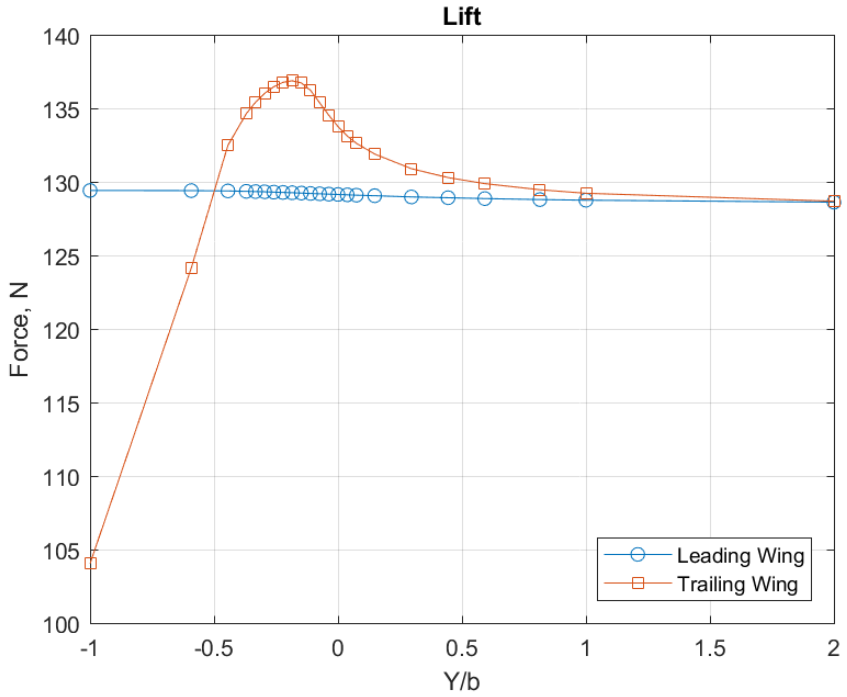

Figure 5.3: Lift comparison between the leading and trailing wings

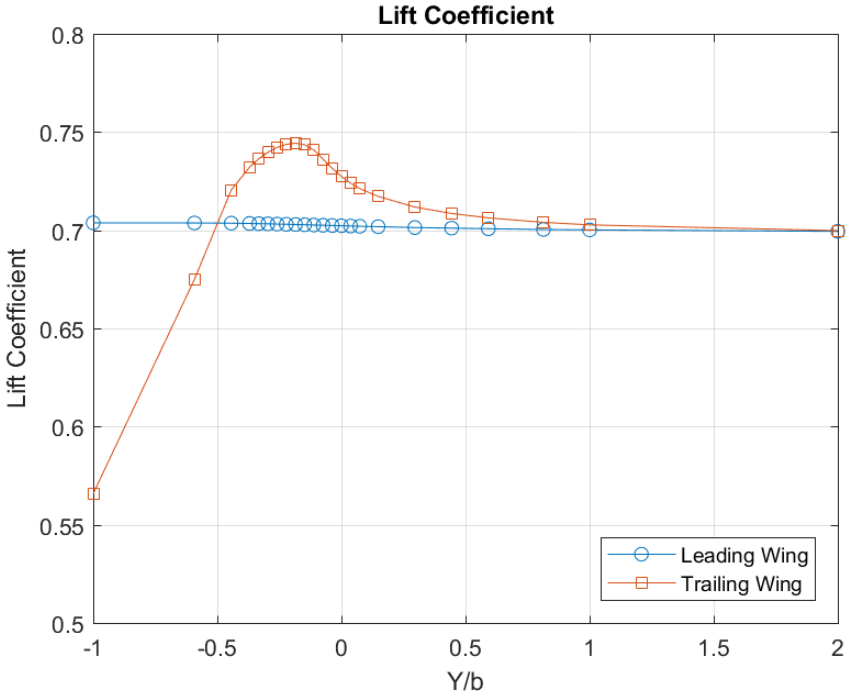

Figure 5.4: Lift coefficient comparison between the leading and trailing wings

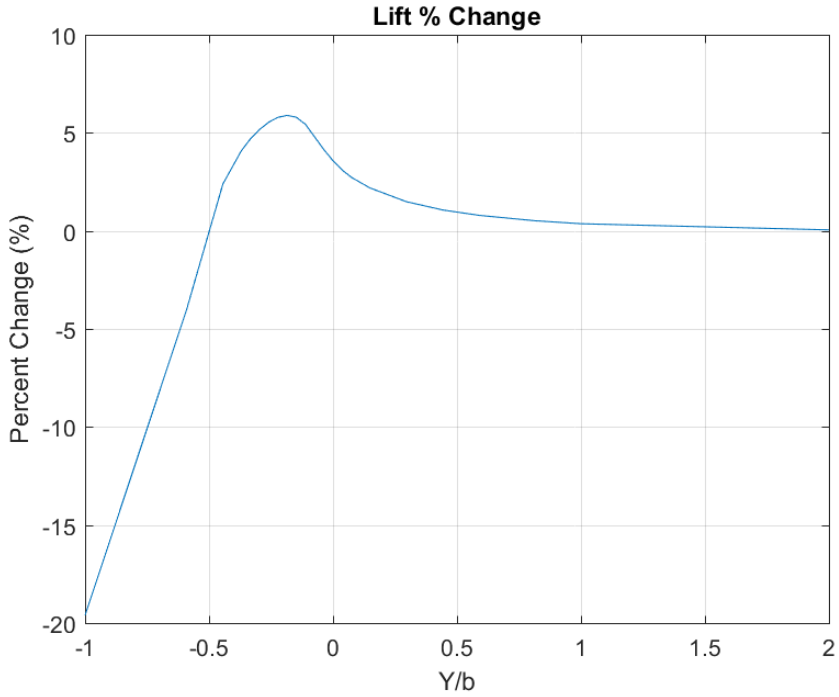

Figure 5.5: Percent change in lift of the trailing wing compared to the leading wing

5.2.2. Drag

The total drag output from STAR-CCM+ for both wings is plotted in Figure 5.6. Figure 5.7 plots the comparison of the total drag coefficient of the leading and trailing wings as calculated by Equations 5.6 and 5.7 respectively. The total drag percent change for the following wing as compared to the leading wing is plotted in Figure 5.8 as computed by Equation 5.8. When looking at these graphs the impression is that they are almost the inverse of lift shown in Figure 5.5. Like lift, there is a discrepancy between the leading and trailing wing at Y/b = 2, here with a change of 1.38% less drag for the following wing. This again indicates that there are still some benefits even at the Y/b = 2 position and that more separation would be required for the trailing wing to see no drag reduction. The average total drag coefficient for the leading wing is 0.031 across all 23 cases. As the wingtip separation decreases the total drag for the trailing wing gradually, then more rapidly, declines. The lowest drag for the wing is then seen at Y/b = -0.259. This optimal location sees an additional 11.1% overlap than the hypothesized position at Y/b = -0.148, showing that there is an

increased benefit for drag further inboard. At this optimal position there is a total drag reduction of 17.69% for the trailing wing (as seen in Figure 5.8). The total drag coefficient here decreased from 0.031 for the leading wing to 0.025 for the trailing wing. Figure 5.8 for percent change displays a small hiccup at the Y/b = 0.148 and the reason behind this is unknown and may just be an artifact from the simulation. When the trailing wing moves laterally to a complete overlap the drag rapidly increases to the point where there is an increase in drag of 35.60%. As for the leading wing, it does see some benefits as well when there is overlap. The total drag decreases by 1.38% from the Y/b = 2 to Y/b = -1.

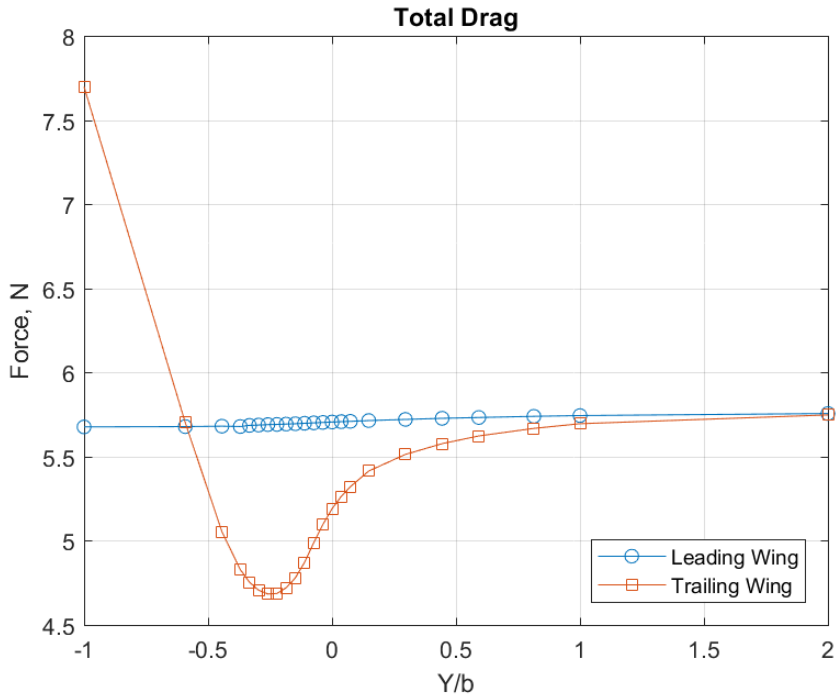

Figure 5.6: Total drag comparison between the leading and trailing wings

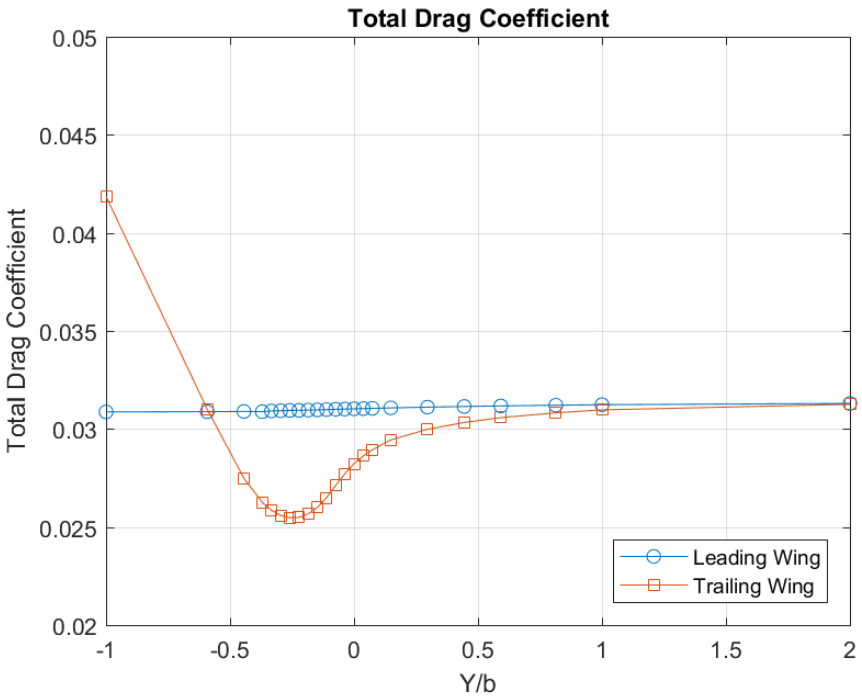

Figure 5.7: Total drag coefficient comparison between the leading and trailing wings

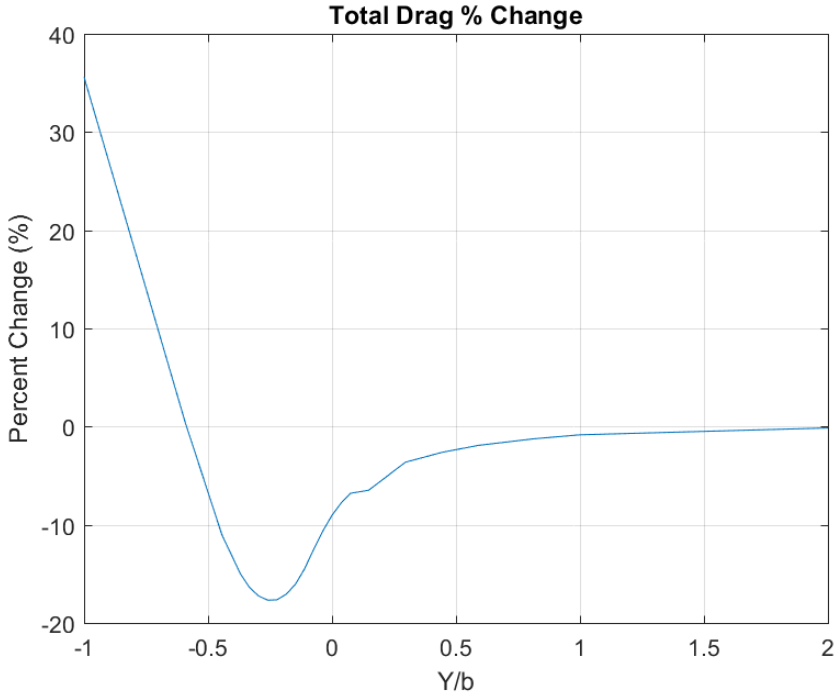

Figure 5.8: Percent change in total drag of the trailing wing compared to the leading wing

5.2.3. Lift-to-Drag Ratio

With the lift and total drag analyzed a comparison of the lift-to-drag ratio was examined. As both lift and drag are aerodynamic forces, this ratio is considered a good indication of the aerodynamic efficiency of an aircraft. Figure 5.9 plots the lift over drag as calculated by Equations 5.9 and 5.10 for the leading and trailing wings respectively, while Figure 5.10 plots the percent change of the lift-to-drag ratio for the trailing wing as compared to the leading (as determined via Equation 5.11). The average lift-to-drag ratio for the leading wing is 22.64 with a S.D. of 0.125 for the 23 analyzed cases. The peak increase in the lift over drag ratio occurs at Y/b = -0.222. This is halfway between the beneficial lift increase location at Y/b = -0.185 and drag reduction at Y/b = -0.259. At this positioning, the trailing wing's lift-to-drag ratio increases by 28.47%. With complete overlap the trailing wing sees a reduction in L/D by 40.72%. Like lift and drag, there is still a slight difference for this aerodynamic parameter for the two-wingspan separated case, an increase of 0.21%.

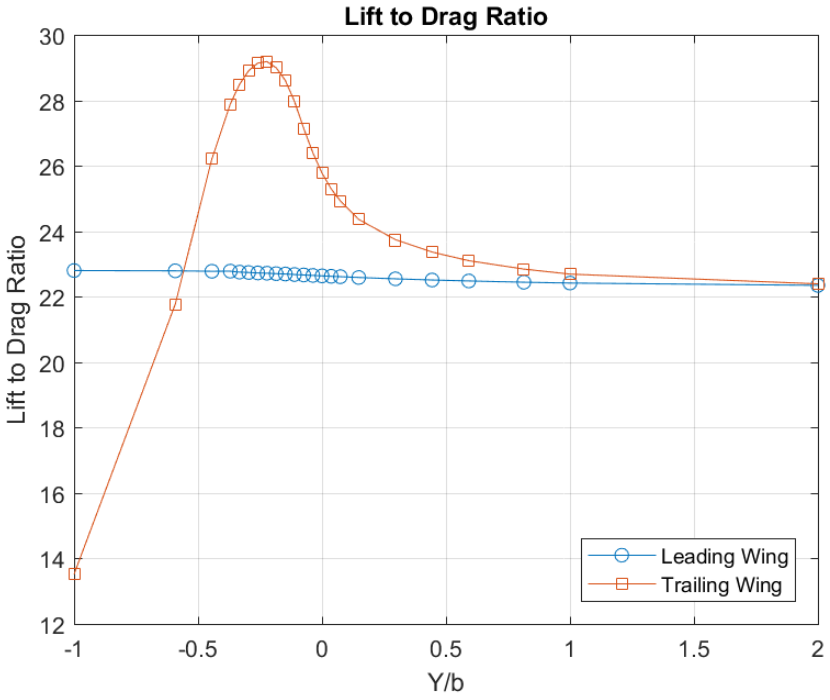

Figure 5.9: Lift-to-drag ratio comparison between the leading and trailing wings

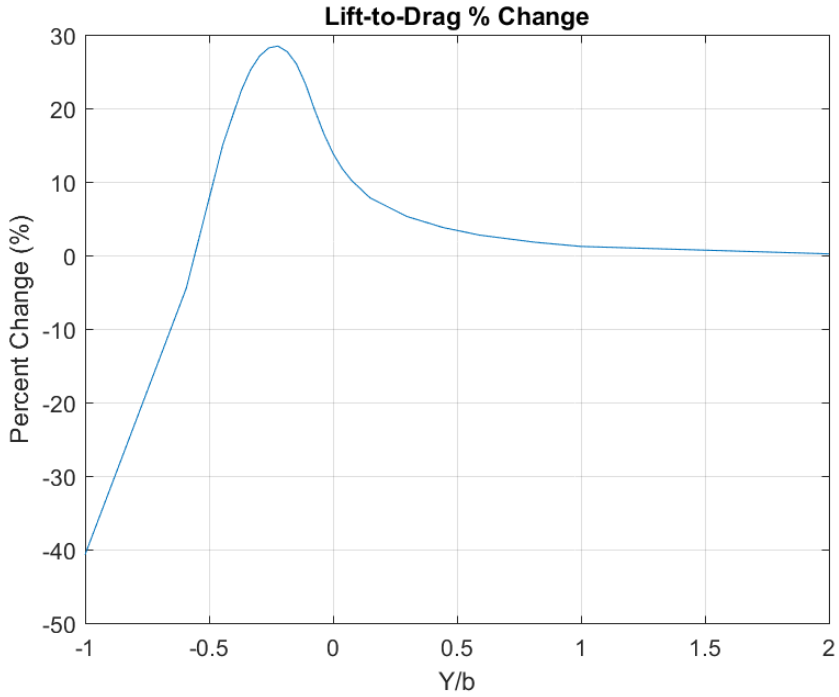

Figure 5.10: Percent change of the lift-to-drag ratio of the trailing wing compared to the leading wing

5.2.4. Skin Friction and Pressure Drag

The two subcomponents of drag, skin friction and pressure drag, which were direct outputs from STAR-CCM+ were also analyzed. Combined, when added together, they sum up to the total drag. Table 5.3 displays the percent of total drag each subcomponent makes up for the two wings. For the leading wing the skin friction drag makes up on average 34.91% of the total drag, while for the pressure drag it is around 65.09%. For both parameters there is a S.D. of 0.125%. For the trailing wing cases, except for the Y/b = -0.59 and Y/b = -1 cases, the percentage skin friction drag increased while the pressure drag decreased. The largest difference occurred at Y/b = -0.222 with a change in the components of total drag by ± 6.84% as the skin friction drag became more prominent.

Table 5.3: Percentage of Total Drag for Skin Friction and Pressure Drags

	Leading Wing		Trailing Wing		Difference	
Wing Spacing, Y/b	**Skin Friction Drag (%)**	**Pressure Drag (%)**	**Skin Friction Drag (%)**	**Pressure Drag (%)**	**Skin Friction Drag (%)**	**Pressure Drag (%)**
-1.000	35.06	64.94	26.67	73.33	- 8.39	+ 8.39
-0.592	35.05	64.95	34.82	65.18	- 0.23	+ 0.23
-0.444	35.04	64.96	38.95	61.05	+ 3.91	- 3.91
-0.370	35.10	64.90	40.63	59.37	+ 5.53	- 5.53
-0.333	35.01	64.99	41.22	58.78	+ 6.21	- 6.21
-0.296	35.00	65.00	41.61	58.39	+ 6.61	- 6.61
-0.259	35.00	65.00	41.79	58.21	+ 6.79	- 6.79
-0.222	34.98	65.02	41.82	58.18	+ 6.84	- 6.84
-0.185	34.97	65.03	41.53	58.47	+ 6.56	- 6.56
-0.148	34.96	65.04	41.09	58.91	+ 6.13	- 6.13
-0.111	34.94	65.06	40.40	59.60	+ 5.46	- 5.46
-0.074	34.93	65.07	39.53	60.47	+ 4.60	- 4.60
-0.037	34.92	65.08	38.75	61.25	+ 3.83	- 3.83
0.000	34.90	65.10	38.10	61.90	+ 3.20	- 3.20
0.037	34.89	65.11	37.60	62.40	+ 2.71	- 2.71
0.074	34.88	65.12	37.23	62.77	+ 2.35	- 2.35
0.148	34.85	65.15	36.64	63.36	+ 1.78	- 1.78
0.296	34.81	65.19	36.02	63.98	+ 1.21	- 1.21
0.444	34.78	65.22	35.67	64.33	+ 0.89	- 0.89
0.592	34.75	65.25	35.38	64.62	+ 0.62	- 0.62
0.814	34.71	65.29	35.12	64.88	+ 0.40	- 0.40
1.000	34.69	65.31	35.07	64.93	+ 0.38	- 0.38
2.000	34.62	65.38	34.67	65.33	+ 0.04	- 0.04

The forces in newtons of the pressure drag and skin friction drag outputs from STAR-CCM+ for both wings are plotted in Figures 5.11 and 5.13 respectively. Figures 5.12 and 5.14 plot the percent change for the trailing wing compared to the leading wing for these two drag components as calculated using Equations 5.12 and 5.13. The plots follow the same trends as the total drag plots. Key to point out is that again the best location for the trailing wing for a reduction in drag is at Y/b = -0.259. At this position the wing sees a decrease in skin friction drag of 1.72% and pressure drag of 26.29%. The greater decrease in pressure drag shows why the skin friction drag becomes more prominent in Table 5.3. Of all the plots created in this report, the results in Figure 5.14 seem

the most scattered, although a smooth curve can be visually drawn skipping a few of the outlying points. These skewed points can be seen in the skin friction drag of the leading wing at Y/b = -0.259 and Y/b = -0.370 as well as the trailing wing at Y/b = -0.370 in Figure 5.13. These three cases were run again in STAR-CCM+ after remeshing with very little change and it was determined that some artifact was causing the distorted results. As the error was between 0.15 and 0.30% for these forces no further investigation was pursued. For an overall view of the drag forces Figure 5.15 plots the total drag, skin friction drag, and pressure drag of each wing. This plot indicates how the reduction in pressure drag from a loss in surface loading is the primary reason there is a reduction in total drag for the trailing wing.

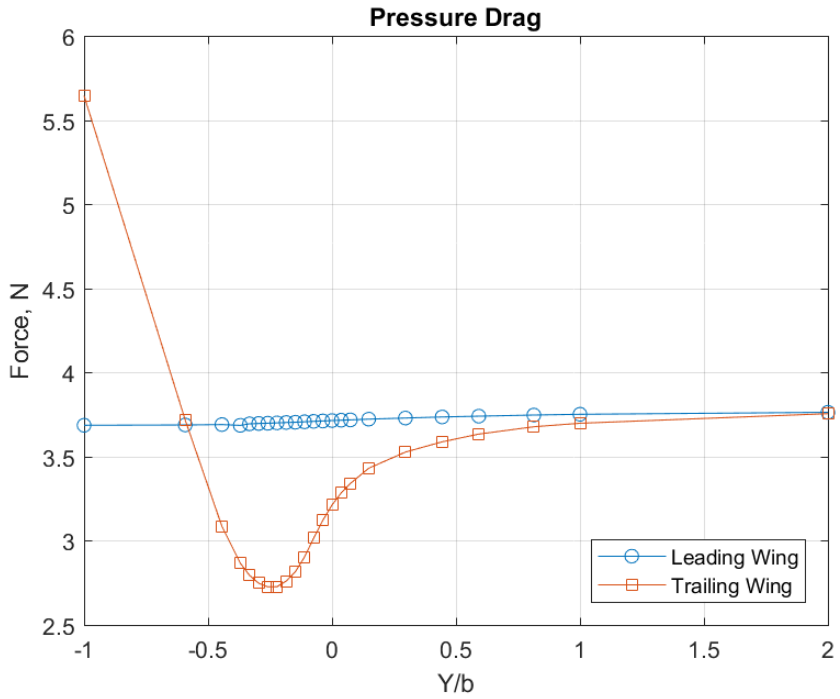

Figure 5.11: Pressure drag comparison between the leading and trailing wings

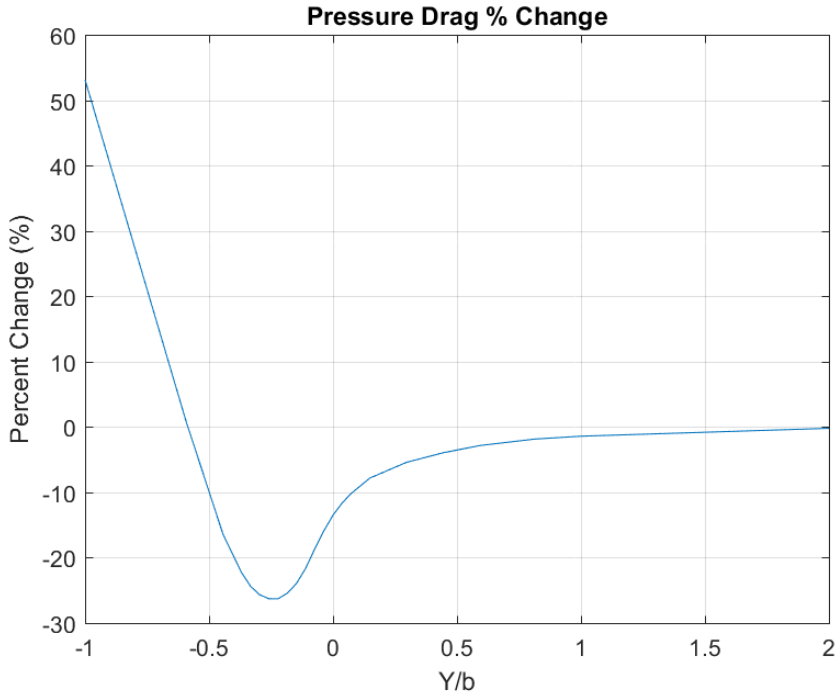

Figure 5.12: Percent change in pressure drag of the trailing wing compared to the leading wing

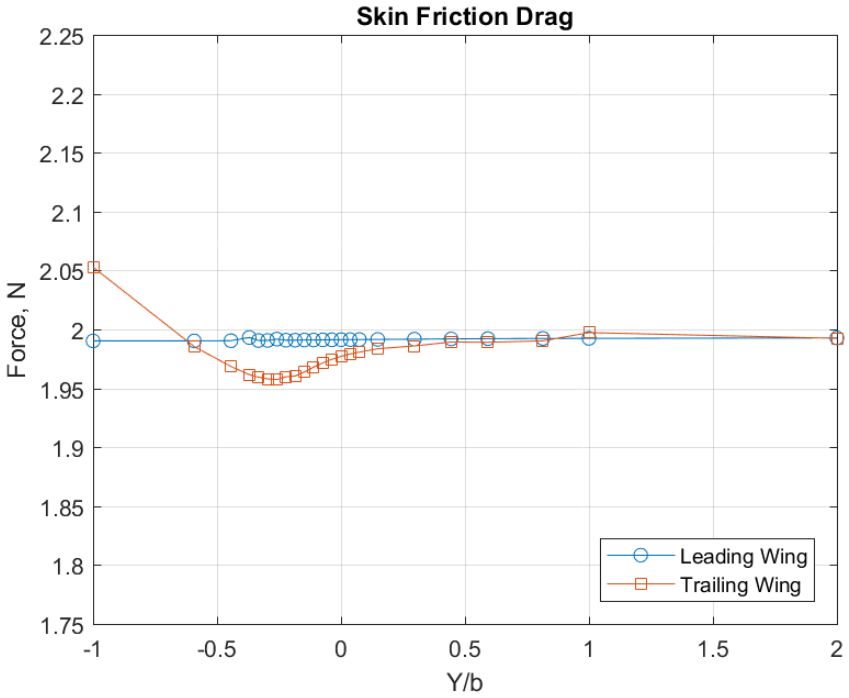

Figure 5.13: Skin friction drag comparison between the leading and trailing wings

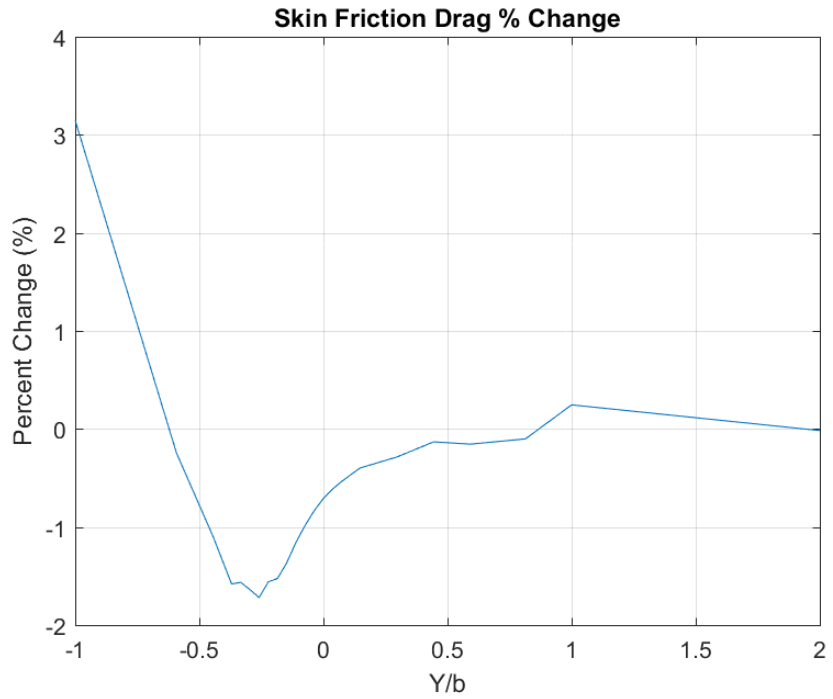

Figure 5.14: Percent change in skin friction drag of the trailing wing compared to the leading wing

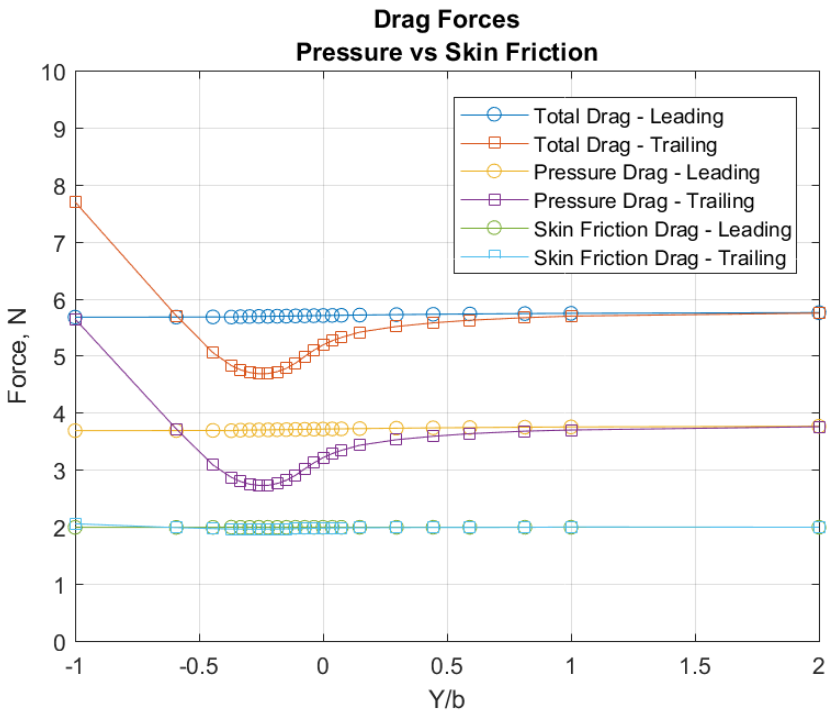

Figure 5.15: Total drag, pressure drag, and skin friction drag for the leading and trailing wings

5.2.5. Results Summary

The subsections above discussed the simulation results based on several monitored parameters. The results focused on the changes to the parameters due to the gained efficiency of formation flight. They are reported for both the leading wing and the trailing wing.

The baseline for comparison is the Y/b = 2 position separation for the trailing wing where it is expected that there is little formation effect. However, some effect was calculated, reflected from the leading wing and its turbulence. It was concluded that additional points further apart may have found an unchanged baseline. This location saw an improvement on lift of +0.05%, on total drag of -1.38%, and on the lift/drag ratio of +0.21%. These are minimal but noticeable values, but they made no difference in the conclusions and so were accepted.

The leading wing also saw changes in parameters due to effects from the trailing wing. The figures in the section plot the leading wing values. They show small changes (such as +0.62% for lift), but they are not significant. All values can be reviewed in tables in Appendix F if desired.

The parameters for the trailing wing, when plotted, have similar graphical representations. They are near flatline out at Y/b = 2.00 and 1.00, then they slope up continuously to a rounded crest (or mirrored trough), a rough positioned top, and a steep dive to negative values. The Y/b = 2.00 point is baseline for comparison on efficiency gains. Table 5.4 summarizes the positions at the crest for each basic parameter, as well as the change from the baseline value.

Table 5.4: Optimal Prandtl-D Position for Various Aerodynamic Parameters

Aerodynamic Parameter	Wing Spacing, Y/b	Percent Difference, %
Lift	-0.185	5.89
Total Drag	-0.259	-17.69
Lift-to-Drag Ratio	-0.222	28.47

One of the original expectations of this study was that the optimal position would be where the trailing wingtip lines up with the leading wing vortex, at Y/b = -0.148. But the findings shown in this table make it clear that this hypothesis needs to be revised. The vortex position is further

overlapped by 0.037b to 0.111b (at Y/b = -0.185 and -0.259 respectively) depending on the aerodynamic parameter.

The worst location for the trailing wing is directly behind the lead wing, centerline to centerline (Y/b = -1.00). The corresponding differences for the parameters are: Lift -19.61%, Total Drag +35.60%, and Lift/Drag Ratio -40.72% (see Appendix F). At this position, the trailing wing suffers from the full lead wing downwash, which overrides whatever vortex and upwash benefits there may be.

This Section 5.2 discussed the output processing procedure and emphasis. It presented the overall results in both tabular and graphical form. Additional tables are available if Appendix F. The analysis of these results is discussed further in Section 5.4 and in the Chapter 6 Conclusion.

5.3. Trefftz Plane Analysis

From the literature review into induced drag on elliptically loaded wings in Section 2.4, the average maximum induced drag reduction for the two wing system was 25.25% (averaged from [18], [19], [20], and [21]). To try to determine the reduction of induced drag for the two wing system in formation flight, as well as the induced drag on the leading wing, the Trefftz plane analysis was used. The methodology behind this approach is described in Section 2.2. For the current analysis two Trefftz planes were set up: one 6 m behind the nose of the leading wing (80% of the wingspan) and the other 7.5 m behind the nose of the trailing wing (100% of the wingspan). An array of point probes was made in STAR-CCM+ on these planes with a grid size of 1 cm by 1 cm. An attempt to increase the density of probes was made but the software would crash with anything larger than 15 million points. Even at this density outputting the X, Y, and Z velocity perturbations at each probe took a little over 5 hours for the computer to process a single case and output the file. The number of probes for the leading wing and system Trefftz planes is tabulated in Appendix G and ranged from 3.75 to 7.36 million points, varying from case to case due to the change in the domain size. There are some small discrepancies between the number of points in the

two planes due to how the grid was positioned in the domain, ie. closer to one wall for one plane thus cutting off a row of points, as per STAR-CCM+.

Once the grid was set up the velocity perturbation data for each point probe was outputted and saved as comma separated value files (.csv). This data for both planes was then processed in MATLAB using Equation 2.42 where the area for each point (dS) was 1 cm^2. The resulting output is plotted below in the figures of this section and is tabulated in Appendix G There was no S.D. from this data as only the last iteration in the simulations were analyzed after convergence to conserve computing time.

Figure 5.16 plots the far-field induced drag of the leading wing. The slope from left to right is gradual, changing only 1% between the positioning at Y/b = 2 and Y/b = -0.37, after which it declines more rapidly. As the Trefftz plane is only 1.5 m in front of the trailing wing it is concluded that the upstream affects of the lifting body reduces the velocity perturbations seen at the grid point probes and lowers the induced drag. It is also present that even at the point when the Prandtl-D wings are two spans apart that the trend sloping upwards continues, and it is hypothesized that the curve may increase a little more before the plot plateaus. Though this is the best understanding as to the induced drag of a single wing from this study, a future study with the same grid spacing for the point probes without the trailing wing may reveal more pertinent results.

$$C_{D,i} = \frac{D_i}{\frac{1}{2}\rho S {V_\infty}^2} \tag{5.14}$$

Using Equation 5.14 the induced drag coefficient was calculated as seen by the Trefftz plane behind the leading wing. Across all 23 cases the coefficient ranges from 0.01202 to 0.01244 with an average of 0.01233 and a S.D. of 0.00008. This is plotted in Figure 5.17.

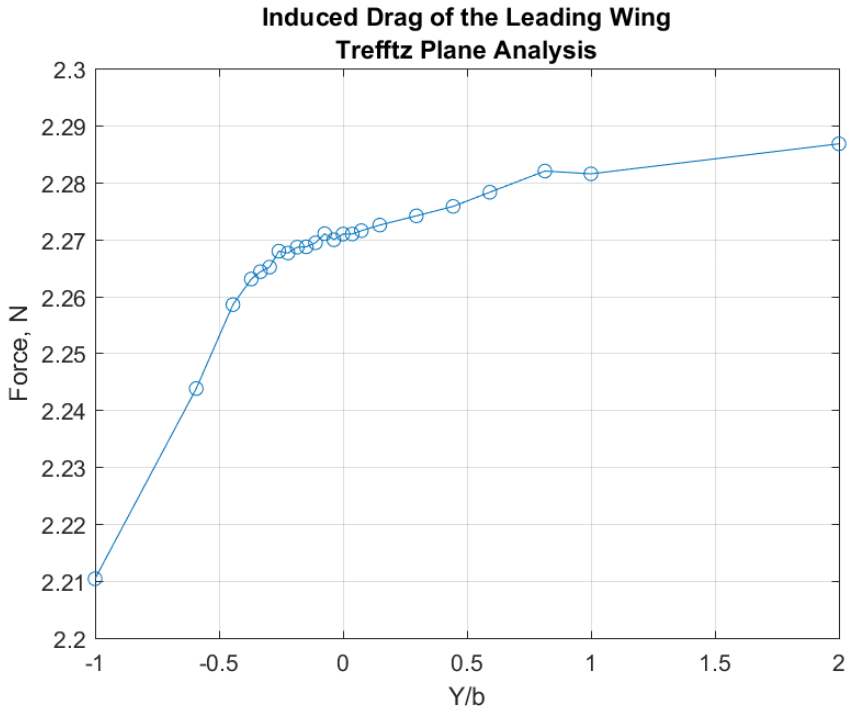

Figure 5.16: Induced drag of the leading wing using the Trefftz plane analysis

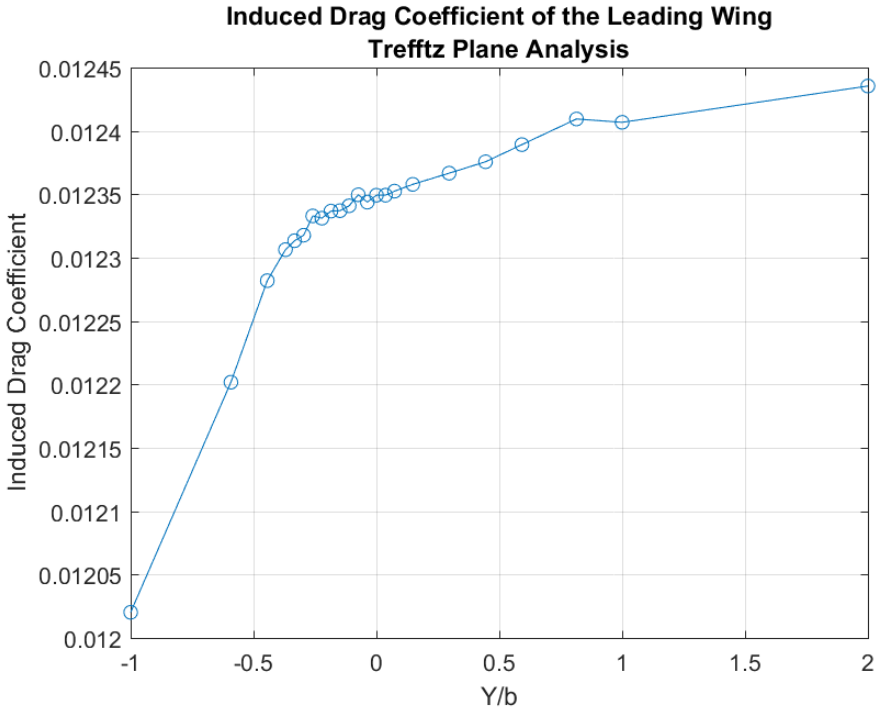

Figure 5.17: Induced drag coefficient of the leading wing using the Trefftz plane analysis

There are a few reasons caveat to this approach where 100% of the energy dissipated into the surroundings is not captured. The first, as mentioned above, is due to the proximity of the Trefftz plane to the trailing wing which reduces the drag by weakening the velocity perturbations of the leading wings wake. The second possibility is due to a restriction of the domain. Even though it was concluded during the mesh refinement stage that there was very little change on the result of the lift and total drag on the wing, an analysis was not made at this stage on the effects of the domain on the induced drag calculated by the Trefftz plane. In theory, by restricting the domain to a specific size all potential point probes outside of this boundary now read zero, when in actuality there should still be some change. If the domain were bigger and these additional points were included the induced drag would now be higher. This can be seen slightly as the slope of induced drag increases as more space is given between the two wings; a larger domain thus more accurately calculates the induced drag. The third reason can be confirmed by an early study during the analysis of the baseline configuration with a grid spacing of 5 mm by 5 mm. With the finer spacing the induced drag for this plane was found to be 2.349 N, or 3.49% more than the 1 cm by 1 cm grid spacing presented in this section. From this it is concluded that a finer grid spacing shows a more accurate representation of the far field induced drag and that this more precise value is higher than what is plotted for the Trefftz plane analysis here. As mentioned before, a finer grid size was not pursued as it was reasonable for the computational time required for this report and not significant for the conclusions. Just this one case where there are four times as many points resulted in more than 24 hours to tabulate the results into a .cvs file and would have taken an additional four weeks to output the data for all 23 cases. Even though there can be some discrepancies, it is predicted that the induced drag of the Trefftz plane analysis is close to that which Ludwig Prandtl theorized, and may be as much as 6% lower than actuality.

With the analysis of the first Trefftz plane finished the study continues to review the second plane, which captures the far field induced drag of the two wings as a system. It is impossible to distinguish how much induced drag is being produced from each individual wing using this

approach. Therefore, the coefficient of induced drag is also not calculated. It is also assumed that two of the reasons listed above, a course point probe grid and a restricted domain, also apply here and that the induced drag calculated for the system using the Trefftz plane is slightly lower than actuality. For the baseline case, the system induced drag for the finer 5 mm by 5 mm grid spacing was 5.19 percent higher. Yet, even with discrepancies the trend still holds true.

Figure 5.18 plots the far field induced drag of the system. The drag at Y/b = 2, the case with the largest separation, is 4.334 N. The lowest drag seen at Y/b = -0.259 is 3.022 N while the greatest drag occurring at Y/b = -1 is 6.514 N. This indicates that for the lowest induced drag of the system it is best to position the wings almost to the point where the vortices align. This overlap of 25.9% was also determined to be the best location for a reduction in drag for the trailing wing as an individual.

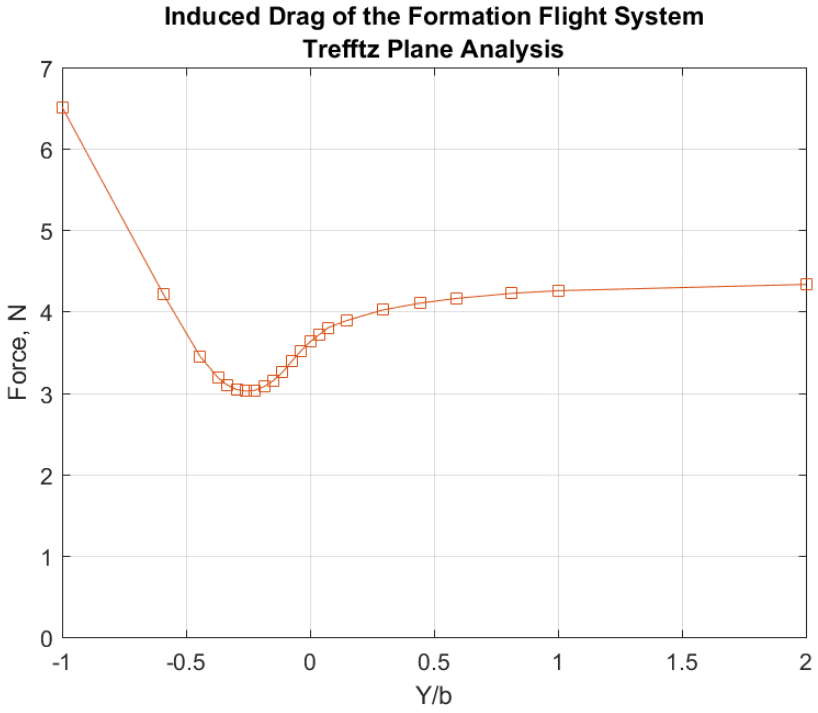

Figure 5.18: Induced drag of the two wing system using the Trefftz plane analysis

Figure 5.19 takes the far field induced drag of both the leading wing and the system and plots it on a single graph. The dotted blue line is positioned at double the induced drag of the leading wing at Y/b = 2. In theory, when the wings are far apart and there is no influence on one another

then the system induced drag should be twice that of a single wing. From this a percent difference can be calculated. Why the system drag at Y/b = 2 does not match up with this theory has a few possible reasons, namely the same ones listed above. First and foremost, if the point probe density increases so will the accuracy of the calculated induced drag value. Also, increasing the domain size and testing with a larger spacing between wings would also be of benefit to the study.

As Figure 5.20 shows, the system has a decrease of 33.93% for induced drag at Y/b = -0.259. For simplicity, the difference percentage is also calculated using the Y/b = 2 case for the system, at which the same positioning sees a reduction of 30.27% for the system. In either case, it is significantly greater than the average of 25.25% as seen for the optimal positioning of an ELD wing from the aircraft literature. So, not only does a single wing with the BSLD have an 11.11% reduction of induced drag, but as it flies in a two-wing echelon formation, the BSLD system sees a 5-9% reduction in induced drag over the elliptically loaded wing system.

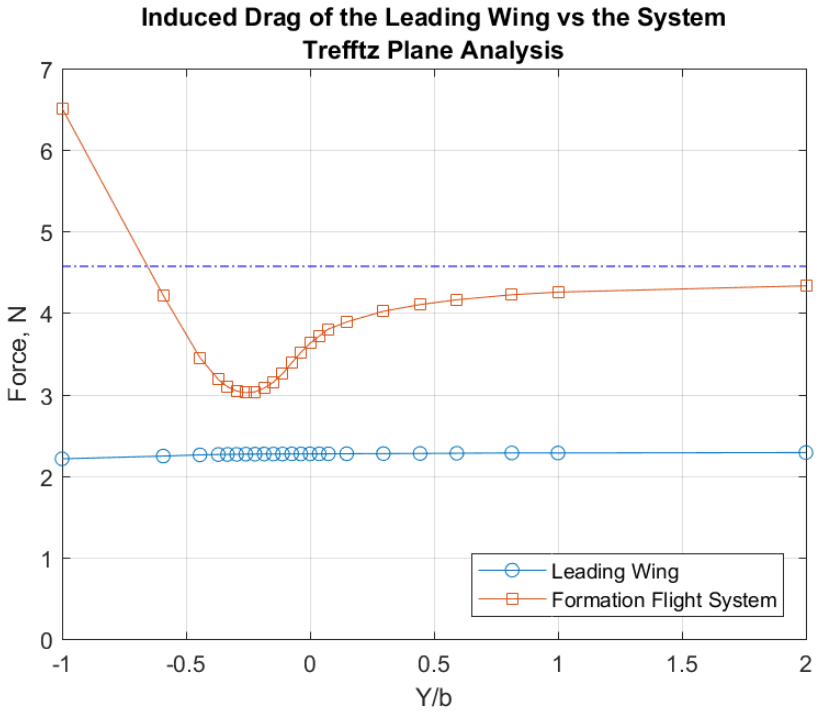

Figure 5.19: Induced drag comparison between the leading wing and the two wing system using the Trefftz plane analysis

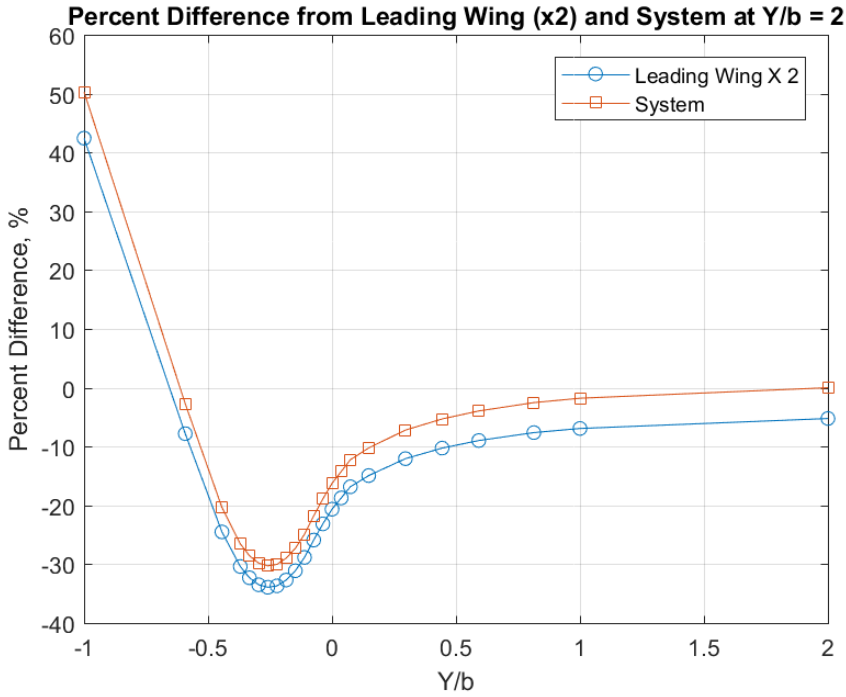

Figure 5.20: Percent difference in induced drag for the system – from double the leading wing's induced drag and from the system's induced drag at -200%

Section 5.3 presented the set up and results from several Trefftz plane analyses of the leading wing and the two-wing system. For the system induced drag reduction the same trend is found as that of the total drag of the trailing wing with the optimal wing position at Y/b = -0.259 for both.

5.4. The Optimal Wing Position and Beneficial Range

This section takes selected values from the results presented in Section 5.2 and uses them to identify the optimal trailing wing positioning as well as the beneficial range. This presentation and discussion specifically addresses one of the hypotheses of this study.

So, what is the optimal position for formation flight? It really depends on what parameter is used for the optimization, and whether it is an optimization for the system or for the trailing wing alone. Table 5.5 tabulates the optimal position and beneficial range of the trailing wing from three of the aerodynamic parameters observed in the study: lift, total drag, and the lift-to-drag ratio of as seen by the trailing wing. The table also includes the optimal position and beneficial range of the trailing wing for the best reduction of induced drag as seen by the system. With the trailing aircraft's

wingtip lined up with the leading aircraft's vortex at an overlap of 14.8% of the wingspan (Y/b = -0.148), the data indicates that an additional 3.7% overlap is preferred for maximum lift. This is presumed to be due to the fact that even though an additional overlap means the following wing sees some downwash near the wingtip, having an additional inboard portion of the wing area in the upwash field from nearer to the leading wingtip outweighs the negative effects of the weak vortex downwash. Reflect back to the study of birds in Section 2.4. There on average the various species found themselves flying at Y/b = -0.185, the same exact positioning found. This immediately suggests that the trailing bird fly in formation to benefit from feeling an increase in lift from the additional upwash from the leading bird. This is not like that of the aircraft studied that look to benefit from the greatest drag reduction.

As for total drag, having the following wing almost at the point where the two aircraft have their vortices lined up (Y/b = -0.296) sees greater results with a reduction of -17.69%. So a pilot of an aircraft in formation flight with wings matching the BSLD has to choose what the flight objectives are and whether to fly with a greater decrease in drag, saving fuel and reducing operational costs, or to fly with an increase in lift. A more ideal approach may then be to fly between the two optimal positions to allow for the best lift-to-drag ratio and increase in efficiency. Note that for the range of Y/b = -0.148 to Y/b = -0.296 there is no more than a 2.5% difference in the percent change from the optimal position for the three parameters as indicated in Table 5.6. If the maximum savings is taken in each column (shaded), significant savings can still be achieved at other positions close to the optimal. If a range is selected within 50% of the maximum values, it would be 0.41b (Y/b = +0.037 to -0.370) for Lift, 0.44b (Y/b = 0.000 to -0.444) for Drag, and 0.41 (Y/b = -0.037 to -0.444) for Lift-to-Drag Ratio. This shows that the trailing wing can wander laterally quite a lot and still see great benefit. This is also tabulated as the 50% modal in Table 5.5. Reflect back to the avian reports that show a beneficial range between 0.42b and 1.19b, averaging at 0.735b. This suggests that even though the birds have found the optimal position at Y/b = -0.185 they tend to wonder a lot more, which may be due to the stability of flight in a more complex flow field, as well

as the flexibility of a birds wing which can conform and change shape for additive benefits. This is unlike an elliptically loaded wing that has a tight region in which the trailing wing must fly (b_e = 0.25 in Table 2.4), moving out of this region greatly reduces the ELD wing's increased efficiency.

Table 5.5: Optimal Position and Beneficial Range for Various Aerodynamic Parameters for the Prandtl-D

Aerodynamic Parameter	Optimal Wing Position, Y/b	Percent Difference, %	Beneficial Range	
			Y/b	b
Lift	-0.185	5.89	-0.370 to 0.037	0.407
Total Drag	-0.259	-17.69	-0.444 to 0.000	0.444
Lift-to-Drag Ratio	-0.222	28.47	-0.444 to -0.037	0.407
System Induced Drag	-0.259	-33.93	-0.444 to 0.037	0.481

Table 5.6: Aerodynamic Parameter Percent Change Between Y/b = 0.148 and -0.444 for the Trailing Wing Compared to the Leading Wing

Wing Spacing, Y/b	Lift Percent Change, %	Total Drag Percent Change, %	Lift-to-Drag Ratio Percent Change, %	System Induced Drag Percent Change, %
0.148	2.195	-6.489	7.855	-14.939
0.074	2.734	-6.805	10.234	-16.840
0.037	3.101	-7.785	11.805	-18.746
0.000	3.576	-9.040	13.870	-20.656
-0.037	4.147	-10.645	16.555	-23.155
-0.074	4.789	-12.517	19.783	-25.907
-0.111	5.430	-14.511	23.326	-28.851
-0.148	5.797	-16.083	26.072	-31.123
-0.185	5.891	-17.090	27.718	-32.704
-0.222	5.795	-17.652	28.473	-33.696
-0.259	5.547	-17.690	28.231	-33.930
-0.296	5.176	-17.264	27.123	-33.504
-0.333	4.697	-16.387	25.216	-32.316
-0.370	4.082	-14.978	22.418	-30.396
-0.444	2.396	-11.037	15.100	-24.522

Table 5.5 also indicates the optimal wing overlap position for a reduction of induced drag for the two-wing echelon formation flight system at Y/b = -0.259 which has 11.1% more overlap from the predicted flight configuration at an overlap at Y/b =-0.148. At this optimal position, the system sees a reduction of induced drag of 33.93%. This is interesting when compared to a two-wing echelon formation of elliptically loaded wings. Table 5.7 tabulates the optimal wing spacing (Y/b_e) and system induced drag reductions of the studies reviewed in Section 2.5. The extra overlap seen

in these reports from the predicted optimal flight position at Y/b_e = -0.128, 12.8% inboard of the leading wing vortex to trailing wingtip alignment at Y/b_e = 0.0. This is nearly the same as the 11.1% vortex overlap of the Prandtl-D trailing wingtip. The similar results suggest a similar reasoning for the vortex overlap. Another comparison that can be made is the reduction in induced drag for the system. For the elliptically loaded wing there is a decrease of 25% on average while in this study it was found that the BSLD wing had a comparable reduction at 34%.

Table 5.7: Optimal Elliptical Wing Position and Reduction in System Induced Drag from Various Studies

Report Author	Wing Spacing, Y/b_e	System induced drag reduction, %
Ning [18]	-0.15	-30.0
Shin [19]	Not listed	-26.0
Blake [20]	-0.15	-25.0
Vachon [21]	-0.13	-20.0
Hansen [22]	-0.13	Not listed
Frazier [23]	-0.11	Not listed
Kless [24]	-0.10	Not listed
Average	-0.128	-25.25

Figure 5.21 plots the percent change of the lift, total drag, L/D, and system induced drag for the Prandtl-D wing on a plot of a non-dimensional index vs wing overlap percent. This shows the optimal flight position of the two aircraft. Some data manipulation was performed to create this plot. First, the total drag percent change trend was inverted so that the low point became a peak. The percentages across all the parameters were then scaled down so that the peaks of each data set were at the same value and that the lowest point in each data set right of the peaks were at the same value. To do this Equation 5.15 was used where x was the point at the peak, y was the lowest point left of the peak, z was the point being scaled, and Z' is the repositioned point. In general the curves all follow a similar trend, though it should be pointed out that the peak for lift is further right (outboard) than the others and the slope left (inboard) of this peak is steeper as there is a greater impact on lift when the trailing wing is behind the leading wing.

$$Z' = \frac{(z - y)}{(x - y)} \tag{5.15}$$

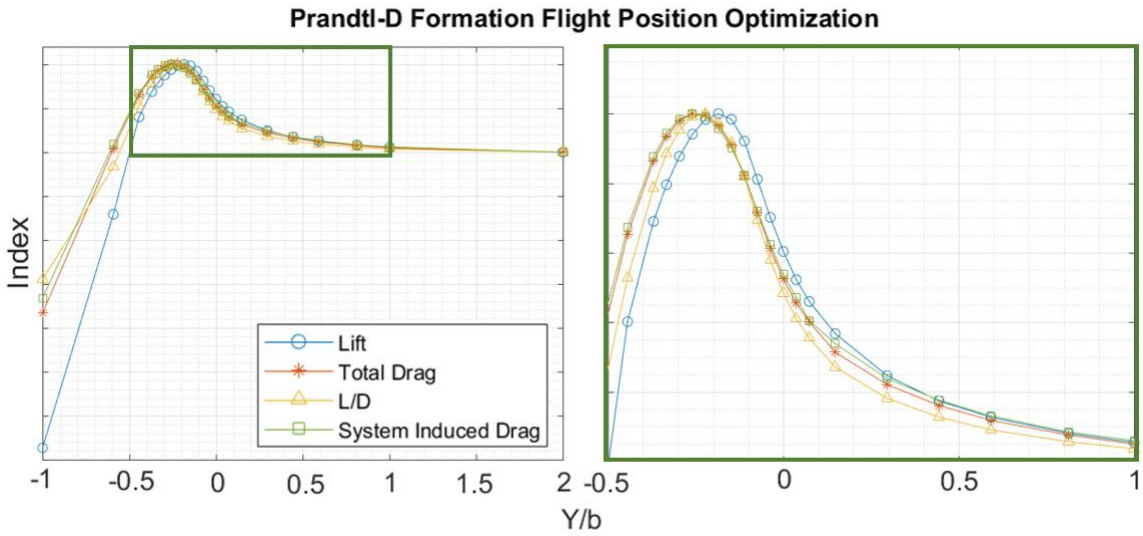

Figure 5.21: Wing positions for optimization of key aerodynamic parameters

This data manipulation was done in preparation for a comparison of the Prandtl-D wing to birds in formation flight. As indicated in the literary review it is determined that birds in formation flight seek out the greatest upwash. This statement indicates that birds fly with the benefit of lift in mind and may not directly sense how much drag reduction they get; let alone how much reduction the group of birds get. To test this theory and to compare the results of this study to the analysis of bird formations, Figure 5.22 was produced. To create this, the flight positioning frequency data published by Hainsworth [13], Speakman & Banks [15], and Portugal [16] was scaled and converted to a new coordinate system (Section 2.4). This data in their original form is seen in Figures 2.13, 2.15, and 2.16. Note that there are error bars for the geese data provided from histograms. First using a web-based tool, the data was extracted from the plots. Then the x-axes were converted to Y/b. The method used to find Y/b depends on how the data was presented in its original form. As most data sets were plotted with wingtip spacing (WTS) on the x-axis Equation 5.16 is used. For Portugal's data which was plotted with the distance to the side of the center of the leading wing, Equation 5.17 was used where 'Distance' was the provided X location. The span (b)

of the birds for these calculations follows as 1.5 m for Canadian geese [13], 1.439 m for Greylag geese [15], and 1.2 m for ibises [16]. After modifying the x-axis, the frequency data sets were scaled on the y-axis as well, following the same method approach to produce Figure 5.21 using Equation 5.15. The data before and after manipulation is tabulated in Appendix D. Data for the change in lift and change in lift-to-drag ratio of the Prandtl-D wing as discovered in this study are plotted together with the formation flight data of the birds for comparison.

$$Y/b = \frac{b + WTS}{b} - 1 \tag{5.16}$$

$$Y/b = -\frac{b - Distance}{b} \tag{5.17}$$

It is quite evident reviewing the plot that there is a strong correlation between the location data of birds in formation flight and lift optimization for the Prandtl-D wing. This is a clear indication that birds fly positioning themselves to seek out the maximum upwash from the leading bird. The wide range of trailing bird frequency of position matches closely with the wide range of high lift benefits provided by bell-shaped loading. It further demonstrates why, as discussed in Bowers article [2], the BSLD methodology should be used when studying the flight of birds. It also graphically explains the observational positioning data collected for the bird formation studies without resorting to hypothetical explanations. These results are further discussed in the conclusions in Chapter 6.

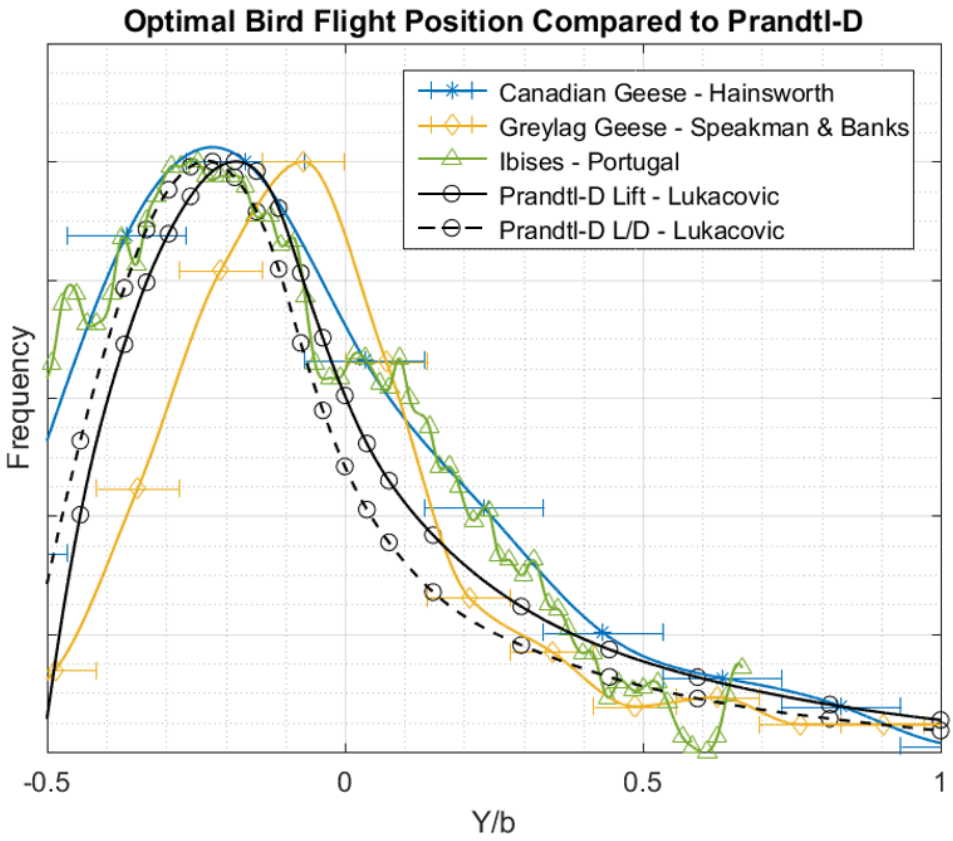

Figure 5.22: Frequency distribution of following bird positions from data sets collected by Hainsworth [13], Speakman & Banks [15], and Portugal [16] overlaid with the optimal Lift and L/D positions of the Prandtl-D wing

5.5. Pressure Profile Data

This section presents additional studies performed to identify the changes in parameter values along the full trailing wingspan at different lateral positions. This highlights the skewed effects of beneficial forces on the wing.

With the bulk of the analysis complete an additional investigation was done to examine the effects of the lateral movement of the trailing wing has on the lift distribution and local lift coefficient distribution. The method of creating these distributions, as mentioned in Section 4.5, was applied to both the leading and trailing wing. Additional plots for this section can be found in Appendix I for all cases while only a select few are presented in the following figures.

Figure 5.23 shows the lift distribution of the leading and trailing wing as compared to the theory of a selected six cases. For the leading wing, the spanload does not change across the 23 cases and there is no difference in the loading between the right and left side of the wing (Figure 5.24). As for the trailing wing there is some noticeable change and progression through the 23 cases. Though the total lift of the trailing wing is 19.6% less than the leading wing with a 100% wing overlap, when comparing to the local lift force at the center of the wing, the trailing wing sees higher loading at the wingtips from about 70% of the semispan and outwards. This additional lift towards the wingtip of the trailing wing is from the updraft of the leading wing and it is direct evidence of the location of the vortex core at .704 of the semispan. As the trailing wing is directly behind the leading wing there is no evident change between the loading on the left and right sides of the trailing wing, as evident in Figure 5.25(a). This updraft region from the leading wing can be seen on the right side of the trailing wing up in cases less than Y/b = 0.592 and slowly transitions from the center of the trailing toward the wingtip, Figure 5.25(b) through Figure 5.25(e). For the Y/b = -0.296 wing overlap case, the vortices of the leading and trailing wing line up, which can be seen in Figure 5.23(b) as the loading on the right side of the trailing wing crosses from being more to less than the leading wing at 0.704 due to the upwash and downwash effect. The vortex core of the leading wing moves to 0.852 for the right side of the trailing wing at Y/b =-0.148, Figure 5.23(c), then further out to 1 at the 0% wing overlap case, Figure 5.23(d).

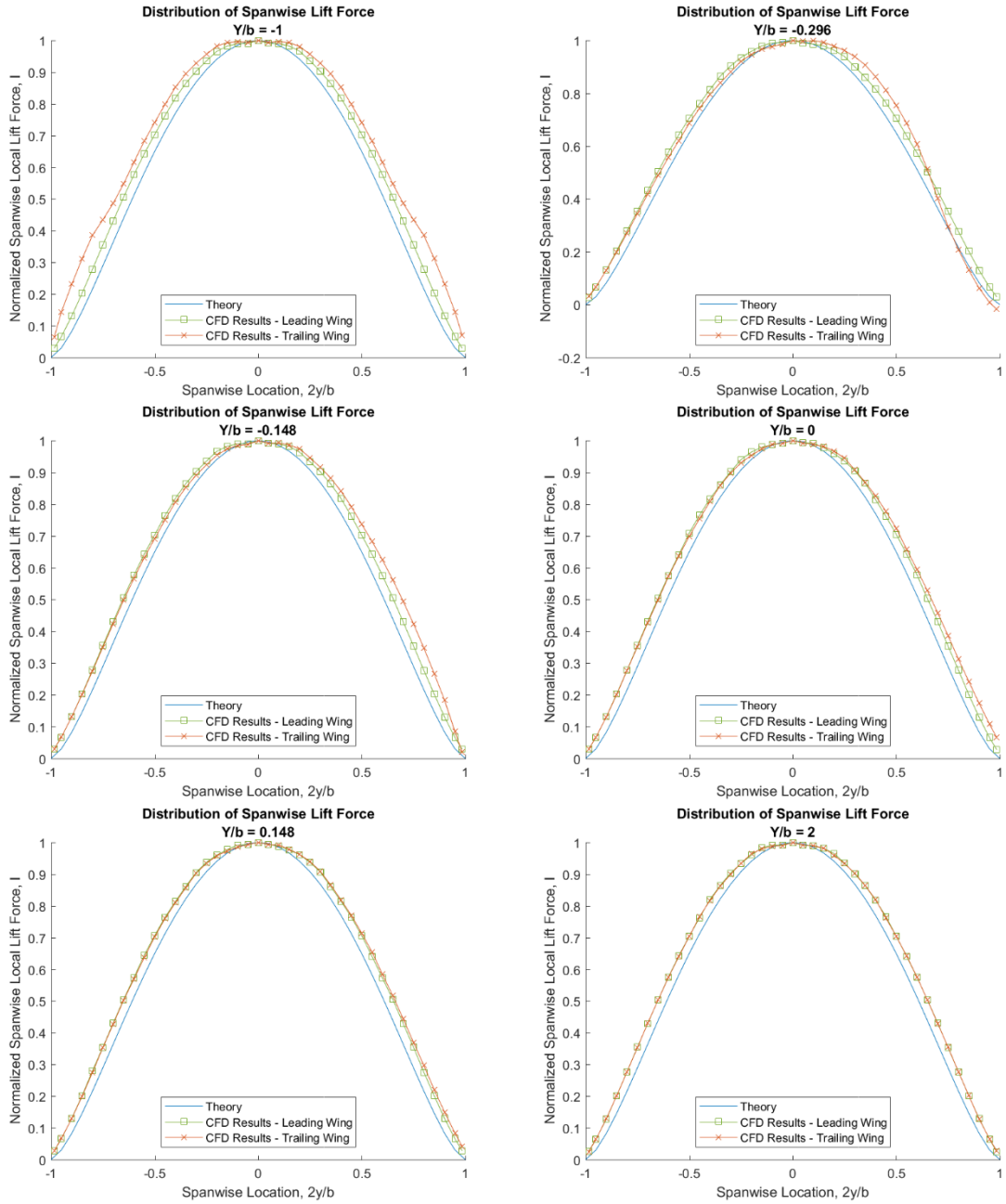

Figure 5.23: Lift distribution of leading and trailing wing compared to the theory for the Y/b = (a) -1, (b) -0.296, (c) -0.148, (d) 0, (e) 0.148, and (f) 2 cases

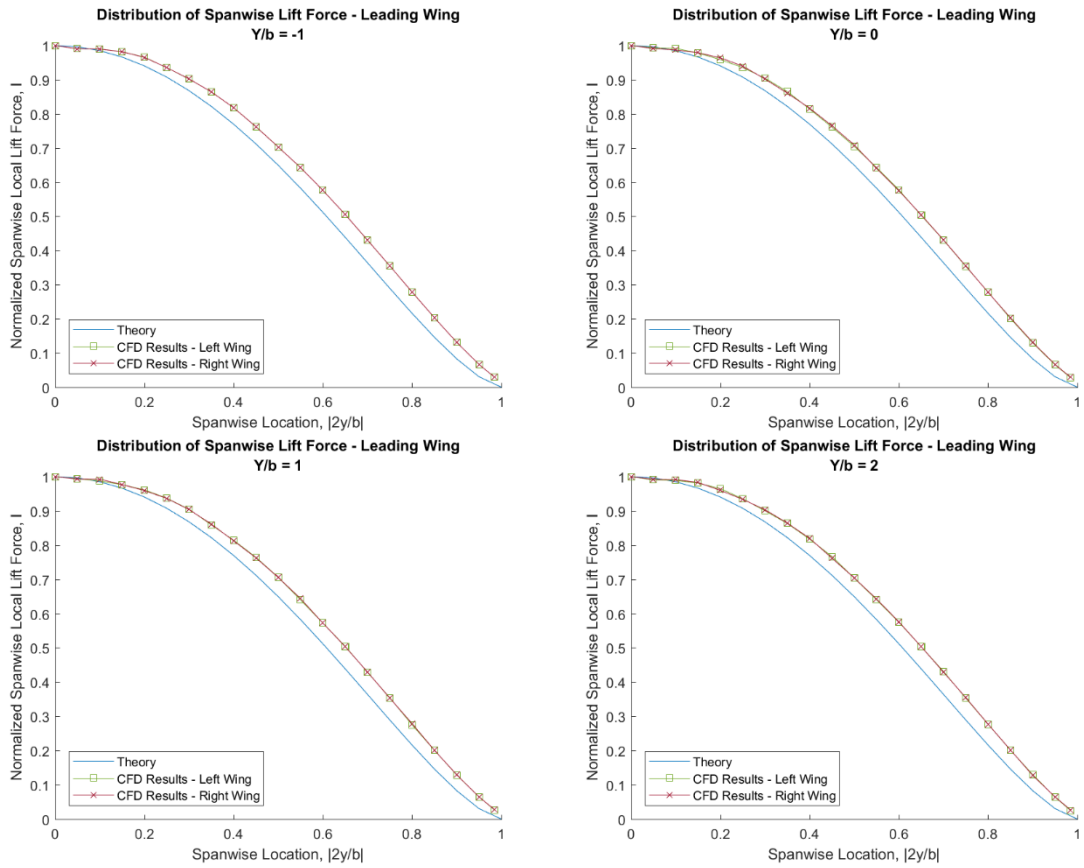

Figure 5.24: Lift distribution of the left and right side of the leading wing compared to the theory for the Y/b = (a) -1, (b) 0, (c) 1, and (d) 2 cases

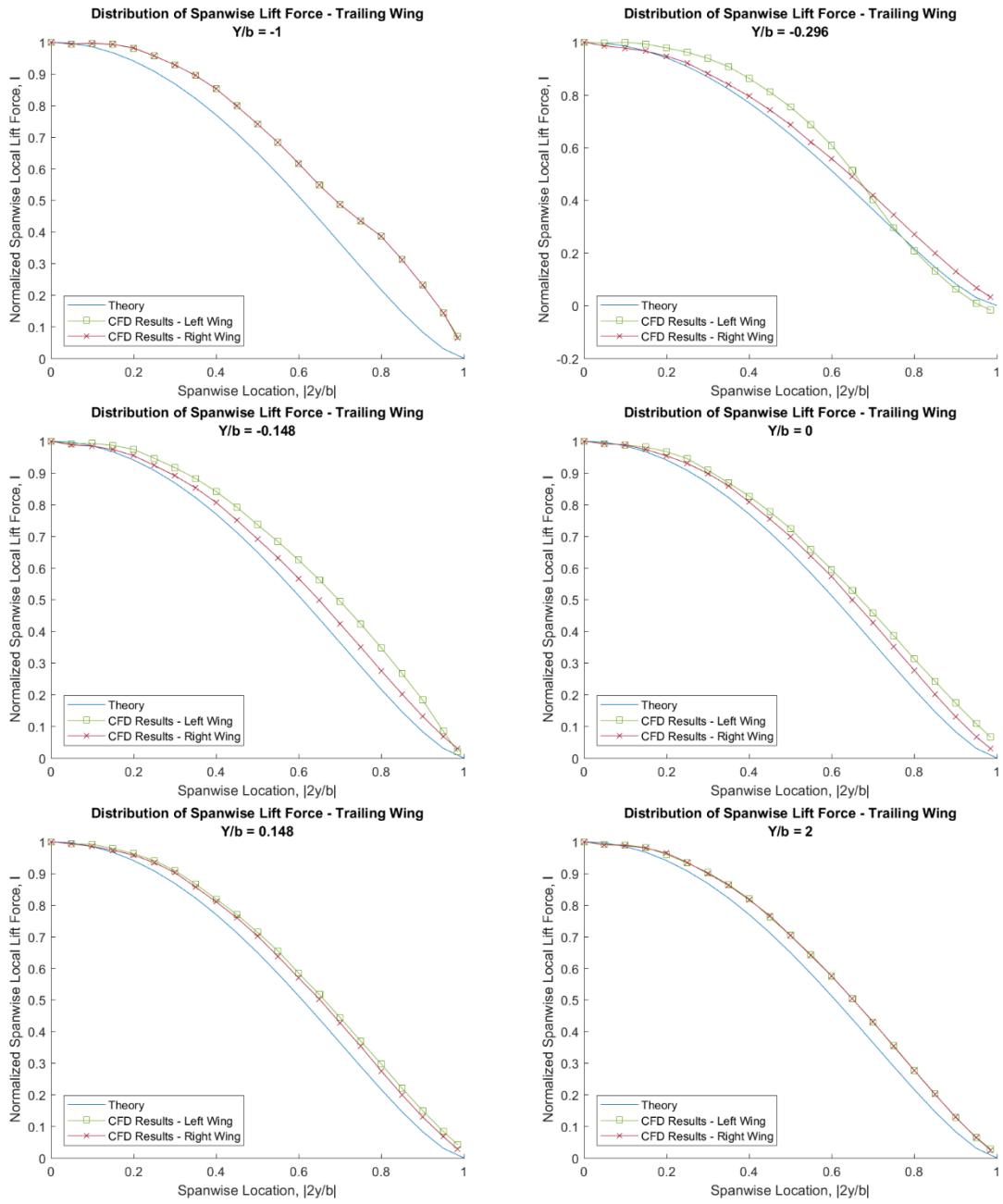

Figure 5.25: Lift distribution of the left and right side of the trailing wing compared to the theory for the Y/b = (a) -1, (b) -0.296, (c) -0.148, (d) 0, (e) 0.148, and (f) -2 cases

Chapter 6

CONCLUSION

This study furthers the analysis of the bell-shape lift distribution (BSLD) method for wing design. Using the dimension parameters of the NASA experimental aircraft known as the Prandtl-D (published 2016 by Bowers and Murillo [2]), this study used CFD modeling to demonstrate the benefits of formation flight of the BSLD wing.

Several hypotheses have been presented for this study. The analyses have bourne out some of these and have modified and enhanced others. The expectations for this thesis were: (1) Formation flight of the BSLD wing is highly beneficial; (2) The trailing wing benefits most when its tip is aligned with the leading wing vortex; (3) Bird formation flight is better modeled using BSLD rather than elliptical lift distribution (ELD). The findings and conclusions for these hypotheses are discussed in the following paragraphs.

Note that since no new lab or field observations were performed for this study, and since little has been published directly on the flight of such airfoils and nothing at all on formation flight, this report relies on observation data collected and published by others on bird formation flight to validate some of the study conclusions.

6.1. The Bell-Shaped Lift Distribution Benefits

The study confirmed that formation flight of the BSLD wing is highly beneficial for a two-wing system. Within the parameters of wing design, relative velocity, and X and Z axis positions, the CFD modeling resulted in an increased L/D ratio of 28.5% and a reduced system induced drag of 33.9% (see Table 6.1). Note that this is not a direct comparison to the ELD wing formation efficiency savings, but literature research of studies of aircraft in differing configurations reported comparable induced drag reduction of 20-30% (see Subsection 2.5.1).

Table 6.1: Optimal Prandtl-D Position for Various Aerodynamic Parameters

Aerodynamic Parameter	Wing Spacing, Y/b	Percent Difference, %
Lift	-0.185	5.891
Total Drag	-0.259	-17.690
Lift-to-Drag Ratio	-0.222	28.473
System Induced Drag	-0.259	-33.930

6.2. The Optimal Wing Position and Beneficial Range

The expectation that the trailing wing benefits most when its tip is aligned with the leading wing vortex proved incorrect to a degree. It was found through CFD modeling of the BSLD wing as well as in the aircraft literature review for ELD that the optimal position has the trailing wing partially overlapping the vortex position. When considering the induced drag parameter, for example, the optimal position for the BSLD wing is Y/b = -0.259 whereas the vortex originates from the -0.148 position, for an overlap of 0.11b. The aircraft literature review provides a confirming comparison (Subsection 2.5.2). The ELD design aircraft wings showed an average optimal position at Y/b_e = -0.128 where the vortex is at the wingtip (Y/b_e = 0.00). The reason for this partial overlap of the vortex was not part of this study, but it is hypothesized that the overlap exposed more of the higher loaded wing area to the beneficial upwash of the vortex than it exposed to the downwash.

An additional finding of this study concerns the wide range of beneficial positioning presented by the BSLD design. Take Table 5.5 for the four parameters analyzed, when a range is selected within 50% of the maximum values, the range was identified as between 0.407b and 0.481b. This wide range of beneficial positioning of 0.407b (41% of the full wingspan) or greater was not originally anticipated. But the literature search on aircraft in formation flight emphasized the importance of this range. Some of the aircraft studies noted savings in induced drag and the associated ranges. The average range for these ELD wings was a narrower $0.25b_e$ (Subsections 2.5.3 and 2.5.5). This shows a definitive difference between the distribution methods. This difference can be ascribed to the wider vortex created by a BSLD design, and therefore the wider

range of beneficial positioning available to the trailing wing. This is discussed further under Vortices below (Section 6.4). Tables 2.3, 2.4, and 5.5 are consolidated in Table 6.2 for the optimal position and range from this report and from the literature review.

Table 6.2: Optimal Position and Beneficial Range from Avian, ELD, and BSLD research

	Optimal Position, Y/b (Y/b_e)	Beneficial Range, b (b_e)
Avian Flight (BSLD – Lift)	-0.185	0.735
ELD - System Induced Drag	-0.128	0.250
BSLD - Lift	-0.185	0.407
BSLD - Total Drag	-0.259	0.444
BSLD - Lift-to-Drag Ratio	-0.222	0.407
BSLD - System Induced Drag	-0.259	0.481

6.3. Bird Formation Flight

In their paper [2], Bowers and Murillo theorized that bird flight, which has traditionally been analyzed using the ELD wing loading, would be better described by the BSLD method. They presented several arguments concerning overlapping trailing wings, lack of a vertical tail control, proverse vs adverse yaw, and wing shape (see Section 2.4, first paragraph). The findings of this thesis further add to this conclusion.

The CFD analysis of the BSLD wing determined an optimal lift (Figure 5.5) at the Y/b = -0.185 position. The optimal frequency positions directly reported in the bird formation literature differ from Y/b = -0.122 to -0.246 (Table 2.3) and average Y/b = -0.185, an evident match. It indicates an inboard rather than wingtip vortex. Taken by itself, it may seem coincidental, but in light of the other considerations discussed above and below it adds weight to the conclusion that bird flight is better informed by BSLD.

Observational data from bird formation flight literature shows clearly that the beneficial range of lateral position selected by the birds is much wider than predicted by the published authors using ELD methods. As discussed above, the ELD aircraft formation literature found a beneficial range averaging $0.25b_e$. However, the data from the bird formation literature averaged a much wider beneficial range of 0.73b (see Table 2.3). In this report for the Prandtl-D wing the beneficial range

for lift was found to be 0.41b. This suggests that even if birds can sense the optimal position to benefit from lift, they can still wander over a wide range and get appreciable lift benefits. They may also shift positions often due to the changes in lead bird turbulence in a bird's flight path.

The optimal position and the range of the bird studies are superimposed and the data normalized in Figure 5.22. This graph visually summarizes the wide range of positions selected by the birds and how it reasonably tracks the benefit curves of the BSLD wing parameters of Lift and Lift/Drag Ratio. These traits are confirmed by BSLD loading first because the wing vortex derives not from the wingtip of a BLSD wing, but further inboard, and second because the vortex is weaker and wider for the BSLD, so the beneficial position range is wider but still provides more total benefits because it acts over a larger wing area. These primary characteristics of the data collected and published in past studies could not be properly evaluated or explained by their authors using ELD models. They are well explained by BSLD models. It is recommended here that future bird flight evaluations should use the BSLD method.

Note two basic assumptions made for the analysis of the observational data for bird formation flight: (1) Birds are fairly adept at sensing and maintaining upwash positioning and (2) it is assumed that the bird position frequency is directly proportional to the magnitude of lift benefit at that position. The literature did not explain why such a wide range of positioning was selected by the birds. Several authors used the explanation that maybe the birds were imperfect in positioning or insensitive to upwash. Portugal [16], however, indicated that the birds were very adept at beneficial positioning. Considering the amount of seemingly easy and instinctive maneuvering birds make to maintain flight position, it seems that Portugal is correct in his conclusion. The second assumption, equating frequency of position with benefits gained, follows onto the first assumption. If birds are adept at sensing upwash opportunity, then they would more often frequent those beneficial positions. The wider vortices of BSLD wings provides a wider range of beneficial positions that the birds maintain. Tighter vortices, such as ELD produce, would result in tight grouping (as was expected by the authors). With this reasoning, the two assumptions appear appropriate.

6.4. Vortices

Subsections 2.4.5 (birds) and 2.5.4 (aircraft) discuss vortices as presented by the literature authors. Although vortex properties and characteristics were not specifically subjects included in this study, they appeared to be important considerations in evaluating the study results. Two conclusions are drawn concerning vortices. The first is that a BSLD wing vortex is wider and weaker than an ELD wingtip vortex. The second is that any inboard vortex contraction occurs far field and not immediately off the wing.

A vortex is created by a wing at the upwash - downwash interface where air vectors in opposite directions swirl into a vortex. The greater the shear (the difference in velocity), the stronger and tighter the angular momentum of the vortex. A characteristic of the BSLD wing is that the vortex generated is wider and less intense than that of an elliptical lift distribution wing because the shear velocities of the adjacent downwash and upwash are much less pronounced (see Figure 2.4). The location of this vortex-creating shear is also at a different point along the wing than the current standard. The elliptical design has a vortex initiated at the wingtip, whereas the bell-shape design is inboard (at s = 0.704 for the Prandtl-D wing). Although the total energy contained in these two types of vortices may be the same, the active cross sections differ significantly. Even though the core diameters were not directly calculated, the literature reviewed provided some input. Kless [24] performed CFD analyses on extended formation flight and utilized specific vortex modeling. He reported the core diameter off the ELD wingtips as b/d = 80 (d = core diameter). Spedding [12], performing observational experiments with a kestrel falcon, calculated a b/d of 7 (or d/b = 0.15). The vortex core of the Prandtl-D wing was not calculated, but a visual in Figure 2.9 shows a rollup coming off the wing from the vortex center at Y/b = -0.148 to the wingtip. This would indicate a d/b = 0.30. Two (of many) hypotheses can be drawn from this: (1) A trailing wing can gain similar lift from the wider vortex because it acts over a greater wing surface area, and (2) the vortices created by birds are better represented by the BSLD method as opposed to the ELD.

The second vortex conclusion is that an airfoil vortex does not contract immediately. In 1966 Milne-Thompson published a wonderful aerodynamics textbook [17] that quickly became an academic standard of its time. One of its numerous chapters and sections discussed the possibility of a contraction of vortex cores towards each other in "the wake far down wind" (see discussion in Subsection 2.4.5). There was also a discussion of a previous classical "horseshoe theory" that also postulated a far field contraction of the vortices. He theorized they could contract up to a factor of $\pi/4b$. Lissaman and Schollenberger [11], in a 1970 bird formation article, took this as a magical value and misapplied it as an immediate near-field contraction. Lissaman was cited directly over the following decades by other bird researchers who grabbed hold of this lifeline to explain why their observational data indicated a vortex inboard off the wing as opposed to off the wingtip. However, the literature on aircraft, including flight data, wind tunnel data, and specific CFD vortex modeling, give no results indicating contraction, near field or far field. A conclusion is that such studies should not assume immediate vortex contraction in their analysis. A deduction from this is that the data gathered by the bird formation flight research further verifies that the BSLD model with an inboard vortex, better represents bird flight.

6.5. Summary

The discussions above explain and demonstrate the conclusions from this thesis:

1. BSLD wings in formation flight can provide significant energy efficiency for the system.
2. Vortices created by a BSLD wing are inboard from the wingtips and are wider than ELD wingtip vortices.
3. The optimal position for a trailing wing is partially overlapping a vortex core.
4. Bird flight research would be better informed and modeled using the BSLD method as opposed to the traditional ELD method. Birds fly for optimization of lift.

REFERENCES

[1] Prandtl, Ludwig. “Zeitschrift Für Flugtecknik Und Motorluftschiffahrt.” *Über Tragflügel Kleinsten Induzierten Widerstandes*, 28 Dec. 1932, pp. 713–740.

[2] Bowers, Albion H., and Oscar J. Murillo. *On Wings of the Minimum Induced Drag: Spanload Implications for Aircraft and Birds*. NASA TP-2016-219072, Mar. 2016, www.ntrs.nasa.gov/archive/nasa/casi.ntrs.nasa.gov/20160003578.pdf

[3] Prandtl, Ludwig, and Albert Betz. *Vier Abhandlungen zur Hydrodynamik und Aerodynamik*. Kaiser Wilhem Institute for Flow Research. 1927, pp 31

[4] Jones, Robert T. *The Spanwise Distribution of Lift for Minimum Induced Drag of Wings Having a Given Lift and a Given Bending Moment.* NASA TN 2249, Dec. 1950 www.ntrs.nasa.gov/archive/nasa/casi.ntrs.nasa.gov/19760012005.pdf

[5] Klein, Armin, and Sathy.P. Viswanathan. “Zeitschrift für angewandte Mathematik und Physik ZAMP.” *Minimum Induced Drag of Wings with Given Lift and Root-Bending Moment*, Nov. 1973, pp. 886-892.

[6] Klein, Armin, and Sathy.P. Viswanathan. “Journal of Aircraft.” *Approximate Solution for Minimum Induced Drag of Wings with Given Structural Weight.* AIAA, Feb. 1975, pp. 124-126.

[7] Drela, Mark. *Flight Vehicle Aerodynamics*. Massachusetts Institute of Technology, 2014.

[8] Tschida, Tom. “The Prandtl-D makes one of its early flights.” *NASA*, 2015, www.nasa.gov/sites/default/files/thumbnails/image/ed13-0279-54.jpg.

[9] Christensen, Nancy. “Laysan Albatross.” *Macaulay Library*, ML59515111, Cornell University, 27 May 2017, www.macaulaylibrary.org/asset/59515111/.

[10] Kisbenedek, Attila. “Common cranes in formation flight” AFP, Nov. 20, 2013, www.news.com.au/technology/science/study-birds-fly-in-v-formation-to-save-energy/news-story/e68f8ec38051b2b92352184319d60b16

[11] Lissaman, P.B.S. and Carl A. Shollenberger. “Science.” *Formation Flight of Birds.* Science vol. 138, 22 May 1970, pp. 1003-1005. DOI: 10.1126/science 168.3934.1003.

[12] Spedding, G.R. “Journal of Experimental Biology.” *The Wake of a Kestrel (Falco Tinnunculus) in Gliding Flight.* 1987 Issue 127, pp. 45-57.

[13] Hainsworth, F. Reed. ‘Journal of Experimental Science.” *Precision and Dynamics of Positioning by Canada Geese Flying in Formation.* 1987, issue 128, pp. 445-468.

[14] Hainsworth, F. Reed. “Journal of Experimental Biology.” *Induced Drag Savings from Ground Effect and Formation Flight in Brown Pelicans.* 1988 Issue 135, pp. 431-444.

[15] Speakman, J.R. and Banks, D. “International Journal of Avian Science (IBIS).” *The Function of Flight Formations in Greylag Geese anser anser; Energy Savings or Orientation?*, 1998, issue 140, pp.280-287.

[16] Portugal, Steven, T. Hubel, J. Fritz, S. Heese, D. Trube, B. Voelkl, S. Hailes, A. Wilson, and J.R. Usherwood. “Upwash Exploitation and Downwash Avoidance by Flap Phasing in Ibis Formation Flight.” *Nature*, vol. 505, 14 Jan. 2014, pp. 399–494., doi:10.1038/nature12939.

[17] Milne–Thompson, L.M. (1966). “Theoretical Aerodynamics”. Dover Publishing. New York.

[18] Ning, Andrew, Flanzer, Tristan, and Kroo, Ilan. “Journal of Aircraft, Vol. 48, No. 3.” *Aerodynamic Performance of Extended Formation Flight.* BYU, May 2011, pp. 855-865. DOI: 10.2514/1.C031046.

[19] Shin, H.S., Antoniadis, A. F., and Tsourdos, A. “Journal of Intelligent & Robotic Systems.” *Parametric Study on Formation Flying Effectiveness for a Blended-Wing UAV.* IRS, 26 Apr., 2008. DOI: 10.1007 / s10846-018-0842-4.

[20] Blake, William B., and Gingras, David R. *Comparison of Predicted and Measured Formation Flight Interference Effects.* AFRL Conference August 2001, AIAA 2001-4136.

[21] Vachon, M.J., Ray, R.J., Walsh, K.R., and Ennix, K. *F/A-18 Aircraft Performance Benefits Measured During the Autonomous Formation Flight Project.* AIAA 2002-4491. DOI: 10.2514-6.2002-4491.

[22] Hansen, Jennifer L., and Cobleigh, Brent R. *Induced Moment Effects of Formation Flight Using Two F/A-18 Aircraft.* NASA TM-2002-210732, August 2002.

[23] Frazier, James W.,and Gopalarathnam, Ashok. "Journal of Aircraft, Vol 40, No.4." *Optimum Downwash Behind Wings in Formation Flight.* AIAA, July 2003, pp. 799-803. DOI: 10.2514/2.3162.

[24] Kless, J.E., Aftosmis, M.J., Ning, S.A., and Nemec, M. "AIAA Journal, Vol 51, No. 7." *Inviscid Analysis of Extended-Formation Flight.* AIAA July, 2013, pp. 1703-1705. DOI: 10.2514/1.J052224.

[25] Yoo, Seung Y. "Applied Aerodynamics Conference." *Computational Fluid Dynamics Analysis of the Stall Characteristics of a Wing Designed Based on Prandtl's Minimum Induced Drag.* AIAA, 24 Jun. 2018, doi:10.2514/6.2018-3009

[26] White, Frank M. *Viscous Fluid Flow*. McGraw-Hill Higher Education, third edition, 2011.

[27] Roache, Patrick J. "Quantification of uncertainty in computational fluid dynamics." Annual Review of Fluid Mechanics, vol. 29, 1997, pp. 123-160.

APPENDICES

Appendix A

AIRFOIL INFO

A.1 Wingtip & Centerline Airfoil Section Points

Table A.1: Centerline Airfoil Section

X	Y	X	Y	X	Y	X	Y
0.99839	0.01595	0.33928	0.09971	0.00107	-0.00520	0.40245	-0.01754
0.98664	0.01580	0.30866	0.09846	0.00428	-0.00882	0.43474	-0.01602
0.95215	0.01710	0.27886	0.09632	0.00961	-0.01205	0.46730	-0.01451
0.89696	0.0255	0.25000	0.09339	0.01704	-0.01502	0.50000	-0.01301
0.82387	0.03690	0.22221	0.08978	0.02653	-0.01800	0.53270	-0.01156
0.80438	0.04073	0.19562	0.08553	0.03806	-0.02062	0.56526	-0.01017
0.77779	0.04590	0.17033	0.08072	0.05156	-0.02237	0.59755	-0.00885
0.75000	0.05124	0.14645	0.07539	0.06699	-0.02406	0.62941	-0.00761
0.72114	0.05668	0.12408	0.06963	0.08427	-0.02524	0.66072	-0.00646
0.69134	0.06218	0.10332	0.06345	0.10332	-0.02598	0.69134	-0.00542
0.66072	0.06768	0.08427	0.05691	0.12408	-0.02642	0.72114	-0.00448
0.62941	0.07312	0.06699	0.05017	0.14645	-0.02653	0.75000	-0.00364
0.59755	0.07840	0.05156	0.04318	0.17033	-0.02631	0.77779	-0.00291
0.56526	0.08341	0.03806	0.03575	0.19562	-0.02584	0.80438	-0.00227
0.53270	0.08800	0.02653	0.02897	0.22221	-0.02512	0.82005	-0.00194
0.50000	0.09201	0.01704	0.02201	0.25000	-0.02419	0.89553	0.00255
0.46730	0.09530	0.00961	0.01424	0.27886	-0.02308	0.95184	0.00908
0.43474	0.09777	0.00428	0.00784	0.30866	-0.02184	0.98662	0.01411
0.40245	0.09936	0.00107	0.00353	0.33928	-0.02047	0.99839	0.01595
0.37059	0.10000	0.00000	0.00000	0.37059	-0.01904		

Table A.2: Wingtip Airfoil Section

X	Y	X	Y	X	Y	X	Y
1.00000	0.00070	0.40620	0.04556	0.00002	-0.00038	0.46904	-0.04274
0.96091	0.00428	0.38108	0.04644	0.00028	-0.00161	0.48162	-0.04208
0.94833	0.00540	0.36853	0.04682	0.00174	-0.00435	0.49420	-0.04139
0.93571	0.00654	0.35599	0.04716	0.00460	-0.00763	0.50678	-0.04067
0.92307	0.00769	0.34346	0.04745	0.00681	-0.00956	0.54455	-0.03836
0.89778	0.00999	0.33093	0.04770	0.01384	-0.01430	0.55715	-0.03754
0.88515	0.01114	0.29342	0.04814	0.01925	-0.01718	0.56975	-0.03670
0.84728	0.01455	0.26848	0.04816	0.02619	-0.02030	0.59495	-0.03496
0.82206	0.01679	0.25604	0.04807	0.03452	-0.02347	0.60756	-0.03406
0.80944	0.01789	0.24362	0.04791	0.06460	-0.03186	0.62017	-0.03315
0.79683	0.01898	0.23122	0.04767	0.07556	-0.03415	0.65801	-0.03031
0.78422	0.02006	0.21885	0.04736	0.09825	-0.03801	0.67063	-0.02933
0.77160	0.02113	0.20652	0.04696	0.12166	-0.04103	0.68325	-0.02834
0.73374	0.02428	0.15762	0.04434	0.13355	-0.04229	0.69587	-0.02734
0.72112	0.02531	0.14554	0.04338	0.14554	-0.04338	0.72112	-0.02531
0.69587	0.02734	0.13355	0.04229	0.15762	-0.04434	0.73374	-0.02428
0.68325	0.02834	0.12166	0.04103	0.20652	-0.04696	0.77160	-0.02113
0.67063	0.02933	0.09825	0.03801	0.21885	-0.04736	0.78422	-0.02006
0.65801	0.03031	0.07556	0.03415	0.23122	-0.04767	0.79683	-0.01898
0.62017	0.03315	0.06460	0.03186	0.24362	-0.04791	0.80944	-0.01789
0.60756	0.03406	0.03452	0.02347	0.25604	-0.04807	0.82206	-0.01679
0.59495	0.03496	0.02619	0.02030	0.26848	-0.04816	0.84728	-0.01455
0.56975	0.03670	0.01925	0.01718	0.29342	-0.04814	0.88515	-0.01114
0.55715	0.03754	0.01384	0.01430	0.33093	-0.04770	0.89778	-0.00999
0.54455	0.03836	0.00681	0.00956	0.34346	-0.04745	0.92307	-0.00769
0.50678	0.04067	0.00460	0.00763	0.35599	-0.04716	0.93571	-0.00654
0.49420	0.04139	0.00174	0.00435	0.36853	-0.04682	0.94833	-0.00540
0.48162	0.04208	0.00028	0.00161	0.38108	-0.04644	0.96091	-0.00428
0.46904	0.04274	0.00002	0.00038	0.40620	-0.04556	1.00000	0.00070
0.43132	0.04453	0.00000	0.00000	0.43132	-0.04453		

A.2 Twist Distribution

Table A.3: Wing Twist Distribution Along Semispan

Semispan location, percent	Angle, degrees	Semispan location, percent	Angle, degrees
0	8.3274	55	7.2592
5	8.5524	60	6.6634
10	8.7259	65	5.9579
15	8.8441	70	5.1362
20	8.903	75	4.1927
25	8.8984	80	3.1253
30	8.8257	85	1.9394
35	8.6801	90	0.6589
40	8.4565	95	-0.6417
45	8.1492	100	-1.6726
50	7.7522		

A.3 Chosen Wingtip Airfoil Section Points

Table A.1: Chosen Wingtip Airfoil Section Point

X	Y	X	Y	X	Y	X	Y
1.00000	0.00070	0.38108	0.04644	0.00028	-0.00161	0.43132	-0.04453
0.96091	0.00428	0.35599	0.04716	0.00174	-0.00435	0.46904	-0.04274
0.93571	0.00654	0.33093	0.04770	0.00681	-0.00956	0.50678	-0.04067
0.89778	0.00999	0.29342	0.04814	0.01384	-0.01430	0.54455	-0.03836
0.88515	0.01114	0.26848	0.04816	0.02619	-0.02030	0.56975	-0.03670
0.84728	0.01455	0.25604	0.04807	0.03452	-0.02347	0.59495	-0.03496
0.80944	0.01789	0.23122	0.04767	0.06460	-0.03186	0.62017	-0.03315
0.77160	0.02113	0.20652	0.04696	0.07556	-0.03415	0.65801	-0.03031
0.73374	0.02428	0.15762	0.04434	0.09825	-0.03801	0.67063	-0.02933
0.69587	0.02734	0.12166	0.04103	0.12166	-0.04103	0.69587	-0.02734
0.67063	0.02933	0.09825	0.03801	0.15762	-0.04434	0.73374	-0.02428
0.65801	0.03031	0.07556	0.03415	0.20652	-0.04696	0.77160	-0.02113
0.62017	0.03315	0.06460	0.03186	0.23122	-0.04767	0.80944	-0.01789
0.59495	0.03496	0.03452	0.02347	0.25604	-0.04807	0.84728	-0.01455
0.56975	0.03670	0.02619	0.02030	0.26848	-0.04816	0.88515	-0.01114
0.54455	0.03836	0.01384	0.01430	0.29342	-0.04814	0.89778	-0.00999
0.50678	0.04067	0.00681	0.00956	0.33093	-0.04770	0.93571	-0.00654
0.46904	0.04274	0.00174	0.00435	0.35599	-0.04716	0.96091	-0.00428
0.43132	0.04453	0.00028	0.00161	0.38108	-0.04644	1.00000	0.000700
0.40620	0.04556	0.00000	0.00000	0.40620	-0.04556		

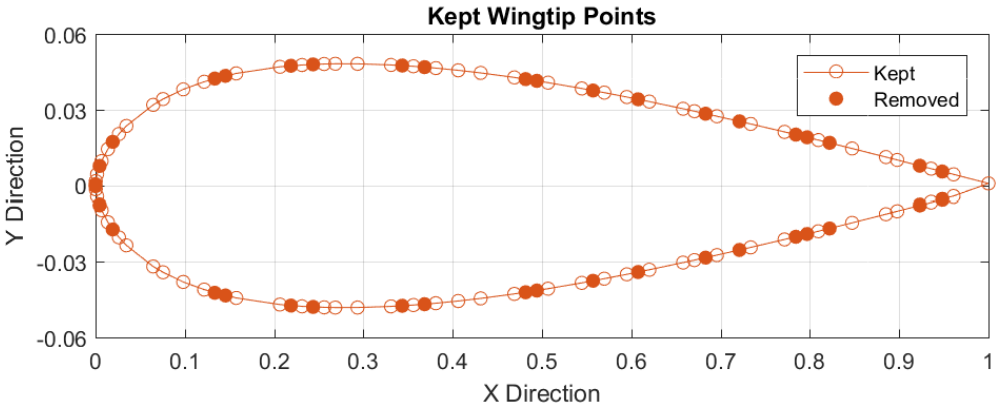

Figure A.1: Plot of nondimensional removed and kept wingtip airfoil points

Appendix B

MATLAB CODE

B.1 Airfoil Section Code (ChordFunction.m)

```
clc
clear all
close all

Tip = importdata('tip.txt', '\t');
Center = importdata('center.txt', '\t');
Twist = importdata('twist.txt', '\t');
sweep = 24; % sweep in deg
dihedral = 2.645; % equates to 2.5 deg at the 3/4 chord when 2.645 deg is applied at the leading edge
scale = 2;
centerchord = 15.75*0.0254*scale %m
wingtipchord = 3.94*0.0254*scale %m
hspan = 1.87452*scale; %The half-span of the aircraft, in meters, scaled for P3C
n = 79; % number of points

Choordinates = zeros(n,3,21); %create matrix of points
Quarter75 = zeros ([21 3]); %create matrix of points
Chord75 = zeros ([21 3]); %create matrix of points
ChoordinatesTop = zeros(40,3,21); %create matrix of points
ChoordinatesBottom = zeros(40,3,21); %create matrix of points
Choordlength = zeros(21,1);

%% Populate the airfoil matrix

%Load Tip and Center chord coordinates into array
for ii = 1:2
   for jj = 1:n
      Choordinates( jj, ii, 1) = centerchord * Center(jj, ii);
      Choordinates(jj, ii, 21) = wingtipchord * Tip(jj, ii);

      %Find a linear interpolation between the tip and the center chord
      Cvector = linspace(Choordinates(jj,ii,1), Choordinates(jj,ii,21),21);

      %Put the coordinates into Choordinates in their corresponding places
      for kk = 2:20
         Choordinates(jj,ii,kk) = Cvector(kk);
      end
   end
end
junk = 1;

%% Twist
% Angles
sweep = sweep * pi/180; %Convert the sweep into radians
dihedral = dihedral * pi/180; %Convert the dihedral into radians
span = linspace(0, hspan, 21); %Create a vector of spanwise locations for the airfoils

for kk = 1:21
   figure(kk)
   hold on;
   plot(Choordinates(:,1,kk), Choordinates(:,2,kk));

   %Convert the twist into radians
   Twist(kk) = -pi * Twist(kk) / 180;
```

```
    %Get a scaling factor
    r = sqrt(Choordinates(1,1,kk)^2 + Choordinates(1,2,kk)^2);

    for jj = 1:n
        %Populate vectors to be rotated
        xr(jj) = Choordinates(jj,1,kk);
        yr(jj) = Choordinates(jj,2,kk);
        Choordinates(jj,3,kk) = span(kk);
    end

    %Create Rotatoin Point at 75% of chord
    xc75(kk) = Choordinates(1,1,kk)/4*3;
    yc75(kk) = Choordinates(1,2,kk)/4*3;

    %Find Chord at 75% location.
    Quarter75(:,1,kk) = xc75(kk);
    Quarter75(:,2,kk) = yc75(kk);
    Quarter75(:,3,kk) = Choordinates(1,3,kk);
    Chord75(kk,:) = Quarter75(1,:,kk);

    %Rotate vectors
    [xr, yr, sf] = RotationMatrix(xr, yr, xc75(kk), yc75(kk), Twist(kk), r);

    %Store the rotated vectors
    Choordinates(:,1,kk) = xr * sf;
    Choordinates(:,2,kk) = yr * sf;

    %Plot to compare to prior rotation
    plot(Choordinates(:,1,kk), Choordinates(:,2,kk));
    axis equal;
end

%% Translate, Dihedral, Sweep

%Find center leading edge
    dx = Choordinates(40,1,1);
    dy = Choordinates(40,2,1);

for kk = 1:21
    %Transtlate center back to zero
    Choordinates(:,1,kk) = Choordinates(:,1,kk) - dx;
    Choordinates(:,2,kk) = Choordinates(:,2,kk) - dy;
    Chord75(kk,1) = Chord75(kk,1)- dx;
    Chord75(kk,2) = Chord75(kk,2)- dy;

    %Plot to compare to prior translation
    hold on;
    figure(kk)
    plot(Choordinates(:,1,kk), Choordinates(:,2,kk));
    axis equal;

    %get the distance needed to shift for sweep/dihedral
    y = span(kk) * tan(sweep);
    z = span(kk) * tan(dihedral);

    %Shift chord back by the sweep distance at that span location.
    Chord75(kk,1) = Chord75(kk,1) + y;

    %Shift chord up by the dihedral distance at that span location.
    Chord75(kk,2) = Chord75(kk,2) + z;

    %Shift each airfoil back by the sweep distance at that span location.
```

```
    for jj = 1:n
        Choordinates(jj, 1, kk) = Choordinates(jj, 1, kk) + y;
    end
    %Shift each airfoil up by the dihedral distance at that span location.
    for ii = 1:n
        Choordinates(ii, 2, kk) = Choordinates(ii, 2, kk) + z;
    end

    plot(Choordinates(:,1,kk), Choordinates(:,2,kk));
    hold on;
    title('Prandtl Wing Sections')
    xlabel('Chord (m)')
    ylabel('Thickness (m)')
    xlim([0 1])
    ylim([-.1 .15])
    legend('Initial', 'Rotation', 'Translation', 'Sweep & Dihedral');
    hold off;
end
close all

% Re-order for X,Y,Z point location
ChoordinatesR = Choordinates(:,[3 2 1],:);
ChoordinatesL = Choordinates(:,[3 2 1],:);
ChoordinatesL(:,1,:) = -1*ChoordinatesL(:,1,:);
Chord75 = Chord75(:,[3 2 1]);

%% Find Top and bottom surfaces RHS
for kk = 1:21
    for jj = 1:40
        for ii = 1:3
        ChoordinatesTopR(jj, ii, kk) = Choordinates(jj, ii, kk);
        ChoordinatesBottomR(jj, ii, kk) = Choordinates((jj+39), ii, kk);
        end
    end
end

%% Get leading and trailing edge line sets RHS
for kk = 1:21
    TrailingEdgeR (kk,:) = Choordinates(1,:,kk);
    LeadingEdgeR (kk,:) = Choordinates(40,:,kk);
end

%% Find Top and bottom surfaces LHS
for kk = 1:21
    for jj = 1:40
        for ii = 1:3
        ChoordinatesTopL(jj, ii, kk) = Choordinates(jj, ii, kk);
        ChoordinatesBottomL(jj, ii, kk) = Choordinates((jj+39), ii, kk);

        end
    end
end
ChoordinatesTopL(:,3,:) = -1*ChoordinatesTopR(:,3,:);
ChoordinatesBottomL(:,3,:) = -1*ChoordinatesBottomR(:,3,:);

%% Get leading and trailing edge line sets LHS
for kk = 1:21
    TrailingEdgeL (kk,:) = Choordinates(1,:,kk);
    LeadingEdgeL (kk,:) = Choordinates(40,:,kk);
end
TrailingEdgeL (:,3) = -1*TrailingEdgeL (:,3);
LeadingEdgeL (:,3) = -1*LeadingEdgeL (:,3);
```

```
%% Get choord lengths of each section

for kk = 1:21
   Choordlength(kk) = sqrt((LeadingEdgeL(kk,1)-TrailingEdgeL(kk,1))^2+(LeadingEdgeL(kk,2)-
TrailingEdgeL(kk,2))^2);
end

%% Print to RHS
dlmwrite('Final Airfoil 1R.txt',ChoordinatesR(:,:,1),'delimiter','\t','precision',6);
dlmwrite('Final Airfoil 2R.txt',ChoordinatesR(:,:,2),'delimiter','\t','precision',6);
dlmwrite('Final Airfoil 3R.txt',ChoordinatesR(:,:,3),'delimiter','\t','precision',6);
dlmwrite('Final Airfoil 4R.txt',ChoordinatesR(:,:,4),'delimiter','\t','precision',6);
dlmwrite('Final Airfoil 5R.txt',ChoordinatesR(:,:,5),'delimiter','\t','precision',6);
dlmwrite('Final Airfoil 6R.txt',ChoordinatesR(:,:,6),'delimiter','\t','precision',6);
dlmwrite('Final Airfoil 7R.txt',ChoordinatesR(:,:,7),'delimiter','\t','precision',6);
dlmwrite('Final Airfoil 8R.txt',ChoordinatesR(:,:,8),'delimiter','\t','precision',6);
dlmwrite('Final Airfoil 9R.txt',ChoordinatesR(:,:,9),'delimiter','\t','precision',6);
dlmwrite('Final Airfoil 10R.txt',ChoordinatesR(:,:,10),'delimiter','\t','precision',6);
dlmwrite('Final Airfoil 11R.txt',ChoordinatesR(:,:,11),'delimiter','\t','precision',6);
dlmwrite('Final Airfoil 12R.txt',ChoordinatesR(:,:,12),'delimiter','\t','precision',6);
dlmwrite('Final Airfoil 13R.txt',ChoordinatesR(:,:,13),'delimiter','\t','precision',6);
dlmwrite('Final Airfoil 14R.txt',ChoordinatesR(:,:,14),'delimiter','\t','precision',6);
dlmwrite('Final Airfoil 15R.txt',ChoordinatesR(:,:,15),'delimiter','\t','precision',6);
dlmwrite('Final Airfoil 16R.txt',ChoordinatesR(:,:,16),'delimiter','\t','precision',6);
dlmwrite('Final Airfoil 17R.txt',ChoordinatesR(:,:,17),'delimiter','\t','precision',6);
dlmwrite('Final Airfoil 18R.txt',ChoordinatesR(:,:,18),'delimiter','\t','precision',6);
dlmwrite('Final Airfoil 19R.txt',ChoordinatesR(:,:,19),'delimiter','\t','precision',6);
dlmwrite('Final Airfoil 20R.txt',ChoordinatesR(:,:,20),'delimiter','\t','precision',6);
dlmwrite('Final Airfoil 21R.txt',ChoordinatesR(:,:,21),'delimiter','\t','precision',6);
dlmwrite('Final Airfoil 1R Top.txt',ChoordinatesTopR(:,:,1),'delimiter','\t','precision',6);
dlmwrite('Final Airfoil 2R Top.txt',ChoordinatesTopR(:,:,2),'delimiter','\t','precision',6);
dlmwrite('Final Airfoil 3R Top.txt',ChoordinatesTopR(:,:,3),'delimiter','\t','precision',6);
dlmwrite('Final Airfoil 4R Top.txt',ChoordinatesTopR(:,:,4),'delimiter','\t','precision',6);
dlmwrite('Final Airfoil 5R Top.txt',ChoordinatesTopR(:,:,5),'delimiter','\t','precision',6);
dlmwrite('Final Airfoil 6R Top.txt',ChoordinatesTopR(:,:,6),'delimiter','\t','precision',6);
dlmwrite('Final Airfoil 7R Top.txt',ChoordinatesTopR(:,:,7),'delimiter','\t','precision',6);
dlmwrite('Final Airfoil 8R Top.txt',ChoordinatesTopR(:,:,8),'delimiter','\t','precision',6);
dlmwrite('Final Airfoil 9R Top.txt',ChoordinatesTopR(:,:,9),'delimiter','\t','precision',6);
dlmwrite('Final Airfoil 10R Top.txt',ChoordinatesTopR(:,:,10),'delimiter','\t','precision',6);
dlmwrite('Final Airfoil 11R Top.txt',ChoordinatesTopR(:,:,11),'delimiter','\t','precision',6);
dlmwrite('Final Airfoil 12R Top.txt',ChoordinatesTopR(:,:,12),'delimiter','\t','precision',6);
dlmwrite('Final Airfoil 13R Top.txt',ChoordinatesTopR(:,:,13),'delimiter','\t','precision',6);
dlmwrite('Final Airfoil 14R Top.txt',ChoordinatesTopR(:,:,14),'delimiter','\t','precision',6);
dlmwrite('Final Airfoil 15R Top.txt',ChoordinatesTopR(:,:,15),'delimiter','\t','precision',6);
dlmwrite('Final Airfoil 16R Top.txt',ChoordinatesTopR(:,:,16),'delimiter','\t','precision',6);
dlmwrite('Final Airfoil 17R Top.txt',ChoordinatesTopR(:,:,17),'delimiter','\t','precision',6);
dlmwrite('Final Airfoil 18R Top.txt',ChoordinatesTopR(:,:,18),'delimiter','\t','precision',6);
dlmwrite('Final Airfoil 19R Top.txt',ChoordinatesTopR(:,:,19),'delimiter','\t','precision',6);
dlmwrite('Final Airfoil 20R Top.txt',ChoordinatesTopR(:,:,20),'delimiter','\t','precision',6);
dlmwrite('Final Airfoil 21R Top.txt',ChoordinatesTopR(:,:,21),'delimiter','\t','precision',6);
dlmwrite('Final Airfoil 1R Bottom.txt',ChoordinatesBottomR(:,:,1),'delimiter','\t','precision',6);
dlmwrite('Final Airfoil 2R Bottom.txt',ChoordinatesBottomR(:,:,2),'delimiter','\t','precision',6);
dlmwrite('Final Airfoil 3R Bottom.txt',ChoordinatesBottomR(:,:,3),'delimiter','\t','precision',6);
dlmwrite('Final Airfoil 4R Bottom.txt',ChoordinatesBottomR(:,:,4),'delimiter','\t','precision',6);
dlmwrite('Final Airfoil 5R Bottom.txt',ChoordinatesBottomR(:,:,5),'delimiter','\t','precision',6);
dlmwrite('Final Airfoil 6R Bottom.txt',ChoordinatesBottomR(:,:,6),'delimiter','\t','precision',6);
dlmwrite('Final Airfoil 7R Bottom.txt',ChoordinatesBottomR(:,:,7),'delimiter','\t','precision',6);
dlmwrite('Final Airfoil 8R Bottom.txt',ChoordinatesBottomR(:,:,8),'delimiter','\t','precision',6);
dlmwrite('Final Airfoil 9R Bottom.txt',ChoordinatesBottomR(:,:,9),'delimiter','\t','precision',6);
dlmwrite('Final Airfoil 10R Bottom.txt',ChoordinatesBottomR(:,:,10),'delimiter','\t','precision',6);
dlmwrite('Final Airfoil 11R Bottom.txt',ChoordinatesBottomR(:,:,11),'delimiter','\t','precision',6);
```

```
dlmwrite('Final Airfoil 12R Bottom.txt',ChoordinatesBottomR(:,:,12),'delimiter','\t','precision',6);
dlmwrite('Final Airfoil 13R Bottom.txt',ChoordinatesBottomR(:,:,13),'delimiter','\t','precision',6);
dlmwrite('Final Airfoil 14R Bottom.txt',ChoordinatesBottomR(:,:,14),'delimiter','\t','precision',6);
dlmwrite('Final Airfoil 15R Bottom.txt',ChoordinatesBottomR(:,:,15),'delimiter','\t','precision',6);
dlmwrite('Final Airfoil 16R Bottom.txt',ChoordinatesBottomR(:,:,16),'delimiter','\t','precision',6);
dlmwrite('Final Airfoil 17R Bottom.txt',ChoordinatesBottomR(:,:,17),'delimiter','\t','precision',6);
dlmwrite('Final Airfoil 18R Bottom.txt',ChoordinatesBottomR(:,:,18),'delimiter','\t','precision',6);
dlmwrite('Final Airfoil 19R Bottom.txt',ChoordinatesBottomR(:,:,19),'delimiter','\t','precision',6);
dlmwrite('Final Airfoil 20R Bottom.txt',ChoordinatesBottomR(:,:,20),'delimiter','\t','precision',6);
dlmwrite('Final Airfoil 21R Bottom.txt',ChoordinatesBottomR(:,:,21),'delimiter','\t','precision',6);
dlmwrite('TrailingEdgeR.txt',TrailingEdgeR,'delimiter','\t','precision',6);
dlmwrite('LeadingEdgeR.txt',LeadingEdgeR,'delimiter','\t','precision',6);
dlmwrite('Chord75.txt',Chord75,'delimiter','\t','precision',6);
%% Print to LHS
dlmwrite('Final Airfoil 1L.txt',ChoordinatesL(:,:,1),'delimiter','\t','precision',6);
dlmwrite('Final Airfoil 2L.txt',ChoordinatesL(:,:,2),'delimiter','\t','precision',6);
dlmwrite('Final Airfoil 3L.txt',ChoordinatesL(:,:,3),'delimiter','\t','precision',6);
dlmwrite('Final Airfoil 4L.txt',ChoordinatesL(:,:,4),'delimiter','\t','precision',6);
dlmwrite('Final Airfoil 5L.txt',ChoordinatesL(:,:,5),'delimiter','\t','precision',6);
dlmwrite('Final Airfoil 6L.txt',ChoordinatesL(:,:,6),'delimiter','\t','precision',6);
dlmwrite('Final Airfoil 7L.txt',ChoordinatesL(:,:,7),'delimiter','\t','precision',6);
dlmwrite('Final Airfoil 8L.txt',ChoordinatesL(:,:,8),'delimiter','\t','precision',6);
dlmwrite('Final Airfoil 9L.txt',ChoordinatesL(:,:,9),'delimiter','\t','precision',6);
dlmwrite('Final Airfoil 10L.txt',ChoordinatesL(:,:,10),'delimiter','\t','precision',6);
dlmwrite('Final Airfoil 11L.txt',ChoordinatesL(:,:,11),'delimiter','\t','precision',6);
dlmwrite('Final Airfoil 12L.txt',ChoordinatesL(:,:,12),'delimiter','\t','precision',6);
dlmwrite('Final Airfoil 13L.txt',ChoordinatesL(:,:,13),'delimiter','\t','precision',6);
dlmwrite('Final Airfoil 14L.txt',ChoordinatesL(:,:,14),'delimiter','\t','precision',6);
dlmwrite('Final Airfoil 15L.txt',ChoordinatesL(:,:,15),'delimiter','\t','precision',6);
dlmwrite('Final Airfoil 16L.txt',ChoordinatesL(:,:,16),'delimiter','\t','precision',6);
dlmwrite('Final Airfoil 17L.txt',ChoordinatesL(:,:,17),'delimiter','\t','precision',6);
dlmwrite('Final Airfoil 18L.txt',ChoordinatesL(:,:,18),'delimiter','\t','precision',6);
dlmwrite('Final Airfoil 19L.txt',ChoordinatesL(:,:,19),'delimiter','\t','precision',6);
dlmwrite('Final Airfoil 20L.txt',ChoordinatesL(:,:,20),'delimiter','\t','precision',6);
dlmwrite('Final Airfoil 21L.txt',ChoordinatesL(:,:,21),'delimiter','\t','precision',6);
dlmwrite('Final Airfoil 1L Top.txt',ChoordinatesTopL(:,:,1),'delimiter','\t','precision',6);
dlmwrite('Final Airfoil 2L Top.txt',ChoordinatesTopL(:,:,2),'delimiter','\t','precision',6);
dlmwrite('Final Airfoil 3L Top.txt',ChoordinatesTopL(:,:,3),'delimiter','\t','precision',6);
dlmwrite('Final Airfoil 4L Top.txt',ChoordinatesTopL(:,:,4),'delimiter','\t','precision',6);
dlmwrite('Final Airfoil 5L Top.txt',ChoordinatesTopL(:,:,5),'delimiter','\t','precision',6);
dlmwrite('Final Airfoil 6L Top.txt',ChoordinatesTopL(:,:,6),'delimiter','\t','precision',6);
dlmwrite('Final Airfoil 7L Top.txt',ChoordinatesTopL(:,:,7),'delimiter','\t','precision',6);
dlmwrite('Final Airfoil 8L Top.txt',ChoordinatesTopL(:,:,8),'delimiter','\t','precision',6);
dlmwrite('Final Airfoil 9L Top.txt',ChoordinatesTopL(:,:,9),'delimiter','\t','precision',6);
dlmwrite('Final Airfoil 10L Top.txt',ChoordinatesTopL(:,:,10),'delimiter','\t','precision',6);
dlmwrite('Final Airfoil 11L Top.txt',ChoordinatesTopL(:,:,11),'delimiter','\t','precision',6);
dlmwrite('Final Airfoil 12L Top.txt',ChoordinatesTopL(:,:,12),'delimiter','\t','precision',6);
dlmwrite('Final Airfoil 13L Top.txt',ChoordinatesTopL(:,:,13),'delimiter','\t','precision',6);
dlmwrite('Final Airfoil 14L Top.txt',ChoordinatesTopL(:,:,14),'delimiter','\t','precision',6);
dlmwrite('Final Airfoil 15L Top.txt',ChoordinatesTopL(:,:,15),'delimiter','\t','precision',6);
dlmwrite('Final Airfoil 16L Top.txt',ChoordinatesTopL(:,:,16),'delimiter','\t','precision',6);
dlmwrite('Final Airfoil 17L Top.txt',ChoordinatesTopL(:,:,17),'delimiter','\t','precision',6);
dlmwrite('Final Airfoil 18L Top.txt',ChoordinatesTopL(:,:,18),'delimiter','\t','precision',6);
dlmwrite('Final Airfoil 19L Top.txt',ChoordinatesTopL(:,:,19),'delimiter','\t','precision',6);
dlmwrite('Final Airfoil 20L Top.txt',ChoordinatesTopL(:,:,20),'delimiter','\t','precision',6);
dlmwrite('Final Airfoil 21L Top.txt',ChoordinatesTopL(:,:,21),'delimiter','\t','precision',6);
dlmwrite('Final Airfoil 1L Bottom.txt',ChoordinatesBottomL(:,:,1),'delimiter','\t','precision',6);
dlmwrite('Final Airfoil 2L Bottom.txt',ChoordinatesBottomL(:,:,2),'delimiter','\t','precision',6);
dlmwrite('Final Airfoil 3L Bottom.txt',ChoordinatesBottomL(:,:,3),'delimiter','\t','precision',6);
dlmwrite('Final Airfoil 4L Bottom.txt',ChoordinatesBottomL(:,:,4),'delimiter','\t','precision',6);
dlmwrite('Final Airfoil 5L Bottom.txt',ChoordinatesBottomL(:,:,5),'delimiter','\t','precision',6);
dlmwrite('Final Airfoil 6L Bottom.txt',ChoordinatesBottomL(:,:,6),'delimiter','\t','precision',6);
```

```
dlmwrite('Final Airfoil 7L Bottom.txt',ChoordinatesBottomL(:,:,7),'delimiter','\t','precision',6);
dlmwrite('Final Airfoil 8L Bottom.txt',ChoordinatesBottomL(:,:,8),'delimiter','\t','precision',6);
dlmwrite('Final Airfoil 9L Bottom.txt',ChoordinatesBottomL(:,:,9),'delimiter','\t','precision',6);
dlmwrite('Final Airfoil 10L Bottom.txt',ChoordinatesBottomL(:,:,10),'delimiter','\t','precision',6);
dlmwrite('Final Airfoil 11L Bottom.txt',ChoordinatesBottomL(:,:,11),'delimiter','\t','precision',6);
dlmwrite('Final Airfoil 12L Bottom.txt',ChoordinatesBottomL(:,:,12),'delimiter','\t','precision',6);
dlmwrite('Final Airfoil 13L Bottom.txt',ChoordinatesBottomL(:,:,13),'delimiter','\t','precision',6);
dlmwrite('Final Airfoil 14L Bottom.txt',ChoordinatesBottomL(:,:,14),'delimiter','\t','precision',6);
dlmwrite('Final Airfoil 15L Bottom.txt',ChoordinatesBottomL(:,:,15),'delimiter','\t','precision',6);
dlmwrite('Final Airfoil 16L Bottom.txt',ChoordinatesBottomL(:,:,16),'delimiter','\t','precision',6);
dlmwrite('Final Airfoil 17L Bottom.txt',ChoordinatesBottomL(:,:,17),'delimiter','\t','precision',6);
dlmwrite('Final Airfoil 18L Bottom.txt',ChoordinatesBottomL(:,:,18),'delimiter','\t','precision',6);
dlmwrite('Final Airfoil 19L Bottom.txt',ChoordinatesBottomL(:,:,19),'delimiter','\t','precision',6);
dlmwrite('Final Airfoil 20L Bottom.txt',ChoordinatesBottomL(:,:,20),'delimiter','\t','precision',6);
dlmwrite('Final Airfoil 21L Bottom.txt',ChoordinatesBottomL(:,:,21),'delimiter','\t','precision',6);
dlmwrite('TrailingEdgeL.txt',TrailingEdgeL,'delimiter','\t','precision',6);
dlmwrite('LeadingEdgeL.txt',LeadingEdgeL,'delimiter','\t','precision',6);
dlmwrite('ChordLength.txt',Choordlength,'delimiter','\t','precision',6);
```

B.2 Rotation Matrix Code (RotationMatrix.m)

```
function [x_rotated, y_rotated, sf] = RotationMatrix(x,y, xc, yc, theta, r)

% create a matrix of these points, which will be useful in future calculations
v = [x;y];
% choose a point which will be the center of rotation
x_center = xc;
y_center = yc;

% create a matrix which will be used later in calculations
center = repmat([x_center; y_center], 1, length(x));

% define a rotation matrix
R = [cos(theta) -sin(theta); sin(theta) cos(theta)];
% do the rotation...
s = v - center;     % shift points in the plane so that the center of rotation is at the origin
so = R*s;           % apply the rotation about the origin
vo = so + center;   % shift again so the origin goes back to the desired center of rotation
% this can be done in one line as:
% vo = R*(v - center) + center
% pick out the vectors of rotated x- and y-data
x_rotated = vo(1,:);
y_rotated = vo(2,:);

%Get the scale factor
r2 = sqrt(vo(1,1)^2 + vo(2,1)^2);
sf = r2/r;

end
```

Appendix C

TABULATED AIRFOIL SECTION POINTS

Airfoils are tabulated below starting with the left wingtip section (Airfoil L21) and ending with the right wingtip section (Airfoil R21). The centerline was both Airfoils L1 and R1 from the output MATLAB code in Appendix B. For simplicity, both the top and bottom surface of each airfoil are tabulated together. In total there are 41 airfoil sections that made up the entirety of the wing. All coordinate points have been rounded to 1 micrometer, or 6 decimal places.

C.1 Airfoil L21 (Left Wingtip)

Table C.1 Airfoil L21 (Left Wingtip)

X	Y	Z	X	Y	Z	X	Y	Z
1.864370	-3.749040	0.088097	1.705370	-3.749040	0.092716	1.718320	-3.749040	0.074049
1.856530	-3.749040	0.088584	1.695600	-3.749040	0.091906	1.723310	-3.749040	0.074198
1.851480	-3.749040	0.088889	1.688420	-3.749040	0.091034	1.730810	-3.749040	0.074506
1.843870	-3.749040	0.089358	1.683760	-3.749040	0.090293	1.735820	-3.749040	0.074760
1.841340	-3.749040	0.089514	1.679240	-3.749040	0.089388	1.740830	-3.749040	0.075051
1.833740	-3.749040	0.089975	1.677060	-3.749040	0.088866	1.745850	-3.749040	0.075373
1.826150	-3.749040	0.090422	1.671100	-3.749040	0.087012	1.750870	-3.749040	0.075726
1.818560	-3.749040	0.090849	1.669450	-3.749040	0.086329	1.758410	-3.749040	0.076305
1.810970	-3.749040	0.091258	1.667010	-3.749040	0.085056	1.765950	-3.749040	0.076939
1.803380	-3.749040	0.091649	1.665630	-3.749040	0.084067	1.773490	-3.749040	0.077622
1.798320	-3.749040	0.091900	1.664650	-3.749040	0.082995	1.778520	-3.749040	0.078101
1.795780	-3.749040	0.092022	1.664370	-3.749040	0.082439	1.783550	-3.749040	0.078597
1.788200	-3.749040	0.092369	1.664330	-3.749040	0.082115	1.788590	-3.749040	0.079106
1.783140	-3.749040	0.092584	1.664390	-3.749040	0.081794	1.796140	-3.749040	0.079895
1.778090	-3.749040	0.092785	1.664700	-3.749040	0.081255	1.798660	-3.749040	0.080165
1.773040	-3.749040	0.092970	1.665740	-3.749040	0.080242	1.803700	-3.749040	0.080710
1.765470	-3.749040	0.093211	1.667180	-3.749040	0.079335	1.811250	-3.749040	0.081544
1.757910	-3.749040	0.093405	1.669680	-3.749040	0.078207	1.818810	-3.749040	0.082395
1.750350	-3.749040	0.093543	1.671370	-3.749040	0.077621	1.826360	-3.749040	0.083264
1.745320	-3.749040	0.093602	1.677440	-3.749040	0.076119	1.833910	-3.749040	0.084154
1.740290	-3.749040	0.093631	1.679640	-3.749040	0.075725	1.841470	-3.749040	0.085057
1.735270	-3.749040	0.093629	1.684200	-3.749040	0.075085	1.843990	-3.749040	0.085361
1.730250	-3.749040	0.093590	1.688900	-3.749040	0.074617	1.851550	-3.749040	0.086273
1.722740	-3.749040	0.093459	1.696120	-3.749040	0.074165	1.856580	-3.749040	0.086872
1.717750	-3.749040	0.093318	1.705920	-3.749040	0.073927	1.864370	-3.749040	0.088097
1.715270	-3.749040	0.093227	1.710860	-3.749040	0.073929			
1.710300	-3.749040	0.093002	1.715830	-3.749040	0.073994			

C.2 Airfoil L20

Table C.2 Airfoil L20

X	Y	Z	X	Y	Z	X	Y	Z
1.810880	-3.561588	0.079252	1.625810	-3.561588	0.088353	1.640870	-3.561588	0.066414
1.802970	-3.561588	0.079838	1.615620	-3.561588	0.087511	1.646720	-3.561588	0.066520
1.796790	-3.561588	0.080250	1.607970	-3.561588	0.086548	1.655000	-3.561588	0.066741
1.787360	-3.561588	0.081059	1.602760	-3.561588	0.085654	1.660960	-3.561588	0.066960
1.782030	-3.561588	0.081752	1.597770	-3.561588	0.084595	1.666950	-3.561588	0.067219
1.774040	-3.561588	0.082464	1.595080	-3.561588	0.083849	1.672980	-3.561588	0.067511
1.765770	-3.561588	0.083213	1.588840	-3.561588	0.081887	1.679030	-3.561588	0.067834
1.757460	-3.561588	0.083950	1.586800	-3.561588	0.080990	1.687490	-3.561588	0.068330
1.749090	-3.561588	0.084673	1.584090	-3.561588	0.079540	1.695960	-3.561588	0.068879
1.740690	-3.561588	0.085381	1.582470	-3.561588	0.078310	1.704440	-3.561588	0.069474
1.734660	-3.561588	0.085912	1.581310	-3.561588	0.077050	1.710540	-3.561588	0.069916
1.731010	-3.561588	0.086275	1.580910	-3.561588	0.076352	1.716630	-3.561588	0.070370
1.722530	-3.561588	0.086931	1.580820	-3.561588	0.075904	1.722710	-3.561588	0.070835
1.716440	-3.561588	0.087408	1.580920	-3.561588	0.075391	1.731170	-3.561588	0.071520
1.710340	-3.561588	0.087854	1.581330	-3.561588	0.074730	1.734820	-3.561588	0.071793
1.704230	-3.561588	0.088261	1.582520	-3.561588	0.073623	1.740840	-3.561588	0.072280
1.695740	-3.561588	0.088737	1.584170	-3.561588	0.072621	1.749220	-3.561588	0.072994
1.687250	-3.561588	0.089135	1.586910	-3.561588	0.071392	1.757570	-3.561588	0.073720
1.678780	-3.561588	0.089444	1.588960	-3.561588	0.070707	1.765870	-3.561588	0.074458
1.672730	-3.561588	0.089597	1.595240	-3.561588	0.069112	1.774120	-3.561588	0.075211
1.666700	-3.561588	0.089686	1.597950	-3.561588	0.068639	1.781940	-3.561588	0.075960
1.660700	-3.561588	0.089705	1.602960	-3.561588	0.067914	1.787360	-3.561588	0.076419
1.654750	-3.561588	0.089656	1.608180	-3.561588	0.067369	1.796810	-3.561588	0.077443
1.646460	-3.561588	0.089529	1.615860	-3.561588	0.066808	1.802990	-3.561588	0.078143
1.640610	-3.561588	0.089323	1.626050	-3.561588	0.066419	1.810880	-3.561588	0.079252
1.637180	-3.561588	0.089098	1.631710	-3.561588	0.066357			
1.631460	-3.561588	0.088765	1.637440	-3.561588	0.066363			

C.3 Airfoil L19

Table C.3 Airfoil L19

X	Y	Z	X	Y	Z	X	Y	Z
1.757360	-3.374136	0.069831	1.546420	-3.374136	0.085347	1.563360	-3.374136	0.059974
1.749380	-3.374136	0.070556	1.535820	-3.374136	0.084536	1.570070	-3.374136	0.059975
1.742090	-3.374136	0.071151	1.527670	-3.374136	0.083539	1.579140	-3.374136	0.060039
1.730860	-3.374136	0.072418	1.521910	-3.374136	0.082538	1.586040	-3.374136	0.060156
1.722750	-3.374136	0.073786	1.516430	-3.374136	0.081366	1.593010	-3.374136	0.060315
1.714380	-3.374136	0.074803	1.513210	-3.374136	0.080431	1.600040	-3.374136	0.060507
1.705450	-3.374136	0.075922	1.506690	-3.374136	0.078400	1.607120	-3.374136	0.060731
1.696420	-3.374136	0.077036	1.504250	-3.374136	0.077315	1.616500	-3.374136	0.061068
1.687300	-3.374136	0.078144	1.501250	-3.374136	0.075712	1.625910	-3.374136	0.061453
1.678110	-3.374136	0.079241	1.499370	-3.374136	0.074258	1.635340	-3.374136	0.061881
1.671120	-3.374136	0.080120	1.498010	-3.374136	0.072823	1.642500	-3.374136	0.062214
1.666350	-3.374136	0.080787	1.497480	-3.374136	0.071990	1.649650	-3.374136	0.062556
1.657000	-3.374136	0.081828	1.497340	-3.374136	0.071419	1.656780	-3.374136	0.062906
1.649880	-3.374136	0.082637	1.497470	-3.374136	0.070712	1.666150	-3.374136	0.063409
1.642740	-3.374136	0.083400	1.497980	-3.374136	0.069923	1.670930	-3.374136	0.063622
1.635590	-3.374136	0.084102	1.499310	-3.374136	0.068710	1.677930	-3.374136	0.063984
1.626180	-3.374136	0.084890	1.501150	-3.374136	0.067598	1.687140	-3.374136	0.064504
1.616790	-3.374136	0.085568	1.504120	-3.374136	0.066244	1.696280	-3.374136	0.065034
1.607410	-3.374136	0.086126	1.506540	-3.374136	0.065436	1.705330	-3.374136	0.065572
1.600340	-3.374136	0.086444	1.513020	-3.374136	0.063710	1.714280	-3.374136	0.066122
1.593320	-3.374136	0.086660	1.516220	-3.374136	0.063125	1.722360	-3.374136	0.066669
1.586350	-3.374136	0.086770	1.521680	-3.374136	0.062273	1.730680	-3.374136	0.067140
1.579450	-3.374136	0.086775	1.527410	-3.374136	0.061603	1.742030	-3.374136	0.068154
1.570380	-3.374136	0.086724	1.535540	-3.374136	0.060878	1.749360	-3.374136	0.068879
1.563660	-3.374136	0.086516	1.546140	-3.374136	0.060276	1.757360	-3.374136	0.069831
1.559290	-3.374136	0.086210	1.552490	-3.374136	0.060092			
1.552790	-3.374136	0.085828	1.558990	-3.374136	0.059983			

C.4 Airfoil L18

Table C.4 Airfoil L18

X	Y	Z	X	Y	Z	X	Y	Z
1.703780	-3.186684	0.060097	1.467210	-3.186684	0.083118	1.485870	-3.186684	0.054228
1.695740	-3.186684	0.060960	1.456170	-3.186684	0.082355	1.493450	-3.186684	0.054086
1.687340	-3.186684	0.061786	1.447520	-3.186684	0.081342	1.503290	-3.186684	0.053961
1.674320	-3.186684	0.063588	1.441220	-3.186684	0.080256	1.511140	-3.186684	0.053936
1.663470	-3.186684	0.065754	1.435240	-3.186684	0.078993	1.519080	-3.186684	0.053954
1.654730	-3.186684	0.067091	1.431480	-3.186684	0.077891	1.527120	-3.186684	0.054004
1.645140	-3.186684	0.068604	1.424670	-3.186684	0.075801	1.535230	-3.186684	0.054085
1.635420	-3.186684	0.070126	1.421820	-3.186684	0.074544	1.545530	-3.186684	0.054223
1.625560	-3.186684	0.071650	1.418520	-3.186684	0.072799	1.555870	-3.186684	0.054407
1.615590	-3.186684	0.073168	1.416380	-3.186684	0.071132	1.566230	-3.186684	0.054629
1.607660	-3.186684	0.074436	1.414820	-3.186684	0.069529	1.574450	-3.186684	0.054807
1.601780	-3.186684	0.075455	1.414150	-3.186684	0.068568	1.582660	-3.186684	0.054992
1.591570	-3.186684	0.076918	1.413960	-3.186684	0.067877	1.590830	-3.186684	0.055182
1.583440	-3.186684	0.078103	1.414100	-3.186684	0.066973	1.601110	-3.186684	0.055466
1.575280	-3.186684	0.079227	1.414700	-3.186684	0.066052	1.607020	-3.186684	0.055571
1.567100	-3.186684	0.080268	1.416160	-3.186684	0.064728	1.615000	-3.186684	0.055765
1.556780	-3.186684	0.081405	1.418210	-3.186684	0.063495	1.625030	-3.186684	0.056059
1.546480	-3.186684	0.082403	1.421400	-3.186684	0.062008	1.634950	-3.186684	0.056360
1.536210	-3.186684	0.083246	1.424170	-3.186684	0.061060	1.644740	-3.186684	0.056667
1.528130	-3.186684	0.083772	1.430850	-3.186684	0.059196	1.654380	-3.186684	0.056986
1.520110	-3.186684	0.084159	1.434540	-3.186684	0.058478	1.662720	-3.186684	0.057324
1.512170	-3.186684	0.084400	1.440440	-3.186684	0.057479	1.673950	-3.186684	0.057679
1.504330	-3.186684	0.084501	1.446690	-3.186684	0.056665	1.687200	-3.186684	0.058601
1.494480	-3.186684	0.084557	1.455270	-3.186684	0.055758	1.695680	-3.186684	0.059302
1.486890	-3.186684	0.084384	1.466250	-3.186684	0.054927	1.703780	-3.186684	0.060097
1.481570	-3.186684	0.084039	1.473310	-3.186684	0.054594			
1.474300	-3.186684	0.083639	1.480570	-3.186684	0.054336			

C.5 Airfoil L17

Table C.5 Airfoil L17

X	Y	Z	X	Y	Z	X	Y	Z
1.650140	-2.999232	0.050161	1.388140	-2.999232	0.081406	1.408440	-2.999232	0.048945
1.642040	-2.999232	0.051153	1.376680	-2.999232	0.080689	1.416870	-2.999232	0.048637
1.632530	-2.999232	0.052243	1.367530	-2.999232	0.079667	1.427490	-2.999232	0.048305
1.617740	-2.999232	0.054637	1.360660	-2.999232	0.078510	1.436270	-2.999232	0.048111
1.604170	-2.999232	0.057701	1.354190	-2.999232	0.077165	1.445190	-2.999232	0.047959
1.595070	-2.999232	0.059358	1.349890	-2.999232	0.075913	1.454230	-2.999232	0.047836
1.584850	-2.999232	0.061280	1.342790	-2.999232	0.073765	1.463360	-2.999232	0.047743
1.574440	-2.999232	0.063224	1.339530	-2.999232	0.072349	1.474570	-2.999232	0.047661
1.563850	-2.999232	0.065178	1.335920	-2.999232	0.070469	1.485840	-2.999232	0.047620
1.553110	-2.999232	0.067136	1.333500	-2.999232	0.068596	1.497130	-2.999232	0.047614
1.544250	-2.999232	0.068820	1.331740	-2.999232	0.066832	1.506410	-2.999232	0.047605
1.537290	-2.999232	0.070229	1.330930	-2.999232	0.065746	1.515670	-2.999232	0.047602
1.526220	-2.999232	0.072135	1.330670	-2.999232	0.064937	1.524880	-2.999232	0.047600
1.517090	-2.999232	0.073726	1.330830	-2.999232	0.063837	1.536060	-2.999232	0.047644
1.507920	-2.999232	0.075241	1.331520	-2.999232	0.062780	1.543090	-2.999232	0.047601
1.498720	-2.999232	0.076652	1.333110	-2.999232	0.061340	1.552050	-2.999232	0.047598
1.487510	-2.999232	0.078162	1.335350	-2.999232	0.059982	1.562890	-2.999232	0.047647
1.476310	-2.999232	0.079500	1.338760	-2.999232	0.058357	1.573590	-2.999232	0.047702
1.465150	-2.999232	0.080651	1.341880	-2.999232	0.057258	1.584110	-2.999232	0.047764
1.456060	-2.999232	0.081415	1.348760	-2.999232	0.055257	1.594440	-2.999232	0.047838
1.447050	-2.999232	0.082002	1.352940	-2.999232	0.054391	1.603030	-2.999232	0.047969
1.438150	-2.999232	0.082403	1.359280	-2.999232	0.053237	1.617160	-2.999232	0.048101
1.429370	-2.999232	0.082627	1.366040	-2.999232	0.052266	1.632300	-2.999232	0.048874
1.418740	-2.999232	0.082808	1.375070	-2.999232	0.051171	1.641950	-2.999232	0.049515
1.410280	-2.999232	0.082695	1.386430	-2.999232	0.050113	1.650140	-2.999232	0.050161
1.404010	-2.999232	0.082342	1.394190	-2.999232	0.049611			
1.395960	-2.999232	0.081947	1.402200	-2.999232	0.049185			

C.6 Airfoil L16

Table C.6 Airfoil L16

X	Y	Z	X	Y	Z	X	Y	Z
1.596430	-2.811780	0.040099	1.309210	-2.811780	0.080029	1.331070	-2.811780	0.043968
1.588280	-2.811780	0.041205	1.297320	-2.811780	0.079352	1.340360	-2.811780	0.043477
1.577670	-2.811780	0.042583	1.287670	-2.811780	0.078322	1.351750	-2.811780	0.042931
1.561130	-2.811780	0.045608	1.280240	-2.811780	0.077102	1.361460	-2.811780	0.042548
1.544870	-2.811780	0.049649	1.273260	-2.811780	0.075682	1.371350	-2.811780	0.042206
1.535410	-2.811780	0.051623	1.268410	-2.811780	0.074291	1.381380	-2.811780	0.041890
1.524560	-2.811780	0.053957	1.261020	-2.811780	0.072081	1.391530	-2.811780	0.041602
1.513470	-2.811780	0.056328	1.257340	-2.811780	0.070515	1.403650	-2.811780	0.041287
1.502160	-2.811780	0.058721	1.253430	-2.811780	0.068504	1.415840	-2.811780	0.041008
1.490670	-2.811780	0.061127	1.250730	-2.811780	0.066431	1.428050	-2.811780	0.040760
1.480890	-2.811780	0.063246	1.248760	-2.811780	0.064509	1.438380	-2.811780	0.040543
1.472850	-2.811780	0.065073	1.247810	-2.811780	0.063302	1.448690	-2.811780	0.040329
1.460940	-2.811780	0.067432	1.247490	-2.811780	0.062376	1.458940	-2.811780	0.040114
1.450820	-2.811780	0.069450	1.247650	-2.811780	0.061080	1.471000	-2.811780	0.039905
1.440650	-2.811780	0.071378	1.248420	-2.811780	0.059885	1.479160	-2.811780	0.039685
1.430430	-2.811780	0.073180	1.250140	-2.811780	0.058328	1.489080	-2.811780	0.039466
1.418330	-2.811780	0.075074	1.252580	-2.811780	0.056841	1.500740	-2.811780	0.039260
1.406250	-2.811780	0.076766	1.256210	-2.811780	0.055075	1.512200	-2.811780	0.039062
1.394210	-2.811780	0.078237	1.259680	-2.811780	0.053818	1.523450	-2.811780	0.038871
1.384120	-2.811780	0.079260	1.266760	-2.811780	0.051686	1.534460	-2.811780	0.038695
1.374130	-2.811780	0.080067	1.271420	-2.811780	0.050661	1.543300	-2.811780	0.038626
1.364250	-2.811780	0.080648	1.278200	-2.811780	0.049346	1.560310	-2.811780	0.038452
1.354540	-2.811780	0.081013	1.285460	-2.811780	0.048212	1.577350	-2.811780	0.039031
1.343130	-2.811780	0.081328	1.294940	-2.811780	0.046931	1.588150	-2.811780	0.039587
1.333810	-2.811780	0.081291	1.306690	-2.811780	0.045653	1.596430	-2.811780	0.040099
1.326580	-2.811780	0.080955	1.315140	-2.811780	0.044971			
1.317750	-2.811780	0.080578	1.323900	-2.811780	0.044363			

C.7 Airfoil L15

Table C.7 Airfoil L15

X	Y	Z	X	Y	Z	X	Y	Z
1.542680	-2.624328	0.029965	1.230370	-2.624328	0.078853	1.253760	-2.624328	0.039176
1.534460	-2.624328	0.031170	1.218050	-2.624328	0.078205	1.263900	-2.624328	0.038491
1.522760	-2.624328	0.032853	1.207910	-2.624328	0.077163	1.276050	-2.624328	0.037728
1.504470	-2.624328	0.036535	1.199910	-2.624328	0.075882	1.286700	-2.624328	0.037145
1.485550	-2.624328	0.041612	1.192430	-2.624328	0.074389	1.297550	-2.624328	0.036601
1.475740	-2.624328	0.043896	1.187040	-2.624328	0.072869	1.308570	-2.624328	0.036078
1.464270	-2.624328	0.046642	1.179350	-2.624328	0.070591	1.319730	-2.624328	0.035581
1.452510	-2.624328	0.049440	1.175250	-2.624328	0.068881	1.332760	-2.624328	0.035028
1.440490	-2.624328	0.052273	1.171040	-2.624328	0.066741	1.345860	-2.624328	0.034505
1.428250	-2.624328	0.055128	1.168060	-2.624328	0.064471	1.359000	-2.624328	0.034010
1.417550	-2.624328	0.057693	1.165870	-2.624328	0.062394	1.370380	-2.624328	0.033570
1.408440	-2.624328	0.059960	1.164780	-2.624328	0.061069	1.381720	-2.624328	0.033130
1.395710	-2.624328	0.062776	1.164380	-2.624328	0.060028	1.393000	-2.624328	0.032688
1.384610	-2.624328	0.065234	1.164550	-2.624328	0.058535	1.405950	-2.624328	0.032222
1.373430	-2.624328	0.067588	1.165410	-2.624328	0.057201	1.415230	-2.624328	0.031803
1.362220	-2.624328	0.069796	1.167250	-2.624328	0.055525	1.426110	-2.624328	0.031355
1.349240	-2.624328	0.072079	1.169880	-2.624328	0.053907	1.438570	-2.624328	0.030892
1.336280	-2.624328	0.074130	1.173730	-2.624328	0.052000	1.450800	-2.624328	0.030437
1.323360	-2.624328	0.075926	1.177550	-2.624328	0.050580	1.462770	-2.624328	0.029992
1.312270	-2.624328	0.077221	1.184830	-2.624328	0.048325	1.474450	-2.624328	0.029566
1.301290	-2.624328	0.078262	1.189980	-2.624328	0.047133	1.483530	-2.624328	0.029309
1.290460	-2.624328	0.079035	1.197200	-2.624328	0.045658	1.503430	-2.624328	0.028763
1.279810	-2.624328	0.079553	1.204960	-2.624328	0.044357	1.522350	-2.624328	0.029119
1.267630	-2.624328	0.080005	1.214880	-2.624328	0.042894	1.534310	-2.624328	0.029574
1.257440	-2.624328	0.080054	1.227010	-2.624328	0.041409	1.542680	-2.624328	0.029965
1.249260	-2.624328	0.079753	1.236150	-2.624328	0.040541			
1.239650	-2.624328	0.079403	1.245660	-2.624328	0.039743			

C.8 Airfoil L14

Table C.8 Airfoil L14

X	Y	Z	X	Y	Z	X	Y	Z
1.488880	-2.436876	0.019805	1.151620	-2.436876	0.077766	1.176500	-2.436876	0.034468
1.480600	-2.436876	0.021094	1.138870	-2.436876	0.077134	1.187490	-2.436876	0.033586
1.467820	-2.436876	0.023090	1.128220	-2.436876	0.076074	1.200400	-2.436876	0.032608
1.447790	-2.436876	0.027445	1.119660	-2.436876	0.074733	1.211980	-2.436876	0.031819
1.426220	-2.436876	0.033601	1.111670	-2.436876	0.073167	1.223790	-2.436876	0.031066
1.416060	-2.436876	0.036184	1.105730	-2.436876	0.071522	1.235800	-2.436876	0.030330
1.403970	-2.436876	0.039337	1.097760	-2.436876	0.069168	1.247970	-2.436876	0.029616
1.391540	-2.436876	0.042559	1.093230	-2.436876	0.067319	1.261900	-2.436876	0.028824
1.378820	-2.436876	0.045828	1.088710	-2.436876	0.065049	1.275910	-2.436876	0.028057
1.365830	-2.436876	0.049130	1.085450	-2.436876	0.062585	1.289970	-2.436876	0.027314
1.354240	-2.436876	0.052147	1.083050	-2.436876	0.060353	1.302390	-2.436876	0.026643
1.344070	-2.436876	0.054867	1.081810	-2.436876	0.058913	1.314770	-2.436876	0.025969
1.330500	-2.436876	0.058139	1.081350	-2.436876	0.057758	1.327070	-2.436876	0.025292
1.318430	-2.436876	0.061045	1.081510	-2.436876	0.056068	1.340900	-2.436876	0.024569
1.306270	-2.436876	0.063832	1.082450	-2.436876	0.054593	1.351290	-2.436876	0.023936
1.294050	-2.436876	0.066452	1.084430	-2.436876	0.052798	1.363130	-2.436876	0.023253
1.280200	-2.436876	0.069125	1.087250	-2.436876	0.051048	1.376390	-2.436876	0.022534
1.266360	-2.436876	0.071535	1.091320	-2.436876	0.049001	1.389380	-2.436876	0.021826
1.252570	-2.436876	0.073655	1.095490	-2.436876	0.047416	1.402070	-2.436876	0.021131
1.240490	-2.436876	0.075230	1.102970	-2.436876	0.045046	1.414420	-2.436876	0.020458
1.228530	-2.436876	0.076511	1.108600	-2.436876	0.043684	1.423730	-2.436876	0.020025
1.216740	-2.436876	0.077484	1.116250	-2.436876	0.042049	1.446510	-2.436876	0.019060
1.205160	-2.436876	0.078162	1.124520	-2.436876	0.040584	1.467320	-2.436876	0.019176
1.192200	-2.436876	0.078747	1.134880	-2.436876	0.038945	1.480430	-2.436876	0.019518
1.181140	-2.436876	0.078889	1.147390	-2.436876	0.037267	1.488880	-2.436876	0.019805
1.172010	-2.436876	0.078635	1.157220	-2.436876	0.036210			
1.161620	-2.436876	0.078314	1.167480	-2.436876	0.035220			

C.9 Airfoil L13

Table C.9 Airfoil L13

X	Y	Z	X	Y	Z	X	Y	Z
1.435060	-2.249424	0.009655	1.072910	-2.249424	0.076678	1.099290	-2.249424	0.029765
1.426710	-2.249424	0.011014	1.059730	-2.249424	0.076047	1.111120	-2.249424	0.028684
1.412840	-2.249424	0.013326	1.048580	-2.249424	0.074961	1.124800	-2.249424	0.027497
1.391090	-2.249424	0.018359	1.039460	-2.249424	0.073558	1.137300	-2.249424	0.026501
1.366890	-2.249424	0.025621	1.030970	-2.249424	0.071915	1.150070	-2.249424	0.025537
1.356380	-2.249424	0.028493	1.024470	-2.249424	0.070148	1.163060	-2.249424	0.024585
1.343670	-2.249424	0.032045	1.016210	-2.249424	0.067709	1.176240	-2.249424	0.023652
1.330580	-2.249424	0.035684	1.011260	-2.249424	0.065722	1.191070	-2.249424	0.022625
1.317150	-2.249424	0.039384	1.006430	-2.249424	0.063321	1.205980	-2.249424	0.021619
1.303430	-2.249424	0.043127	1.002880	-2.249424	0.060663	1.220950	-2.249424	0.020632
1.290930	-2.249424	0.046597	1.000280	-2.249424	0.058279	1.234410	-2.249424	0.019726
1.279700	-2.249424	0.049777	0.998887	-2.249424	0.056724	1.247830	-2.249424	0.018816
1.265320	-2.249424	0.053500	0.998361	-2.249424	0.055455	1.261160	-2.249424	0.017902
1.252270	-2.249424	0.056855	0.998519	-2.249424	0.053569	1.275870	-2.249424	0.016926
1.239130	-2.249424	0.060078	0.999539	-2.249424	0.051954	1.287370	-2.249424	0.016071
1.225920	-2.249424	0.063112	1.001640	-2.249424	0.050039	1.300160	-2.249424	0.015151
1.211190	-2.249424	0.066171	1.004660	-2.249424	0.048158	1.314210	-2.249424	0.014182
1.196480	-2.249424	0.068934	1.008950	-2.249424	0.045974	1.327960	-2.249424	0.013227
1.181820	-2.249424	0.071375	1.013460	-2.249424	0.044221	1.341360	-2.249424	0.012287
1.168750	-2.249424	0.073232	1.021150	-2.249424	0.041746	1.354380	-2.249424	0.011375
1.155820	-2.249424	0.074756	1.027260	-2.249424	0.040212	1.363930	-2.249424	0.010778
1.143070	-2.249424	0.075929	1.035350	-2.249424	0.038421	1.389580	-2.249424	0.009365
1.130550	-2.249424	0.076768	1.044120	-2.249424	0.036794	1.412260	-2.249424	0.009233
1.116820	-2.249424	0.077483	1.054930	-2.249424	0.034989	1.426520	-2.249424	0.009458
1.104890	-2.249424	0.077717	1.067820	-2.249424	0.033132	1.435060	-2.249424	0.009655
1.094810	-2.249424	0.077516	1.078340	-2.249424	0.031888			
1.083640	-2.249424	0.077225	1.089340	-2.249424	0.030706			

C.10 Airfoil L12

Table C.10 Airfoil L12

X	Y	Z	X	Y	Z	X	Y	Z
1.381220	-2.061972	-0.000452	0.994219	-2.061972	0.075511	1.022110	-2.061972	0.024993
1.372810	-2.061972	0.000961	0.980611	-2.061972	0.074866	1.034780	-2.061972	0.023718
1.357850	-2.061972	0.003588	0.968960	-2.061972	0.073744	1.049220	-2.061972	0.022330
1.334370	-2.061972	0.009298	0.959275	-2.061972	0.072273	1.062640	-2.061972	0.021129
1.307550	-2.061972	0.017680	0.950278	-2.061972	0.070548	1.076370	-2.061972	0.019957
1.296690	-2.061972	0.020829	0.943231	-2.061972	0.068659	1.090350	-2.061972	0.018791
1.283370	-2.061972	0.024771	0.934683	-2.061972	0.066125	1.104530	-2.061972	0.017642
1.269620	-2.061972	0.028816	0.929311	-2.061972	0.064001	1.120260	-2.061972	0.016389
1.255490	-2.061972	0.032937	0.924181	-2.061972	0.061468	1.136080	-2.061972	0.015150
1.241020	-2.061972	0.037111	0.920345	-2.061972	0.058615	1.151960	-2.061972	0.013927
1.227630	-2.061972	0.041031	0.917529	-2.061972	0.056077	1.166460	-2.061972	0.012789
1.215350	-2.061972	0.044676	0.915991	-2.061972	0.054407	1.180900	-2.061972	0.011646
1.200140	-2.061972	0.048841	0.915396	-2.061972	0.053025	1.195250	-2.061972	0.010497
1.186130	-2.061972	0.052642	0.915550	-2.061972	0.050943	1.210840	-2.061972	0.009276
1.172000	-2.061972	0.056298	0.916651	-2.061972	0.049187	1.223450	-2.061972	0.008195
1.157800	-2.061972	0.059745	0.918886	-2.061972	0.047155	1.237190	-2.061972	0.007042
1.142200	-2.061972	0.063180	0.922101	-2.061972	0.045143	1.252030	-2.061972	0.005831
1.126610	-2.061972	0.066290	0.926613	-2.061972	0.042824	1.266540	-2.061972	0.004637
1.111080	-2.061972	0.069042	0.931470	-2.061972	0.040904	1.280650	-2.061972	0.003463
1.097020	-2.061972	0.071179	0.939369	-2.061972	0.038335	1.294340	-2.061972	0.002322
1.083120	-2.061972	0.072943	0.945958	-2.061972	0.036629	1.304120	-2.061972	0.001573
1.069410	-2.061972	0.074315	0.954487	-2.061972	0.034687	1.332630	-2.061972	-0.000304
1.055970	-2.061972	0.075313	0.963758	-2.061972	0.032903	1.357190	-2.061972	-0.000684
1.041460	-2.061972	0.076148	0.975016	-2.061972	0.030943	1.372600	-2.061972	-0.000574
1.028660	-2.061972	0.076471	0.988284	-2.061972	0.028923	1.381220	-2.061972	-0.000452
1.017630	-2.061972	0.076326	0.999494	-2.061972	0.027496			
1.005680	-2.061972	0.076061	1.011230	-2.061972	0.026127			

C.11 Airfoil L11

Table C.11 Airfoil L11

X	Y	Z	X	Y	Z	X	Y	Z
1.327370	-1.874520	-0.010491	0.915526	-1.874520	0.074197	0.944942	-1.874520	0.020091
1.318890	-1.874520	-0.009036	0.901487	-1.874520	0.073522	0.958458	-1.874520	0.018628
1.302850	-1.874520	-0.006100	0.889335	-1.874520	0.072352	0.973658	-1.874520	0.017051
1.277650	-1.874520	0.000278	0.879086	-1.874520	0.070807	0.988005	-1.874520	0.015652
1.248210	-1.874520	0.009782	0.869587	-1.874520	0.068994	1.002690	-1.874520	0.014278
1.237000	-1.874520	0.013196	0.861989	-1.874520	0.066980	1.017650	-1.874520	0.012906
1.223060	-1.874520	0.017515	0.853156	-1.874520	0.064342	1.032840	-1.874520	0.011546
1.208650	-1.874520	0.021955	0.847361	-1.874520	0.062079	1.049460	-1.874520	0.010077
1.193820	-1.874520	0.026485	0.841927	-1.874520	0.059408	1.066190	-1.874520	0.008617
1.178610	-1.874520	0.031080	0.837809	-1.874520	0.056360	1.082980	-1.874520	0.007169
1.164320	-1.874520	0.035443	0.834783	-1.874520	0.053667	1.098520	-1.874520	0.005806
1.150990	-1.874520	0.039549	0.833099	-1.874520	0.051883	1.113990	-1.874520	0.004435
1.134960	-1.874520	0.044146	0.832436	-1.874520	0.050388	1.129360	-1.874520	0.003057
1.119980	-1.874520	0.048387	0.832585	-1.874520	0.048109	1.145820	-1.874520	0.001602
1.104870	-1.874520	0.052469	0.833768	-1.874520	0.046213	1.159540	-1.874520	0.000298
1.089670	-1.874520	0.056321	0.836135	-1.874520	0.044064	1.174230	-1.874520	-0.001083
1.073200	-1.874520	0.060122	0.839547	-1.874520	0.041924	1.189870	-1.874520	-0.002524
1.056740	-1.874520	0.063567	0.844283	-1.874520	0.039473	1.205120	-1.874520	-0.003945
1.040340	-1.874520	0.066622	0.849487	-1.874520	0.037389	1.219950	-1.874520	-0.005342
1.025290	-1.874520	0.069032	0.857599	-1.874520	0.034734	1.234300	-1.874520	-0.006701
1.010410	-1.874520	0.071029	0.864668	-1.874520	0.032859	1.244310	-1.874520	-0.007587
0.995756	-1.874520	0.072593	0.873637	-1.874520	0.030774	1.275680	-1.874520	-0.009933
0.981375	-1.874520	0.073743	0.883412	-1.874520	0.028840	1.302120	-1.874520	-0.010552
0.966090	-1.874520	0.074687	0.895118	-1.874520	0.026735	1.318680	-1.874520	-0.010551
0.952430	-1.874520	0.075094	0.908770	-1.874520	0.024568	1.327370	-1.874520	-0.010491
0.940446	-1.874520	0.075003	0.920667	-1.874520	0.022966			
0.927717	-1.874520	0.074757	0.933151	-1.874520	0.021416			

C.12 Airfoil L10

Table C.12 Airfoil L10

X	Y	Z	X	Y	Z	X	Y	Z
1.273540	-1.687068	-0.020436	0.836806	-1.687068	0.072678	0.867789	-1.687068	0.015007
1.264990	-1.687068	-0.018953	0.822336	-1.687068	0.071957	0.882149	-1.687068	0.013365
1.247860	-1.687068	-0.015718	0.809683	-1.687068	0.070726	0.898110	-1.687068	0.011612
1.220930	-1.687068	-0.008687	0.798871	-1.687068	0.069098	0.913381	-1.687068	0.010024
1.188880	-1.687068	0.001931	0.788870	-1.687068	0.067189	0.929021	-1.687068	0.008458
1.177310	-1.687068	0.005596	0.780721	-1.687068	0.065046	0.944970	-1.687068	0.006888
1.162750	-1.687068	0.010279	0.771605	-1.687068	0.062293	0.961164	-1.687068	0.005329
1.147670	-1.687068	0.015101	0.765389	-1.687068	0.059887	0.978677	-1.687068	0.003658
1.132140	-1.687068	0.020026	0.759654	-1.687068	0.057075	0.996313	-1.687068	0.001990
1.116190	-1.687068	0.025028	0.755253	-1.687068	0.053827	1.014010	-1.687068	0.000331
1.101000	-1.687068	0.029824	0.752020	-1.687068	0.050978	1.030590	-1.687068	-0.001248
1.086610	-1.687068	0.034387	0.750191	-1.687068	0.049078	1.047090	-1.687068	-0.002837
1.069760	-1.687068	0.039401	0.749461	-1.687068	0.047470	1.063480	-1.687068	-0.004434
1.053810	-1.687068	0.044072	0.749607	-1.687068	0.044996	1.080820	-1.687068	-0.006108
1.037720	-1.687068	0.048571	0.750872	-1.687068	0.042960	1.095640	-1.687068	-0.007631
1.021530	-1.687068	0.052819	0.753373	-1.687068	0.040695	1.111290	-1.687068	-0.009230
1.004190	-1.687068	0.056973	0.756984	-1.687068	0.038430	1.127710	-1.687068	-0.010887
0.986851	-1.687068	0.060739	0.761947	-1.687068	0.035852	1.143720	-1.687068	-0.012520
0.969577	-1.687068	0.064080	0.767498	-1.687068	0.033607	1.159260	-1.687068	-0.014127
0.953542	-1.687068	0.066754	0.775828	-1.687068	0.030876	1.174270	-1.687068	-0.015689
0.937687	-1.687068	0.068976	0.783378	-1.687068	0.028837	1.184510	-1.687068	-0.016701
0.922072	-1.687068	0.070723	0.792788	-1.687068	0.026615	1.218750	-1.687068	-0.019506
0.906759	-1.687068	0.072015	0.803069	-1.687068	0.024540	1.247060	-1.687068	-0.020349
0.890697	-1.687068	0.073055	0.815226	-1.687068	0.022304	1.264760	-1.687068	-0.020448
0.876170	-1.687068	0.073535	0.829263	-1.687068	0.020007	1.273540	-1.687068	-0.020436
0.863236	-1.687068	0.073493	0.841849	-1.687068	0.018238			
0.849727	-1.687068	0.073257	0.855077	-1.687068	0.016516			

C.13 Airfoil L9

Table C.13 Airfoil L9

X	Y	Z	X	Y	Z	X	Y	Z
1.219720	-1.499616	-0.030266	0.758037	-1.499616	0.070901	0.790635	-1.499616	0.009690
1.211100	-1.499616	-0.028767	0.743135	-1.499616	0.070115	0.805841	-1.499616	0.007881
1.192880	-1.499616	-0.025247	0.729982	-1.499616	0.068810	0.822564	-1.499616	0.005968
1.164230	-1.499616	-0.017583	0.718608	-1.499616	0.067090	0.838760	-1.499616	0.004204
1.129550	-1.499616	-0.005869	0.708106	-1.499616	0.065075	0.855358	-1.499616	0.002458
1.117630	-1.499616	-0.001966	0.699409	-1.499616	0.062797	0.872291	-1.499616	0.000704
1.102440	-1.499616	0.003066	0.690012	-1.499616	0.059918	0.889492	-1.499616	-0.001043
1.086690	-1.499616	0.008255	0.683375	-1.499616	0.057365	0.907902	-1.499616	-0.002899
1.070450	-1.499616	0.013560	0.677341	-1.499616	0.054406	0.926444	-1.499616	-0.004758
1.053760	-1.499616	0.018952	0.672662	-1.499616	0.050956	0.945058	-1.499616	-0.006612
1.037660	-1.499616	0.024170	0.669223	-1.499616	0.047946	0.962667	-1.499616	-0.008394
1.022220	-1.499616	0.029179	0.667251	-1.499616	0.045931	0.980206	-1.499616	-0.010187
1.004540	-1.499616	0.034595	0.666454	-1.499616	0.044209	0.997614	-1.499616	-0.011990
0.987620	-1.499616	0.039683	0.666598	-1.499616	0.041539	1.015820	-1.499616	-0.013867
0.970543	-1.499616	0.044586	0.667947	-1.499616	0.039364	1.031750	-1.499616	-0.015599
0.953358	-1.499616	0.049217	0.670585	-1.499616	0.036987	1.048350	-1.499616	-0.017403
0.935137	-1.499616	0.053706	0.674396	-1.499616	0.034599	1.065570	-1.499616	-0.019260
0.916923	-1.499616	0.057778	0.679589	-1.499616	0.031899	1.082330	-1.499616	-0.021091
0.898774	-1.499616	0.061391	0.685489	-1.499616	0.029496	1.098580	-1.499616	-0.022892
0.881748	-1.499616	0.064315	0.694042	-1.499616	0.026699	1.114260	-1.499616	-0.024642
0.864916	-1.499616	0.066748	0.702074	-1.499616	0.024502	1.124740	-1.499616	-0.025765
0.848344	-1.499616	0.068665	0.711927	-1.499616	0.022154	1.161830	-1.499616	-0.029013
0.832097	-1.499616	0.070088	0.722717	-1.499616	0.019947	1.192020	-1.499616	-0.030059
0.815256	-1.499616	0.071208	0.735326	-1.499616	0.017592	1.210870	-1.499616	-0.030243
0.799862	-1.499616	0.071750	0.749753	-1.499616	0.015182	1.219720	-1.499616	-0.030266
0.785978	-1.499616	0.071748	0.763028	-1.499616	0.013258			
0.771689	-1.499616	0.071511	0.777002	-1.499616	0.011375			

C.14 Airfoil L8

Table C.14 Airfoil L8

X	Y	Z	X	Y	Z	X	Y	Z
1.165940	-1.312164	-0.039963	0.679201	-1.312164	0.068820	0.713473	-1.312164	0.004098
1.157230	-1.312164	-0.038460	0.663867	-1.312164	0.067952	0.729525	-1.312164	0.002137
1.137920	-1.312164	-0.034670	0.650214	-1.312164	0.066558	0.747014	-1.312164	0.000081
1.107530	-1.312164	-0.026400	0.638279	-1.312164	0.064733	0.764136	-1.312164	-0.001844
1.070220	-1.312164	-0.013614	0.627278	-1.312164	0.062601	0.781693	-1.312164	-0.003754
1.057940	-1.312164	-0.009488	0.618033	-1.312164	0.060181	0.799612	-1.312164	-0.005677
1.042130	-1.312164	-0.004123	0.608359	-1.312164	0.057165	0.817821	-1.312164	-0.007597
1.025710	-1.312164	0.001416	0.601304	-1.312164	0.054458	0.837130	-1.312164	-0.009620
1.008750	-1.312164	0.007084	0.594974	-1.312164	0.051347	0.856582	-1.312164	-0.011651
0.991305	-1.312164	0.012850	0.590018	-1.312164	0.047689	0.876109	-1.312164	-0.013681
0.974304	-1.312164	0.018474	0.586377	-1.312164	0.044517	0.894756	-1.312164	-0.015649
0.957807	-1.312164	0.023917	0.584263	-1.312164	0.042383	0.913328	-1.312164	-0.017632
0.939291	-1.312164	0.029717	0.583401	-1.312164	0.040548	0.931758	-1.312164	-0.019624
0.921395	-1.312164	0.035207	0.583545	-1.312164	0.037682	0.950844	-1.312164	-0.021687
0.903328	-1.312164	0.040498	0.584980	-1.312164	0.035369	0.967879	-1.312164	-0.023614
0.885143	-1.312164	0.045496	0.587757	-1.312164	0.032881	0.985434	-1.312164	-0.025607
0.866040	-1.312164	0.050303	0.591772	-1.312164	0.030374	1.003440	-1.312164	-0.027647
0.846944	-1.312164	0.054661	0.597197	-1.312164	0.027557	1.020960	-1.312164	-0.029658
0.827916	-1.312164	0.058528	0.603449	-1.312164	0.025003	1.037930	-1.312164	-0.031636
0.809897	-1.312164	0.061687	0.612227	-1.312164	0.022151	1.054270	-1.312164	-0.033558
0.792085	-1.312164	0.064317	0.620744	-1.312164	0.019802	1.064990	-1.312164	-0.034780
0.774553	-1.312164	0.066388	0.631043	-1.312164	0.017337	1.104940	-1.312164	-0.038442
0.757372	-1.312164	0.067926	0.642344	-1.312164	0.015010	1.137000	-1.312164	-0.039664
0.739750	-1.312164	0.069109	0.655409	-1.312164	0.012550	1.157000	-1.312164	-0.039917
0.723488	-1.312164	0.069698	0.670228	-1.312164	0.010045	1.165940	-1.312164	-0.039963
0.708653	-1.312164	0.069725	0.684195	-1.312164	0.007977			
0.693583	-1.312164	0.069472	0.698917	-1.312164	0.005948			

C.15 Airfoil L7

Table C.15 Airfoil L7

X	Y	Z	X	Y	Z	X	Y	Z
1.112190	-1.124712	-0.049509	0.600283	-1.124712	0.066392	0.636294	-1.124712	-0.001807
1.103400	-1.124712	-0.048014	0.584517	-1.124712	0.065424	0.653196	-1.124712	-0.003904
1.083000	-1.124712	-0.043973	0.570364	-1.124712	0.063925	0.671453	-1.124712	-0.006085
1.050860	-1.124712	-0.035126	0.557870	-1.124712	0.061984	0.689504	-1.124712	-0.008153
1.010910	-1.124712	-0.021304	0.546371	-1.124712	0.059724	0.708022	-1.124712	-0.010210
0.998262	-1.124712	-0.016967	0.536581	-1.124712	0.057152	0.726929	-1.124712	-0.012284
0.981813	-1.124712	-0.011287	0.526631	-1.124712	0.053986	0.746148	-1.124712	-0.014357
0.964714	-1.124712	-0.005416	0.519161	-1.124712	0.051120	0.766359	-1.124712	-0.016527
0.947031	-1.124712	0.000597	0.512537	-1.124712	0.047848	0.786721	-1.124712	-0.018709
0.928833	-1.124712	0.006719	0.507308	-1.124712	0.043979	0.807164	-1.124712	-0.020895
0.910920	-1.124712	0.012731	0.503468	-1.124712	0.040640	0.826853	-1.124712	-0.023032
0.893359	-1.124712	0.018593	0.501214	-1.124712	0.038386	0.846460	-1.124712	-0.025184
0.874004	-1.124712	0.024757	0.500289	-1.124712	0.036436	0.865914	-1.124712	-0.027349
0.855126	-1.124712	0.030631	0.500436	-1.124712	0.033375	0.885880	-1.124712	-0.029575
0.836064	-1.124712	0.036292	0.501960	-1.124712	0.030925	0.904024	-1.124712	-0.031683
0.816874	-1.124712	0.041640	0.504878	-1.124712	0.028329	0.922535	-1.124712	-0.033848
0.796884	-1.124712	0.046744	0.509099	-1.124712	0.025707	0.941341	-1.124712	-0.036051
0.776901	-1.124712	0.051369	0.514760	-1.124712	0.022779	0.959620	-1.124712	-0.038223
0.756990	-1.124712	0.055469	0.521366	-1.124712	0.020079	0.977299	-1.124712	-0.040359
0.737973	-1.124712	0.058846	0.530375	-1.124712	0.017182	0.994308	-1.124712	-0.042435
0.719180	-1.124712	0.061653	0.539378	-1.124712	0.014690	1.005260	-1.124712	-0.043743
0.700685	-1.124712	0.063861	0.550127	-1.124712	0.012119	1.048090	-1.124712	-0.047783
0.682567	-1.124712	0.065497	0.561942	-1.124712	0.009683	1.082020	-1.124712	-0.049150
0.664163	-1.124712	0.066724	0.575466	-1.124712	0.007134	1.103170	-1.124712	-0.049452
0.647031	-1.124712	0.067344	0.590681	-1.124712	0.004550	1.112190	-1.124712	-0.049509
0.631246	-1.124712	0.067386	0.605342	-1.124712	0.002355			
0.615395	-1.124712	0.067103	0.620813	-1.124712	0.000195			

C.16 Airfoil L6

Table C.16 Airfoil L6

X	Y	Z	X	Y	Z	X	Y	Z
1.058480	-0.937260	-0.058890	0.521267	-0.937260	0.063579	0.559093	-0.937260	-0.008061
1.049610	-0.937260	-0.057412	0.505069	-0.937260	0.062492	0.576848	-0.937260	-0.010276
1.028110	-0.937260	-0.053143	0.490418	-0.937260	0.060873	0.595875	-0.937260	-0.012560
0.994213	-0.937260	-0.043753	0.477366	-0.937260	0.058801	0.614857	-0.937260	-0.014753
0.951602	-0.937260	-0.028933	0.465371	-0.937260	0.056399	0.634340	-0.937260	-0.016937
0.938586	-0.937260	-0.024402	0.455039	-0.937260	0.053665	0.654238	-0.937260	-0.019141
0.921496	-0.937260	-0.018424	0.444817	-0.937260	0.050339	0.674470	-0.937260	-0.021348
0.903711	-0.937260	-0.012240	0.436933	-0.937260	0.047304	0.695585	-0.937260	-0.023642
0.885301	-0.937260	-0.005902	0.430020	-0.937260	0.043866	0.716862	-0.937260	-0.025954
0.866339	-0.937260	0.000555	0.424522	-0.937260	0.039778	0.738224	-0.937260	-0.028273
0.847506	-0.937260	0.006937	0.420486	-0.937260	0.036268	0.758956	-0.937260	-0.030556
0.828875	-0.937260	0.013200	0.418095	-0.937260	0.033892	0.779601	-0.937260	-0.032858
0.808674	-0.937260	0.019707	0.417109	-0.937260	0.031826	0.800081	-0.937260	-0.035173
0.788808	-0.937260	0.025944	0.417262	-0.937260	0.028570	0.820930	-0.937260	-0.037543
0.768744	-0.937260	0.031955	0.418876	-0.937260	0.025985	0.840187	-0.937260	-0.039811
0.748542	-0.937260	0.037632	0.421940	-0.937260	0.023284	0.859656	-0.937260	-0.042128
0.727659	-0.937260	0.043012	0.426370	-0.937260	0.020551	0.879261	-0.937260	-0.044474
0.706783	-0.937260	0.047882	0.432270	-0.937260	0.017518	0.898302	-0.937260	-0.046787
0.685984	-0.937260	0.052193	0.439234	-0.937260	0.014680	0.916699	-0.937260	-0.049061
0.665966	-0.937260	0.055767	0.448476	-0.937260	0.011749	0.934379	-0.937260	-0.051272
0.646187	-0.937260	0.058732	0.457969	-0.937260	0.009122	0.945573	-0.937260	-0.052653
0.626727	-0.937260	0.061058	0.469171	-0.937260	0.006458	0.991268	-0.937260	-0.057028
0.607670	-0.937260	0.062772	0.481502	-0.937260	0.003927	1.027080	-0.937260	-0.058503
0.588481	-0.937260	0.064023	0.495489	-0.937260	0.001303	1.049380	-0.937260	-0.058832
0.570478	-0.937260	0.064655	0.511103	-0.937260	-0.001341	1.058480	-0.937260	-0.058890
0.553742	-0.937260	0.064695	0.526461	-0.937260	-0.003648			
0.537110	-0.937260	0.064364	0.542685	-0.937260	-0.005924			

C.17 Airfoil L5

Table C.17 Airfoil L5

X	Y	Z	X	Y	Z	X	Y	Z
1.004810	-0.749808	-0.068090	0.442144	-0.749808	0.060345	0.481866	-0.749808	-0.014694
0.995865	-0.749808	-0.066641	0.425514	-0.749808	0.059121	0.500476	-0.749808	-0.017008
0.973252	-0.749808	-0.062166	0.410366	-0.749808	0.057365	0.520278	-0.749808	-0.019374
0.937593	-0.749808	-0.052272	0.396758	-0.749808	0.055147	0.540194	-0.749808	-0.021671
0.892306	-0.749808	-0.036501	0.384270	-0.749808	0.052591	0.560644	-0.749808	-0.023959
0.878914	-0.749808	-0.031790	0.373397	-0.749808	0.049683	0.581536	-0.749808	-0.026272
0.861176	-0.749808	-0.025534	0.362906	-0.749808	0.046184	0.602784	-0.749808	-0.028589
0.842697	-0.749808	-0.019056	0.354613	-0.749808	0.042972	0.624806	-0.749808	-0.030984
0.823551	-0.749808	-0.012413	0.347413	-0.749808	0.039359	0.647001	-0.749808	-0.033401
0.803818	-0.749808	-0.005643	0.341651	-0.749808	0.035047	0.669285	-0.749808	-0.035829
0.784058	-0.749808	0.001088	0.337423	-0.749808	0.031362	0.691065	-0.749808	-0.038237
0.764349	-0.749808	0.007732	0.334897	-0.749808	0.028860	0.712751	-0.749808	-0.040665
0.743294	-0.749808	0.014558	0.333852	-0.749808	0.026677	0.734261	-0.749808	-0.043108
0.722432	-0.749808	0.021138	0.334014	-0.749808	0.023225	0.755996	-0.749808	-0.045596
0.701359	-0.749808	0.027476	0.335723	-0.749808	0.020507	0.776368	-0.749808	-0.048004
0.680139	-0.749808	0.033459	0.338934	-0.749808	0.017705	0.796798	-0.749808	-0.050452
0.658357	-0.749808	0.039092	0.343577	-0.749808	0.014866	0.817206	-0.749808	-0.052918
0.636581	-0.749808	0.044183	0.349720	-0.749808	0.011735	0.837012	-0.749808	-0.055350
0.614888	-0.749808	0.048682	0.357045	-0.749808	0.008766	0.856131	-0.749808	-0.057742
0.593865	-0.749808	0.052430	0.366524	-0.749808	0.005811	0.874484	-0.749808	-0.060068
0.573096	-0.749808	0.055532	0.376511	-0.749808	0.003061	0.885919	-0.749808	-0.061508
0.552667	-0.749808	0.057953	0.388169	-0.749808	0.000316	0.934492	-0.749808	-0.066168
0.532668	-0.749808	0.059724	0.401020	-0.749808	-0.002297	0.972183	-0.749808	-0.067712
0.512693	-0.749808	0.060977	0.415473	-0.749808	-0.004980	0.995633	-0.749808	-0.068043
0.493818	-0.749808	0.061601	0.431490	-0.749808	-0.007666	1.004810	-0.749808	-0.068090
0.476130	-0.749808	0.061621	0.447548	-0.749808	-0.010068			
0.458716	-0.749808	0.061223	0.464528	-0.749808	-0.012440			

C.18 Airfoil L4

Table C.18 Airfoil L4

X	Y	Z	X	Y	Z	X	Y	Z
0.951201	-0.562356	-0.077098	0.362903	-0.562356	0.056661	0.404610	-0.562356	-0.021736
0.942166	-0.562356	-0.075687	0.345844	-0.562356	0.055280	0.424079	-0.562356	-0.024126
0.918441	-0.562356	-0.071034	0.330200	-0.562356	0.053370	0.444658	-0.562356	-0.026552
0.881002	-0.562356	-0.060674	0.316038	-0.562356	0.050991	0.465512	-0.562356	-0.028929
0.833020	-0.562356	-0.044006	0.303059	-0.562356	0.048265	0.486932	-0.562356	-0.031299
0.819246	-0.562356	-0.039129	0.291649	-0.562356	0.045170	0.508822	-0.562356	-0.033697
0.800852	-0.562356	-0.032615	0.280893	-0.562356	0.041487	0.531089	-0.562356	-0.036100
0.781671	-0.562356	-0.025866	0.272194	-0.562356	0.038089	0.554022	-0.562356	-0.038570
0.761782	-0.562356	-0.018940	0.264711	-0.562356	0.034291	0.577138	-0.562356	-0.041067
0.741268	-0.562356	-0.011878	0.258689	-0.562356	0.029749	0.600348	-0.562356	-0.043578
0.720573	-0.562356	-0.004820	0.254273	-0.562356	0.025883	0.623179	-0.562356	-0.046085
0.699778	-0.562356	0.002181	0.251616	-0.562356	0.023253	0.645909	-0.562356	-0.048614
0.677860	-0.562356	0.009303	0.250514	-0.562356	0.020952	0.668452	-0.562356	-0.051160
0.655994	-0.562356	0.016201	0.250690	-0.562356	0.017305	0.691077	-0.562356	-0.053743
0.633903	-0.562356	0.022843	0.252495	-0.562356	0.014455	0.712568	-0.562356	-0.056268
0.611658	-0.562356	0.029108	0.255858	-0.562356	0.011555	0.733963	-0.562356	-0.058822
0.588969	-0.562356	0.034968	0.260716	-0.562356	0.008616	0.755177	-0.562356	-0.061385
0.566287	-0.562356	0.040256	0.267106	-0.562356	0.005394	0.775751	-0.562356	-0.063913
0.543695	-0.562356	0.044918	0.274796	-0.562356	0.002302	0.795595	-0.562356	-0.066402
0.521660	-0.562356	0.048817	0.284517	-0.562356	-0.000667	0.814626	-0.562356	-0.068822
0.499897	-0.562356	0.052031	0.295000	-0.562356	-0.003528	0.826304	-0.562356	-0.070309
0.478497	-0.562356	0.054524	0.307117	-0.562356	-0.006341	0.877760	-0.562356	-0.075197
0.457554	-0.562356	0.056329	0.320492	-0.562356	-0.009022	0.917336	-0.562356	-0.076766
0.436789	-0.562356	0.057562	0.335415	-0.562356	-0.011746	0.941937	-0.562356	-0.077071
0.417041	-0.562356	0.058156	0.351838	-0.562356	-0.014456	0.951201	-0.562356	-0.077098
0.398401	-0.562356	0.058135	0.368600	-0.562356	-0.016935			
0.380205	-0.562356	0.057651	0.386339	-0.562356	-0.019384			

C.19 Airfoil L3

Table C.19 Airfoil L3

X	Y	Z	X	Y	Z	X	Y	Z
0.897639	-0.374904	-0.085902	0.283540	-0.374904	0.052497	0.327324	-0.374904	-0.029210
0.888517	-0.374904	-0.084539	0.266051	-0.374904	0.050941	0.347654	-0.374904	-0.031654
0.863673	-0.374904	-0.079735	0.249914	-0.374904	0.048858	0.369014	-0.374904	-0.034117
0.824442	-0.374904	-0.068955	0.235200	-0.374904	0.046301	0.390810	-0.374904	-0.036550
0.773742	-0.374904	-0.051445	0.221733	-0.374904	0.043391	0.413203	-0.374904	-0.038976
0.759580	-0.374904	-0.046419	0.209790	-0.374904	0.040096	0.436094	-0.374904	-0.041432
0.740522	-0.374904	-0.039668	0.198773	-0.374904	0.036216	0.459384	-0.374904	-0.043896
0.720631	-0.374904	-0.032668	0.189671	-0.374904	0.032621	0.483232	-0.374904	-0.046415
0.699989	-0.374904	-0.025481	0.181910	-0.374904	0.028631	0.507272	-0.374904	-0.048965
0.678686	-0.374904	-0.018152	0.175633	-0.374904	0.023850	0.531412	-0.374904	-0.051533
0.657047	-0.374904	-0.010792	0.171034	-0.374904	0.019799	0.555297	-0.374904	-0.054112
0.635157	-0.374904	-0.003458	0.168248	-0.374904	0.017038	0.579075	-0.374904	-0.056716
0.612367	-0.374904	0.003936	0.167093	-0.374904	0.014617	0.602655	-0.374904	-0.059339
0.589488	-0.374904	0.011126	0.167286	-0.374904	0.010774	0.626173	-0.374904	-0.061990
0.566372	-0.374904	0.018046	0.169192	-0.374904	0.007795	0.648787	-0.374904	-0.064605
0.543093	-0.374904	0.024567	0.172710	-0.374904	0.004802	0.671152	-0.374904	-0.067241
0.519489	-0.374904	0.030628	0.177787	-0.374904	0.001767	0.693175	-0.374904	-0.069876
0.495895	-0.374904	0.036087	0.184428	-0.374904	-0.001539	0.714520	-0.374904	-0.072478
0.472396	-0.374904	0.040886	0.192486	-0.374904	-0.004745	0.735093	-0.374904	-0.075040
0.449346	-0.374904	0.044910	0.202451	-0.374904	-0.007716	0.754805	-0.374904	-0.077532
0.426585	-0.374904	0.048210	0.213435	-0.374904	-0.010677	0.766728	-0.374904	-0.079053
0.404209	-0.374904	0.050750	0.226015	-0.374904	-0.013543	0.821076	-0.374904	-0.084108
0.382318	-0.374904	0.052565	0.239917	-0.374904	-0.016276	0.862539	-0.374904	-0.085655
0.360763	-0.374904	0.053753	0.255313	-0.374904	-0.019026	0.888293	-0.374904	-0.085906
0.340141	-0.374904	0.054294	0.272145	-0.374904	-0.021742	0.897639	-0.374904	-0.085902
0.320547	-0.374904	0.054210	0.289614	-0.374904	-0.024278			
0.301570	-0.374904	0.053618	0.308116	-0.374904	-0.026784			

C.20 Airfoil L2

Table C.20 Airfoil L2

X	Y	Z	X	Y	Z	X	Y	Z
0.844130	-0.187452	-0.094492	0.204049	-0.187452	0.047827	0.250007	-0.187452	-0.037140
0.834919	-0.187452	-0.093186	0.186133	-0.187452	0.046076	0.271203	-0.187452	-0.039614
0.808950	-0.187452	-0.088261	0.169504	-0.187452	0.043803	0.293347	-0.187452	-0.042089
0.767911	-0.187452	-0.077107	0.154242	-0.187452	0.041052	0.316087	-0.187452	-0.044552
0.714471	-0.187452	-0.058819	0.140291	-0.187452	0.037941	0.339458	-0.187452	-0.047008
0.699915	-0.187452	-0.053658	0.127817	-0.187452	0.034432	0.363353	-0.187452	-0.049496
0.680185	-0.187452	-0.046691	0.116543	-0.187452	0.030344	0.387669	-0.187452	-0.051992
0.659574	-0.187452	-0.039463	0.107043	-0.187452	0.026540	0.412436	-0.187452	-0.054533
0.638171	-0.187452	-0.032040	0.099009	-0.187452	0.022349	0.437404	-0.187452	-0.057108
0.616070	-0.187452	-0.024466	0.092483	-0.187452	0.017323	0.462477	-0.187452	-0.059705
0.593477	-0.187452	-0.016830	0.087705	-0.187452	0.013079	0.487420	-0.187452	-0.062327
0.570483	-0.187452	-0.009189	0.084793	-0.187452	0.010184	0.512250	-0.187452	-0.064978
0.546811	-0.187452	-0.001551	0.083587	-0.187452	0.007641	0.536871	-0.187452	-0.067649
0.522910	-0.187452	0.005905	0.083804	-0.187452	0.003604	0.561286	-0.187452	-0.070341
0.498759	-0.187452	0.013075	0.085813	-0.187452	0.000497	0.585027	-0.187452	-0.073020
0.474438	-0.187452	0.019825	0.089489	-0.187452	-0.002586	0.608364	-0.187452	-0.075711
0.449912	-0.187452	0.026061	0.094790	-0.187452	-0.005709	0.631200	-0.187452	-0.078394
0.425398	-0.187452	0.031663	0.101685	-0.187452	-0.009092	0.653321	-0.187452	-0.081044
0.400988	-0.187452	0.036571	0.110115	-0.187452	-0.012402	0.674626	-0.187452	-0.083656
0.376916	-0.187452	0.040693	0.120328	-0.187452	-0.015365	0.695022	-0.187452	-0.086198
0.353152	-0.187452	0.044053	0.131816	-0.187452	-0.018412	0.707191	-0.187452	-0.087741
0.329797	-0.187452	0.046614	0.144863	-0.187452	-0.021318	0.764440	-0.187452	-0.092895
0.306957	-0.187452	0.048412	0.159295	-0.187452	-0.024086	0.807793	-0.187452	-0.094371
0.284609	-0.187452	0.049530	0.175167	-0.187452	-0.026844	0.834700	-0.187452	-0.094536
0.263111	-0.187452	0.049994	0.192413	-0.187452	-0.029548	0.844130	-0.187452	-0.094492
0.242564	-0.187452	0.049824	0.210592	-0.187452	-0.032121			
0.222807	-0.187452	0.049101	0.229859	-0.187452	-0.034662			

C.21 Airfoils L1 & R1 (Centerline)

Table C.21 Airfoils L1 & R1 (Centerline)

X	Y	Z	X	Y	Z	X	Y	Z
0.790670	0.000000	-0.102860	0.124429	0.000000	0.042629	0.172663	0.000000	-0.045546
0.781369	0.000000	-0.101620	0.106088	0.000000	0.040665	0.194727	0.000000	-0.048025
0.754269	0.000000	-0.096604	0.088971	0.000000	0.038183	0.217657	0.000000	-0.050485
0.711410	0.000000	-0.085126	0.073163	0.000000	0.035219	0.241346	0.000000	-0.052952
0.655205	0.000000	-0.066125	0.058731	0.000000	0.031892	0.265697	0.000000	-0.055411
0.640249	0.000000	-0.060845	0.045731	0.000000	0.028154	0.290600	0.000000	-0.057902
0.619838	0.000000	-0.053685	0.034206	0.000000	0.023844	0.315946	0.000000	-0.060401
0.598499	0.000000	-0.046252	0.024312	0.000000	0.019821	0.341634	0.000000	-0.062935
0.576326	0.000000	-0.038616	0.016009	0.000000	0.015419	0.367535	0.000000	-0.065507
0.553417	0.000000	-0.030824	0.009240	0.000000	0.010140	0.393544	0.000000	-0.068104
0.529860	0.000000	-0.022938	0.004288	0.000000	0.005699	0.419548	0.000000	-0.070740
0.505752	0.000000	-0.015019	0.001254	0.000000	0.002665	0.445434	0.000000	-0.073407
0.481190	0.000000	-0.007162	0.000000	0.000000	0.000000	0.471099	0.000000	-0.076098
0.456257	0.000000	0.000530	0.000244	0.000000	-0.004232	0.496415	0.000000	-0.078803
0.431062	0.000000	0.007923	0.002362	0.000000	-0.007464	0.521286	0.000000	-0.081515
0.405690	0.000000	0.014873	0.006199	0.000000	-0.010632	0.545599	0.000000	-0.084235
0.380234	0.000000	0.021254	0.011726	0.000000	-0.013838	0.569253	0.000000	-0.086939
0.354794	0.000000	0.026971	0.018880	0.000000	-0.017290	0.592152	0.000000	-0.089613
0.329466	0.000000	0.031961	0.027686	0.000000	-0.020693	0.614194	0.000000	-0.092250
0.304367	0.000000	0.036152	0.038150	0.000000	-0.023637	0.635276	0.000000	-0.094819
0.279596	0.000000	0.039543	0.050146	0.000000	-0.026757	0.647695	0.000000	-0.096371
0.255258	0.000000	0.042097	0.063663	0.000000	-0.029688	0.707851	0.000000	-0.101552
0.231466	0.000000	0.043852	0.078628	0.000000	-0.032476	0.753097	0.000000	-0.102905
0.208325	0.000000	0.044875	0.094980	0.000000	-0.035224	0.781158	0.000000	-0.102953
0.185951	0.000000	0.045237	0.112642	0.000000	-0.037898	0.790670	0.000000	-0.102860
0.164450	0.000000	0.044954	0.131535	0.000000	-0.040486			
0.143913	0.000000	0.044078	0.151571	0.000000	-0.043039			

C.22 Airfoil R2

Table C.22 Airfoil R2

X	Y	Z	X	Y	Z	X	Y	Z
0.844130	0.187452	-0.094492	0.204049	0.187452	0.047827	0.250007	0.187452	-0.037140
0.834919	0.187452	-0.093186	0.186133	0.187452	0.046076	0.271203	0.187452	-0.039614
0.808950	0.187452	-0.088261	0.169504	0.187452	0.043803	0.293347	0.187452	-0.042089
0.767911	0.187452	-0.077107	0.154242	0.187452	0.041052	0.316087	0.187452	-0.044552
0.714471	0.187452	-0.058819	0.140291	0.187452	0.037941	0.339458	0.187452	-0.047008
0.699915	0.187452	-0.053658	0.127817	0.187452	0.034432	0.363353	0.187452	-0.049496
0.680185	0.187452	-0.046691	0.116543	0.187452	0.030344	0.387669	0.187452	-0.051992
0.659574	0.187452	-0.039463	0.107043	0.187452	0.026540	0.412436	0.187452	-0.054533
0.638171	0.187452	-0.032040	0.099009	0.187452	0.022349	0.437404	0.187452	-0.057108
0.616070	0.187452	-0.024466	0.092483	0.187452	0.017323	0.462477	0.187452	-0.059705
0.593477	0.187452	-0.016830	0.087705	0.187452	0.013079	0.487420	0.187452	-0.062327
0.570483	0.187452	-0.009189	0.084793	0.187452	0.010184	0.512250	0.187452	-0.064978
0.546811	0.187452	-0.001551	0.083587	0.187452	0.007641	0.536871	0.187452	-0.067649
0.522910	0.187452	0.005905	0.083804	0.187452	0.003604	0.561286	0.187452	-0.070341
0.498759	0.187452	0.013075	0.085813	0.187452	0.000497	0.585027	0.187452	-0.073020
0.474438	0.187452	0.019825	0.089489	0.187452	-0.002586	0.608364	0.187452	-0.075711
0.449912	0.187452	0.026061	0.094790	0.187452	-0.005709	0.631200	0.187452	-0.078394
0.425398	0.187452	0.031663	0.101685	0.187452	-0.009092	0.653321	0.187452	-0.081044
0.400988	0.187452	0.036571	0.110115	0.187452	-0.012402	0.674626	0.187452	-0.083656
0.376916	0.187452	0.040693	0.120328	0.187452	-0.015365	0.695022	0.187452	-0.086198
0.353152	0.187452	0.044053	0.131816	0.187452	-0.018412	0.707191	0.187452	-0.087741
0.329797	0.187452	0.046614	0.144863	0.187452	-0.021318	0.764440	0.187452	-0.092895
0.306957	0.187452	0.048412	0.159295	0.187452	-0.024086	0.807793	0.187452	-0.094371
0.284609	0.187452	0.049530	0.175167	0.187452	-0.026844	0.834700	0.187452	-0.094536
0.263111	0.187452	0.049994	0.192413	0.187452	-0.029548	0.844130	0.187452	-0.094492
0.242564	0.187452	0.049824	0.210592	0.187452	-0.032121			
0.222807	0.187452	0.049101	0.229859	0.187452	-0.034662			

C.23 Airfoil R3

Table C.23 Airfoil R3

X	Y	Z	X	Y	Z	X	Y	Z
0.897639	0.374904	-0.085902	0.283540	0.374904	0.052497	0.327324	0.374904	-0.029210
0.888517	0.374904	-0.084539	0.266051	0.374904	0.050941	0.347654	0.374904	-0.031654
0.863673	0.374904	-0.079735	0.249914	0.374904	0.048858	0.369014	0.374904	-0.034117
0.824442	0.374904	-0.068955	0.235200	0.374904	0.046301	0.390810	0.374904	-0.036550
0.773742	0.374904	-0.051445	0.221733	0.374904	0.043391	0.413203	0.374904	-0.038976
0.759580	0.374904	-0.046419	0.209790	0.374904	0.040096	0.436094	0.374904	-0.041432
0.740522	0.374904	-0.039668	0.198773	0.374904	0.036216	0.459384	0.374904	-0.043896
0.720631	0.374904	-0.032668	0.189671	0.374904	0.032621	0.483232	0.374904	-0.046415
0.699989	0.374904	-0.025481	0.181910	0.374904	0.028631	0.507272	0.374904	-0.048965
0.678686	0.374904	-0.018152	0.175633	0.374904	0.023850	0.531412	0.374904	-0.051533
0.657047	0.374904	-0.010792	0.171034	0.374904	0.019799	0.555297	0.374904	-0.054112
0.635157	0.374904	-0.003458	0.168248	0.374904	0.017038	0.579075	0.374904	-0.056716
0.612367	0.374904	0.003936	0.167093	0.374904	0.014617	0.602655	0.374904	-0.059339
0.589488	0.374904	0.011126	0.167286	0.374904	0.010774	0.626173	0.374904	-0.061990
0.566372	0.374904	0.018046	0.169192	0.374904	0.007795	0.648787	0.374904	-0.064605
0.543093	0.374904	0.024567	0.172710	0.374904	0.004802	0.671152	0.374904	-0.067241
0.519489	0.374904	0.030628	0.177787	0.374904	0.001767	0.693175	0.374904	-0.069876
0.495895	0.374904	0.036087	0.184428	0.374904	-0.001539	0.714520	0.374904	-0.072478
0.472396	0.374904	0.040886	0.192486	0.374904	-0.004745	0.735093	0.374904	-0.075040
0.449346	0.374904	0.044910	0.202451	0.374904	-0.007716	0.754805	0.374904	-0.077532
0.426585	0.374904	0.048210	0.213435	0.374904	-0.010677	0.766728	0.374904	-0.079053
0.404209	0.374904	0.050750	0.226015	0.374904	-0.013543	0.821076	0.374904	-0.084108
0.382318	0.374904	0.052565	0.239917	0.374904	-0.016276	0.862539	0.374904	-0.085655
0.360763	0.374904	0.053753	0.255313	0.374904	-0.019026	0.888293	0.374904	-0.085906
0.340141	0.374904	0.054294	0.272145	0.374904	-0.021742	0.897639	0.374904	-0.085902
0.320547	0.374904	0.054210	0.289614	0.374904	-0.024278			
0.301570	0.374904	0.053618	0.308116	0.374904	-0.026784			

C.24 Airfoil R4

Table C.24 Airfoil R4

X	Y	Z	X	Y	Z	X	Y	Z
0.951201	0.562356	-0.077098	0.362903	0.562356	0.056661	0.404610	0.562356	-0.021736
0.942166	0.562356	-0.075687	0.345844	0.562356	0.055280	0.424079	0.562356	-0.024126
0.918441	0.562356	-0.071034	0.330200	0.562356	0.053370	0.444658	0.562356	-0.026552
0.881002	0.562356	-0.060674	0.316038	0.562356	0.050991	0.465512	0.562356	-0.028929
0.833020	0.562356	-0.044006	0.303059	0.562356	0.048265	0.486932	0.562356	-0.031299
0.819246	0.562356	-0.039129	0.291649	0.562356	0.045170	0.508822	0.562356	-0.033697
0.800852	0.562356	-0.032615	0.280893	0.562356	0.041487	0.531089	0.562356	-0.036100
0.781671	0.562356	-0.025866	0.272194	0.562356	0.038089	0.554022	0.562356	-0.038570
0.761782	0.562356	-0.018940	0.264711	0.562356	0.034291	0.577138	0.562356	-0.041067
0.741268	0.562356	-0.011878	0.258689	0.562356	0.029749	0.600348	0.562356	-0.043578
0.720573	0.562356	-0.004820	0.254273	0.562356	0.025883	0.623179	0.562356	-0.046085
0.699778	0.562356	0.002181	0.251616	0.562356	0.023253	0.645909	0.562356	-0.048614
0.677860	0.562356	0.009303	0.250514	0.562356	0.020952	0.668452	0.562356	-0.051160
0.655994	0.562356	0.016201	0.250690	0.562356	0.017305	0.691077	0.562356	-0.053743
0.633903	0.562356	0.022843	0.252495	0.562356	0.014455	0.712568	0.562356	-0.056268
0.611658	0.562356	0.029108	0.255858	0.562356	0.011555	0.733963	0.562356	-0.058822
0.588969	0.562356	0.034968	0.260716	0.562356	0.008616	0.755177	0.562356	-0.061385
0.566287	0.562356	0.040256	0.267106	0.562356	0.005394	0.775751	0.562356	-0.063913
0.543695	0.562356	0.044918	0.274796	0.562356	0.002302	0.795595	0.562356	-0.066402
0.521660	0.562356	0.048817	0.284517	0.562356	-0.000667	0.814626	0.562356	-0.068822
0.499897	0.562356	0.052031	0.295000	0.562356	-0.003528	0.826304	0.562356	-0.070309
0.478497	0.562356	0.054524	0.307117	0.562356	-0.006341	0.877760	0.562356	-0.075197
0.457554	0.562356	0.056329	0.320492	0.562356	-0.009022	0.917336	0.562356	-0.076766
0.436789	0.562356	0.057562	0.335415	0.562356	-0.011746	0.941937	0.562356	-0.077071
0.417041	0.562356	0.058156	0.351838	0.562356	-0.014456	0.951201	0.562356	-0.077098
0.398401	0.562356	0.058135	0.368600	0.562356	-0.016935			
0.380205	0.562356	0.057651	0.386339	0.562356	-0.019384			

C.25 Airfoil R5

Table C.25 Airfoil R5

X	Y	Z	X	Y	Z	X	Y	Z
1.004810	0.749808	-0.068090	0.442144	0.749808	0.060345	0.481866	0.749808	-0.014694
0.995865	0.749808	-0.066641	0.425514	0.749808	0.059121	0.500476	0.749808	-0.017008
0.973252	0.749808	-0.062166	0.410366	0.749808	0.057365	0.520278	0.749808	-0.019374
0.937593	0.749808	-0.052272	0.396758	0.749808	0.055147	0.540194	0.749808	-0.021671
0.892306	0.749808	-0.036501	0.384270	0.749808	0.052591	0.560644	0.749808	-0.023959
0.878914	0.749808	-0.031790	0.373397	0.749808	0.049683	0.581536	0.749808	-0.026272
0.861176	0.749808	-0.025534	0.362906	0.749808	0.046184	0.602784	0.749808	-0.028589
0.842697	0.749808	-0.019056	0.354613	0.749808	0.042972	0.624806	0.749808	-0.030984
0.823551	0.749808	-0.012413	0.347413	0.749808	0.039359	0.647001	0.749808	-0.033401
0.803818	0.749808	-0.005643	0.341651	0.749808	0.035047	0.669285	0.749808	-0.035829
0.784058	0.749808	0.001088	0.337423	0.749808	0.031362	0.691065	0.749808	-0.038237
0.764349	0.749808	0.007732	0.334897	0.749808	0.028860	0.712751	0.749808	-0.040665
0.743294	0.749808	0.014558	0.333852	0.749808	0.026677	0.734261	0.749808	-0.043108
0.722432	0.749808	0.021138	0.334014	0.749808	0.023225	0.755996	0.749808	-0.045596
0.701359	0.749808	0.027476	0.335723	0.749808	0.020507	0.776368	0.749808	-0.048004
0.680139	0.749808	0.033459	0.338934	0.749808	0.017705	0.796798	0.749808	-0.050452
0.658357	0.749808	0.039092	0.343577	0.749808	0.014866	0.817206	0.749808	-0.052918
0.636581	0.749808	0.044183	0.349720	0.749808	0.011735	0.837012	0.749808	-0.055350
0.614888	0.749808	0.048682	0.357045	0.749808	0.008766	0.856131	0.749808	-0.057742
0.593865	0.749808	0.052430	0.366524	0.749808	0.005811	0.874484	0.749808	-0.060068
0.573096	0.749808	0.055532	0.376511	0.749808	0.003061	0.885919	0.749808	-0.061508
0.552667	0.749808	0.057953	0.388169	0.749808	0.000316	0.934492	0.749808	-0.066168
0.532668	0.749808	0.059724	0.401020	0.749808	-0.002297	0.972183	0.749808	-0.067712
0.512693	0.749808	0.060977	0.415473	0.749808	-0.004980	0.995633	0.749808	-0.068043
0.493818	0.749808	0.061601	0.431490	0.749808	-0.007666	1.004810	0.749808	-0.068090
0.476130	0.749808	0.061621	0.447548	0.749808	-0.010068			
0.458716	0.749808	0.061223	0.464528	0.749808	-0.012440			

C.26 Airfoil R6

Table C.26 Airfoil R6

X	Y	Z	X	Y	Z	X	Y	Z
1.058480	0.937260	-0.058890	0.521267	0.937260	0.063579	0.559093	0.937260	-0.008061
1.049610	0.937260	-0.057412	0.505069	0.937260	0.062492	0.576848	0.937260	-0.010276
1.028110	0.937260	-0.053143	0.490418	0.937260	0.060873	0.595875	0.937260	-0.012560
0.994213	0.937260	-0.043753	0.477366	0.937260	0.058801	0.614857	0.937260	-0.014753
0.951602	0.937260	-0.028933	0.465371	0.937260	0.056399	0.634340	0.937260	-0.016937
0.938586	0.937260	-0.024402	0.455039	0.937260	0.053665	0.654238	0.937260	-0.019141
0.921496	0.937260	-0.018424	0.444817	0.937260	0.050339	0.674470	0.937260	-0.021348
0.903711	0.937260	-0.012240	0.436933	0.937260	0.047304	0.695585	0.937260	-0.023642
0.885301	0.937260	-0.005902	0.430020	0.937260	0.043866	0.716862	0.937260	-0.025954
0.866339	0.937260	0.000555	0.424522	0.937260	0.039778	0.738224	0.937260	-0.028273
0.847506	0.937260	0.006937	0.420486	0.937260	0.036268	0.758956	0.937260	-0.030556
0.828875	0.937260	0.013200	0.418095	0.937260	0.033892	0.779601	0.937260	-0.032858
0.808674	0.937260	0.019707	0.417109	0.937260	0.031826	0.800081	0.937260	-0.035173
0.788808	0.937260	0.025944	0.417262	0.937260	0.028570	0.820930	0.937260	-0.037543
0.768744	0.937260	0.031955	0.418876	0.937260	0.025985	0.840187	0.937260	-0.039811
0.748542	0.937260	0.037632	0.421940	0.937260	0.023284	0.859656	0.937260	-0.042128
0.727659	0.937260	0.043012	0.426370	0.937260	0.020551	0.879261	0.937260	-0.044474
0.706783	0.937260	0.047882	0.432270	0.937260	0.017518	0.898302	0.937260	-0.046787
0.685984	0.937260	0.052193	0.439234	0.937260	0.014680	0.916699	0.937260	-0.049061
0.665966	0.937260	0.055767	0.448476	0.937260	0.011749	0.934379	0.937260	-0.051272
0.646187	0.937260	0.058732	0.457969	0.937260	0.009122	0.945573	0.937260	-0.052653
0.626727	0.937260	0.061058	0.469171	0.937260	0.006458	0.991268	0.937260	-0.057028
0.607670	0.937260	0.062772	0.481502	0.937260	0.003927	1.027080	0.937260	-0.058503
0.588481	0.937260	0.064023	0.495489	0.937260	0.001303	1.049380	0.937260	-0.058832
0.570478	0.937260	0.064655	0.511103	0.937260	-0.001341	1.058480	0.937260	-0.058890
0.553742	0.937260	0.064695	0.526461	0.937260	-0.003648			
0.537110	0.937260	0.064364	0.542685	0.937260	-0.005924			

C.27 Airfoil R7

Table C.27 Airfoil R7

X	Y	Z	X	Y	Z	X	Y	Z
1.112190	1.124712	-0.049509	0.600283	1.124712	0.066392	0.636294	1.124712	-0.001807
1.103400	1.124712	-0.048014	0.584517	1.124712	0.065424	0.653196	1.124712	-0.003904
1.083000	1.124712	-0.043973	0.570364	1.124712	0.063925	0.671453	1.124712	-0.006085
1.050860	1.124712	-0.035126	0.557870	1.124712	0.061984	0.689504	1.124712	-0.008153
1.010910	1.124712	-0.021304	0.546371	1.124712	0.059724	0.708022	1.124712	-0.010210
0.998262	1.124712	-0.016967	0.536581	1.124712	0.057152	0.726929	1.124712	-0.012284
0.981813	1.124712	-0.011287	0.526631	1.124712	0.053986	0.746148	1.124712	-0.014357
0.964714	1.124712	-0.005416	0.519161	1.124712	0.051120	0.766359	1.124712	-0.016527
0.947031	1.124712	0.000597	0.512537	1.124712	0.047848	0.786721	1.124712	-0.018709
0.928833	1.124712	0.006719	0.507308	1.124712	0.043979	0.807164	1.124712	-0.020895
0.910920	1.124712	0.012731	0.503468	1.124712	0.040640	0.826853	1.124712	-0.023032
0.893359	1.124712	0.018593	0.501214	1.124712	0.038386	0.846460	1.124712	-0.025184
0.874004	1.124712	0.024757	0.500289	1.124712	0.036436	0.865914	1.124712	-0.027349
0.855126	1.124712	0.030631	0.500436	1.124712	0.033375	0.885880	1.124712	-0.029575
0.836064	1.124712	0.036292	0.501960	1.124712	0.030925	0.904024	1.124712	-0.031683
0.816874	1.124712	0.041640	0.504878	1.124712	0.028329	0.922535	1.124712	-0.033848
0.796884	1.124712	0.046744	0.509099	1.124712	0.025707	0.941341	1.124712	-0.036051
0.776901	1.124712	0.051369	0.514760	1.124712	0.022779	0.959620	1.124712	-0.038223
0.756990	1.124712	0.055469	0.521366	1.124712	0.020079	0.977299	1.124712	-0.040359
0.737973	1.124712	0.058846	0.530375	1.124712	0.017182	0.994308	1.124712	-0.042435
0.719180	1.124712	0.061653	0.539378	1.124712	0.014690	1.005260	1.124712	-0.043743
0.700685	1.124712	0.063861	0.550127	1.124712	0.012119	1.048090	1.124712	-0.047783
0.682567	1.124712	0.065497	0.561942	1.124712	0.009683	1.082020	1.124712	-0.049150
0.664163	1.124712	0.066724	0.575466	1.124712	0.007134	1.103170	1.124712	-0.049452
0.647031	1.124712	0.067344	0.590681	1.124712	0.004550	1.112190	1.124712	-0.049509
0.631246	1.124712	0.067386	0.605342	1.124712	0.002355			
0.615395	1.124712	0.067103	0.620813	1.124712	0.000195			

C.28 Airfoil R8

Table C.28 Airfoil R8

X	Y	Z	X	Y	Z	X	Y	Z
1.165940	1.312164	-0.039963	0.679201	1.312164	0.068820	0.713473	1.312164	0.004098
1.157230	1.312164	-0.038460	0.663867	1.312164	0.067952	0.729525	1.312164	0.002137
1.137920	1.312164	-0.034670	0.650214	1.312164	0.066558	0.747014	1.312164	0.000081
1.107530	1.312164	-0.026400	0.638279	1.312164	0.064733	0.764136	1.312164	-0.001844
1.070220	1.312164	-0.013614	0.627278	1.312164	0.062601	0.781693	1.312164	-0.003754
1.057940	1.312164	-0.009488	0.618033	1.312164	0.060181	0.799612	1.312164	-0.005677
1.042130	1.312164	-0.004123	0.608359	1.312164	0.057165	0.817821	1.312164	-0.007597
1.025710	1.312164	0.001416	0.601304	1.312164	0.054458	0.837130	1.312164	-0.009620
1.008750	1.312164	0.007084	0.594974	1.312164	0.051347	0.856582	1.312164	-0.011651
0.991305	1.312164	0.012850	0.590018	1.312164	0.047689	0.876109	1.312164	-0.013681
0.974304	1.312164	0.018474	0.586377	1.312164	0.044517	0.894756	1.312164	-0.015649
0.957807	1.312164	0.023917	0.584263	1.312164	0.042383	0.913328	1.312164	-0.017632
0.939291	1.312164	0.029717	0.583401	1.312164	0.040548	0.931758	1.312164	-0.019624
0.921395	1.312164	0.035207	0.583545	1.312164	0.037682	0.950844	1.312164	-0.021687
0.903328	1.312164	0.040498	0.584980	1.312164	0.035369	0.967879	1.312164	-0.023614
0.885143	1.312164	0.045496	0.587757	1.312164	0.032881	0.985434	1.312164	-0.025607
0.866040	1.312164	0.050303	0.591772	1.312164	0.030374	1.003440	1.312164	-0.027647
0.846944	1.312164	0.054661	0.597197	1.312164	0.027557	1.020960	1.312164	-0.029658
0.827916	1.312164	0.058528	0.603449	1.312164	0.025003	1.037930	1.312164	-0.031636
0.809897	1.312164	0.061687	0.612227	1.312164	0.022151	1.054270	1.312164	-0.033558
0.792085	1.312164	0.064317	0.620744	1.312164	0.019802	1.064990	1.312164	-0.034780
0.774553	1.312164	0.066388	0.631043	1.312164	0.017337	1.104940	1.312164	-0.038442
0.757372	1.312164	0.067926	0.642344	1.312164	0.015010	1.137000	1.312164	-0.039664
0.739750	1.312164	0.069109	0.655409	1.312164	0.012550	1.157000	1.312164	-0.039917
0.723488	1.312164	0.069698	0.670228	1.312164	0.010045	1.165940	1.312164	-0.039963
0.708653	1.312164	0.069725	0.684195	1.312164	0.007977			
0.693583	1.312164	0.069472	0.698917	1.312164	0.005948			

C.29 Airfoil R9

Table C.29 Airfoil R9

X	Y	Z	X	Y	Z	X	Y	Z
1.219720	1.499616	-0.030266	0.758037	1.499616	0.070901	0.790635	1.499616	0.009690
1.211100	1.499616	-0.028767	0.743135	1.499616	0.070115	0.805841	1.499616	0.007881
1.192880	1.499616	-0.025247	0.729982	1.499616	0.068810	0.822564	1.499616	0.005968
1.164230	1.499616	-0.017583	0.718608	1.499616	0.067090	0.838760	1.499616	0.004204
1.129550	1.499616	-0.005869	0.708106	1.499616	0.065075	0.855358	1.499616	0.002458
1.117630	1.499616	-0.001966	0.699409	1.499616	0.062797	0.872291	1.499616	0.000704
1.102440	1.499616	0.003066	0.690012	1.499616	0.059918	0.889492	1.499616	-0.001043
1.086690	1.499616	0.008255	0.683375	1.499616	0.057365	0.907902	1.499616	-0.002899
1.070450	1.499616	0.013560	0.677341	1.499616	0.054406	0.926444	1.499616	-0.004758
1.053760	1.499616	0.018952	0.672662	1.499616	0.050956	0.945058	1.499616	-0.006612
1.037660	1.499616	0.024170	0.669223	1.499616	0.047946	0.962667	1.499616	-0.008394
1.022220	1.499616	0.029179	0.667251	1.499616	0.045931	0.980206	1.499616	-0.010187
1.004540	1.499616	0.034595	0.666454	1.499616	0.044209	0.997614	1.499616	-0.011990
0.987620	1.499616	0.039683	0.666598	1.499616	0.041539	1.015820	1.499616	-0.013867
0.970543	1.499616	0.044586	0.667947	1.499616	0.039364	1.031750	1.499616	-0.015599
0.953358	1.499616	0.049217	0.670585	1.499616	0.036987	1.048350	1.499616	-0.017403
0.935137	1.499616	0.053706	0.674396	1.499616	0.034599	1.065570	1.499616	-0.019260
0.916923	1.499616	0.057778	0.679589	1.499616	0.031899	1.082330	1.499616	-0.021091
0.898774	1.499616	0.061391	0.685489	1.499616	0.029496	1.098580	1.499616	-0.022892
0.881748	1.499616	0.064315	0.694042	1.499616	0.026699	1.114260	1.499616	-0.024642
0.864916	1.499616	0.066748	0.702074	1.499616	0.024502	1.124740	1.499616	-0.025765
0.848344	1.499616	0.068665	0.711927	1.499616	0.022154	1.161830	1.499616	-0.029013
0.832097	1.499616	0.070088	0.722717	1.499616	0.019947	1.192020	1.499616	-0.030059
0.815256	1.499616	0.071208	0.735326	1.499616	0.017592	1.210870	1.499616	-0.030243
0.799862	1.499616	0.071750	0.749753	1.499616	0.015182	1.219720	1.499616	-0.030266
0.785978	1.499616	0.071748	0.763028	1.499616	0.013258			
0.771689	1.499616	0.071511	0.777002	1.499616	0.011375			

C.30 Airfoil R10

Table C.30 Airfoil R10

X	Y	Z	X	Y	Z	X	Y	Z
1.273540	1.687068	-0.020436	0.836806	1.687068	0.072678	0.867789	1.687068	0.015007
1.264990	1.687068	-0.018953	0.822336	1.687068	0.071957	0.882149	1.687068	0.013365
1.247860	1.687068	-0.015718	0.809683	1.687068	0.070726	0.898110	1.687068	0.011612
1.220930	1.687068	-0.008687	0.798871	1.687068	0.069098	0.913381	1.687068	0.010024
1.188880	1.687068	0.001931	0.788870	1.687068	0.067189	0.929021	1.687068	0.008458
1.177310	1.687068	0.005596	0.780721	1.687068	0.065046	0.944970	1.687068	0.006888
1.162750	1.687068	0.010279	0.771605	1.687068	0.062293	0.961164	1.687068	0.005329
1.147670	1.687068	0.015101	0.765389	1.687068	0.059887	0.978677	1.687068	0.003658
1.132140	1.687068	0.020026	0.759654	1.687068	0.057075	0.996313	1.687068	0.001990
1.116190	1.687068	0.025028	0.755253	1.687068	0.053827	1.014010	1.687068	0.000331
1.101000	1.687068	0.029824	0.752020	1.687068	0.050978	1.030590	1.687068	-0.001248
1.086610	1.687068	0.034387	0.750191	1.687068	0.049078	1.047090	1.687068	-0.002837
1.069760	1.687068	0.039401	0.749461	1.687068	0.047470	1.063480	1.687068	-0.004434
1.053810	1.687068	0.044072	0.749607	1.687068	0.044996	1.080820	1.687068	-0.006108
1.037720	1.687068	0.048571	0.750872	1.687068	0.042960	1.095640	1.687068	-0.007631
1.021530	1.687068	0.052819	0.753373	1.687068	0.040695	1.111290	1.687068	-0.009230
1.004190	1.687068	0.056973	0.756984	1.687068	0.038430	1.127710	1.687068	-0.010887
0.986851	1.687068	0.060739	0.761947	1.687068	0.035852	1.143720	1.687068	-0.012520
0.969577	1.687068	0.064080	0.767498	1.687068	0.033607	1.159260	1.687068	-0.014127
0.953542	1.687068	0.066754	0.775828	1.687068	0.030876	1.174270	1.687068	-0.015689
0.937687	1.687068	0.068976	0.783378	1.687068	0.028837	1.184510	1.687068	-0.016701
0.922072	1.687068	0.070723	0.792788	1.687068	0.026615	1.218750	1.687068	-0.019506
0.906759	1.687068	0.072015	0.803069	1.687068	0.024540	1.247060	1.687068	-0.020349
0.890697	1.687068	0.073055	0.815226	1.687068	0.022304	1.264760	1.687068	-0.020448
0.876170	1.687068	0.073535	0.829263	1.687068	0.020007	1.273540	1.687068	-0.020436
0.863236	1.687068	0.073493	0.841849	1.687068	0.018238			
0.849727	1.687068	0.073257	0.855077	1.687068	0.016516			

C.31 Airfoil R11

Table C.31 Airfoil R11

X	Y	Z	X	Y	Z	X	Y	Z
1.327370	1.874520	-0.010491	0.915526	1.874520	0.074197	0.944942	1.874520	0.020091
1.318890	1.874520	-0.009036	0.901487	1.874520	0.073522	0.958458	1.874520	0.018628
1.302850	1.874520	-0.006100	0.889335	1.874520	0.072352	0.973658	1.874520	0.017051
1.277650	1.874520	0.000278	0.879086	1.874520	0.070807	0.988005	1.874520	0.015652
1.248210	1.874520	0.009782	0.869587	1.874520	0.068994	1.002690	1.874520	0.014278
1.237000	1.874520	0.013196	0.861989	1.874520	0.066980	1.017650	1.874520	0.012906
1.223060	1.874520	0.017515	0.853156	1.874520	0.064342	1.032840	1.874520	0.011546
1.208650	1.874520	0.021955	0.847361	1.874520	0.062079	1.049460	1.874520	0.010077
1.193820	1.874520	0.026485	0.841927	1.874520	0.059408	1.066190	1.874520	0.008617
1.178610	1.874520	0.031080	0.837809	1.874520	0.056360	1.082980	1.874520	0.007169
1.164320	1.874520	0.035443	0.834783	1.874520	0.053667	1.098520	1.874520	0.005806
1.150990	1.874520	0.039549	0.833099	1.874520	0.051883	1.113990	1.874520	0.004435
1.134960	1.874520	0.044146	0.832436	1.874520	0.050388	1.129360	1.874520	0.003057
1.119980	1.874520	0.048387	0.832585	1.874520	0.048109	1.145820	1.874520	0.001602
1.104870	1.874520	0.052469	0.833768	1.874520	0.046213	1.159540	1.874520	0.000298
1.089670	1.874520	0.056321	0.836135	1.874520	0.044064	1.174230	1.874520	-0.001083
1.073200	1.874520	0.060122	0.839547	1.874520	0.041924	1.189870	1.874520	-0.002524
1.056740	1.874520	0.063567	0.844283	1.874520	0.039473	1.205120	1.874520	-0.003945
1.040340	1.874520	0.066622	0.849487	1.874520	0.037389	1.219950	1.874520	-0.005342
1.025290	1.874520	0.069032	0.857599	1.874520	0.034734	1.234300	1.874520	-0.006701
1.010410	1.874520	0.071029	0.864668	1.874520	0.032859	1.244310	1.874520	-0.007587
0.995756	1.874520	0.072593	0.873637	1.874520	0.030774	1.275680	1.874520	-0.009933
0.981375	1.874520	0.073743	0.883412	1.874520	0.028840	1.302120	1.874520	-0.010552
0.966090	1.874520	0.074687	0.895118	1.874520	0.026735	1.318680	1.874520	-0.010551
0.952430	1.874520	0.075094	0.908770	1.874520	0.024568	1.327370	1.874520	-0.010491
0.940446	1.874520	0.075003	0.920667	1.874520	0.022966			
0.927717	1.874520	0.074757	0.933151	1.874520	0.021416			

C.32 Airfoil R12

Table C.32 Airfoil R12

X	Y	Z	X	Y	Z	X	Y	Z
1.381220	2.061972	-0.000452	0.994219	2.061972	0.075511	1.022110	2.061972	0.024993
1.372810	2.061972	0.000961	0.980611	2.061972	0.074866	1.034780	2.061972	0.023718
1.357850	2.061972	0.003588	0.968960	2.061972	0.073744	1.049220	2.061972	0.022330
1.334370	2.061972	0.009298	0.959275	2.061972	0.072273	1.062640	2.061972	0.021129
1.307550	2.061972	0.017680	0.950278	2.061972	0.070548	1.076370	2.061972	0.019957
1.296690	2.061972	0.020829	0.943231	2.061972	0.068659	1.090350	2.061972	0.018791
1.283370	2.061972	0.024771	0.934683	2.061972	0.066125	1.104530	2.061972	0.017642
1.269620	2.061972	0.028816	0.929311	2.061972	0.064001	1.120260	2.061972	0.016389
1.255490	2.061972	0.032937	0.924181	2.061972	0.061468	1.136080	2.061972	0.015150
1.241020	2.061972	0.037111	0.920345	2.061972	0.058615	1.151960	2.061972	0.013927
1.227630	2.061972	0.041031	0.917529	2.061972	0.056077	1.166460	2.061972	0.012789
1.215350	2.061972	0.044676	0.915991	2.061972	0.054407	1.180900	2.061972	0.011646
1.200140	2.061972	0.048841	0.915396	2.061972	0.053025	1.195250	2.061972	0.010497
1.186130	2.061972	0.052642	0.915550	2.061972	0.050943	1.210840	2.061972	0.009276
1.172000	2.061972	0.056298	0.916651	2.061972	0.049187	1.223450	2.061972	0.008195
1.157800	2.061972	0.059745	0.918886	2.061972	0.047155	1.237190	2.061972	0.007042
1.142200	2.061972	0.063180	0.922101	2.061972	0.045143	1.252030	2.061972	0.005831
1.126610	2.061972	0.066290	0.926613	2.061972	0.042824	1.266540	2.061972	0.004637
1.111080	2.061972	0.069042	0.931470	2.061972	0.040904	1.280650	2.061972	0.003463
1.097020	2.061972	0.071179	0.939369	2.061972	0.038335	1.294340	2.061972	0.002322
1.083120	2.061972	0.072943	0.945958	2.061972	0.036629	1.304120	2.061972	0.001573
1.069410	2.061972	0.074315	0.954487	2.061972	0.034687	1.332630	2.061972	-0.000304
1.055970	2.061972	0.075313	0.963758	2.061972	0.032903	1.357190	2.061972	-0.000684
1.041460	2.061972	0.076148	0.975016	2.061972	0.030943	1.372600	2.061972	-0.000574
1.028660	2.061972	0.076471	0.988284	2.061972	0.028923	1.381220	2.061972	-0.000452
1.017630	2.061972	0.076326	0.999494	2.061972	0.027496			
1.005680	2.061972	0.076061	1.011230	2.061972	0.026127			

C.33 Airfoil R13

Table C.33 Airfoil R13

X	Y	Z	X	Y	Z	X	Y	Z
1.435060	2.249424	0.009655	1.072910	2.249424	0.076678	1.099290	2.249424	0.029765
1.426710	2.249424	0.011014	1.059730	2.249424	0.076047	1.111120	2.249424	0.028684
1.412840	2.249424	0.013326	1.048580	2.249424	0.074961	1.124800	2.249424	0.027497
1.391090	2.249424	0.018359	1.039460	2.249424	0.073558	1.137300	2.249424	0.026501
1.366890	2.249424	0.025621	1.030970	2.249424	0.071915	1.150070	2.249424	0.025537
1.356380	2.249424	0.028493	1.024470	2.249424	0.070148	1.163060	2.249424	0.024585
1.343670	2.249424	0.032045	1.016210	2.249424	0.067709	1.176240	2.249424	0.023652
1.330580	2.249424	0.035684	1.011260	2.249424	0.065722	1.191070	2.249424	0.022625
1.317150	2.249424	0.039384	1.006430	2.249424	0.063321	1.205980	2.249424	0.021619
1.303430	2.249424	0.043127	1.002880	2.249424	0.060663	1.220950	2.249424	0.020632
1.290930	2.249424	0.046597	1.000280	2.249424	0.058279	1.234410	2.249424	0.019726
1.279700	2.249424	0.049777	0.998887	2.249424	0.056724	1.247830	2.249424	0.018816
1.265320	2.249424	0.053500	0.998361	2.249424	0.055455	1.261160	2.249424	0.017902
1.252270	2.249424	0.056855	0.998519	2.249424	0.053569	1.275870	2.249424	0.016926
1.239130	2.249424	0.060078	0.999539	2.249424	0.051954	1.287370	2.249424	0.016071
1.225920	2.249424	0.063112	1.001640	2.249424	0.050039	1.300160	2.249424	0.015151
1.211190	2.249424	0.066171	1.004660	2.249424	0.048158	1.314210	2.249424	0.014182
1.196480	2.249424	0.068934	1.008950	2.249424	0.045974	1.327960	2.249424	0.013227
1.181820	2.249424	0.071375	1.013460	2.249424	0.044221	1.341360	2.249424	0.012287
1.168750	2.249424	0.073232	1.021150	2.249424	0.041746	1.354380	2.249424	0.011375
1.155820	2.249424	0.074756	1.027260	2.249424	0.040212	1.363930	2.249424	0.010778
1.143070	2.249424	0.075929	1.035350	2.249424	0.038421	1.389580	2.249424	0.009365
1.130550	2.249424	0.076768	1.044120	2.249424	0.036794	1.412260	2.249424	0.009233
1.116820	2.249424	0.077483	1.054930	2.249424	0.034989	1.426520	2.249424	0.009458
1.104890	2.249424	0.077717	1.067820	2.249424	0.033132	1.435060	2.249424	0.009655
1.094810	2.249424	0.077516	1.078340	2.249424	0.031888			
1.083640	2.249424	0.077225	1.089340	2.249424	0.030706			

C.34 Airfoil R14

Table C.34 Airfoil R14

X	Y	Z	X	Y	Z	X	Y	Z
1.488880	2.436876	0.019805	1.151620	2.436876	0.077766	1.176500	2.436876	0.034468
1.480600	2.436876	0.021094	1.138870	2.436876	0.077134	1.187490	2.436876	0.033586
1.467820	2.436876	0.023090	1.128220	2.436876	0.076074	1.200400	2.436876	0.032608
1.447790	2.436876	0.027445	1.119660	2.436876	0.074733	1.211980	2.436876	0.031819
1.426220	2.436876	0.033601	1.111670	2.436876	0.073167	1.223790	2.436876	0.031066
1.416060	2.436876	0.036184	1.105730	2.436876	0.071522	1.235800	2.436876	0.030330
1.403970	2.436876	0.039337	1.097760	2.436876	0.069168	1.247970	2.436876	0.029616
1.391540	2.436876	0.042559	1.093230	2.436876	0.067319	1.261900	2.436876	0.028824
1.378820	2.436876	0.045828	1.088710	2.436876	0.065049	1.275910	2.436876	0.028057
1.365830	2.436876	0.049130	1.085450	2.436876	0.062585	1.289970	2.436876	0.027314
1.354240	2.436876	0.052147	1.083050	2.436876	0.060353	1.302390	2.436876	0.026643
1.344070	2.436876	0.054867	1.081810	2.436876	0.058913	1.314770	2.436876	0.025969
1.330500	2.436876	0.058139	1.081350	2.436876	0.057758	1.327070	2.436876	0.025292
1.318430	2.436876	0.061045	1.081510	2.436876	0.056068	1.340900	2.436876	0.024569
1.306270	2.436876	0.063832	1.082450	2.436876	0.054593	1.351290	2.436876	0.023936
1.294050	2.436876	0.066452	1.084430	2.436876	0.052798	1.363130	2.436876	0.023253
1.280200	2.436876	0.069125	1.087250	2.436876	0.051048	1.376390	2.436876	0.022534
1.266360	2.436876	0.071535	1.091320	2.436876	0.049001	1.389380	2.436876	0.021826
1.252570	2.436876	0.073655	1.095490	2.436876	0.047416	1.402070	2.436876	0.021131
1.240490	2.436876	0.075230	1.102970	2.436876	0.045046	1.414420	2.436876	0.020458
1.228530	2.436876	0.076511	1.108600	2.436876	0.043684	1.423730	2.436876	0.020025
1.216740	2.436876	0.077484	1.116250	2.436876	0.042049	1.446510	2.436876	0.019060
1.205160	2.436876	0.078162	1.124520	2.436876	0.040584	1.467320	2.436876	0.019176
1.192200	2.436876	0.078747	1.134880	2.436876	0.038945	1.480430	2.436876	0.019518
1.181140	2.436876	0.078889	1.147390	2.436876	0.037267	1.488880	2.436876	0.019805
1.172010	2.436876	0.078635	1.157220	2.436876	0.036210			
1.161620	2.436876	0.078314	1.167480	2.436876	0.035220			

C.35 Airfoil R15

Table C.35 Airfoil R15

X	Y	Z	X	Y	Z	X	Y	Z
1.542680	2.624328	0.029965	1.230370	2.624328	0.078853	1.253760	2.624328	0.039176
1.534460	2.624328	0.031170	1.218050	2.624328	0.078205	1.263900	2.624328	0.038491
1.522760	2.624328	0.032853	1.207910	2.624328	0.077163	1.276050	2.624328	0.037728
1.504470	2.624328	0.036535	1.199910	2.624328	0.075882	1.286700	2.624328	0.037145
1.485550	2.624328	0.041612	1.192430	2.624328	0.074389	1.297550	2.624328	0.036601
1.475740	2.624328	0.043896	1.187040	2.624328	0.072869	1.308570	2.624328	0.036078
1.464270	2.624328	0.046642	1.179350	2.624328	0.070591	1.319730	2.624328	0.035581
1.452510	2.624328	0.049440	1.175250	2.624328	0.068881	1.332760	2.624328	0.035028
1.440490	2.624328	0.052273	1.171040	2.624328	0.066741	1.345860	2.624328	0.034505
1.428250	2.624328	0.055128	1.168060	2.624328	0.064471	1.359000	2.624328	0.034010
1.417550	2.624328	0.057693	1.165870	2.624328	0.062394	1.370380	2.624328	0.033570
1.408440	2.624328	0.059960	1.164780	2.624328	0.061069	1.381720	2.624328	0.033130
1.395710	2.624328	0.062776	1.164380	2.624328	0.060028	1.393000	2.624328	0.032688
1.384610	2.624328	0.065234	1.164550	2.624328	0.058535	1.405950	2.624328	0.032222
1.373430	2.624328	0.067588	1.165410	2.624328	0.057201	1.415230	2.624328	0.031803
1.362220	2.624328	0.069796	1.167250	2.624328	0.055525	1.426110	2.624328	0.031355
1.349240	2.624328	0.072079	1.169880	2.624328	0.053907	1.438570	2.624328	0.030892
1.336280	2.624328	0.074130	1.173730	2.624328	0.052000	1.450800	2.624328	0.030437
1.323360	2.624328	0.075926	1.177550	2.624328	0.050580	1.462770	2.624328	0.029992
1.312270	2.624328	0.077221	1.184830	2.624328	0.048325	1.474450	2.624328	0.029566
1.301290	2.624328	0.078262	1.189980	2.624328	0.047133	1.483530	2.624328	0.029309
1.290460	2.624328	0.079035	1.197200	2.624328	0.045658	1.503430	2.624328	0.028763
1.279810	2.624328	0.079553	1.204960	2.624328	0.044357	1.522350	2.624328	0.029119
1.267630	2.624328	0.080005	1.214880	2.624328	0.042894	1.534310	2.624328	0.029574
1.257440	2.624328	0.080054	1.227010	2.624328	0.041409	1.542680	2.624328	0.029965
1.249260	2.624328	0.079753	1.236150	2.624328	0.040541			
1.239650	2.624328	0.079403	1.245660	2.624328	0.039743			

C.36 Airfoil R16

Table C.36 Airfoil R16

X	Y	Z	X	Y	Z	X	Y	Z
1.596430	2.811780	0.040099	1.309210	2.811780	0.080029	1.331070	2.811780	0.043968
1.588280	2.811780	0.041205	1.297320	2.811780	0.079352	1.340360	2.811780	0.043477
1.577670	2.811780	0.042583	1.287670	2.811780	0.078322	1.351750	2.811780	0.042931
1.561130	2.811780	0.045608	1.280240	2.811780	0.077102	1.361460	2.811780	0.042548
1.544870	2.811780	0.049649	1.273260	2.811780	0.075682	1.371350	2.811780	0.042206
1.535410	2.811780	0.051623	1.268410	2.811780	0.074291	1.381380	2.811780	0.041890
1.524560	2.811780	0.053957	1.261020	2.811780	0.072081	1.391530	2.811780	0.041602
1.513470	2.811780	0.056328	1.257340	2.811780	0.070515	1.403650	2.811780	0.041287
1.502160	2.811780	0.058721	1.253430	2.811780	0.068504	1.415840	2.811780	0.041008
1.490670	2.811780	0.061127	1.250730	2.811780	0.066431	1.428050	2.811780	0.040760
1.480890	2.811780	0.063246	1.248760	2.811780	0.064509	1.438380	2.811780	0.040543
1.472850	2.811780	0.065073	1.247810	2.811780	0.063302	1.448690	2.811780	0.040329
1.460940	2.811780	0.067432	1.247490	2.811780	0.062376	1.458940	2.811780	0.040114
1.450820	2.811780	0.069450	1.247650	2.811780	0.061080	1.471000	2.811780	0.039905
1.440650	2.811780	0.071378	1.248420	2.811780	0.059885	1.479160	2.811780	0.039685
1.430430	2.811780	0.073180	1.250140	2.811780	0.058328	1.489080	2.811780	0.039466
1.418330	2.811780	0.075074	1.252580	2.811780	0.056841	1.500740	2.811780	0.039260
1.406250	2.811780	0.076766	1.256210	2.811780	0.055075	1.512200	2.811780	0.039062
1.394210	2.811780	0.078237	1.259680	2.811780	0.053818	1.523450	2.811780	0.038871
1.384120	2.811780	0.079260	1.266760	2.811780	0.051686	1.534460	2.811780	0.038695
1.374130	2.811780	0.080067	1.271420	2.811780	0.050661	1.543300	2.811780	0.038626
1.364250	2.811780	0.080648	1.278200	2.811780	0.049346	1.560310	2.811780	0.038452
1.354540	2.811780	0.081013	1.285460	2.811780	0.048212	1.577350	2.811780	0.039031
1.343130	2.811780	0.081328	1.294940	2.811780	0.046931	1.588150	2.811780	0.039587
1.333810	2.811780	0.081291	1.306690	2.811780	0.045653	1.596430	2.811780	0.040099
1.326580	2.811780	0.080955	1.315140	2.811780	0.044971			
1.317750	2.811780	0.080578	1.323900	2.811780	0.044363			

C.37 Airfoil R17

Table C.37 Airfoil R17

X	Y	Z	X	Y	Z	X	Y	Z
1.650140	2.999232	0.050161	1.388140	2.999232	0.081406	1.408440	2.999232	0.048945
1.642040	2.999232	0.051153	1.376680	2.999232	0.080689	1.416870	2.999232	0.048637
1.632530	2.999232	0.052243	1.367530	2.999232	0.079667	1.427490	2.999232	0.048305
1.617740	2.999232	0.054637	1.360660	2.999232	0.078510	1.436270	2.999232	0.048111
1.604170	2.999232	0.057701	1.354190	2.999232	0.077165	1.445190	2.999232	0.047959
1.595070	2.999232	0.059358	1.349890	2.999232	0.075913	1.454230	2.999232	0.047836
1.584850	2.999232	0.061280	1.342790	2.999232	0.073765	1.463360	2.999232	0.047743
1.574440	2.999232	0.063224	1.339530	2.999232	0.072349	1.474570	2.999232	0.047661
1.563850	2.999232	0.065178	1.335920	2.999232	0.070469	1.485840	2.999232	0.047620
1.553110	2.999232	0.067136	1.333500	2.999232	0.068596	1.497130	2.999232	0.047614
1.544250	2.999232	0.068820	1.331740	2.999232	0.066832	1.506410	2.999232	0.047605
1.537290	2.999232	0.070229	1.330930	2.999232	0.065746	1.515670	2.999232	0.047602
1.526220	2.999232	0.072135	1.330670	2.999232	0.064937	1.524880	2.999232	0.047600
1.517090	2.999232	0.073726	1.330830	2.999232	0.063837	1.536060	2.999232	0.047644
1.507920	2.999232	0.075241	1.331520	2.999232	0.062780	1.543090	2.999232	0.047601
1.498720	2.999232	0.076652	1.333110	2.999232	0.061340	1.552050	2.999232	0.047598
1.487510	2.999232	0.078162	1.335350	2.999232	0.059982	1.562890	2.999232	0.047647
1.476310	2.999232	0.079500	1.338760	2.999232	0.058357	1.573590	2.999232	0.047702
1.465150	2.999232	0.080651	1.341880	2.999232	0.057258	1.584110	2.999232	0.047764
1.456060	2.999232	0.081415	1.348760	2.999232	0.055257	1.594440	2.999232	0.047838
1.447050	2.999232	0.082002	1.352940	2.999232	0.054391	1.603030	2.999232	0.047969
1.438150	2.999232	0.082403	1.359280	2.999232	0.053237	1.617160	2.999232	0.048101
1.429370	2.999232	0.082627	1.366040	2.999232	0.052266	1.632300	2.999232	0.048874
1.418740	2.999232	0.082808	1.375070	2.999232	0.051171	1.641950	2.999232	0.049515
1.410280	2.999232	0.082695	1.386430	2.999232	0.050113	1.650140	2.999232	0.050161
1.404010	2.999232	0.082342	1.394190	2.999232	0.049611			
1.395960	2.999232	0.081947	1.402200	2.999232	0.049185			

C.38 Airfoil R18

Table C.38 Airfoil R18

X	Y	Z	X	Y	Z	X	Y	Z
1.703780	3.186684	0.060097	1.467210	3.186684	0.083118	1.485870	3.186684	0.054228
1.695740	3.186684	0.060960	1.456170	3.186684	0.082355	1.493450	3.186684	0.054086
1.687340	3.186684	0.061786	1.447520	3.186684	0.081342	1.503290	3.186684	0.053961
1.674320	3.186684	0.063588	1.441220	3.186684	0.080256	1.511140	3.186684	0.053936
1.663470	3.186684	0.065754	1.435240	3.186684	0.078993	1.519080	3.186684	0.053954
1.654730	3.186684	0.067091	1.431480	3.186684	0.077891	1.527120	3.186684	0.054004
1.645140	3.186684	0.068604	1.424670	3.186684	0.075801	1.535230	3.186684	0.054085
1.635420	3.186684	0.070126	1.421820	3.186684	0.074544	1.545530	3.186684	0.054223
1.625560	3.186684	0.071650	1.418520	3.186684	0.072799	1.555870	3.186684	0.054407
1.615590	3.186684	0.073168	1.416380	3.186684	0.071132	1.566230	3.186684	0.054629
1.607660	3.186684	0.074436	1.414820	3.186684	0.069529	1.574450	3.186684	0.054807
1.601780	3.186684	0.075455	1.414150	3.186684	0.068568	1.582660	3.186684	0.054992
1.591570	3.186684	0.076918	1.413960	3.186684	0.067877	1.590830	3.186684	0.055182
1.583440	3.186684	0.078103	1.414100	3.186684	0.066973	1.601110	3.186684	0.055466
1.575280	3.186684	0.079227	1.414700	3.186684	0.066052	1.607020	3.186684	0.055571
1.567100	3.186684	0.080268	1.416160	3.186684	0.064728	1.615000	3.186684	0.055765
1.556780	3.186684	0.081405	1.418210	3.186684	0.063495	1.625030	3.186684	0.056059
1.546480	3.186684	0.082403	1.421400	3.186684	0.062008	1.634950	3.186684	0.056360
1.536210	3.186684	0.083246	1.424170	3.186684	0.061060	1.644740	3.186684	0.056667
1.528130	3.186684	0.083772	1.430850	3.186684	0.059196	1.654380	3.186684	0.056986
1.520110	3.186684	0.084159	1.434540	3.186684	0.058478	1.662720	3.186684	0.057324
1.512170	3.186684	0.084400	1.440440	3.186684	0.057479	1.673950	3.186684	0.057679
1.504330	3.186684	0.084501	1.446690	3.186684	0.056665	1.687200	3.186684	0.058601
1.494480	3.186684	0.084557	1.455270	3.186684	0.055758	1.695680	3.186684	0.059302
1.486890	3.186684	0.084384	1.466250	3.186684	0.054927	1.703780	3.186684	0.060097
1.481570	3.186684	0.084039	1.473310	3.186684	0.054594			
1.474300	3.186684	0.083639	1.480570	3.186684	0.054336			

C.39 Airfoil R19

Table C.39 Airfoil R19

X	Y	Z	X	Y	Z	X	Y	Z
1.757360	3.374136	0.069831	1.546420	3.374136	0.085347	1.563360	3.374136	0.059974
1.749380	3.374136	0.070556	1.535820	3.374136	0.084536	1.570070	3.374136	0.059975
1.742090	3.374136	0.071151	1.527670	3.374136	0.083539	1.579140	3.374136	0.060039
1.730860	3.374136	0.072418	1.521910	3.374136	0.082538	1.586040	3.374136	0.060156
1.722750	3.374136	0.073786	1.516430	3.374136	0.081366	1.593010	3.374136	0.060315
1.714380	3.374136	0.074803	1.513210	3.374136	0.080431	1.600040	3.374136	0.060507
1.705450	3.374136	0.075922	1.506690	3.374136	0.078400	1.607120	3.374136	0.060731
1.696420	3.374136	0.077036	1.504250	3.374136	0.077315	1.616500	3.374136	0.061068
1.687300	3.374136	0.078144	1.501250	3.374136	0.075712	1.625910	3.374136	0.061453
1.678110	3.374136	0.079241	1.499370	3.374136	0.074258	1.635340	3.374136	0.061881
1.671120	3.374136	0.080120	1.498010	3.374136	0.072823	1.642500	3.374136	0.062214
1.666350	3.374136	0.080787	1.497480	3.374136	0.071990	1.649650	3.374136	0.062556
1.657000	3.374136	0.081828	1.497340	3.374136	0.071419	1.656780	3.374136	0.062906
1.649880	3.374136	0.082637	1.497470	3.374136	0.070712	1.666150	3.374136	0.063409
1.642740	3.374136	0.083400	1.497980	3.374136	0.069923	1.670930	3.374136	0.063622
1.635590	3.374136	0.084102	1.499310	3.374136	0.068710	1.677930	3.374136	0.063984
1.626180	3.374136	0.084890	1.501150	3.374136	0.067598	1.687140	3.374136	0.064504
1.616790	3.374136	0.085568	1.504120	3.374136	0.066244	1.696280	3.374136	0.065034
1.607410	3.374136	0.086126	1.506540	3.374136	0.065436	1.705330	3.374136	0.065572
1.600340	3.374136	0.086444	1.513020	3.374136	0.063710	1.714280	3.374136	0.066122
1.593320	3.374136	0.086660	1.516220	3.374136	0.063125	1.722360	3.374136	0.066669
1.586350	3.374136	0.086770	1.521680	3.374136	0.062273	1.730680	3.374136	0.067140
1.579450	3.374136	0.086775	1.527410	3.374136	0.061603	1.742030	3.374136	0.068154
1.570380	3.374136	0.086724	1.535540	3.374136	0.060878	1.749360	3.374136	0.068879
1.563660	3.374136	0.086516	1.546140	3.374136	0.060276	1.757360	3.374136	0.069831
1.559290	3.374136	0.086210	1.552490	3.374136	0.060092			
1.552790	3.374136	0.085828	1.558990	3.374136	0.059983			

C.40 Airfoil R20

Table C.40 Airfoil R20

X	Y	Z	X	Y	Z	X	Y	Z
1.810880	3.561588	0.079252	1.625810	3.561588	0.088353	1.640870	3.561588	0.066414
1.802970	3.561588	0.079838	1.615620	3.561588	0.087511	1.646720	3.561588	0.066520
1.796790	3.561588	0.080250	1.607970	3.561588	0.086548	1.655000	3.561588	0.066741
1.787360	3.561588	0.081059	1.602760	3.561588	0.085654	1.660960	3.561588	0.066960
1.782030	3.561588	0.081752	1.597770	3.561588	0.084595	1.666950	3.561588	0.067219
1.774040	3.561588	0.082464	1.595080	3.561588	0.083849	1.672980	3.561588	0.067511
1.765770	3.561588	0.083213	1.588840	3.561588	0.081887	1.679030	3.561588	0.067834
1.757460	3.561588	0.083950	1.586800	3.561588	0.080990	1.687490	3.561588	0.068330
1.749090	3.561588	0.084673	1.584090	3.561588	0.079540	1.695960	3.561588	0.068879
1.740690	3.561588	0.085381	1.582470	3.561588	0.078310	1.704440	3.561588	0.069474
1.734660	3.561588	0.085912	1.581310	3.561588	0.077050	1.710540	3.561588	0.069916
1.731010	3.561588	0.086275	1.580910	3.561588	0.076352	1.716630	3.561588	0.070370
1.722530	3.561588	0.086931	1.580820	3.561588	0.075904	1.722710	3.561588	0.070835
1.716440	3.561588	0.087408	1.580920	3.561588	0.075391	1.731170	3.561588	0.071520
1.710340	3.561588	0.087854	1.581330	3.561588	0.074730	1.734820	3.561588	0.071793
1.704230	3.561588	0.088261	1.582520	3.561588	0.073623	1.740840	3.561588	0.072280
1.695740	3.561588	0.088737	1.584170	3.561588	0.072621	1.749220	3.561588	0.072994
1.687250	3.561588	0.089135	1.586910	3.561588	0.071392	1.757570	3.561588	0.073720
1.678780	3.561588	0.089444	1.588960	3.561588	0.070707	1.765870	3.561588	0.074458
1.672730	3.561588	0.089597	1.595240	3.561588	0.069112	1.774120	3.561588	0.075211
1.666700	3.561588	0.089686	1.597950	3.561588	0.068639	1.781940	3.561588	0.075960
1.660700	3.561588	0.089705	1.602960	3.561588	0.067914	1.787360	3.561588	0.076419
1.654750	3.561588	0.089656	1.608180	3.561588	0.067369	1.796810	3.561588	0.077443
1.646460	3.561588	0.089529	1.615860	3.561588	0.066808	1.802990	3.561588	0.078143
1.640610	3.561588	0.089323	1.626050	3.561588	0.066419	1.810880	3.561588	0.079252
1.637180	3.561588	0.089098	1.631710	3.561588	0.066357			
1.631460	3.561588	0.088765	1.637440	3.561588	0.066363			

C.41 Airfoil R21

Table C.41 Airfoil R21

X	Y	Z	X	Y	Z	X	Y	Z
1.864370	3.749040	0.088097	1.705370	3.749040	0.092716	1.718320	3.749040	0.074049
1.856530	3.749040	0.088584	1.695600	3.749040	0.091906	1.723310	3.749040	0.074198
1.851480	3.749040	0.088889	1.688420	3.749040	0.091034	1.730810	3.749040	0.074506
1.843870	3.749040	0.089358	1.683760	3.749040	0.090293	1.735820	3.749040	0.074760
1.841340	3.749040	0.089514	1.679240	3.749040	0.089388	1.740830	3.749040	0.075051
1.833740	3.749040	0.089975	1.677060	3.749040	0.088866	1.745850	3.749040	0.075373
1.826150	3.749040	0.090422	1.671100	3.749040	0.087012	1.750870	3.749040	0.075726
1.818560	3.749040	0.090849	1.669450	3.749040	0.086329	1.758410	3.749040	0.076305
1.810970	3.749040	0.091258	1.667010	3.749040	0.085056	1.765950	3.749040	0.076939
1.803380	3.749040	0.091649	1.665630	3.749040	0.084067	1.773490	3.749040	0.077622
1.798320	3.749040	0.091900	1.664650	3.749040	0.082995	1.778520	3.749040	0.078101
1.795780	3.749040	0.092022	1.664370	3.749040	0.082439	1.783550	3.749040	0.078597
1.788200	3.749040	0.092369	1.664330	3.749040	0.082115	1.788590	3.749040	0.079106
1.783140	3.749040	0.092584	1.664390	3.749040	0.081794	1.796140	3.749040	0.079895
1.778090	3.749040	0.092785	1.664700	3.749040	0.081255	1.798660	3.749040	0.080165
1.773040	3.749040	0.092970	1.665740	3.749040	0.080242	1.803700	3.749040	0.080710
1.765470	3.749040	0.093211	1.667180	3.749040	0.079335	1.811250	3.749040	0.081544
1.757910	3.749040	0.093405	1.669680	3.749040	0.078207	1.818810	3.749040	0.082395
1.750350	3.749040	0.093543	1.671370	3.749040	0.077621	1.826360	3.749040	0.083264
1.745320	3.749040	0.093602	1.677440	3.749040	0.076119	1.833910	3.749040	0.084154
1.740290	3.749040	0.093631	1.679640	3.749040	0.075725	1.841470	3.749040	0.085057
1.735270	3.749040	0.093629	1.684200	3.749040	0.075085	1.843990	3.749040	0.085361
1.730250	3.749040	0.093590	1.688900	3.749040	0.074617	1.851550	3.749040	0.086273
1.722740	3.749040	0.093459	1.696120	3.749040	0.074165	1.856580	3.749040	0.086872
1.717750	3.749040	0.093318	1.705920	3.749040	0.073927	1.864370	3.749040	0.088097
1.715270	3.749040	0.093227	1.710860	3.749040	0.073929			
1.710300	3.749040	0.093002	1.715830	3.749040	0.073994			

Appendix D

LEADING AND TRAILING EDGE INFO

D.1 Leading & Trailing Edge Coordinates

Table D.1: Leading Edge Coordinates

X Location (m)	Y Location (m)	Z Location (m)
0.000000	0.000000	0.000000
0.187452	0.083587	0.007641
0.374904	0.167093	0.014617
0.562356	0.250514	0.020952
0.749808	0.333852	0.026677
0.937260	0.417109	0.031826
1.124712	0.500289	0.036436
1.312164	0.583401	0.040548
1.499616	0.666454	0.044209
1.687068	0.749461	0.047470
1.874520	0.832436	0.050388
2.061972	0.915396	0.053025
2.249424	0.998361	0.055455
2.436876	1.081350	0.057758
2.624328	1.164380	0.060028
2.811780	1.247490	0.062376
2.999232	1.330670	0.064937
3.186684	1.413960	0.067877
3.374136	1.497340	0.071419
3.561588	1.580820	0.075904
3.749040	1.664330	0.082115

Table D.2: Trailing Edge Coordinates

X Location (m)	Y Location (m)	Z Location (m)
0.000000	0.790670	-0.102860
0.187452	0.844130	-0.094492
0.374904	0.897639	-0.085902
0.562356	0.951201	-0.077098
0.749808	1.004810	-0.068090
0.937260	1.058480	-0.058890
1.124712	1.112190	-0.049509
1.312164	1.165940	-0.039963
1.499616	1.219720	-0.030266
1.687068	1.273540	-0.020436
1.874520	1.327370	-0.010491
2.061972	1.381220	-0.000452
2.249424	1.435060	0.009655
2.436876	1.488880	0.019805
2.624328	1.542680	0.029965
2.811780	1.596430	0.040099
2.999232	1.650140	0.050161
3.186684	1.703780	0.060097
3.374136	1.757360	0.069831
3.561588	1.810880	0.079252
3.749040	1.864370	0.088097

D.2 Leading & Trailing Edge Plotted

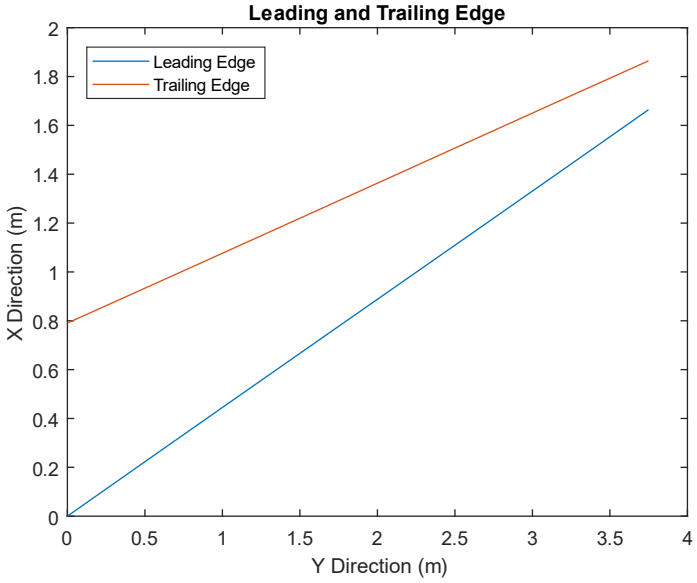

Figure D.1: Leading and Trailing Edges Plotted

Appendix E

RESIDUALS

E.1 Tabulated Residuals

Table E.1: Tabulated Residuals Pt.1

Wing Spacing, Y/b	Continuity		Tdr		Tke	
	Mean	S.D.	Mean	S.D.	Mean	S.D.
-1	2.02E-04	6.18E-07	4.36E-06	1.16E-08	2.72E-05	1.11E-07
-0.592	2.10E-04	7.63E-07	4.53E-06	1.52E-08	3.18E-05	8.66E-08
-0.444	2.22E-04	5.44E-07	4.52E-06	1.37E-08	2.74E-05	6.09E-08
-0.37	2.19E-04	5.90E-07	2.20E-04	7.08E-05	3.15E-05	7.96E-08
-0.333	2.20E-04	5.37E-07	4.48E-06	1.23E-08	2.74E-05	4.04E-08
-0.296	2.16E-04	5.40E-07	4.58E-06	1.31E-08	2.76E-05	4.85E-08
-0.259	2.15E-04	5.18E-07	3.32E-03	8.48E-04	2.90E-05	2.40E-07
-0.222	2.24E-04	4.92E-07	2.21E-03	3.54E-04	3.12E-05	2.07E-07
-0.185	2.21E-04	5.69E-07	4.57E-06	1.07E-08	3.46E-05	2.12E-07
-0.148	2.19E-04	4.32E-07	4.52E-06	1.52E-08	2.56E-05	4.72E-08
-0.111	2.24E-04	5.14E-07	4.53E-06	2.02E-08	3.02E-05	7.91E-08
-0.074	2.29E-04	5.49E-07	5.01E-06	5.54E-08	3.17E-05	7.39E-08
-0.037	2.20E-04	5.01E-07	4.48E-06	1.40E-08	2.30E-05	4.32E-08
0	2.29E-04	5.11E-07	4.58E-06	2.06E-08	3.20E-05	8.13E-08
0.037	2.22E-04	5.22E-07	4.46E-06	1.60E-08	3.01E-05	6.42E-08
0.074	2.21E-04	5.42E-07	4.50E-06	1.40E-08	3.14E-05	8.90E-08
0.148	2.38E-04	5.52E-07	2.51E-01	1.02E-01	8.52E-04	3.52E-04
0.296	2.33E-04	5.59E-07	4.49E-06	1.17E-08	3.06E-05	5.63E-08
0.444	2.47E-04	5.36E-07	2.86E-03	8.14E-04	4.03E-05	5.85E-06
0.592	2.36E-04	4.78E-07	4.40E-06	1.33E-08	2.61E-05	5.99E-08
0.814	2.46E-04	5.65E-07	4.54E-06	1.49E-08	2.82E-05	8.81E-08
1	2.51E-04	4.98E-07	1.09E-01	2.79E-02	1.04E-04	3.09E-05
2	2.81E-04	4.61E-06	4.66E-05	2.63E-05	2.58E-05	1.23E-07

Table E.2: Tabulated Residuals Pt.2

Wing Spacing, Y/b	X Momentum		Y Momentum		Z Momentum	
	Mean	S.D.	Mean	S.D.	Mean	S.D.
-1	1.13E-04	4.82E-07	1.46E-04	1.26E-06	1.62E-05	1.69E-07
-0.592	1.19E-04	5.08E-07	1.61E-04	1.35E-06	1.43E-05	1.23E-07
-0.444	1.24E-04	2.98E-07	1.59E-04	1.31E-06	1.37E-05	1.15E-07
-0.37	1.23E-04	3.61E-07	1.58E-04	1.30E-06	1.35E-05	1.02E-07
-0.333	1.23E-04	3.63E-07	1.54E-04	1.31E-06	1.31E-05	1.19E-07
-0.296	1.22E-04	3.93E-07	1.53E-04	1.29E-06	1.30E-05	1.10E-07

-0.259	1.23E-04	3.88E-07	1.51E-04	1.29E-06	1.29E-05	1.11E-07
-0.222	1.26E-04	5.30E-07	1.51E-04	1.52E-06	1.32E-05	1.77E-07
-0.185	1.24E-04	3.12E-07	1.49E-04	1.20E-06	1.28E-05	9.61E-08
-0.148	1.23E-04	3.33E-07	1.45E-04	1.18E-06	1.26E-05	1.08E-07
-0.111	1.26E-04	3.61E-07	1.45E-04	1.17E-06	1.26E-05	1.01E-07
-0.074	1.29E-04	1.16E-06	1.44E-04	1.65E-06	1.26E-05	1.29E-07
-0.037	1.24E-04	3.79E-07	1.38E-04	1.17E-06	1.21E-05	1.09E-07
0	1.28E-04	4.62E-07	1.38E-04	1.16E-06	1.24E-05	1.04E-07
0.037	1.26E-04	5.42E-07	1.35E-04	1.18E-06	1.21E-05	1.11E-07
0.074	1.25E-04	4.16E-07	1.34E-04	1.16E-06	1.21E-05	1.13E-07
0.148	1.31E-04	4.08E-07	1.32E-04	1.21E-06	1.23E-05	1.39E-07
0.296	1.30E-04	2.81E-07	1.25E-04	1.13E-06	1.18E-05	1.14E-07
0.444	1.35E-04	3.10E-07	1.21E-04	1.03E-06	1.20E-05	1.00E-07
0.592	1.32E-04	3.14E-07	1.17E-04	1.08E-06	1.15E-05	1.12E-07
0.814	1.36E-04	3.88E-07	1.17E-04	1.01E-06	1.16E-05	9.97E-08
1	1.39E-04	3.01E-07	1.17E-04	9.66E-07	1.16E-05	9.10E-08
2	2.27E-03	1.25E-03	3.52E-03	1.97E-03	7.92E-04	4.02E-04

E.2 Additional Residual Plots

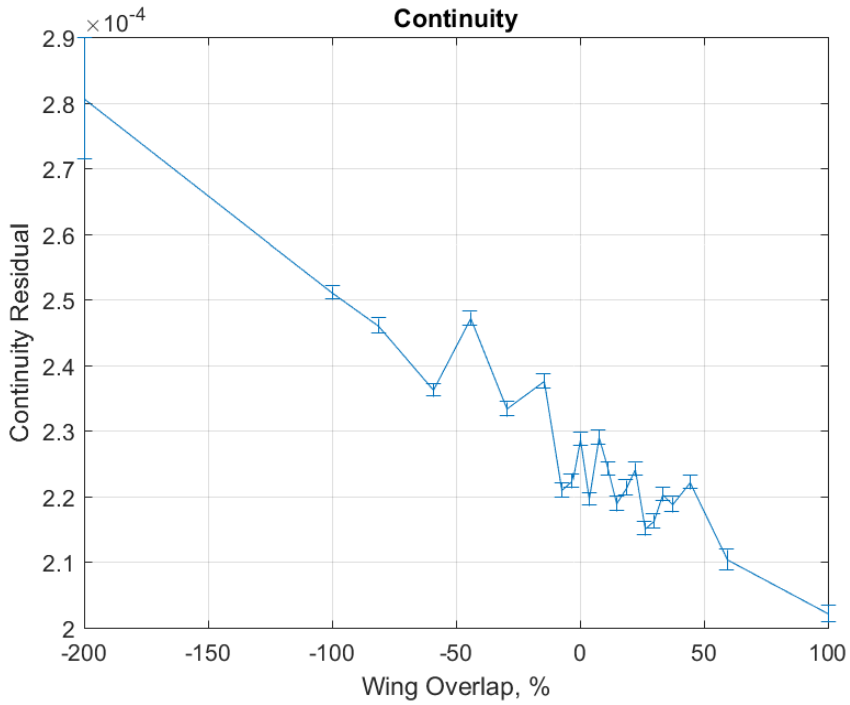

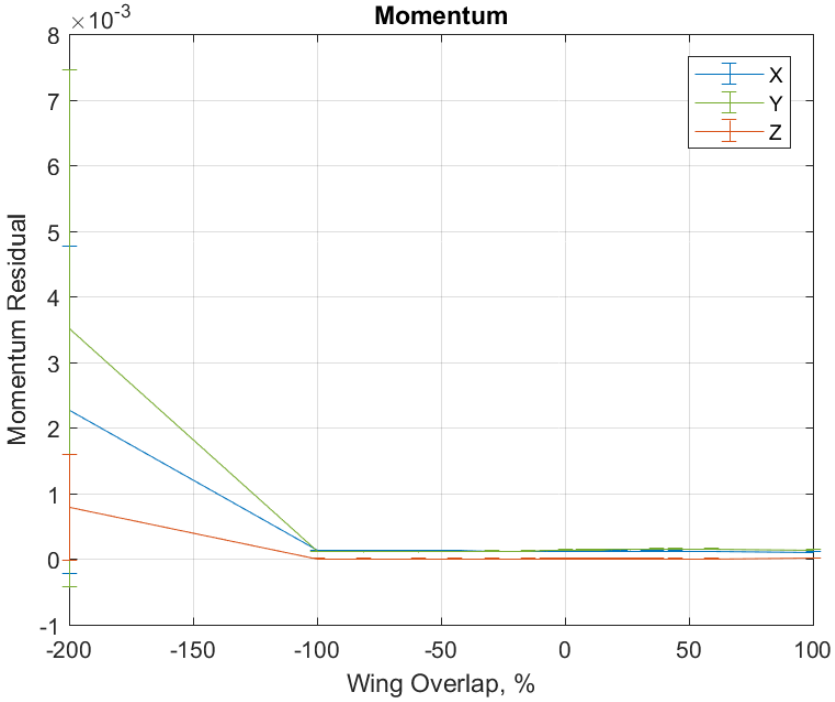
Momentum
×10^-3
8
7
6
5
4
3
2
1
0
-1
Momentum Residual
-200
-150
-100
-50
0
50
100
Wing Overlap, %
X
Y
Z

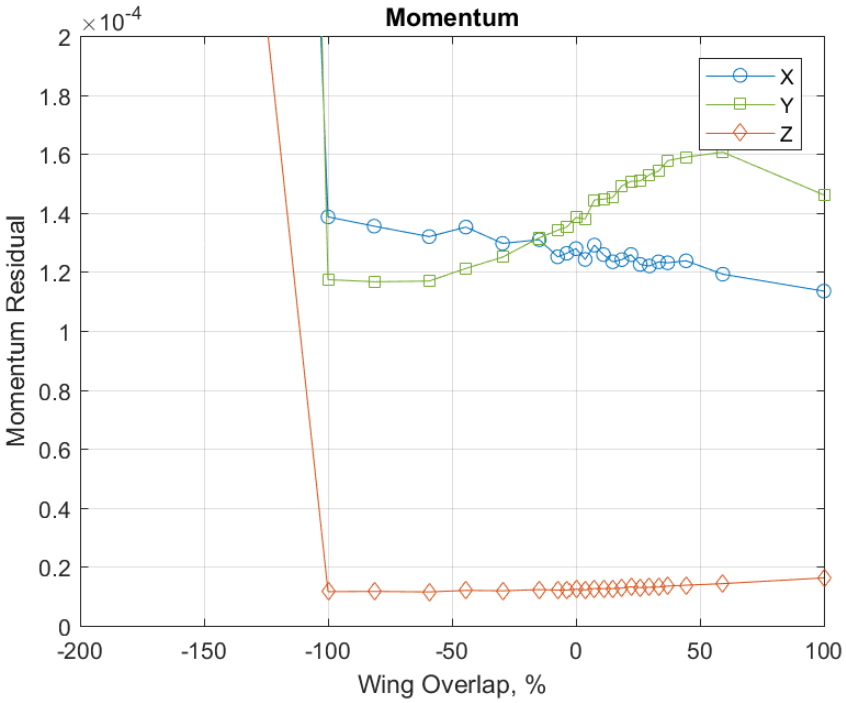
Momentum
×10^-4
2
1.8
1.6
1.4
1.2
1
0.8
0.6
0.4
0.2
0
Momentum Residual
-200
-150
-100
-50
0
50
100
Wing Overlap, %
X
Y
Z

Appendix F

MONITORED DATA

F.1 Tabulated Results from Monitored Data

Table F.1: Tabulated Lift Parameters

Wing Spacing, Y/b	Lift - Leading (N)		Lift – Trailing (N)		Lift % Change	
	Mean	S.D.	Mean	S.D.	Mean	S.D.
-1	129.416	3.71E-04	104.039	1.24E-04	-19.609	2.78E-04
-0.592	129.407	1.40E-04	124.128	1.67E-04	-4.079	1.85E-04
-0.444	129.384	5.88E-05	132.485	1.49E-04	2.396	1.49E-04
-0.37	129.357	7.00E-05	134.638	1.26E-04	4.082	1.15E-04
-0.333	129.340	1.40E-04	135.414	9.07E-05	4.697	1.43E-04
-0.296	129.329	1.34E-04	136.023	7.68E-05	5.176	1.33E-04
-0.259	129.302	1.42E-04	136.474	4.58E-05	5.547	1.24E-04
-0.222	129.282	1.34E-04	136.774	8.33E-05	5.795	1.54E-04
-0.185	129.262	1.36E-04	136.877	5.66E-05	5.891	1.45E-04
-0.148	129.238	1.39E-04	136.729	4.92E-05	5.797	1.44E-04
-0.111	129.210	1.26E-04	136.226	3.65E-05	5.430	1.14E-04
-0.074	129.190	1.76E-04	135.377	2.70E-05	4.789	1.44E-04
-0.037	129.166	1.16E-04	134.523	7.46E-05	4.147	7.41E-05
0	129.145	9.03E-05	133.763	1.96E-05	3.576	7.07E-05
0.037	129.120	1.11E-04	133.123	1.28E-05	3.101	8.63E-05
0.074	129.095	8.23E-05	132.624	1.88E-05	2.734	6.98E-05
0.148	129.059	6.78E-05	131.892	1.28E-05	2.195	4.58E-05
0.296	128.976	7.45E-05	130.897	1.91E-05	1.489	6.39E-05
0.444	128.922	4.17E-05	130.293	1.90E-05	1.063	3.80E-05
0.592	128.864	4.39E-05	129.881	3.81E-05	0.789	4.67E-05
0.814	128.797	2.77E-05	129.464	3.06E-05	0.518	2.05E-05
1	128.754	4.21E-05	129.225	4.27E-05	0.366	1.23E-05
2	128.621	9.46E-05	128.687	1.35E-02	0.051	1.05E-02

Table F.2: Tabulated Lift Coefficient Parameters

Wing Spacing, Y/b	Lift Coefficient - Leading		Lift Coefficient - Trailing		Lift Coefficient % Change	
	Mean	S.D.	Mean	S.D.	Mean	S.D.
-1	0.703765	2.02E-06	0.565763	6.72E-07	-19.609	2.78E-04
-0.592	0.703713	7.62E-07	0.675006	9.09E-07	-4.079	1.85E-04
-0.444	0.703591	3.20E-07	0.720452	8.09E-07	2.396	1.49E-04
-0.37	0.703444	3.81E-07	0.732161	6.87E-07	4.082	1.15E-04
-0.333	0.703350	7.59E-07	0.736383	4.93E-07	4.697	1.43E-04
-0.296	0.703290	7.28E-07	0.739693	4.17E-07	5.176	1.33E-04
-0.259	0.703146	7.73E-07	0.742146	2.49E-07	5.547	1.24E-04
-0.222	0.703034	7.29E-07	0.743774	4.53E-07	5.795	1.54E-04
-0.185	0.702928	7.41E-07	0.744338	3.08E-07	5.891	1.45E-04
-0.148	0.702794	7.55E-07	0.743533	2.67E-07	5.797	1.44E-04
-0.111	0.702646	6.87E-07	0.740798	1.99E-07	5.430	1.14E-04
-0.074	0.702535	9.59E-07	0.736182	1.47E-07	4.789	1.44E-04
-0.037	0.702403	6.30E-07	0.731535	4.06E-07	4.147	7.41E-05
0	0.702289	4.91E-07	0.727405	1.07E-07	3.576	7.07E-05
0.037	0.702152	6.01E-07	0.723924	6.97E-08	3.101	8.63E-05
0.074	0.702017	4.47E-07	0.721207	1.02E-07	2.734	6.98E-05
0.148	0.701822	3.69E-07	0.717228	6.94E-08	2.195	4.58E-05
0.296	0.701373	4.05E-07	0.711815	1.04E-07	1.489	6.39E-05
0.444	0.701077	2.27E-07	0.708532	1.03E-07	1.063	3.80E-05
0.592	0.700763	2.39E-07	0.706294	2.07E-07	0.789	4.67E-05
0.814	0.700397	1.51E-07	0.704027	1.67E-07	0.518	2.05E-05
1	0.700165	2.29E-07	0.702726	2.32E-07	0.366	1.23E-05
2	0.699438	5.14E-07	0.699798	7.34E-05	0.051	1.05E-02

Table F.3: Tabulated Total Drag Parameters

Wing Spacing, Y/b	Total Drag - Leading (N)		Total Drag - Trailing (N)		Drag % Change	
	Mean	S.D.	Mean	S.D.	Mean	S.D.
-1	5.676	4.93E-05	7.697	3.86E-05	35.604	1.60E-03
-0.592	5.678	2.90E-05	5.702	3.49E-05	0.423	9.48E-04
-0.444	5.681	2.34E-05	5.054	3.17E-05	-11.037	7.42E-04
-0.37	5.679	1.88E-05	4.828	2.11E-05	-14.978	5.24E-04
-0.333	5.685	2.31E-05	4.754	2.31E-05	-16.387	5.90E-04
-0.296	5.687	1.81E-05	4.705	2.39E-05	-17.264	6.01E-04
-0.259	5.690	2.57E-05	4.683	2.17E-05	-17.690	5.91E-04
-0.222	5.691	2.96E-05	4.686	2.24E-05	-17.652	6.23E-04
-0.185	5.693	3.02E-05	4.720	2.26E-05	-17.090	7.69E-04
-0.148	5.695	2.49E-05	4.779	1.79E-05	-16.083	5.27E-04
-0.111	5.698	2.34E-05	4.871	1.82E-05	-14.511	5.46E-04
-0.074	5.700	6.12E-04	4.987	2.07E-05	-12.517	9.39E-03
-0.037	5.703	1.70E-05	5.096	1.87E-05	-10.645	4.82E-04
0	5.705	2.19E-05	5.190	2.17E-05	-9.040	5.76E-04
0.037	5.708	2.16E-05	5.263	1.84E-05	-7.785	5.01E-04
0.074	5.709	2.67E-05	4.321	1.36E-05	-6.805	4.48E-04
0.148	5.714	1.66E-05	5.414	1.31E-05	-6.489	2.51E-04
0.296	5.721	1.90E-05	5.513	1.59E-05	-3.633	4.92E-04
0.444	5.727	2.66E-05	5.577	1.23E-05	-2.627	4.59E-04
0.592	5.732	2.60E-05	5.623	2.36E-05	-1.913	5.49E-04
0.814	5.739	1.92E-05	5.668	2.17E-05	-1.248	4.22E-04
1	5.744	1.94E-05	5.695	2.11E-05	-0.842	4.36E-04
2	5.756	2.31E-05	5.748	5.77E-02	-0.144	1.00E+00

Table F.4: Tabulated Total Drag Coefficient Parameters

Wing Spacing, Y/b	Total Drag Coefficient - Leading		Total Drag Coefficient - Trailing		Total Drag Coefficient % Change	
	Mean	S.D.	Mean	S.D.	Mean	S.D.
-1	0.030868	2.68E-07	0.041858	2.10E-07	35.604	1.60E-03
-0.592	0.030878	1.58E-07	0.031009	1.90E-07	0.423	9.48E-04
-0.444	0.030891	1.27E-07	0.027482	1.72E-07	-11.037	7.42E-04
-0.37	0.030881	1.02E-07	0.026256	1.15E-07	-14.978	5.24E-04
-0.333	0.030916	1.26E-07	0.025850	1.25E-07	-16.387	5.90E-04
-0.296	0.030928	9.87E-08	0.025588	1.30E-07	-17.264	6.01E-04
-0.259	0.030942	1.40E-07	0.025469	1.18E-07	-17.690	5.91E-04
-0.222	0.030948	1.61E-07	0.025485	1.22E-07	-17.652	6.23E-04
-0.185	0.030960	1.64E-07	0.025669	1.23E-07	-17.090	7.69E-04
-0.148	0.030970	1.35E-07	0.025989	9.74E-08	-16.083	5.27E-04
-0.111	0.030985	1.27E-07	0.026489	9.91E-08	-14.511	5.46E-04
-0.074	0.030999	3.33E-06	0.027119	1.13E-07	-12.517	9.39E-03
-0.037	0.031012	9.24E-08	0.027711	1.02E-07	-10.645	4.82E-04
0	0.031026	1.19E-07	0.028221	1.18E-07	-9.040	5.76E-04
0.037	0.031038	1.18E-07	0.028621	1.00E-07	-7.785	5.01E-04
0.074	0.031048	1.45E-07	0.028935	7.42E-08	-6.805	4.48E-04
0.148	0.031073	9.02E-08	0.029442	7.12E-08	-6.489	2.51E-04
0.296	0.031110	1.03E-07	0.029979	8.67E-08	-3.633	4.92E-04
0.444	0.031145	1.45E-07	0.030327	6.70E-08	-2.627	4.59E-04
0.592	0.031172	1.41E-07	0.030576	1.28E-07	-1.913	5.49E-04
0.814	0.031210	1.05E-07	0.030820	1.18E-07	-1.248	4.22E-04
1	0.031234	1.06E-07	0.030971	1.15E-07	-0.842	4.36E-04
2	0.031300	1.25E-07	0.031255	3.14E-04	-0.144	1.00E+00

Table F.5: Tabulated Lift-to-Drag Ratio Parameters

Wing Spacing, Y/b	Lift-to-Drag Ratio - Leading		Lift-to-Drag Ratio - Trailing		Lift-to-Drag % Change	
	Mean	S.D.	Mean	S.D.	Mean	S.D.
-1	22.799	1.50E-04	13.516	6.38E-05	-40.716	5.81E-04
-0.592	22.790	1.11E-04	21.768	1.10E-04	-4.483	7.60E-04
-0.444	22.776	9.14E-05	26.216	1.54E-04	15.100	8.82E-04
-0.37	22.779	7.55E-05	27.886	1.06E-04	22.418	6.76E-04
-0.333	22.750	8.94E-05	28.487	1.32E-04	25.216	8.30E-04
-0.296	22.740	6.76E-05	28.907	1.41E-04	27.123	8.63E-04
-0.259	22.724	9.84E-05	29.140	1.33E-04	28.231	8.78E-04
-0.222	22.717	1.14E-04	29.185	1.32E-04	28.473	9.04E-04
-0.185	22.704	1.16E-04	28.997	1.39E-04	27.718	1.18E-03
-0.148	22.693	8.76E-05	28.610	1.05E-04	26.072	7.23E-04
-0.111	22.677	8.59E-05	27.967	1.05E-04	23.326	7.74E-04
-0.074	22.663	2.46E-03	27.147	1.13E-04	19.783	1.30E-02
-0.037	22.649	6.85E-05	26.399	9.50E-05	16.555	6.06E-04
0	22.636	8.52E-05	25.775	1.08E-04	13.870	7.38E-04
0.037	22.623	8.17E-05	25.293	8.84E-05	11.805	6.18E-04
0.074	22.611	1.02E-04	24.925	6.53E-05	10.234	5.30E-04
0.148	22.587	6.03E-05	24.361	6.04E-05	7.855	2.85E-04
0.296	22.545	7.48E-05	23.744	6.96E-05	5.316	5.39E-04
0.444	22.510	1.06E-04	23.363	5.15E-05	3.790	4.91E-04
0.592	22.480	1.04E-04	23.100	9.60E-05	2.755	5.79E-04
0.814	22.442	7.61E-05	22.843	8.67E-05	1.789	4.37E-04
1	22.416	7.53E-05	22.690	8.34E-05	1.218	4.49E-04
2	22.346	8.25E-05	22.392	2.27E-01	0.206	1.02E+00

Table F.6: Tabulated Pressure Drag Parameters

Wing Spacing, Y/b	Pressure Drag - Leading (N)		Pressure Drag - Trailing (N)		Pressure Drag % Change	
	Mean	S.D.	Mean	S.D.	Mean	S.D.
-1	Mean	S.D.	Mean	S.D.	Mean	S.D.
-0.592	3.686	2.47E-05	5.645	1.43E-05	53.127	1.05E-03
-0.444	3.688	1.38E-05	3.717	3.19E-05	0.783	1.06E-03
-0.37	3.690	8.00E-06	3.085	1.20E-05	-16.396	4.08E-04
-0.333	3.686	5.30E-06	2.867	1.22E-05	-22.223	3.97E-04
-0.296	3.695	7.38E-06	2.794	8.39E-06	-24.372	3.32E-04
-0.259	3.697	4.81E-06	2.748	1.31E-05	-25.678	3.94E-04
-0.222	3.698	6.14E-06	2.726	1.17E-05	-26.290	4.13E-04
-0.185	3.700	1.01E-05	2.727	9.07E-06	-26.309	4.32E-04
-0.148	3.703	8.23E-06	2.760	9.48E-06	-25.459	3.86E-04
-0.111	3.704	7.51E-06	2.815	6.87E-06	-23.992	2.82E-04
-0.074	3.707	4.24E-06	2.903	7.68E-06	-21.682	2.25E-04
-0.037	3.709	6.11E-04	3.015	1.09E-05	-18.708	1.34E-02
0	3.712	8.66E-06	3.121	8.26E-06	-15.909	2.70E-04
0.037	3.714	3.83E-06	3.213	1.01E-05	-13.506	3.06E-04
0.074	3.716	3.91E-06	3.284	1.02E-05	-11.628	3.06E-04
0.148	3.718	6.55E-06	3.340	8.71E-06	-10.163	1.16E-04
0.296	3.722	5.81E-06	3.431	4.84E-06	-7.842	1.08E-04
0.444	3.729	4.84E-06	3.527	4.12E-06	-5.421	2.04E-04
0.592	3.735	5.90E-06	3.588	4.61E-06	-3.957	1.30E-04
0.814	3.740	7.95E-06	3.634	5.75E-06	-2.849	1.02E-04
1	3.747	7.04E-06	3.677	5.26E-06	-1.858	1.17E-04
2	3.751	6.13E-06	3.698	5.55E-06	-1.420	9.91E-05

Table F.7: Tabulated Skin Friction Drag Parameters

Wing Spacing, Y/b	Skin Friction Drag - Leading (N)		Skin Friction Drag - Trailing (N)		Skin Friction Drag % Change	
	Mean	S.D.	Mean	S.D.	Mean	S.D.
-1	1.990	3.53E-05	2.053	2.91E-05	3.148	2.91E-03
-0.592	1.990	2.04E-05	1.985	2.01E-05	-0.245	1.44E-03
-0.444	1.990	2.04E-05	1.968	2.92E-05	-1.101	1.89E-03
-0.37	1.993	1.65E-05	1.962	1.54E-05	-1.582	1.12E-03
-0.333	1.991	1.96E-05	1.959	1.94E-05	-1.565	1.36E-03
-0.296	1.991	1.63E-05	1.958	1.64E-05	-1.640	1.30E-03
-0.259	1.992	2.25E-05	1.957	1.59E-05	-1.721	1.22E-03
-0.222	1.991	2.33E-05	1.960	1.76E-05	-1.561	1.21E-03
-0.185	1.991	2.56E-05	1.960	1.90E-05	-1.526	2.02E-03
-0.148	1.991	1.95E-05	1.964	1.51E-05	-1.367	1.19E-03
-0.111	1.991	2.10E-05	1.968	1.61E-05	-1.160	1.53E-03
-0.074	1.991	1.77E-05	1.971	1.78E-05	-0.985	1.20E-03
-0.037	1.991	1.53E-05	1.975	1.71E-05	-0.834	1.22E-03
0	1.991	2.14E-05	1.977	1.93E-05	-0.710	1.63E-03
0.037	1.991	1.96E-05	1.979	1.52E-05	-0.614	1.34E-03
0.074	1.991	2.46E-05	1.981	1.04E-05	-0.535	1.35E-03
0.148	1.991	1.39E-05	1.984	1.18E-05	-0.398	7.45E-04
0.296	1.992	1.82E-05	1.986	1.56E-05	-0.287	1.36E-03
0.444	1.992	2.62E-05	1.989	1.10E-05	-0.132	1.31E-03
0.592	1.992	2.47E-05	1.989	2.21E-05	-0.155	1.58E-03
0.814	1.992	1.78E-05	1.990	2.05E-05	-0.102	1.20E-03
1	1.992	1.74E-05	1.997	1.98E-05	0.245	1.27E-03
2	1.993	1.86E-05	1.992	1.75E-05	-0.017	1.36E-03

Appendix G

TREFFTZ PLANE INFO

G.1 Trefftz Plane Info

Table G.1: Number of points in Trefftz plane

Wing Spacing, Y/b	Leading Wing Trefftz Plane	System Trefftz Plane
-1	3758373	3758159
-0.592	4247643	4247493
-0.444	4425570	4425674
-0.37	4516220	4516424
-0.333	4560982	4561091
-0.296	4602856	4602461
-0.259	4647722	4647373
-0.222	4693921	4693678
-0.185	4735585	4735289
-0.148	4780059	4780109
-0.111	4826304	4826259
-0.074	4871105	4870990
-0.037	4912893	4912474
0	4957484	4957336
0.037	5003862	5003663
0.074	5069568	5069142
0.148	5135273	5134620
0.296	5312652	5312420
0.444	5490119	5490040
0.592	5667190	5667459
0.814	5936764	5936419
1	6156822	6156798
2	7359088	7359079

G.1 Trefftz Plane Results

Table G.2: Trefftz Plane Results

Wing Spacing, Y/b	Induced Drag - Leading	Induced Drag – System	Leading Induced Drag % Change	Induced Drag Coefficient- Leading
-1	2.210	6.514	15.550	0.012
-0.592	2.244	4.216	13.813	0.012
-0.444	2.259	3.452	13.031	0.012
-0.37	2.263	3.183	12.760	0.012
-0.333	2.264	3.096	12.665	0.012
-0.296	2.265	3.041	12.606	0.012
-0.259	2.268	3.022	12.421	0.012
-0.222	2.268	3.032	12.401	0.012
-0.185	2.269	3.078	12.317	0.012
-0.148	2.269	3.150	12.270	0.012
-0.111	2.269	3.254	12.188	0.012
-0.074	2.271	3.389	12.074	0.012
-0.037	2.270	3.515	12.084	0.012
0	2.271	3.629	11.999	0.012
0.037	2.271	3.716	11.955	0.012
0.074	2.272	3.803	11.883	0.012
0.148	2.273	3.890	11.772	0.012
0.296	2.274	4.022	11.549	0.012
0.444	2.276	4.104	11.374	0.012
0.592	2.278	4.163	11.153	0.012
0.814	2.282	4.224	10.856	0.012
1	2.282	4.257	10.806	0.012
2	2.287	4.334	10.321	0.012

Table G.3: Trefftz Plane Results for the System Compared to Identified Values

Wing Spacing, Y/b	Induced Drag difference from 2x leading at Y/b = 2	Induced Drag difference from system at Y/b = 2
-1	42.429	50.300
-0.592	-7.817	-2.723
-0.444	-24.522	-20.351
-0.37	-30.396	-26.550
-0.333	-32.316	-28.576
-0.296	-33.504	-29.829
-0.259	-33.930	-30.279
-0.222	-33.696	-30.032
-0.185	-32.704	-28.985
-0.148	-31.123	-27.317
-0.111	-28.851	-24.920
-0.074	-25.907	-21.813
-0.037	-23.155	-18.908
0	-20.656	-16.271
0.037	-18.746	-14.256
0.074	-16.840	-12.245
0.148	-14.939	-10.239
0.296	-12.064	-7.205
0.444	-10.270	-5.311
0.592	-8.982	-3.952
0.814	-7.635	-2.531
1	-6.931	-1.788
2	-5.237	0.000

Appendix H

BIRD FORMATION FLIGHT DATA AND MANIPULATION

H.1 Canadian Geese – Hainsworth [13]

Table H.1: Canadian Geese Flight Data from Hainsworth Before and After Manipulation

From Report		Manipulated	
Wingtip Spacing (cm)	Number	Wing Spacing, Y/b	Scaled Frequency
-115	6	-0.7667	0.029
-85	38	-0.5667	0.337
-55	94	-0.3667	0.875
-25	107	-0.1667	1.000
5	72	0.0333	0.663
35	46	0.2333	0.413
65	24	0.4333	0.202
95	16	0.6333	0.125
125	11	0.8333	0.077
155	4	1.0333	0.010
185	7	1.2333	0.038
215	4	1.4333	0.010
275	3	1.8333	0.000

H.2 Greylag Geese - Speakman & Banks [15]

Table H.2: Greylag Geese Flight Data from Speakman & Banks Before and After Manipulation

From Report		Manipulated	
Wingtip spacing (cm)	Frequency	Wing Spacing, Y/b	Scaled Frequency
-90	1	-0.6254	0.015
-70	9	-0.4864	0.138
-50	29	-0.3475	0.446
-30	53	-0.2085	0.815
-10	65	-0.0695	1.000
10	43	0.0695	0.662
30	17	0.2085	0.262
50	11	0.3475	0.169
70	5	0.4864	0.077
90	6	0.6254	0.092
110	3	0.7644	0.046
130	3	0.9034	0.046
150	3	1.0424	0.046
170	0	1.1814	0.000

H.3 Ibises - Portugal [16]

Table H.3: Ibises Flight Data from Portugal Before and After Manipulation

From Report		Manipulated	
Distance to side (m)	Flaps in 0.25 m transect	Wing Spacing, Y/b	Scaled Frequency
0.00	13948	-1.00	-0.783
0.02	13792	-0.98	-0.817
0.04	13714	-0.97	-0.833
0.07	13753	-0.94	-0.825
0.09	14026	-0.93	-0.766
0.12	14182	-0.90	-0.733
0.14	14649	-0.88	-0.633
0.16	15000	-0.87	-0.558
0.19	15312	-0.84	-0.491
0.22	15351	-0.82	-0.483
0.24	15662	-0.80	-0.417
0.26	16130	-0.78	-0.317
0.29	16286	-0.76	-0.283
0.31	16870	-0.74	-0.158
0.34	16987	-0.72	-0.133
0.36	17494	-0.70	-0.025
0.39	17942	-0.68	0.071
0.41	18351	-0.66	0.158
0.44	18662	-0.63	0.225
0.46	18935	-0.62	0.283
0.48	19403	-0.60	0.383
0.51	19831	-0.58	0.475
0.53	20065	-0.56	0.525
0.55	20299	-0.54	0.575
0.58	20532	-0.52	0.625
0.61	20688	-0.49	0.658
0.63	21156	-0.48	0.758
0.66	21234	-0.45	0.775
0.68	21000	-0.43	0.725
0.70	21000	-0.42	0.725
0.73	21234	-0.39	0.775
0.75	21682	-0.38	0.871
0.78	21468	-0.35	0.825
0.80	21818	-0.33	0.900
0.82	22013	-0.32	0.942
0.85	22247	-0.29	0.992

0.87	22247	-0.28	0.992
0.90	22286	-0.25	1.000
0.92	22169	-0.23	0.975
0.95	22169	-0.21	0.975
0.97	22169	-0.19	0.975
1.00	22091	-0.17	0.958
1.02	21857	-0.15	0.908
1.05	21857	-0.13	0.908
1.07	21623	-0.11	0.858
1.10	21662	-0.08	0.867
1.12	21214	-0.07	0.771
1.14	20688	-0.05	0.658
1.17	20571	-0.03	0.633
1.19	20571	-0.01	0.633
1.22	20766	0.02	0.675
1.24	20727	0.03	0.667
1.27	20532	0.06	0.625
1.29	20494	0.08	0.617
1.31	20727	0.09	0.667
1.33	20416	0.11	0.600
1.37	20182	0.14	0.550
1.39	19870	0.16	0.483
1.41	19870	0.18	0.483
1.43	19714	0.19	0.450
1.46	19442	0.22	0.392
1.49	19519	0.24	0.408
1.51	19169	0.26	0.333
1.53	19130	0.28	0.325
1.56	19013	0.30	0.300
1.58	19130	0.32	0.325
1.61	18779	0.34	0.250
1.63	18740	0.36	0.242
1.65	18584	0.38	0.208
1.68	18390	0.40	0.167
1.70	18390	0.42	0.167
1.73	18039	0.44	0.092
1.75	18156	0.46	0.117
1.78	18097	0.48	0.104
1.80	18117	0.50	0.108
1.83	18156	0.53	0.117
1.85	18000	0.54	0.083

1.88	17727	0.57	0.025
1.90	17649	0.58	0.008
1.93	17610	0.61	0.000
1.95	17727	0.63	0.025
1.97	18058	0.64	0.096
2.00	18273	0.67	0.142

Appendix I

ALL PLOTS DERIVED FROM PRESSURE PROFILES

I.1 Distribution of Spanwise Lift Force

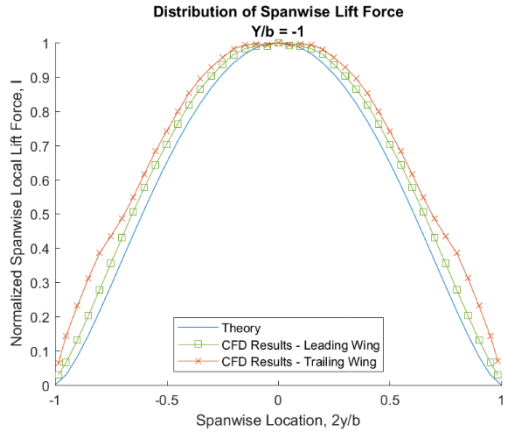

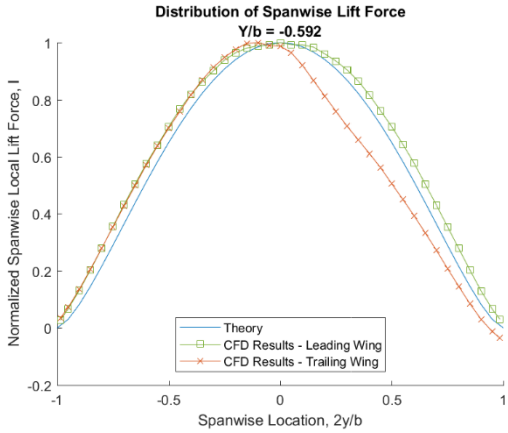

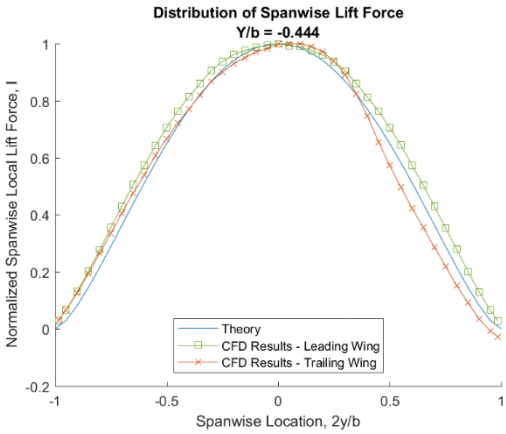

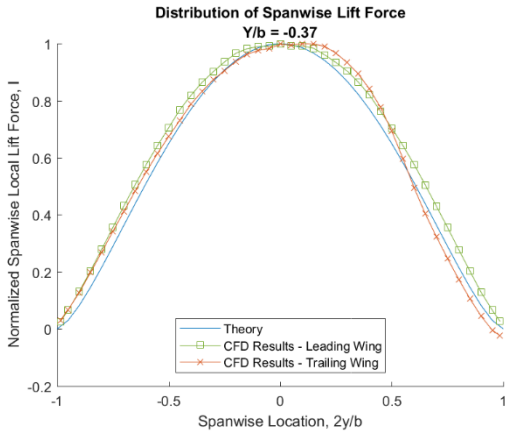

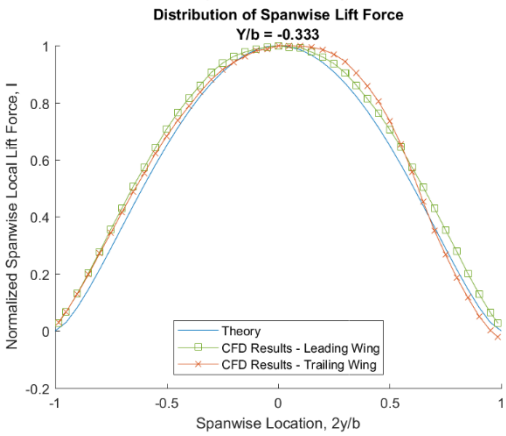

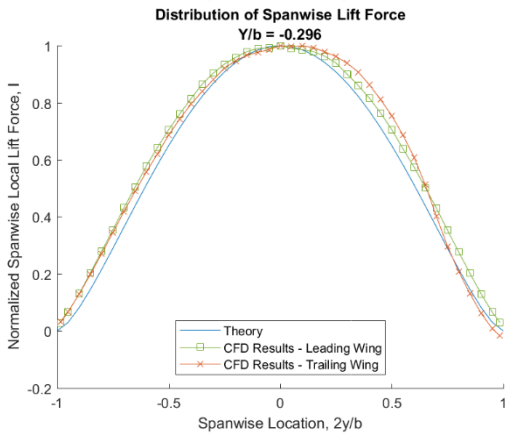

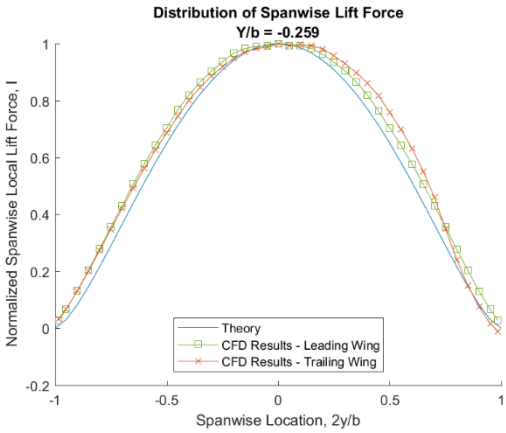
Distribution of Spanwise Lift Force
Y/b = -0.259
Normalized Spanwise Local Lift Force, l
Spanwise Location, 2y/b
Theory
CFD Results - Leading Wing
CFD Results - Trailing Wing

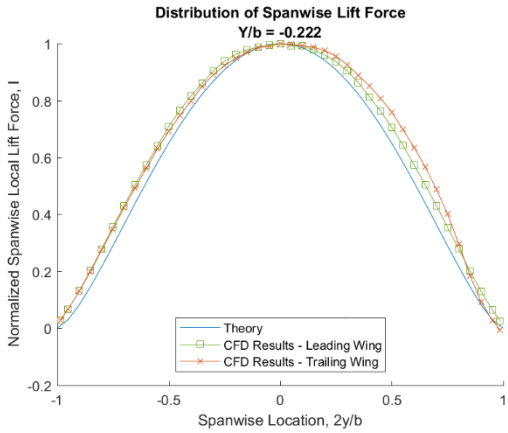
Distribution of Spanwise Lift Force
Y/b = -0.222
Normalized Spanwise Local Lift Force, l
Spanwise Location, 2y/b
Theory
CFD Results - Leading Wing
CFD Results - Trailing Wing

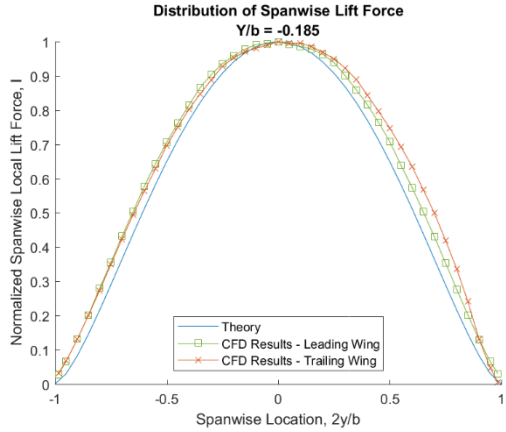
Distribution of Spanwise Lift Force
Y/b = -0.185
Normalized Spanwise Local Lift Force, l
Spanwise Location, 2y/b
Theory
CFD Results - Leading Wing
CFD Results - Trailing Wing

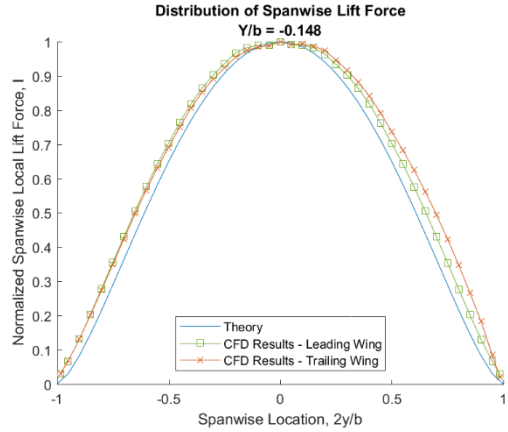
Distribution of Spanwise Lift Force
Y/b = -0.148
Normalized Spanwise Local Lift Force, l
Spanwise Location, 2y/b
Theory
CFD Results - Leading Wing
CFD Results - Trailing Wing

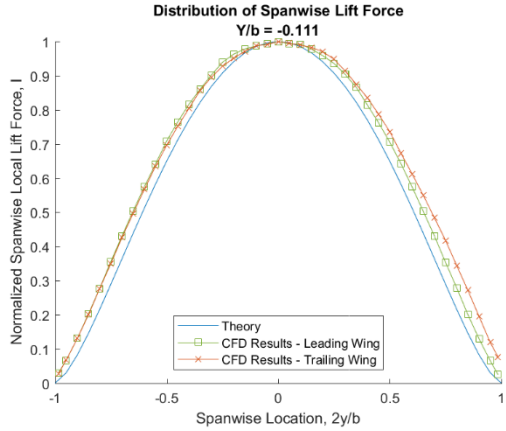
Distribution of Spanwise Lift Force
Y/b = -0.111
Normalized Spanwise Local Lift Force, l
Spanwise Location, 2y/b
Theory
CFD Results - Leading Wing
CFD Results - Trailing Wing

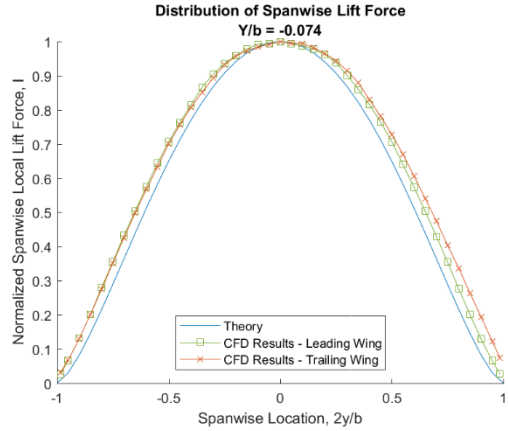
Distribution of Spanwise Lift Force
Y/b = -0.074
Normalized Spanwise Local Lift Force, l
Spanwise Location, 2y/b
Theory
CFD Results - Leading Wing
CFD Results - Trailing Wing

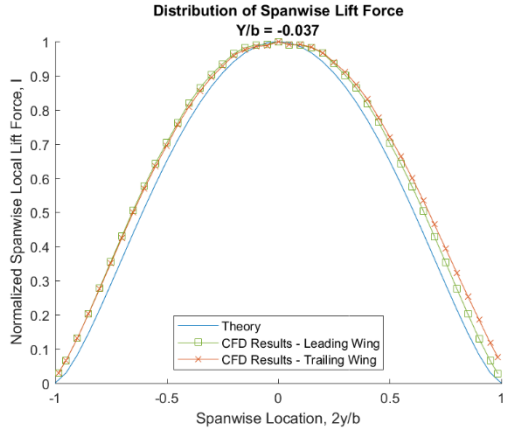
Distribution of Spanwise Lift Force
Y/b = -0.037
Normalized Spanwise Local Lift Force, l
Spanwise Location, 2y/b
Theory
CFD Results - Leading Wing
CFD Results - Trailing Wing

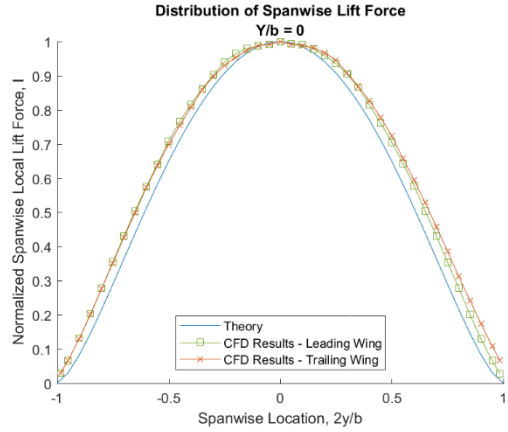
Distribution of Spanwise Lift Force
Y/b = 0
Normalized Spanwise Local Lift Force, l
Spanwise Location, 2y/b
Theory
CFD Results - Leading Wing
CFD Results - Trailing Wing

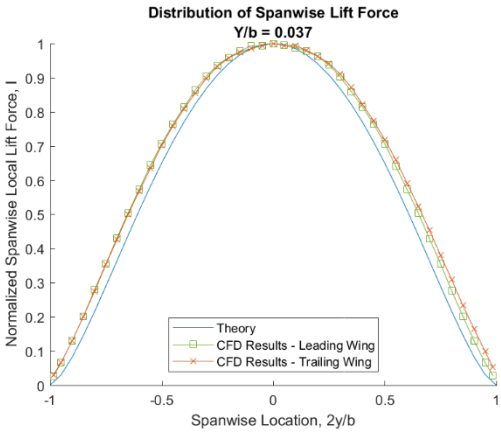
Distribution of Spanwise Lift Force
Y/b = 0.037
Normalized Spanwise Local Lift Force, l
Spanwise Location, 2y/b
Theory
CFD Results - Leading Wing
CFD Results - Trailing Wing

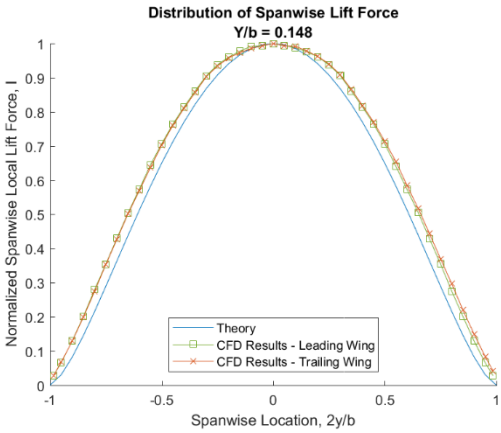
Distribution of Spanwise Lift Force
Y/b = 0.148
Normalized Spanwise Local Lift Force, l
Spanwise Location, 2y/b
Theory
CFD Results - Leading Wing
CFD Results - Trailing Wing

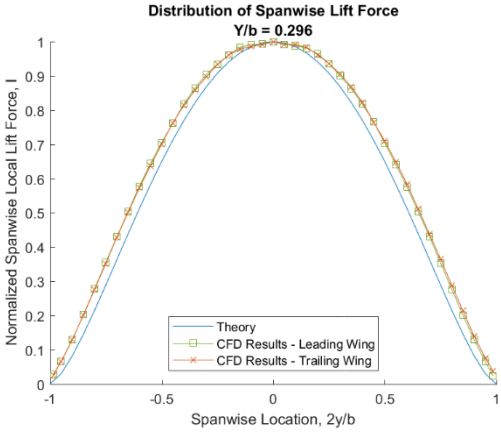
Distribution of Spanwise Lift Force
Y/b = 0.296
Normalized Spanwise Local Lift Force, l
Spanwise Location, 2y/b
Theory
CFD Results - Leading Wing
CFD Results - Trailing Wing

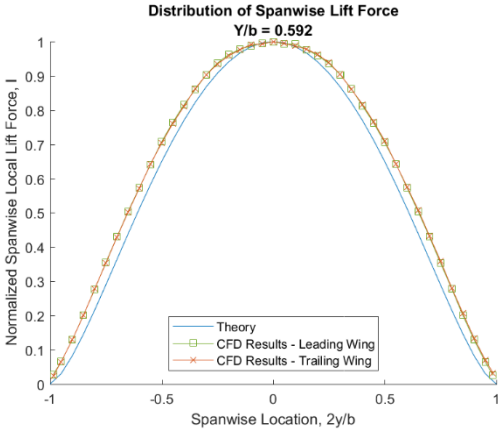
Distribution of Spanwise Lift Force
Y/b = 0.592
Normalized Spanwise Local Lift Force, l
Spanwise Location, 2y/b
Theory
CFD Results - Leading Wing
CFD Results - Trailing Wing

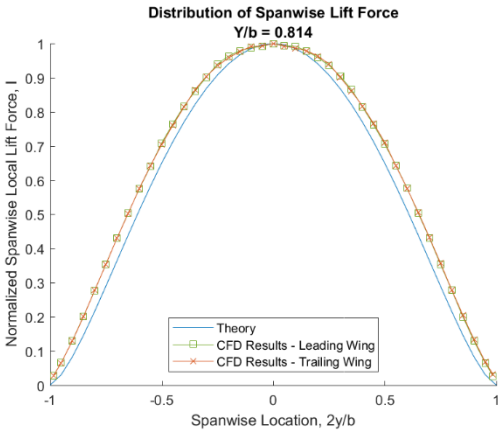
Distribution of Spanwise Lift Force
Y/b = 0.814
Normalized Spanwise Local Lift Force, l
Spanwise Location, 2y/b
Theory
CFD Results - Leading Wing
CFD Results - Trailing Wing

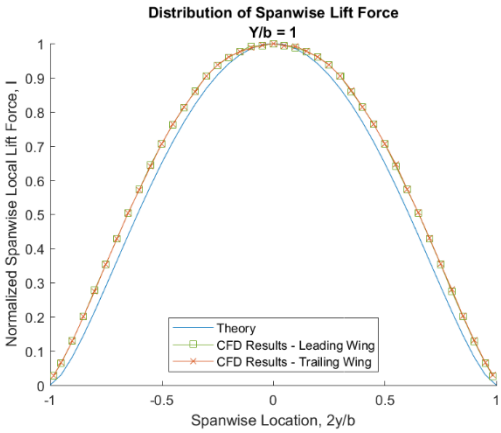
Distribution of Spanwise Lift Force
Y/b = 1
Normalized Spanwise Local Lift Force, l
Spanwise Location, 2y/b
Theory
CFD Results - Leading Wing
CFD Results - Trailing Wing

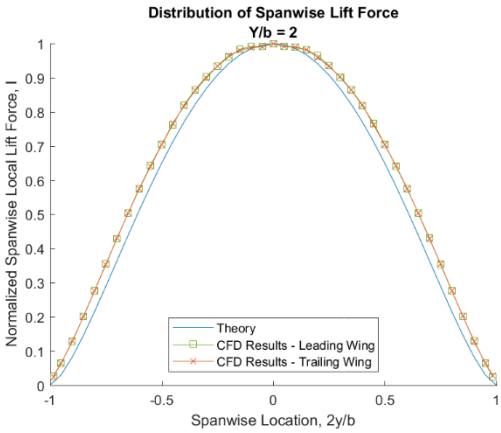
Distribution of Spanwise Lift Force
Y/b = 2
Normalized Spanwise Local Lift Force, l
Spanwise Location, 2y/b
Theory
CFD Results - Leading Wing
CFD Results - Trailing Wing

I.2 Distribution of Spanwise Lift Coefficient

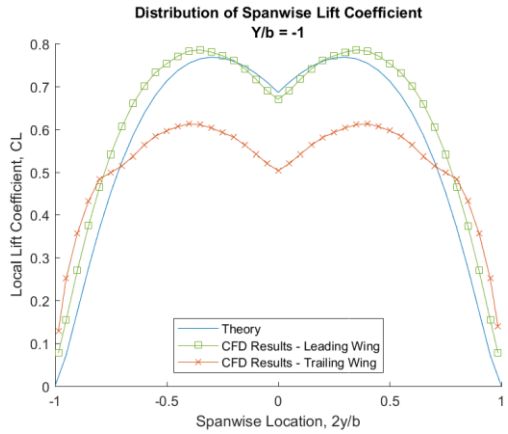

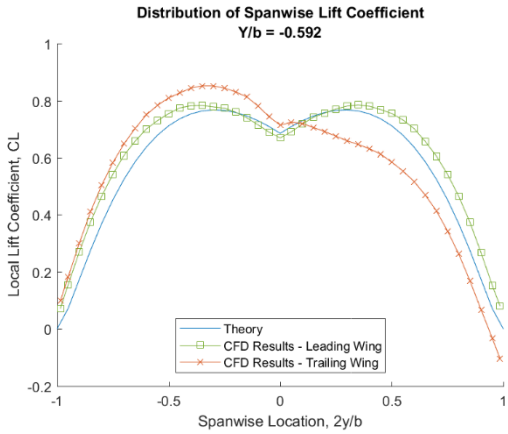

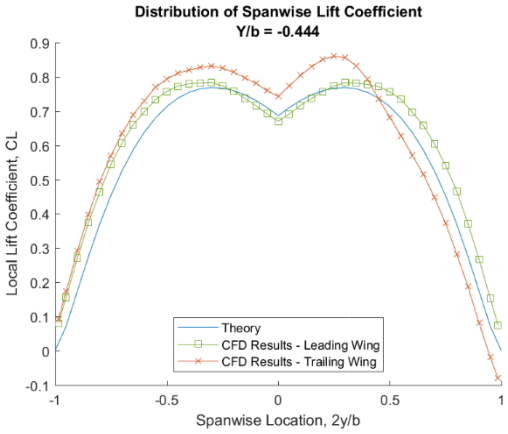

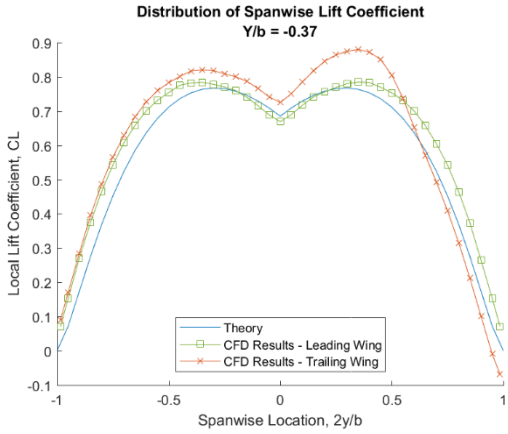

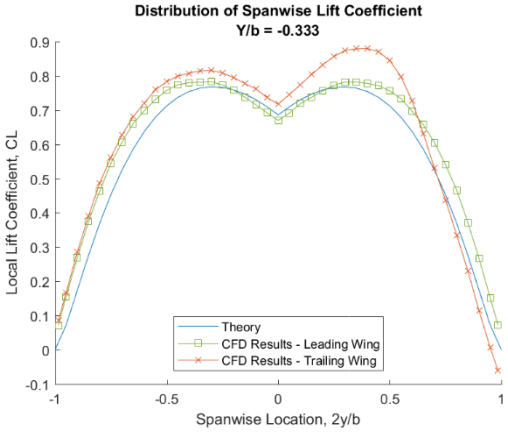

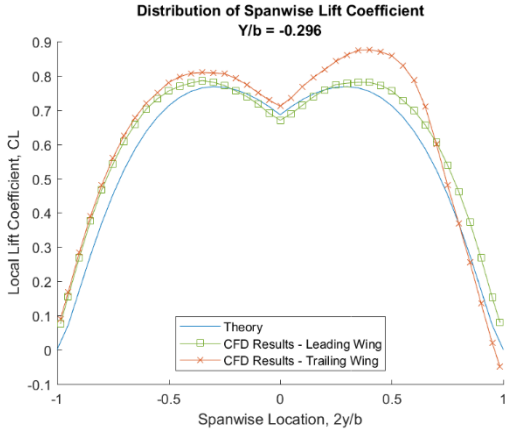

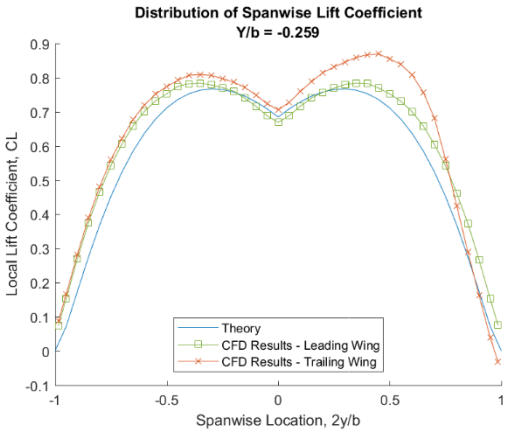
Distribution of Spanwise Lift Coefficient
Y/b = -0.259
Local Lift Coefficient, CL
Spanwise Location, 2y/b
Theory
CFD Results - Leading Wing
CFD Results - Trailing Wing

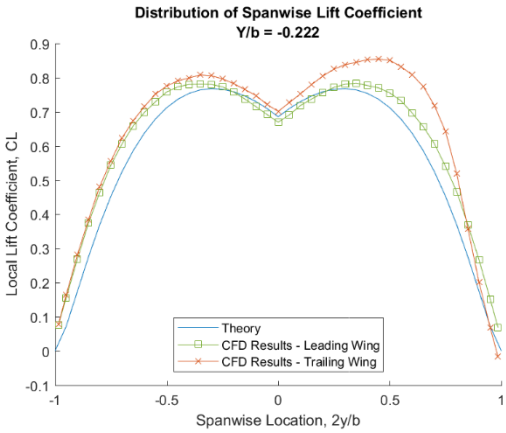
Distribution of Spanwise Lift Coefficient
Y/b = -0.222
Local Lift Coefficient, CL
Spanwise Location, 2y/b
Theory
CFD Results - Leading Wing
CFD Results - Trailing Wing

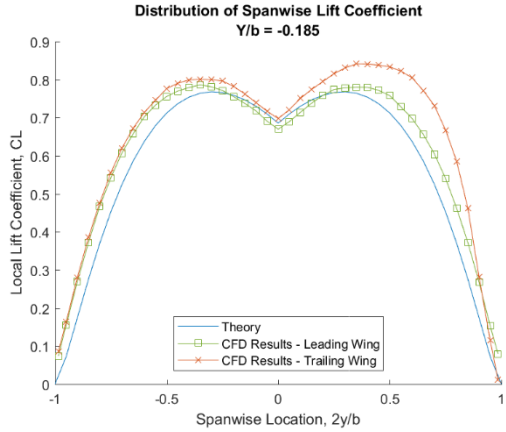
Distribution of Spanwise Lift Coefficient
Y/b = -0.185
Local Lift Coefficient, CL
Spanwise Location, 2y/b
Theory
CFD Results - Leading Wing
CFD Results - Trailing Wing

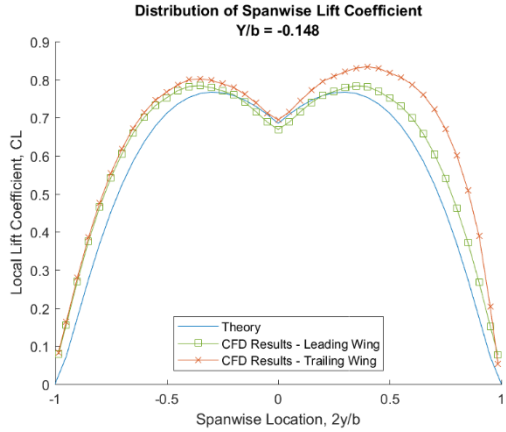
Distribution of Spanwise Lift Coefficient
Y/b = -0.148
Local Lift Coefficient, CL
Spanwise Location, 2y/b
Theory
CFD Results - Leading Wing
CFD Results - Trailing Wing

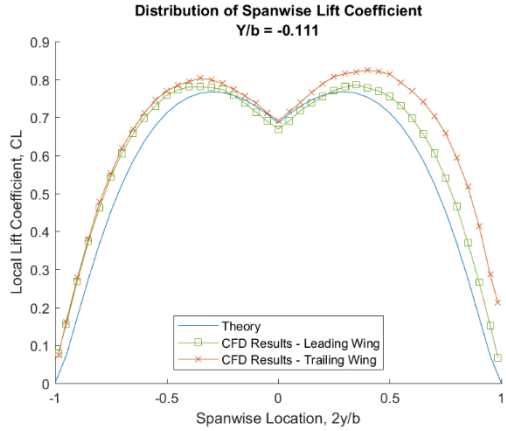
Distribution of Spanwise Lift Coefficient
Y/b = -0.111
Local Lift Coefficient, CL
Spanwise Location, 2y/b
Theory
CFD Results - Leading Wing
CFD Results - Trailing Wing

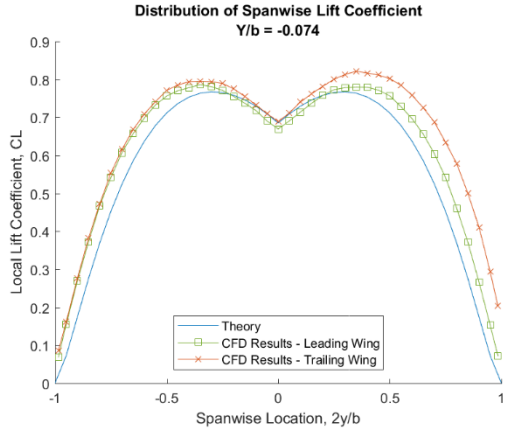
Distribution of Spanwise Lift Coefficient
Y/b = -0.074
Local Lift Coefficient, CL
Spanwise Location, 2y/b
Theory
CFD Results - Leading Wing
CFD Results - Trailing Wing

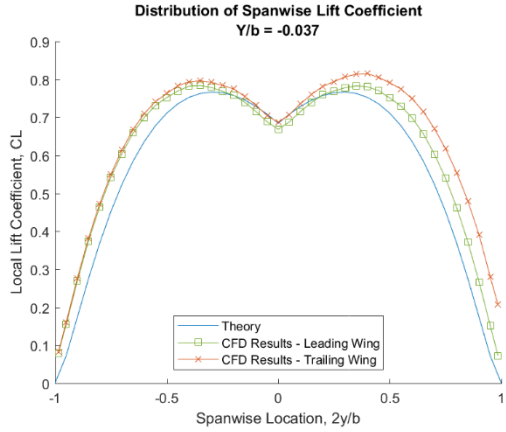
Distribution of Spanwise Lift Coefficient
Y/b = -0.037
Local Lift Coefficient, CL
Spanwise Location, 2y/b
Theory
CFD Results - Leading Wing
CFD Results - Trailing Wing

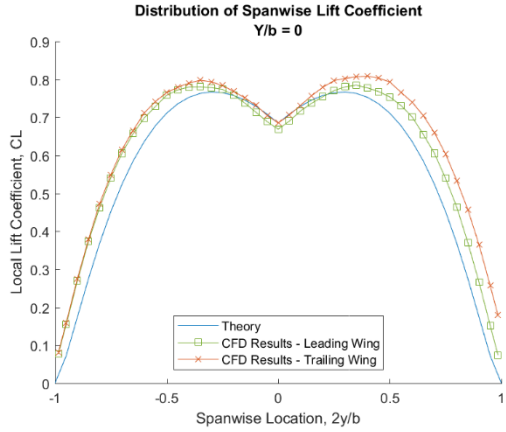
Distribution of Spanwise Lift Coefficient
Y/b = 0
Local Lift Coefficient, CL
Spanwise Location, 2y/b
Theory
CFD Results - Leading Wing
CFD Results - Trailing Wing

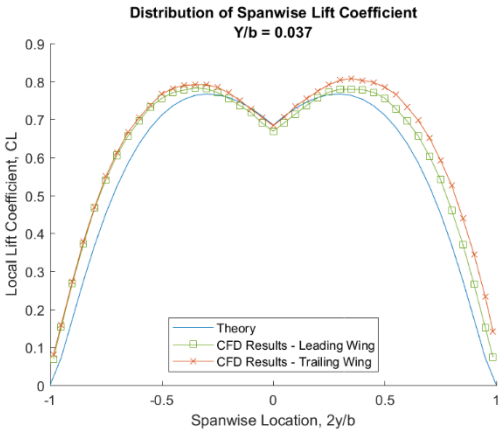
Distribution of Spanwise Lift Coefficient
Y/b = 0.037
Local Lift Coefficient, CL
Spanwise Location, 2y/b
Theory
CFD Results - Leading Wing
CFD Results - Trailing Wing

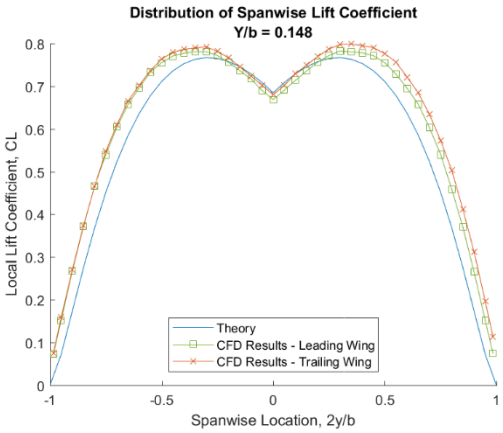
Distribution of Spanwise Lift Coefficient
Y/b = 0.148
Local Lift Coefficient, CL
Spanwise Location, 2y/b
Theory
CFD Results - Leading Wing
CFD Results - Trailing Wing

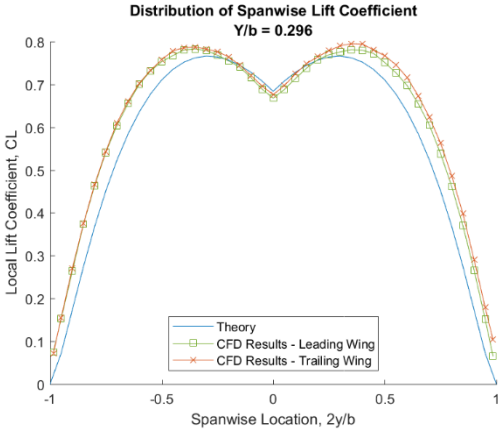
Distribution of Spanwise Lift Coefficient
Y/b = 0.296
Local Lift Coefficient, CL
Spanwise Location, 2y/b
Theory
CFD Results - Leading Wing
CFD Results - Trailing Wing

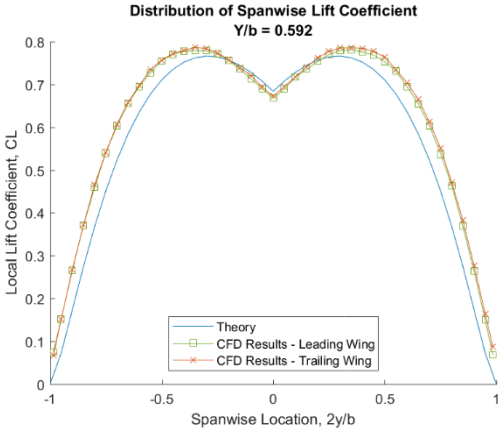
Distribution of Spanwise Lift Coefficient
Y/b = 0.592
Local Lift Coefficient, CL
Spanwise Location, 2y/b
Theory
CFD Results - Leading Wing
CFD Results - Trailing Wing

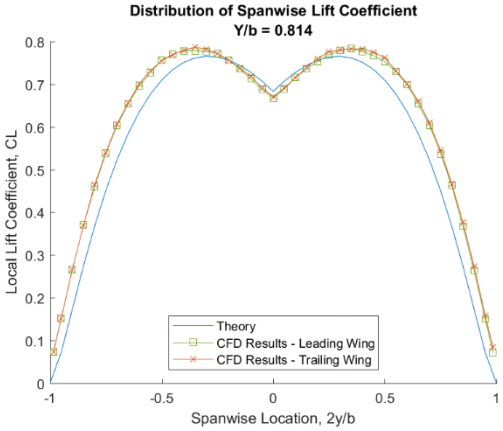
Distribution of Spanwise Lift Coefficient
Y/b = 0.814
Local Lift Coefficient, CL
Spanwise Location, 2y/b
Theory
CFD Results - Leading Wing
CFD Results - Trailing Wing

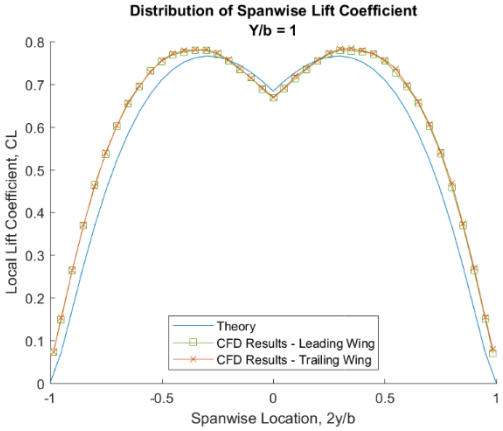
Distribution of Spanwise Lift Coefficient
Y/b = 1
Local Lift Coefficient, CL
Spanwise Location, 2y/b
Theory
CFD Results - Leading Wing
CFD Results - Trailing Wing

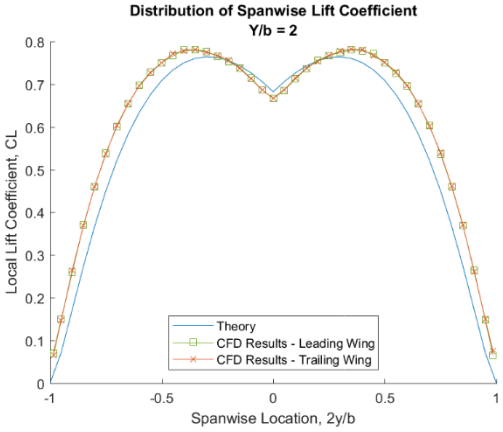
Distribution of Spanwise Lift Coefficient
Y/b = 2
Local Lift Coefficient, CL
Spanwise Location, 2y/b
Theory
CFD Results - Leading Wing
CFD Results - Trailing Wing

I.3 Distribution of Spanwise Lift Force - Leading Wing

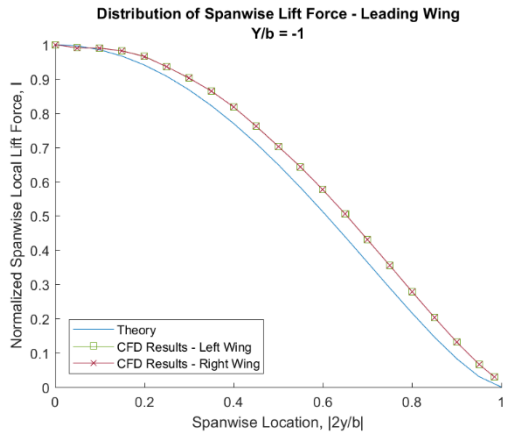

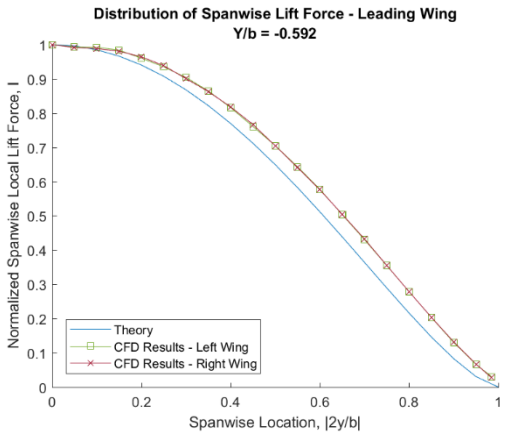

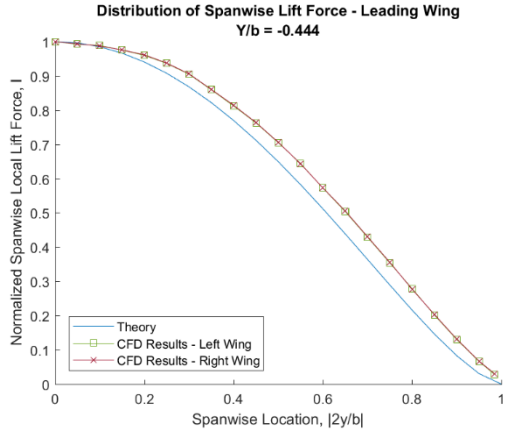

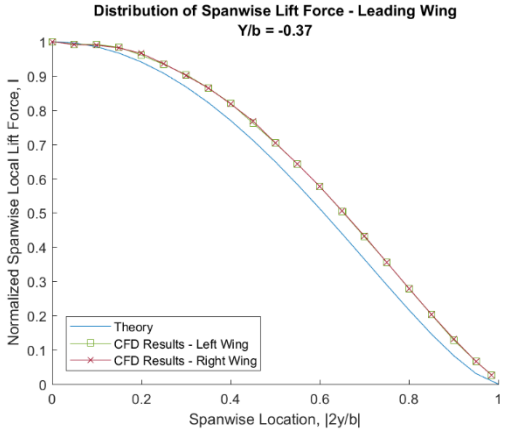

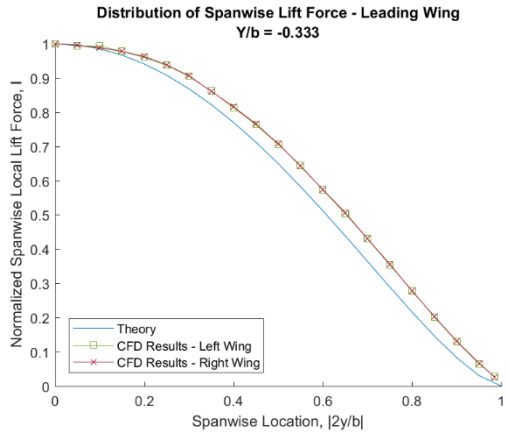

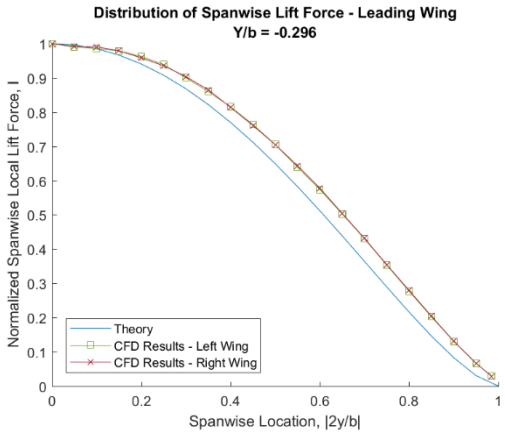

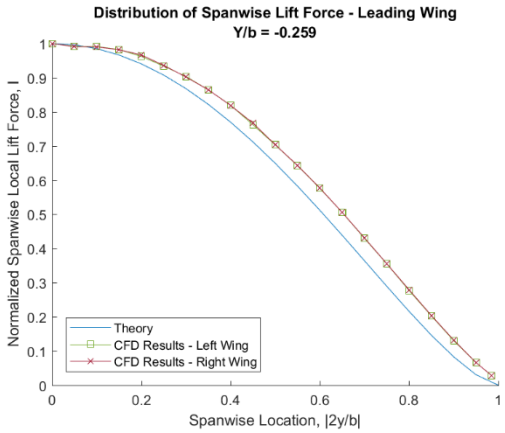
Distribution of Spanwise Lift Force - Leading Wing
Y/b = -0.259
Normalized Spanwise Local Lift Force, l
Spanwise Location, |2y/b|
Theory
CFD Results - Left Wing
CFD Results - Right Wing

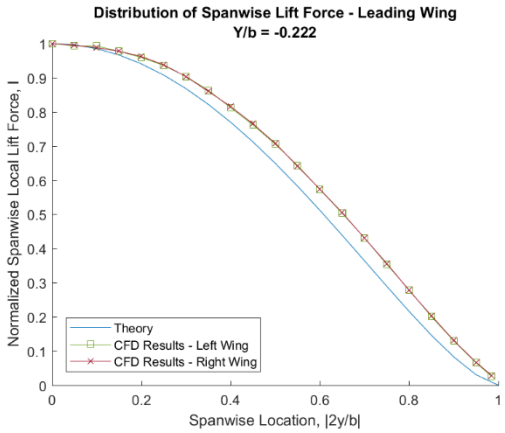
Distribution of Spanwise Lift Force - Leading Wing
Y/b = -0.222
Normalized Spanwise Local Lift Force, l
Spanwise Location, |2y/b|
Theory
CFD Results - Left Wing
CFD Results - Right Wing

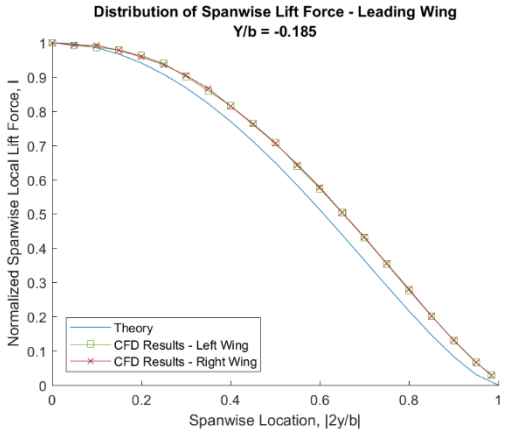
Distribution of Spanwise Lift Force - Leading Wing
Y/b = -0.185
Normalized Spanwise Local Lift Force, l
Spanwise Location, |2y/b|
Theory
CFD Results - Left Wing
CFD Results - Right Wing

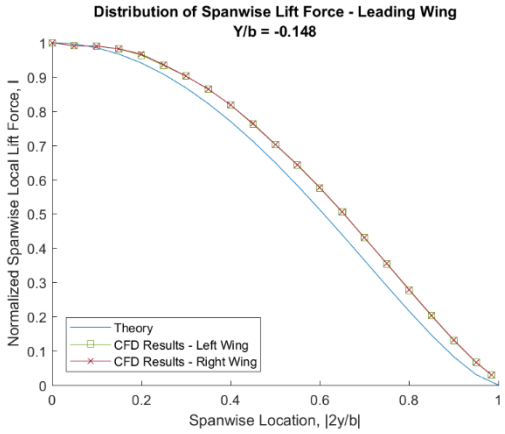
Distribution of Spanwise Lift Force - Leading Wing
Y/b = -0.148
Normalized Spanwise Local Lift Force, l
Spanwise Location, |2y/b|
Theory
CFD Results - Left Wing
CFD Results - Right Wing

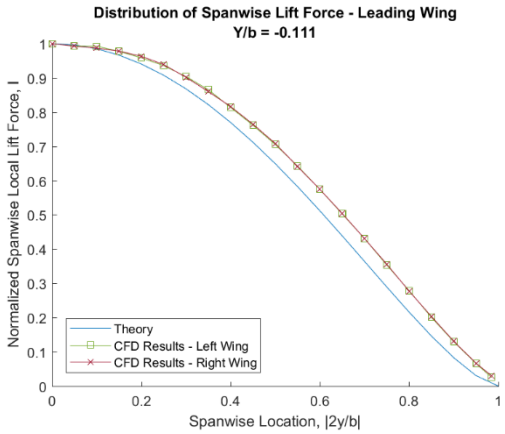
Distribution of Spanwise Lift Force - Leading Wing
Y/b = -0.111
Normalized Spanwise Local Lift Force, l
Spanwise Location, |2y/b|
Theory
CFD Results - Left Wing
CFD Results - Right Wing

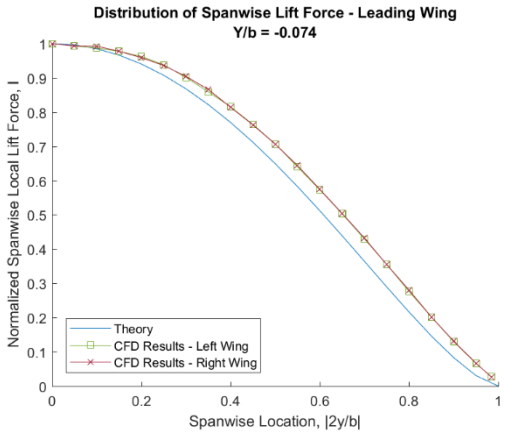
Distribution of Spanwise Lift Force - Leading Wing
Y/b = -0.074
Normalized Spanwise Local Lift Force, l
Spanwise Location, |2y/b|
Theory
CFD Results - Left Wing
CFD Results - Right Wing

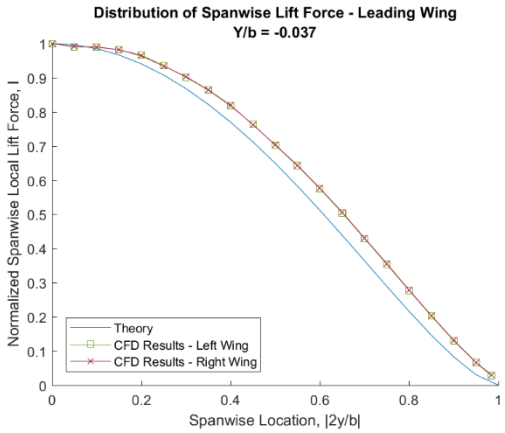
Distribution of Spanwise Lift Force - Leading Wing
Y/b = -0.037
Normalized Spanwise Local Lift Force, l
Spanwise Location, |2y/b|
Theory
CFD Results - Left Wing
CFD Results - Right Wing

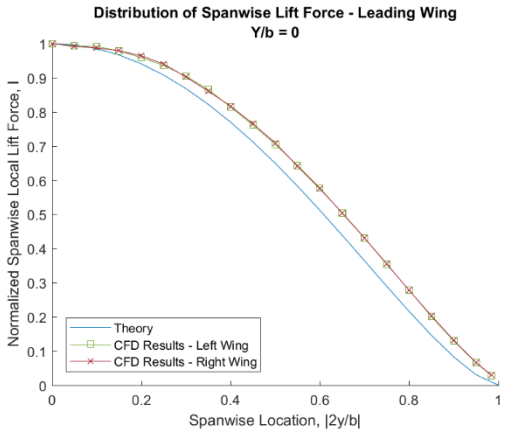
Distribution of Spanwise Lift Force - Leading Wing
Y/b = 0
Normalized Spanwise Local Lift Force, l
Spanwise Location, |2y/b|
Theory
CFD Results - Left Wing
CFD Results - Right Wing

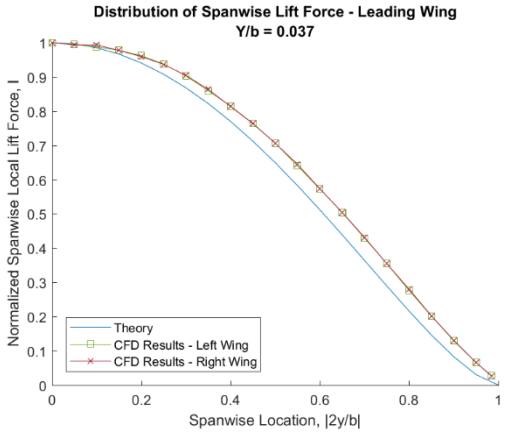
Distribution of Spanwise Lift Force - Leading Wing
Y/b = 0.037
Normalized Spanwise Local Lift Force, l
Spanwise Location, |2y/b|
Theory
CFD Results - Left Wing
CFD Results - Right Wing

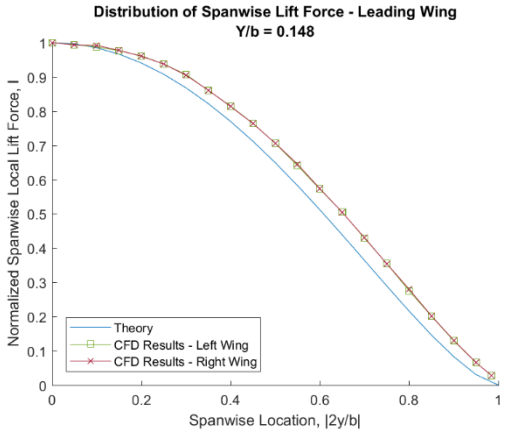
Distribution of Spanwise Lift Force - Leading Wing
Y/b = 0.148
Normalized Spanwise Local Lift Force, l
Spanwise Location, |2y/b|
Theory
CFD Results - Left Wing
CFD Results - Right Wing

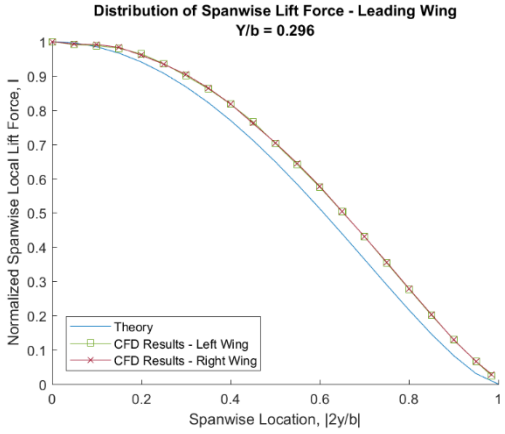
Distribution of Spanwise Lift Force - Leading Wing
Y/b = 0.296
Normalized Spanwise Local Lift Force, l
Spanwise Location, |2y/b|
Theory
CFD Results - Left Wing
CFD Results - Right Wing

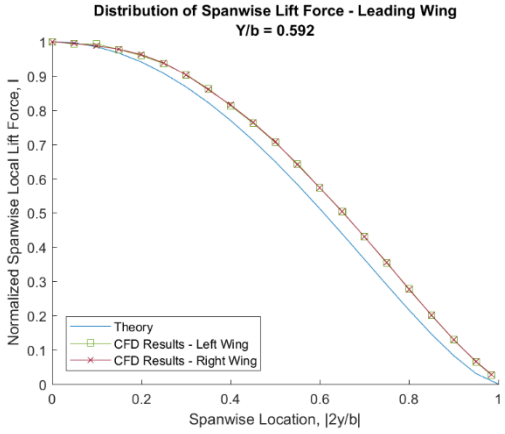
Distribution of Spanwise Lift Force - Leading Wing
Y/b = 0.592
Normalized Spanwise Local Lift Force, l
Spanwise Location, |2y/b|
Theory
CFD Results - Left Wing
CFD Results - Right Wing

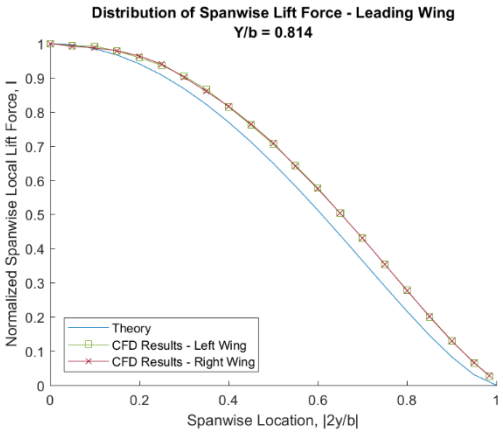
Distribution of Spanwise Lift Force - Leading Wing
Y/b = 0.814
Normalized Spanwise Local Lift Force, l
Spanwise Location, |2y/b|
Theory
CFD Results - Left Wing
CFD Results - Right Wing

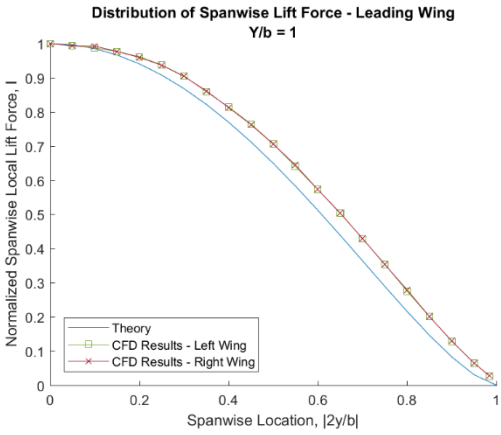
Distribution of Spanwise Lift Force - Leading Wing
Y/b = 1
Normalized Spanwise Local Lift Force, l
Spanwise Location, |2y/b|
Theory
CFD Results - Left Wing
CFD Results - Right Wing

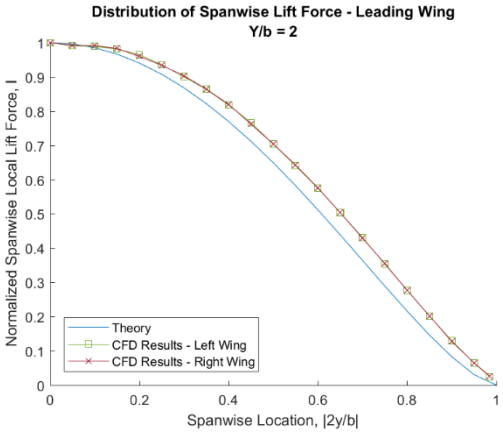
Distribution of Spanwise Lift Force - Leading Wing
Y/b = 2
Normalized Spanwise Local Lift Force, l
Spanwise Location, |2y/b|
Theory
CFD Results - Left Wing
CFD Results - Right Wing

I.4 Distribution of Spanwise Lift Force – Trailing Wing

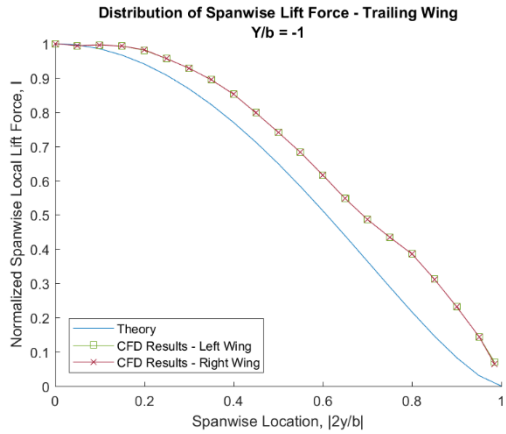

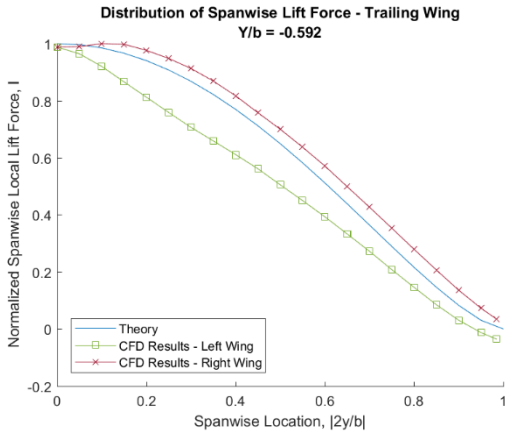

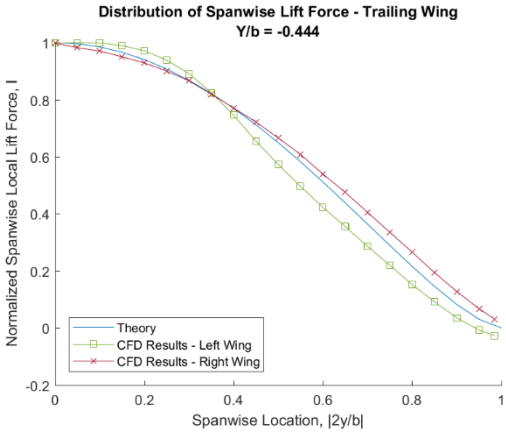

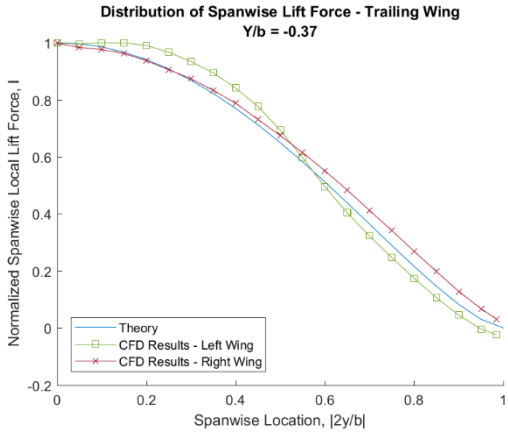

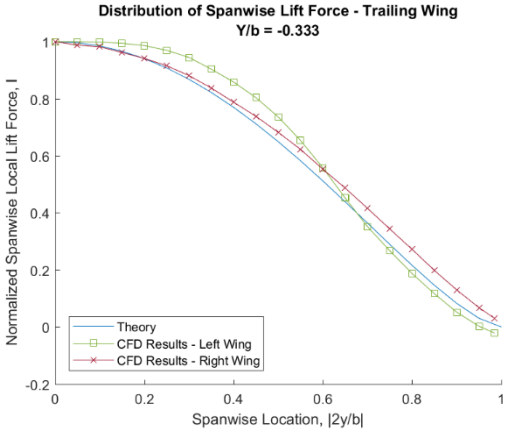

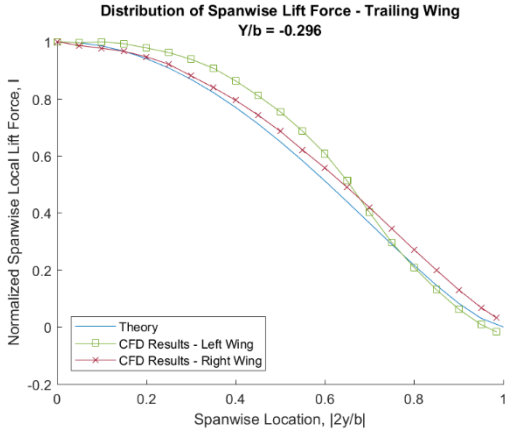

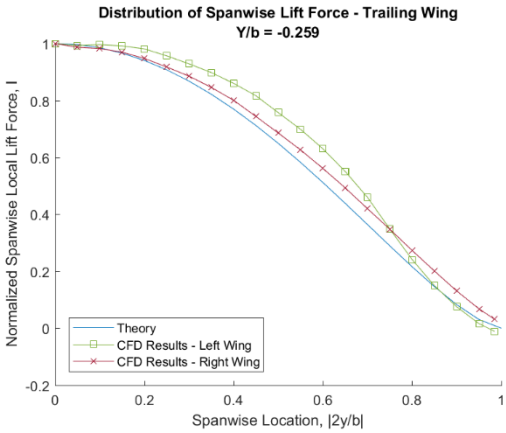
Distribution of Spanwise Lift Force - Trailing Wing
Y/b = -0.259
Normalized Spanwise Local Lift Force, l
Spanwise Location, |2y/b|
Theory
CFD Results - Left Wing
CFD Results - Right Wing

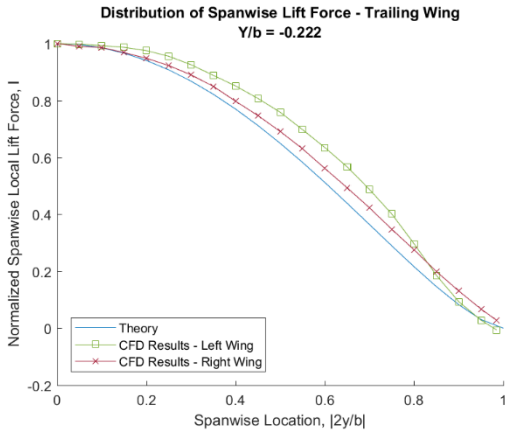
Distribution of Spanwise Lift Force - Trailing Wing
Y/b = -0.222
Normalized Spanwise Local Lift Force, l
Spanwise Location, |2y/b|
Theory
CFD Results - Left Wing
CFD Results - Right Wing

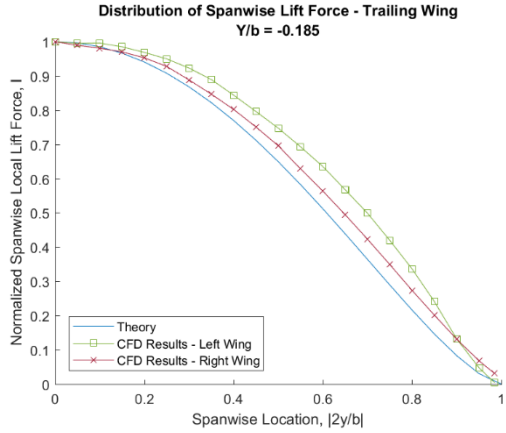
Distribution of Spanwise Lift Force - Trailing Wing
Y/b = -0.185
Normalized Spanwise Local Lift Force, l
Spanwise Location, |2y/b|
Theory
CFD Results - Left Wing
CFD Results - Right Wing

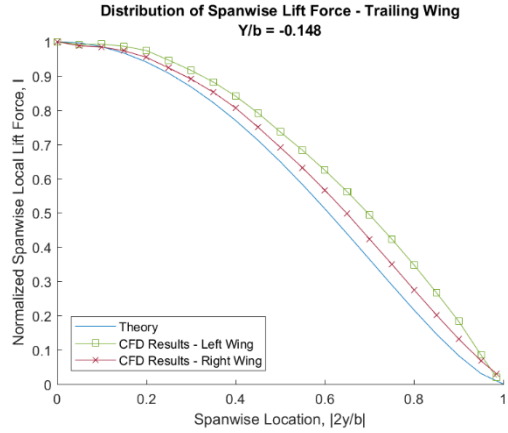
Distribution of Spanwise Lift Force - Trailing Wing
Y/b = -0.148
Normalized Spanwise Local Lift Force, l
Spanwise Location, |2y/b|
Theory
CFD Results - Left Wing
CFD Results - Right Wing

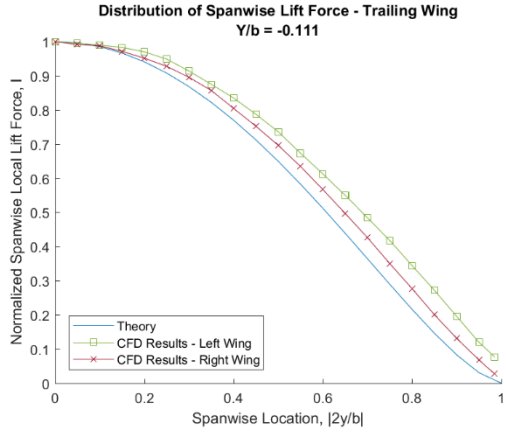
Distribution of Spanwise Lift Force - Trailing Wing
Y/b = -0.111
Normalized Spanwise Local Lift Force, l
Spanwise Location, |2y/b|
Theory
CFD Results - Left Wing
CFD Results - Right Wing

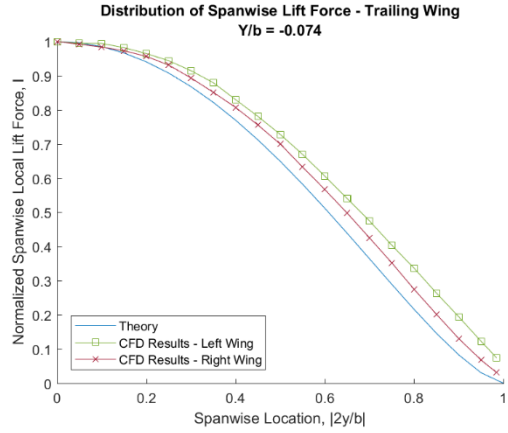
Distribution of Spanwise Lift Force - Trailing Wing
Y/b = -0.074
Normalized Spanwise Local Lift Force, l
Spanwise Location, |2y/b|
Theory
CFD Results - Left Wing
CFD Results - Right Wing

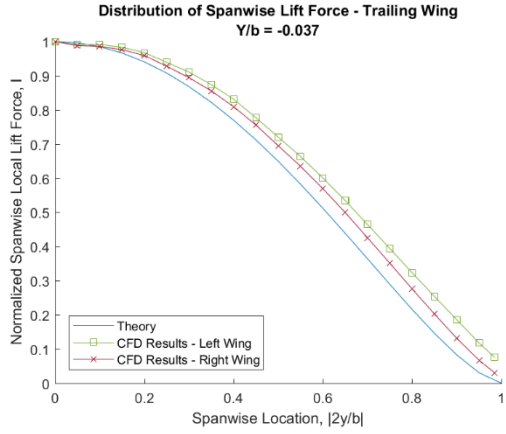
Distribution of Spanwise Lift Force - Trailing Wing
Y/b = -0.037
Normalized Spanwise Local Lift Force, l
Spanwise Location, |2y/b|
Theory
CFD Results - Left Wing
CFD Results - Right Wing

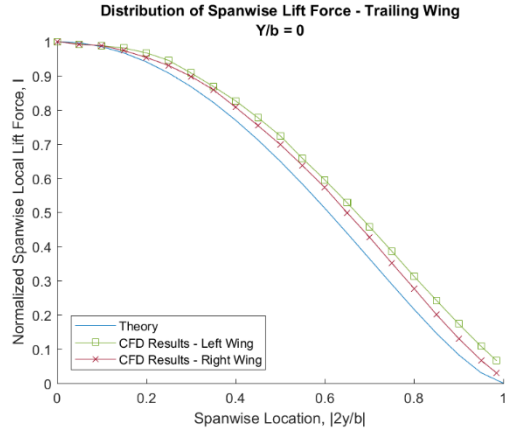
Distribution of Spanwise Lift Force - Trailing Wing
Y/b = 0
Normalized Spanwise Local Lift Force, l
Spanwise Location, |2y/b|
Theory
CFD Results - Left Wing
CFD Results - Right Wing

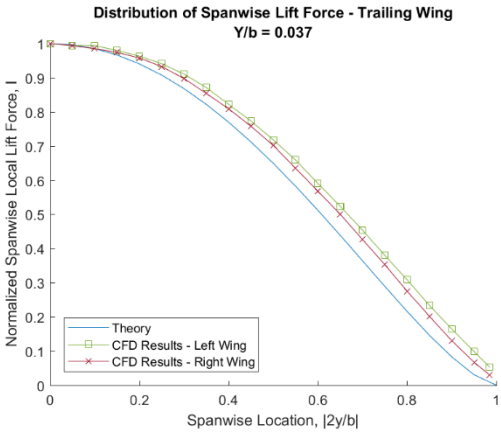
Distribution of Spanwise Lift Force - Trailing Wing
Y/b = 0.037
Normalized Spanwise Local Lift Force, l
Spanwise Location, |2y/b|
Theory
CFD Results - Left Wing
CFD Results - Right Wing

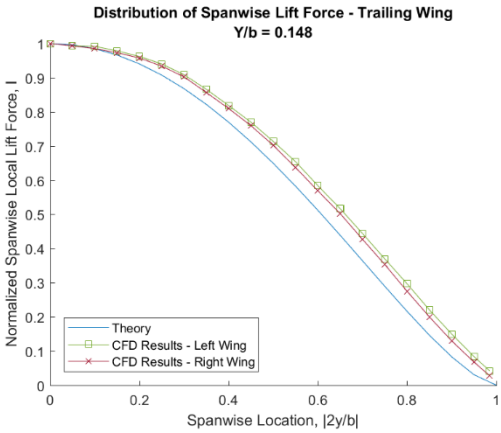
Distribution of Spanwise Lift Force - Trailing Wing
Y/b = 0.148
Normalized Spanwise Local Lift Force, l
Spanwise Location, |2y/b|
Theory
CFD Results - Left Wing
CFD Results - Right Wing

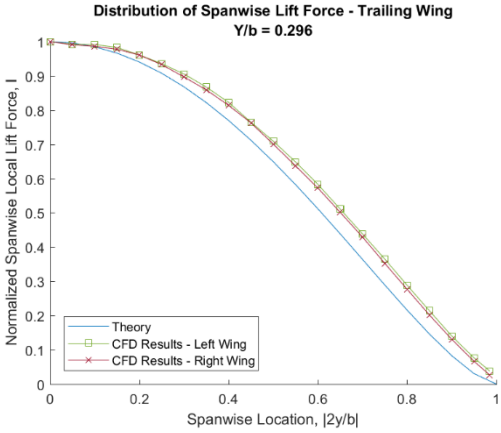
Distribution of Spanwise Lift Force - Trailing Wing
Y/b = 0.296
Normalized Spanwise Local Lift Force, l
Spanwise Location, |2y/b|
Theory
CFD Results - Left Wing
CFD Results - Right Wing

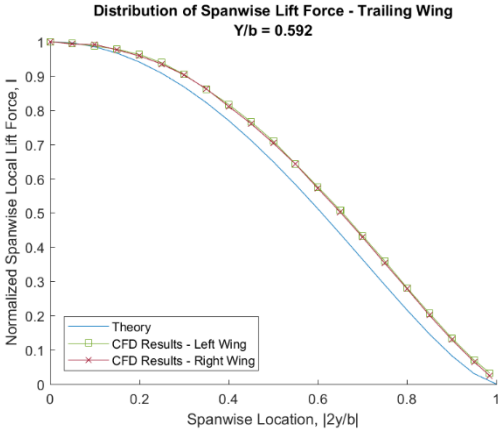
Distribution of Spanwise Lift Force - Trailing Wing
Y/b = 0.592
Normalized Spanwise Local Lift Force, l
Spanwise Location, |2y/b|
Theory
CFD Results - Left Wing
CFD Results - Right Wing

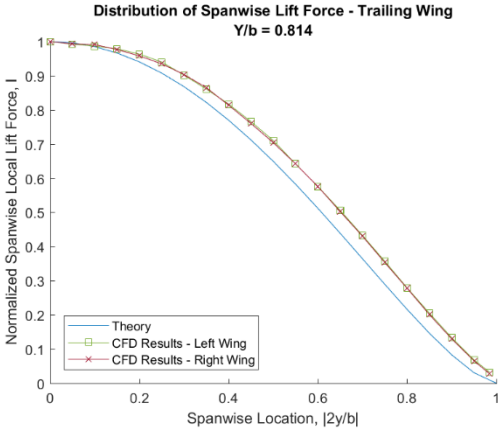
Distribution of Spanwise Lift Force - Trailing Wing
Y/b = 0.814
Normalized Spanwise Local Lift Force, l
Spanwise Location, |2y/b|
Theory
CFD Results - Left Wing
CFD Results - Right Wing

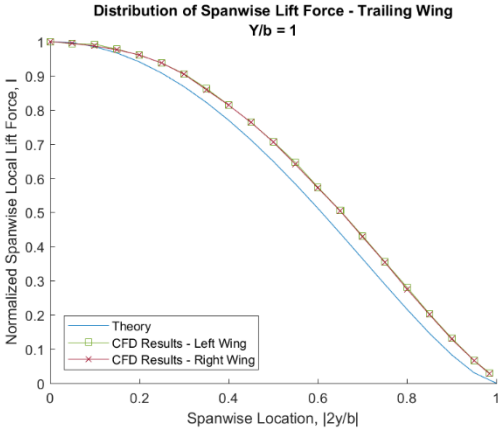
Distribution of Spanwise Lift Force - Trailing Wing
Y/b = 1
Normalized Spanwise Local Lift Force, l
Spanwise Location, |2y/b|
Theory
CFD Results - Left Wing
CFD Results - Right Wing

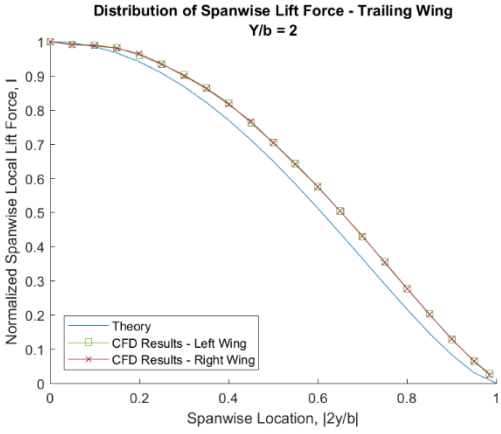
Distribution of Spanwise Lift Force - Trailing Wing
Y/b = 2
Normalized Spanwise Local Lift Force, l
Spanwise Location, |2y/b|
Theory
CFD Results - Left Wing
CFD Results - Right Wing